Investigating the Role of AGO2-RAS Interaction in Mutant RAS Driven Cancers

by

Ronald Francis Siebenaler

A dissertation submitted in partial fulfillment
of the requirements for the degree of
Doctor of Philosophy
(Cellular and Molecular Biology)
in the University of Michigan
2020

Doctoral Committee:

Professor Arul M. Chinnaiyan, Chair
Professor Eric Fearon
Associate Professor Marina Pasca di Magliano
Professor Muneesh Tewari

Ronald F. Siebenaler

rfsiebenaler@gmail.com

ORCID iD: 0000-0003-1583-1547

Dedication

For my Mom and Dad, my family, and my friends

Thank you for all your help and support in the ups and downs of my PhD

Acknowledgements

I first would like to express my deepest thanks and gratitude to my mentor Dr. Arul Chinnaiyan for the opportunity to work on this project. He fostered a deep appreciation for science and provided an unparalleled environment to grow as a physician scientist. He challenged me to develop into a scientist and supported me to follow my career and scientific goals. Thank you Arul for everything. It has been a privilege to work with you.

I would also like to thank all of my committee members: Dr. Eric Fearon, Dr. Marina Pasca Di Magliano, and Dr. Muneesh Tewari. Your feedback and mentorship throughout my graduate school education helped me to grow and develop into a stronger scientific thinker. In particular, I would like to thank Eric for the opportunity to work in his lab during my first rotation. You helped to set me off on this long journey, and I appreciate your guidance throughout graduate school.

I cannot express my gratitude for my fellow scientists in the Chinnaiyan Lab enough. In particular, I would like to thank Dr. Sunita Shankar, your mentorship and welcome into the "RAS" group in lab was foundational to my growth and learning during graduate school. I would also like to thank the other members of the RAS group, Seema Chugh, Jessica Waninger, Lakshmi Dommeti, and Jean Tien. You all helped me through the ups and downs of lab life, and your guidance helped me advance my work and science.

I would also like to thank Dr. Sethu Pitchiaya for his mentorship. You regularly challenged me to think more deeply on my projects and data. Thank you for bringing my thinking into a "single molecule" resolution and for your friendship throughout my time in lab.

In addition, I cannot thank Dr. Steve Kregel enough for both his friendship and mentorship. I would not have made it through these five years in lab without you. Our countless discussions made me a better scientist.

Thank you to all of the Chinnaiyan lab members for your friendship and help during my time in lab: Sisi Gao, Alec Chu, Yashar Niknafs, Pushpinder Bawa, Abhijit Parolia, Jae Eun Choi, Xia Jiang, Dan Robinson, Yi-Mi Wu, Mohan Dhanasekaran, Chandan Kumar, Rahul Mannan, Lanbo Xiao, Ingrid Apel, George Wang, Brendan Veeneman, Yasuyuki Hosono, Rohit Malik, Sandra Carson, Caleb Cheng, Marcin Cieslik, Yuanyuan Qiao, Silvia Zelenka-Wang, Josh Vo, Melissa Dunn, Grace Huang, Sathiya Narayanan, Lisha Wang, Palak Shah, Carl Engelke, Christine Betts, Dianna Banka, Stephanie Ellison, Xavier Owens, Jyoti Athanikar, Nikki Cortis, and Xuhong Cao. I couldn't have accomplished anything without all of your help and support. In particular, I would like to thank all of my undergraduate students that worked for me over the years: Malay Mody, Logan Steiert, Anudeeta Gautam, Nidhi Patel, and Carson Kenum. You all brought a great energy and passion to our projects that always worked to brighten my day.

I would also like to thank the Medical Scientist Training Program: Justine Hein, Gretchen Aland, Liz Bowman, Ellen Elkin, Laurie Koivupalo, and Hilkka Ketola. In particular, I cannot thank Dr. Ronald Koenig enough for his guidance and mentorship as director of the MSTP. Additionally, I would like to thank Dr. Robert Fuller, Lauren Pearl, and Patricia Ocelnik of the Cellular and Molecular program for your guidance and support these last five years.

I also would like to thank my undergraduate mentors from The Ohio State University, in particular, Dr. Michael A. Caligiuri, Dr. Kelsie Bernot, Dr. Nick Zorko, Dr. Ed Briercheck, and Lori Martensen. You all fostered my love of science and set me off on this amazing journey.

I would like to thank my friends and family for everything throughout my medical school and graduate school experience. Someone told me at the beginning of my MD/PhD journey that this would be the hardest thing I will ever do in my educational life, and your support has meant the world to me through the highs and lows if this journey. To Pat, Chelsea, Zach, Steve G., Zee, Bobby, Eric, Amelia, Jess, Steve K., Gauri, Sisi, Sethu, Morgan, Alex, Pushpinder, Alec, Yashar, Jeff, Jay, Mark, Aric, and Chris, you all lifted me up countless times, and I deeply cherish our friendships. In particular, I would like to thank my boyfriend Baldwin Giang for his patience and love throughout my graduate school journey. You always brighten my day when we are together, and I look forward to many more adventures to come.

Finally, I cannot thank and express my gratitude enough to my parents and sister, Lauren. Thank you for your constant encouragement, love, and support over the past seven years. Even when you didn't understand the science or experiment I was struggling with, you were always there to pick me up and improve my mood. I am forever grateful for everything you have given me in life, I couldn't have accomplished anything without your help.

Table of Contents

List of Tables

List of Figures

List of Appendices

Abstract

The *RAS* genes are among the most commonly mutated genes in cancer. These genes code for GTPases that act as growth factor receptor-regulated molecular switches. Mutations in RAS lead to a loss in GTP hydrolysis and cause constitutive RAS-GTP signaling, ultimately promoting cellular transformation and oncogenic growth in approximately 30% of human cancers. In pursuit of uncovering protein binding partners in RAS mutant cancers, the Chinnaiyan Lab recently identified Argonaute 2 (AGO2) of the RNA-induced silencing complex (RISC) as part of a novel interaction with KRAS. Despite showing a role for AGO2-KRAS binding in *KRAS* driven cancer, the precise function of this interaction remained unclear in both normal and cancer biology.

In order to assess the role of *AGO2* in $KRAS^{G12D}$ driven disease, we developed a mouse model of pancreatic cancer with conditional loss of *AGO2*. While *AGO2* knockout did not prevent development of early precursor pancreatic intraepithelial (PanIN) lesions, *AGO2* null lesions displayed increased activation of the EGFR-RAS signaling axis and altered microRNA expression during early PanIN development that led to oncogene induced senescence (OIS). This resulted in a dramatic increase in the survival of mice with AGO2 ablation. Upon loss of *AGO2* and *p53*, progression to PDAC was restored and PanIN lesions bypassed the senescence block. Additionally, we found that EGFR-mediated phosphorylation of $AGO2^{Y393}$ disrupts the interaction between wild-type (WT) and oncogenic KRAS-AGO2 interaction under different conditions.

While *KRAS* is the most commonly mutated isoform in human cancer, we next extended our observations to explore the role of AGO2 interaction with mutant HRAS and NRAS. We

confirmed AGO2-HRAS and AGO2-NRAS interaction, and we observed that AGO2 knockdown led to an induction of OIS that was accompanied with changes in the EGFR-RAS signaling axis in mutant *HRAS* and *NRAS* cells. The EGFR-RAS-ERK signaling observed was associated with an increase in reactive oxygen species (ROS). These high ROS levels inhibited the activity of the phosphatase PTP1B and were associated with increasing pEGFR activation stimulating a feed forward loop resulting in OIS. Finally, knockdown of AGO2 led to an inhibition of mutant *RAS* driven cell migration and metastasis in a zebrafish xenograft model.

We also developed a Single Molecule Toolbox for the use of studying AGO2's interaction with KRAS and other RISC members. Using an *in vitro* translation (IVT) system, we over-expressed a given protein, such as AGO2, in a HeLa based cell extract system. We studied the *in vitro* activity of AGO2 demonstrating a requirement for the presence of RISC members and inhibition by GTP-loaded KRAS. Furthermore, we observed the interaction of AGO2 and KRAS at a single molecule resolution demonstrating their binding at a 1 to 1 stoichiometry. Finally, we observed that IVT generated AGO2 formed higher order clusters *in vitro* that could be disrupted via RNase treatment. This Single Molecule Toolbox represents a new tool to aid in the study of the biochemistry of AGO2 and its interaction with KRAS.

Together, this dissertation describes the role of AGO2-RAS interaction in the development and maintenance of mutant *RAS* driven cancers, uncovering novel insight into these proteins and their role in both normal physiology and cancer biology.

Chapter 1 Introduction

The *RAS* Gene Family and Cancer

Overview

The members of the *RAS* family are among the most commonly mutated genes in human cancer. Since their initial description as proto-oncogenes in 1982 [1], the three *RAS* isoforms (*KRAS, HRAS,* and *NRAS*) have been the subject of intensive functional and biochemical research. Gain of function mutations in *RAS* genes lead to constitutive signaling through its downstream effector proteins, ultimately resulting in cellular transformation. Despite years of research uncovering the intricate signaling mechanisms, protein binding partners, and genetic regulation of RAS proteins, little progress has been made in successfully targeting *RAS* mutations clinically.

RAS Protein Structure

The *RAS* gene superfamily are a highly conserved group of guanosine triphosphatases (GTPases) broadly categorized into the RAS, RAB, ARF, and RHO subfamilies [2]. Together, these GTPases play an important role in cellular signaling in both normal and cancer cellular biology, and in particular, the RAS protein subfamily structure has been extensively characterized. The *RAS* gene family is comprised of 3 isoforms: *KRAS*, *HRAS*, and *NRAS* (**Figure 1.1)**. Additionally, *KRAS* encodes for two alternative splice variants *KRAS4A and KRAS4B* [3].

The four RAS protein isoforms share not only a high degree of structural domains/architecture but also nearly 90% of their amino acid sequence [4]. Together the RAS proteins are comprised of an N-terminal G-domain, a phosphate binding loop, two regulatory

switch regions (Switch I: amino acid (aa) 32-38; Switch II: aa 59-67), and a hypervariable region (HVR) within the C-terminus of the proteins. The G-domain (aa 1-86) is primarily involved in GTP/GDP hydrolysis, and structurally, it contains a six stranded β-sheet with five α-helices [5]. The phosphate binding loop (P-loop; aa 10-17) is critical for nucleotide loading of RAS, specifically binding to the β-phosphate of GDP and the β,γ-phosphates GTP [6]. The Switch I (SI) and Switch II (SII) domains are the primary site of conformational change between the RAS-GDP and RAS-GTP bound states [6]. Furthermore, the switch domains are the main binding sites of downstream effector binding partners such as GAPs (SI) and GEFs (SII) [7]. Intrinsic RAS GTPase activity is directed through residue Q61 mediating GTP hydrolysis and γ-phosphate release [5].

The C-terminal half of RAS proteins contain the highest divergence of sequence identity between RAS isoforms. Unlike the high level of sequence similarity within the G-domain, the allosteric lobe (aa 87-166) contains approximately 82% identity between RAS isoforms and functionally plays a role in the interaction between RAS proteins and the plasma membrane [8]. The hypervariable region (HVR) of the C-terminus (25 aa) of RAS contains the highest level of sequence divergence between RAS isoforms with less than 10% homology [4]. The HVR primarily serves to anchor RAS to the inner plasma membrane following lipid multiple modifications [9] described in detail later. Finally, all three RAS protein isoforms end in a tetrapeptide CAAX motif which is critical to plasma membrane targeting and trafficking following multiple post-translational modifications [10] (**Figure 1.2**).

RAS GTPase Cycle and Growth Factor Signaling

The *RAS* family of GTPases are cellular switches alternating between inactive RAS-GDP bound state and active RAS-GTP bound state based on signaling from growth factor receptors, such as

epidermal growth factor (EGFR) [11] or platelet-derived growth factor (PDGFR) [12], located at the plasma membrane (**Figure 1.3)**. RAS GTPases have high binding affinity for GTP/GDP and have low intrinsic GTPase activity [13]. Thus RAS GTP/GDP cycling is primarily regulated by guanine nucleotide exchange factors (GEFs) and GTPase-activating proteins (GAPs). RAS proteins have a high affinity for bound GDP/GTP nucleotide, leading to slow intrinsic dissociation rates [14]. In order to promote RAS GTP binding, GEF proteins, such as SOS1, activate RAS by increasing the dissociation rate of GDP [15], and since GTP is far more abundant in cells, RAS-GTP loading is favored [16]. Intrinsic RAS GTP hydrolysis is a slow process, and in order to inactivate RAS-GTP signaling, GAP proteins, such as NF1, are required to induce a conformational change in RAS, promoting GTP hydrolysis [17].

RAS GTPase cycling in cells is canonically regulated downstream of mitogenic signaling downstream of growth factor receptors like EGFR or PDGFR [11]. Following binding of associated ligand, growth factor receptor tyrosine kinases (RTK) dimerize, leading to phosphorylation of intracellular tyrosine residues [18]. Growth factor receptor-bound protein 2 (GRB2) is then recruited to the plasma membrane where its SH2 domain binds to phosoho-tyrosine residues on activated RTKs. The SH3 domain of GRB2 then promotes binding of SOS1, ultimately leading to the activation of RAS-GTP loading via SOS1 GEF activity [19]. Thus the RAS GTP cycle and activity is tightly regulated in normal physiologic conditions through the recruitment of activating GEFs downstream of growth factor activation and the presence of inactivating GAP proteins such as NF1.

RAS Mutations and Cancer

While RAS activity is typically under tight control, gain of function mutations in *RAS* genes are common drivers of tumor growth. Nearly 30% of all human cancer contain a point mutation in one of the 3 *RAS* isoforms [20]. Not only are RAS mutations amongst the most commonly mutated oncogenes in cancer, but they are also frequently altered in cancers with some of the highest mortality rates in the United States, including lung, colorectal, and pancreatic cancer [21]. Broadly, oncogenic mutations in RAS inhibit intrinsic and GAP-mediated GTPase activity, leading to constitutively active RAS-GTP signaling independent of growth factor receptor control. This aberrant signaling ultimately drives cellular transformation, proliferation, differentiation, and survival [22].

While missense point mutations in *RAS* isoforms are largely functionally similar, the distribution of mutant *RAS* isoforms varies greatly between different cancer lineages. *KRAS* mutations are the most commonly found in human cancer, comprising nearly 85% of all mutant *RAS* [4, 23]. Pancreatic ductal adenocarcinoma (~95% of all tumors), colorectal adenocarcinoma (~40-50%), and lung adenocarcinoma (~20-50%) are most commonly associated with mutant *KRAS*. Mutations in *NRAS* are the next most common driver of human cancer with approximately 11%, and they are commonly seen in melanoma (~10-30%), acute myeloid leukemia (~10%), and thyroid carcinoma (~15%). Finally, mutant *HRAS* accounts for the smallest percentage (4%) of human cancer, primarily driving urothelial bladder carcinoma (~10%) and squamous cell carcinoma of the head and neck (~6%) [4].

Within the three *RAS* isoforms, activating point mutations are centered around three primary codons G12, G13, and Q61 of the G-domain [22]. Collectively, mutations at these sites lead to an inhibition of both intrinsic and GAP mediated GTPase activity [24]. Specifically,

mutations in glutamine 61 (Q61) directly inhibit GTP hydrolysis of the γ-phosphate. While mutations in glycine 12 (G12) or glycine 13 (G13) of the P-loop, ultimately act to hinder the proper orientation of RAS functional domains to promote intrinsic hydrolysis and block GAP stimulated hydrolysis [17, 22]. In addition to the varying distribution of mutations across the three *RAS* isoforms, there is a great deal of heterogeneity in the pattern of specific site and amino acid changes between RAS proteins and cancer lineages. The G12 residue is most commonly altered in *KRAS*, and *NRAS* mutations occur most frequently at Q61, while *HRAS* alterations are distributed relatively equally between the three hotspots (G12, G13, and Q61). The three isoforms not only show preference for specific sites of mutation but also specific amino acid changes at those residues. For instance, *KRAS* mutations are common in both pancreatic and lung adenocarcinomas, but $KRAS^{G12D}$ is far more common in pancreatic tumors, while $KRAS^{G12C}$ is often seen in the lung [4, 25]. Together, *RAS* mutations account for many of the most aggressive cancer types and remain an important gene of study in human cancers.

RAS Downstream Effectors and Signaling Pathways

Following the loading of GTP into RAS proteins, the switch I and switch II domains undergo a conformational change allowing for interactions with their downstream effector proteins [15]. One of the first RAS binding partners to be described were the RAF kinases which were dependent on RAS-GTP state for their interaction [26]. RAF1 is a serine/threonine kinase containing an N-terminal RAS-binding domain (RBD) which interacts with the RAS switch I domain following GTP loading [27]. During the RAS-RAF interaction, RAF proteins are localized to the plasma membrane, allowing for their activation [28]. RAF then stimulates a signaling cascade through its phosphorylation of MEK1 and MEK2 which in turn induce the activation of the mitogen-activated

protein kinases (MAPKs) ERK1 and ERK2 via phosphorylation [29]. Following its activation, pERK then activates multiple downstream effectors in both the cytoplasm and nucleus, including ETS transcription factors and c-JUN, leading to promotion of cell cycle progression [30]. Ultimately, the RAS-RAF-ERK (MAPK) signaling pathway serves to induce pro-oncogenic proliferation, differentiation, and survival in cells following an activating mutation in *RAS*.

In addition to its activation of the MAPK pathway, RAS has been shown to interact with multiple other signaling molecules. The phosphatidylinositol 3-kinase (PI3K) pathway is also activated downstream of RAS signaling. PI3K interacts with both the switch I and switch II domains of RAS-GTP through its p110 domain [31, 32]. PI3K-RAS binding leads to phosphorylation of the plasma membrane phospholipid PIP_2 (Phosphatidylinositol 4,5-bisphosphate) converting it to PIP_3 (Phosphatidylinositol 3,4,5-trisphosphate). PIP_3 then recruits the serine/threonine kinase AKT to the plasma membrane via its pleckstrin-homology (PH) domain [33, 34], resulting in the phosphorylation of AKT by PKD1 and mTOR2 [35]. AKT then serves to activate multiple downstream effector proteins (including the mTOR pathway) ultimately promoting cellular survival, inhibition of cellular apoptosis, and changes in the actin cytoskeleton [23, 36].

In addition to the RAF-MAPK and PI3K-AKT pathways, RAS has been shown to activate multiple other signaling pathways. The RALa and RALb family of GTPases are activated downstream of RAS-GTP loading. The c-terminus of RALGDS protein binds to RAS's switch I domain, leading to the activation of RAL proteins [37]. RAL signaling has been associated with multiple downstream signaling pathways leading to changes in cell cycle promotion via inhibition of FoxO transcription factors, endocytic/exocytic vesicles, and activation of NF-κB [38-40]. The TIAMI-RAC signaling pathway is another RAS activated pathway leading to changes in cellular

cytoskeleton and migration [23, 41]. Finally, RAS activation of phospholipase Cε (PLC) leads to the hydrolysis of PIP_2 to inositol trisphosphate (IP3) and diacylglycerol (DAG), leading to activation of protein kinase C (PKC) and calcium channel release [42]. Together, these signaling pathways illustrate the central role for RAS GTPases in multiple key cellular processes involved in cellular survival, proliferation, and differentiation in both normal cellular and cancer biology (**Figure 1.4**).

Subcellular Localization and Membrane Trafficking of RAS Proteins

Considering the central role of *RAS* in multiple cellular processes, RAS proteins are highly regulated in their subcellular localization and trafficking to cellular membranes; however, despite their relative similarities in the functional G-domains, the KRAS, NRAS, and HRAS proteins differ substantially in their trafficking within the cell. As described above, the C-terminal hypervariable region (HVR) represents the majority of variance between these three isoforms. The HVR, along with the terminal CAAX tetrapeptide, are responsible for RAS interaction with the plasma membrane, with multiple post-translational modifications producing a hydrophobic C-terminus [10].

Following translation of RAS proteins in the cytoplasm, farneylstransferases (FTases) begin the modification of the CAAX motif by adding a farnesyl lipid to the cysteine. This is a key, rate-limiting step in the membrane trafficking of all RAS isoforms [43, 44]. After farnesylation, RAS is transported to the endoplasmic reticulum (ER) where it undergoes additional modification by RCE1, proteolytic removal of the –AAX tripeptide [45], and ICMT, methylation of the α-carboxyl group [46].

After these steps, the three *RAS* isoforms diverge in their processing and specific membrane trafficking. KRAS4a, HRAS, and NRAS are transported from the ER to the Golgi Apparatus after ICMT mediated methylation. At the Golgi, the HRAS and NRAS isoforms undergo palmitoylation via the DHHC9-GCP16 enzyme increasing the proteins' affinity for the membrane of the Golgi [47, 48]. This allows for transport of RAS proteins from the Golgi to the plasma membrane. As the palmitoylation of RAS is a reversible process, NRAS and HRAS can readily cycle between the plasma membrane and the Golgi apparatus via vesicle transport following depalmitoylation [49].

Unlike the other RAS isoforms, KRAS4b does not undergo palmitoylation following ICMT methylation. KRAS4b's HVR contains a positively charged lysine, polybasic domain that interacts with the plasma membrane [50]. Like HRAS and NRAS, KRAS4b's interaction with the membrane can be dynamically regulated via calmodulin binding or phosphorylation [51]. Together, the dynamic nature of RAS subcellular localization and membrane association is central to RAS signaling (**Figure 1.5**), and considering the central role RAS's interaction with the plasma membrane plays in its downstream signaling, it has been thought to be a potential therapeutic target in cancers driven by mutant *RAS*.

RAS Mutations and Oncogene Induced Senescence

Considering their high prevalence in human cancer, the role of *RAS* mutations in initiating and promoting tumor transformation has been the subject of much inquiry. Early studies demonstrated the ability of mutant *RAS* to drive transformation of NIH 3T3 immortalized mouse fibroblasts [52]; however, primary rodent fibroblasts resisted transformation unless accompanied by additional oncogenes or inactivation of a tumor suppressor [53, 54]. Further exploration demonstrated that while mutant HRAS was capable of inducing oncogenic signaling when introduced to cells, it also

led to the accumulation of tumor suppressors like *p16*^{INK4A} (p16) and *TP53* (p53). Both of these proteins are well studied regulators of cellular senescence, the process by which cells irreversibly undergo cell cycle arrest. Importantly, activation of p53 downstream of cellular stress, such as DNA damage, leads to up-regulation of the p21 protein [55]. Higher levels of p16 and p21 in cells lead to the inhibition of cyclin-dependent kinases and the hypophosphorylation of retinoblastoma protein (pRb). This increases association of pRB with E2F transcription factors leading to repression of E2F gene targets and induction of cell cycle arrest [56]. While oncogenic *RAS* signaling is vital to growth signaling through MAPK and other pathways, constitutive mitogenic signaling has been demonstrated to induce both the p53/p21 and p16 pathways. Thus, the mutation or loss of these senescence mediators is partially required for cellular transformation and oncogenic growth [57, 58]. Furthermore, mutations in *RAS* have been linked to increased production of reactive oxygen species (ROS) which can lead to the additional accumulation of DNA damage and genomic instability within cells [59, 60]. In addition to activation of tumor suppressors like p53 through DNA damage, accumulation of ROS activates p38α MAPK signaling, ultimately leading to the increased transcription of p16 and the induction of cellular senescence within cells [61, 62].

The *in vitro* requirement for activation of *RAS* and loss of tumor suppressors is recapitulated in the development and progression of human cancers driven by mutations in *RAS*. For instance, development of pancreatic ductal adenocarcinoma (PDAC) is commonly driven by mutations in *KRAS* leading to dysplastic growth and the development of pancreatic intraepithelial neoplasia (PanIN lesions). In order for the formation of PDAC, PanIN lesions require the additional accumulation of mutations ultimately leading to the inactivation of tumor suppressors *p16* (intermediate event), *p53*, and *SMAD4* (later events) [63, 64]. A similar progression is seen in

the subset of colorectal adenocarcinoma (CRC) in which inactivation of the *APC* tumor suppressor leads to the formation of adenoma precursor lesions. This is followed by the accumulation of activating mutations in *KRAS* (~50% of CRC) and inactivation of *p53* and *SMAD4* ultimately leading to the formation of metastatic carcinoma [65]. These examples highlight the importance of cooperative activation of oncogenic *RAS* and inactivation of pro-senescence tumor suppressors in the development of *RAS* driven human cancers.

Clinical Targeting of RAS Mutations

Despite years of research into the biochemical properties, cellular signaling effectors, and other aspects of mutant *RAS* biology, few targeted therapies toward *RAS* mutations have made it to the clinic. Considering that *RAS* is the most commonly mutated oncogene and drives some of the deadliest forms of human cancer, there is a great need for the development of effective therapeutic agents to target mutations in all three isoforms of *RAS.* One of the primary difficulties that have prevented effective drug development is RAS's high affinity for GTP which hinders the development of inhibitors that could compete with binding. Additionally, RAS proteins lack hydrophobic pockets for small molecules to readily bind inside [21]. These two features of mutant *RAS* have led to the exploration of other methods, such as targeting RAS binding partners or RAS localization within the cell. Importantly, recent progress has been made to successfully target $KRAS^{G12C}$ mutations directly, and promising clinical results have renewed the promise of direct inhibition of mutant RAS proteins clinically [66, 67].

Much initial work in developing therapeutics targeting *RAS* mutants involved secondary means of inhibiting the downstream effects of oncogenic *RAS* signaling. Since RAS signaling is dependent upon association with the membrane, one of the first methods involved inhibiting RAS

protein localization to the plasma membrane [50]. Farnesyltransferase inhibitors (FTIs) were developed to target the rate limiting step of -CAAX modification necessary for RAS membrane trafficking [68]. However, the efficacy of FTIs were limited by different methods of KRAS and NRAS -CAAX modification through geranylgeranyltransferases (GGTs), leading to continued membrane localization following treatment with FTIs [69]. While the combination of GGT inhibitors and FTIs has demonstrated efficacy in mouse models, toxicity concerns for combination therapy have limited their movement to human patients [70]. Similar off target effects have also hindered the study of inhibitors targeting other steps in RAS membrane trafficking including targeting RCE1, ICMT, PDE6δ, and DHHC9-GCP16 [21].

Other indirect methods of targeting RAS have met similar disappointing fates. Many of the downstream effector pathways of RAS, such as RAF-ERK or PI3K-AKT, have direct inhibitors developed to target their aberrant signaling; however, their use in RAS mutant cancers has been limited by increased signaling through other downstream pathways. While combinations of inhibition of different downstream pathways have shown efficacy *in vitro*, high levels of patient toxicity has prevented successful clinical treatment [21]. In recent years, KRAS protein degraders, anti-sense oligonucleotides (ASOs) targeting KRAS mRNA expression, targeting RAS driven metabolic pathways, and immunotherapy have shown some efficacy in pre-clinical studies suggesting that they may be future options for clinical targeting of RAS [70].

Despite years of setbacks targeting mutant RAS proteins in cancer, recent developments directly targeting $KRAS^{G12C}$ have shown renewed promise in developing novel therapies for cancers driven by these mutations. Utilizing the unique structural biology of the G12C mutant *KRAS*, multiple inhibitors (including ARS-1620) have been developed to irreversibly bind a unique pocket in the switch II domain (S-IIP) locking KRAS in an inactive, GDP-bound state [66, 67].

These drugs have shown promising preclinical ability to specifically inhibit $KRAS^{G12C}$ downstream signaling and decrease tumor size in xenograft studies, and Phase I clinical studies have shown promising results with low toxicity and promising rates of partial response and stable disease [71]. These advancements suggest that direct clinical targeting of *RAS* mutations in human cancer may be possible in the future.

Modeling PDAC Tumors in Genetically Engineered Mouse Models

Since over 90% of pancreatic ductal adenocarcinoma (PDAC) is driven by oncogenic mutations in *KRAS* [72], it is an attractive disease model to elucidate the genetic, biochemical, metabolic, and immunology associated with these mutations. Furthermore, as pancreatic cancer is one of the most common causes of cancer mortality globally and within the USA [73], there is a great need to advance both our molecular and clinical knowledge of *KRAS* driven PDAC.

The natural, histological progression of pancreatic ductal adenocarcinoma is well described and characterized. Pancreatic intraepithelial neoplasia (PanIN) lesions are accepted as the most common originator for formation of PDAC tumors in humans [63]. PanIN lesions are generally thought to arise from regions of acinar ductal metaplasia (ADM) where acinar cells of the pancreas acquire features of ductal cells via transdifferentiation [74]. Additionally, mouse models of PDAC have also indicated pancreatic ductal cells may be the cell of origin, indicating that either cell lineage could give rise to PDAC in human patients [75, 76]. Mutations in KRAS are generally thought to be an initiating event in the development of early, low-grade PanIN-1 lesions [64]. With increasing levels of dysplasia, PanIN lesions progress into intermediate and late precursor lesions, accumulating mutation events. PanIN-2 or intermediate lesions are most commonly associated with inactivating mutations of the tumor suppressor *p16* (*CDKN2A*). PanIN-3 lesions are

associated with mutations in *TP53* and *SMAD4,* both tumor suppressors [63, 77, 78]. While these mutational events are generally thought to drive development of pancreatic cancer, the progression from early lesion to PDAC is marked by the accumulation of many other mutations [72, 79].

Genetically engineered mouse models (GEMMs) provide an important system by which to model the initiation and progression of many different cancer types. While *in vitro* human cell lines and *in vivo* patient derived xenograft (PDX) models are commonly used to study PDAC and other cancers, they fail to fully recapitulate human disease for study as they lack a fully intact immune system and PDX tumors are often implanted outside the pancreas itself limiting the effect of the pancreatic microenvironment [80]. One of the most accurate GEMMs to model the development of human PDAC was generated using a conditional activation of mutant $KRAS^{LSL\text{-}G12D/+}$ driven by the expression of Cre recombinase under the control of a pancreas specific promoter such as *Ptf1a* (*Ptf1a-Cre*). These mice progress from developing PanIN lesions to metastatic PDAC with approximately 20-33% penetrance at 1 year following early embryonic activation of Cre [81, 82]. Since the development of this GEMM, additional mutations or knockout of tumor suppressors such as *p16* or *p53* have been shown to greatly accelerate the development of PDAC in these models and faithfully recapitulate human disease [82, 83]. These models are explored further in **Chapter 2** investigating the role of AGO2 in the development of mutant *KRAS* driven pancreatic adenocarcinoma.

RNA Interference and Argonaute 2

Overview

Gene expression is regulated through a plethora of different cellular mechanisms, ranging from transcription factor activation, epigenetic modifications, and chromatin assembly changes [84, 85].

While much control of gene expression occurs at the level of transcription, cells contain additional levels of control post-transcriptionally, including RNA interference (RNAi). Originally discovered in the 1990s, RNAi is the process by which double-stranded RNA (dsRNA) was found to induce the breakdown of complementary mRNA sequences [86, 87]. Additional characterization of non-coding small RNA transcripts, or MicroRNAS (miRNAs), generated an entirely new field of post-translational gene regulation that has enhanced our understanding of the cellular mechanisms of tight control of genetic expression both in normal cellular and cancer biology.

MicroRNAs and the RNA Induced Silencing Complex

In parallel to the description of RNAi in mRNA transcript control, a new class of small, non-coding RNA transcripts was characterized. These miRNA transcripts are approximately 22 nucleotides in length, that after a series of processing steps negatively regulate the expression of target, complementary mRNA transcripts [88]. The first miRNA, *lin-4*, was described in C. elegans where it was demonstrated to play an important role in the developmental process by negatively regulating the protein expression level of *lin-14*. While *lin-4* did not code for any protein, its sequence was complementary to the 3'-UTR of *lin-14* mRNA transcripts [89]. Since this initial characterization, much research has described the complex biology and role of miRNAs within the cell.

MicroRNAs undergo a complex set of processing steps before their eventual targeting to complementary mRNA transcripts for regulation (**Figure 1.6**). After transcription from their genetic precursors by RNA polymerase II, the primary miRNA (pri-miRNA) transcripts form a hairpin stem-loop structure where complementary sequences of the single-stranded pri-miRNA form a region of dsRNA [90]. While still in the nucleus, a complex of DROSHA and DGCR8

proteins recognize the RNA stem-loop and cleave it from the single-stranded RNA, generating a precursor-miRNA (pre-miRNA) transcript [91, 92]. The pre-miRNA is then transported to the cytoplasm through the nuclear transporter exportin-5 [93].

Once in the cytoplasm, pre-miRNAs are further processed from a dsRNA stem-loop into a single-stranded miRNA. Central to these processing stems is the RNA Induced Silencing Complex (RISC), which is comprised of a number of proteins including DICER, Argonautes 1-4, and TRBP [94]. DICER is an RNAse III enzyme which recognizes the pre-miRNA transcript and cleaves both ends of the dsRNA, leaving behind the core 20-22 nucleotide miRNA duplex [95]. The 5' end of the duplex with less stability is then incorporated into the RISC, and the miRNA duplex is loaded into one of 4 Argonaute (AGO) endonuclease proteins [96, 97]. Argonaute 2 (AGO2) is the most studied member of the argonaute protein family members, and following the loading of the miRNA duplex, AGO2 unwinds the duplex, leading to cleavage of the passenger strand [98]. The fully formed RISC is then complexed with the complementary mRNA transcript to the guide miRNA. The fully formed RISC ultimately results in decreasing target mRNA protein translation. This is accomplished through either 1) cleavage and degradation of mRNA or 2) repression of mRNA translation to protein [99, 100]. Importantly, cleavage of target mRNAs requires both "slicer" activity (unique to AGO2) and perfect alignment between miRNA and target mRNA [101]. Most RISC gene silencing is through translational repression rather than mRNA cleavage [100]. Together, RNAi is an important method of cellular post-transcriptional regulation of gene expression that relies on members of the RNA Induced Silencing Complex including AGO2.

AGO2 Structure and Function

The Argonaute family of proteins is highly evolutionarily conserved with four different isoforms in humans: AGO1, AGO2, AGO3, and AGO4. Of these isoforms, AGO2 has received the most extensive study to date following its identification as the only isoform with "slicer" activity or the ability to cleave mRNA transcripts [101].

Structurally, AGO2 contains multiple domains including four main functional domains (N-terminal, PAZ, MID, and PIWI). The N-terminal domain has been shown to play a key role in the unwinding of miRNA duplex following the formation of RISC [102]. Interestingly, both DICER and AGO2 share the conserved, functional PAZ domain which is critical in binding the 3' end of miRNA transcripts [103]. The other 5' end of miRNA binds within the MID domain of AGO2 along with the 5', 7-methylguanylate cap of target mRNA transcripts [104, 105]. The final functional group of AGO2 is the PIWI domain which contains the main catalytic residues. The PIWI domain is structurally similar to RNAse H family domain. Importantly, this domain relies upon Mg^{2+} and a catalytic triad of D597, D669, and H807 for RNA cleavage [101, 106, 107].

Functionally, AGO2 is the central component of RNAi and RISC activity within the cell as described above. In mammals, most miRNAs imperfectly bind to the 3' UTR of mRNA target transcripts [99]. This leads primarily to translational repression or deadenylation of the mRNA. RISC has been demonstrated to prevent ribosomal binding at the 5'-RNA cap (through binding at the MID domain of AGO2), thus preventing initiation of mRNA translation [108, 109]. The 3' UTR of mRNA transcripts is ended with a 3' polyadenylated (polyA) tail that plays a number of roles in RNA biology including export from the nucleus, mRNA translation, and stability. In fact, as the polyA tail is shorted or removed, mRNA transcripts are subject to degradation [110]. RISC

proteins like TRNC6 (GW182) bring deadenylation complexes, including CCR4-NOT1 and PAN2-PAN3, to the polyA tail of target mRNA ultimately leading to its degradation.

AGO2 Localization and Phase Separation

RNA binding proteins have long been known to localize in granular particles with RNA transcripts in the both the nucleus and cytoplasm of cells. While these foci lack a membrane found in most cellular organelles, they form functional units within the cell that are areas of higher order [111]. In recent years, they have been shown to display liquid properties, condensing as RNA-protein concentration increases, in a process called phase transition or separation [112, 113].

AGO2 and RISC components readily form phase separated particles within the cytoplasm called Processing Bodies or P Bodies [114-116]. These aggregates were first reported with the exonuclease XRN1 which was found to form in the cytoplasm of mouse cells [117]. Further exploration revealed that these structures also contained decapping proteins like DCP2 allowing XRN1 to degrade mRNA transcripts in a 5' to 3' manner [118]. Additionally, RISC proteins such as TNRC6 and deadenylases like CCR4-NOT1 have been shown to localize to P bodies with AGO2, helping to promote mRNA decay [116, 119]. Notably, P body complexes containing AGO2, miRNA, and target mRNA transcripts have been associated with repression of those target mRNAs [120].

Recent work has further expanded the role for precise AGO2 localization and phase transition in RISC formation in accelerating the RNAi and repression of mRNA transcripts. TNRC6 is a large "scaffold" protein that contains many disordered domains which assist in the binding of AGO2 to deadenylase proteins/complexes [121]. The interaction between AGO2 and TRNC6 proteins forms phase separated droplets *in vitro* and *in vivo*. This phase separation

significantly accelerated the rate of mRNA deadenylation, suggesting that these aggregates play a role in the dynamic control of translational repression and degradation of mRNAs [122]. These foci are necessary for some RNAi activity within the cell as their disruption has been demonstrated to lower siRNA mediated repression [123]. AGO2 localization within cells is typically widespread and diffuse within the cytoplasm, and RNAi activity can occur in the absence of visible P body structures [124].

AGO2 Phosphorylation and Post-Translational Modifications

RNA interference plays an important role in cellular, post-transcriptional regulation of gene expression, and as a result, AGO2 is regulated through multiple post-translational modifications (PTMs) that alter its activity, localization, and miRNA binding/processing. The MID domain of AGO2 is critical for binding of the 5' end of miRNA transcripts, and previous work has demonstrated that Y529 is critical for this binding. Phosphorylation of Y529 disrupts this miRNA binding, leading to inhibition of AGO2 RNAi function [125]. This modification has been linked to multiple processes including p38α MAPK signaling leading to the inhibition of miRNA binding in activated macrophages [126] and neuronal differentiation [127]. While phosphorylation at Y529 is considered repressive, other phosphorylation sites have been demonstrated to modulate AGO2 activity through different mechanisms. The S387 residue of AGO2 is phosphorylated downstream of multiple cellular signaling pathways, including MEK-ERK, p38α MAPK, and AKT [128-130]. This event plays a key role in localizing AGO2 to P bodies within cells [129], shifting RNAi from cleavage to translational repression of target mRNAs [130]. Phosphorylation of S387 has also been linked to inhibition of AGO2-miRNA secretion through cellular exosomes in mutant *KRAS* cancer. Finally, Y393 phosphorylation is a major site of AGO2 modification downstream from EGFR

signaling. Interaction between EGFR and AGO2 was found to be enhanced under hypoxic conditions leading to increased phosphorylation at Y393. This modification resulted in decreased interaction of AGO2 with RISC members such as DICER, impeding AGO2 loading and unwinding of long-loop miRNA duplexes [131]. Furthermore, increased phosphorylation of Y393-AGO2 was associated with poor survival in breast cancer patients, suggesting that hypoxia in these may promote aggressive growth and migration in part by altering AGO2 RNAi activity. While other potential phosphorylation sites have been identified on AGO2, such as S253, T303, T307, and S798, modification of these residues has yet to be fully elucidated [132, 133].

While phosphorylation of AGO2 is the most studied group of PTMs, other modifications have also been functionally characterized. Prolyl 4-hydroxylation of the P700 residue on AGO2 leads to increased stability of AGO2 proteins and P body localization through type I collagen prolyl-4-hydoxylase [134]. Conversely, K402 sumoylation has been shown to destabilize AGO2 and increase turnover of the protein in cells [135]. PARylation of AGO2 by PARP decreases RNAi downstream of cellular stressors (such as oxidative stress) [136]. These examples illustrate the myriad of ways AGO2 is post-transcriptionally regulated in a variety of cell conditions to alter its RNAi activity and respond to specific stimuli.

miRNAs in Human Development, Disease, and Cancer

RNA interference and miRNAs play an important role both in the tight regulation of gene expression in normal mammalian development and in aberrant gene dysregulation in human diseases like cancer. Of the four Argonaute protein isoforms, only AGO2 is necessary for normal embryonic development of mice with AGO2 null suffering from multiple defects including incomplete neural tube closure and cardiac failure [101]. Since this initial characterization, specific

miRNAs have been linked to the development of multiple organs, often through cell cycle control. MiRNAs regulate the formation of bone, all types of muscle (cardiac, smooth, and skeletal), vasculature, differentiation of neurons, and hematopoietic cells among others [137]. The requirement of AGO2 for normal embryonic development illustrates the importance of miRNA genetic control in normal cellular development. Not only do miRNAs regulate the development of mammalian organisms, but they also play a role in many diverse cellular processes. Metabolic systems and processes are in part controlled by miRNA production, such as insulin production, cholesterol, and adipose tissue regulation [138]. Similarly, the cardiovascular system, in particular myocardial infarction and heart arrhythmias, have been associated with changes in miRNA expression following cellular stress [139].

While miRNAs play a key role in normal post-transcriptional regulation of genes, they have been shown to be dysregulated in many cancers. Specific miRNAs have also been associated with tumor suppressor and oncogenic functions. As miRNAs serve ultimately to repress the translation of their target mRNA transcripts, many tumor suppressor-linked miRNAs are downregulated in cancer, leading to the upregulation of their target oncogene mRNA. For example, subsets of chronic lymphocytic leukemia (CLL) have been linked to the deletion of chromosome 13q13.4. This event often causes a decrease in the expression of *miR15a* and *miR-16-1*, both of which are known to target BCL2 expression, ultimately promoting survival and inhibiting apoptosis [140]. Another key miRNA tumor suppressor is the *let-7* family of miRNAs. One of the first miRNAs discovered [141], *let-7* plays a wide variety of roles in normal biology including development; however, *let-7* members are also downregulated in many types of cancer such as pancreatic, lung, ovarian, prostate, melanoma, and many others [142]. *RAS* mRNA is one of the primary targets of *let-7* family members in humans, leading to decreased expression of RAS

proteins [143]. Additionally, *let-7* expression has been correlated to increased expression of *KRAS* in non-small cell lung cancer, with low *let-7* expression correlating with lower survival in patients [144]. *Let-7* miRNAs have also been associated with downregulation of cyclin dependent kinases and the oncogene MYC, suggesting that they play a large role in regulating cellular proliferation and survival [145]. While most miRNAs are thought of as tumor suppressors, many have been linked to upregulation and oncogenic properties in cancer. One prime example is the miRNA-17-92 cluster containing multiple family members which are upregulated downstream of MYC activation. These miRNAs inhibit the production of the E2F1 transcription factor [146], and while E2F1 is also upregulated by MYC, miR-17-92 may act to keep E2F1 in balance and prevent induction of apoptosis, promoting survival [147]. Furthermore, this miRNA family has been linked to negatively regulating multiple other tumor suppressors including PTEN, RB, and p21 [148].

A Direct Interaction Between KRAS and AGO2

Overview

While much recent progress has been made in targeting $KRAS^{G12C}$ mutations clinically, there are still relatively few options available for patients with mutant *RAS* driven tumors. As described above, the clinical targeting of RAS effectors and downstream signaling partners has yielded mixed results thus far. In recent years, the Chinnaiyan Lab set out to uncover novel protein interactions with KRAS with the hopes of better understanding RAS GTPase biology and identifying potential future therapeutic targets.

A Novel Interaction between KRAS and AGO2

In *Shankar et al*, the Chinnaiyan Lab utilized a RAS co-immunoprecipitation with tandem mass spectrometry (Co-IP MS) using a pan-RAS antibody targeted towards the Switch I domain of RAS [149]. Surprisingly, AGO2 was found to interact with KRAS across a panel of lung adenocarcinoma, pancreatic adenocarcinoma, and mouse fibroblast cell lines, and the interaction between AGO2 and KRAS was observed regardless of the wild-type (WT) or mutant status of *KRAS* [150].

Further proteomic and biochemical work demonstrated that AGO2's N-terminus was the binding site of KRAS with the K112 and E114 residues as essential for the interaction. As described earlier, the N-terminal domain of AGO2 is primarily responsible for the unwinding of miRNA duplexes following RISC formation [102]. As the RAS10 antibody utilized in the coIP-MS binds at the Switch I domain of RAS [149], AGO2 was found to interact within the Switch II domain of KRAS at the Y64 residue (**Figure 1.1**). Interestingly, AGO2 binding to KRAS occurred regardless of nucleotide loading status, suggesting that the interaction occurs in both KRAS-GTP and KRAS-GDP states.

Following the *in vitro* characterization of AGO2-KRAS binding, *in vivo* cellular studies investigated a functional role for this interaction in cancer biology. AGO2 and RAS were found to co-localize within the membrane of the endoplasmic reticulum. Considering the ubiquitous nature of the AGO2-KRAS interaction in both normal and cancer cell lines, *Shankar et al* next investigated its role in a set of *KRAS* mutant dependent cell lines. Knockdown of AGO2 drastically reduced cell proliferation in H358 (lung adenocarcinoma) and MIA PaCa-2 (pancreatic adenocarcinoma), while FLAG-AGO2 transient overexpression enhanced cell growth. The loss of AGO2 also led to changes in downstream RAS signaling, mainly a decrease in AKT-mTOR

signaling. While both WT and mutant KRAS were found to bind to AGO2, only mutant KRAS expressing cells demonstrated an inhibition of AGO2's ability to unwind *Let-7a* miRNA, a known negative regulator of RAS protein expression as described above [143]. Furthermore, an AGO2 null NIH3T3 demonstrated reduced transformation and colony formation with overexpression of $KRAS^{G12V}$ that was rescued upon overexpression of WT AGO2 but not the KRAS binding deficient $AGO2^{K112A}$ mutant. Finally, NIH3T3 $AGO2^{-/-}$ cells overexpressing $KRAS^{G12V}$ displayed reduced tumor growth in an *in vivo* mouse transplant model. Interestingly, *KRAS* independent cell lines were unperturbed following AGO2 knockdown, suggesting that the requirement for AGO2 is unique to mutant *KRAS* driven oncogenic growth and transformation. *Shankar et al* demonstrated a key role for the interaction between AGO2 and KRAS in promoting mutant *KRAS* driven cancer proliferation and transformation [150].

Exploring AGO2-RAS Interaction in Animal Models of Human Cancer

While the initial characterization of the novel AGO2-KRAS interaction presented an intriguing aspect of mutant *KRAS* biology, the role of this interaction in the initiation and progression of *KRAS* driven cancers remained unclear. Genetically engineered mouse models (GEMMs) of cancer have long been used to study many human cancers from basic cancer biology to translational therapeutic applications [151]. Many *RAS* driven cancers have been extensively studied in GEMMs including pancreatic ductal adenocarcinoma [81, 82], non-small cell lung adenocarcinoma [152], melanoma [153], leukemia [154], and colorectal cancer [155].

Following the identification of AGO2-KRAS interaction in *Shankar et al*, an inducible Cre-recombinase [156] driven mouse model with activation of $Kras^{LSL\text{-}G12D}$ and knockout of $p53^{fl/fl}$ was found to accelerate the development of aggressive diffuse large B-cell lymphoma with

overexpression of Ago2. The overexpression of Ago2 not only led to an increase in aggressive growth, but it also enhanced Kras mediated signaling including Erk and Akt pathways. Notably, this aggressive phenotype was reliant on Ago2-Kras interaction as binding deficient K112A and E114A mutants were unable to enhance proliferation and survival, suggesting that Ago2 was necessary for Kras driven growth in this model [157].

As mutations in *KRAS* driven over 90% of pancreatic ductal adenocarcinoma (PDAC), we employed a series of pancreatic GEMM with activation of $Kras^{LSL\text{-}G12D}$ and knockout of $Ago2^{fl/fl}$ to characterize the role of Ago2-Kras interaction in the oncogenic development, signaling, and tumor survival in PDAC (**CHAPTER 2**).

A Role for AGO2 and the Other RAS Isoforms

While the interaction between AGO2 and KRAS is in the nascent stages of critical study, there is evidence of a role for AGO2 in the development of cancer. As *KRAS* is the most commonly mutated isoform of *RAS* in human cancer, the majority of our scientific inquiry has focused on AGO2-KRAS. However, given the 100% sequence similarity between the three RAS isoforms at their Switch II domains, we asked if AGO2 played a role in mutant *HRAS* and *NRAS* driven cancers, finding a role for AGO2 to prevent oncogene-induced senescence in these cancers (**CHAPTER 3**).

As discussed above, miRNAs have long been connected with the development of cancer, both with tumor suppressive and oncogenic roles. Additionally, *Shankar et al* described an important role for mutant *KRAS* in the inhibition of AGO2 miRNA duplex unwinding, suggesting an important role for this interaction in altering AGO2 RNAi function and contributing to an oncogenic phenotype. In order to better study the biochemical properties of the AGO2-KRAS

interaction, we have developed a single-molecule TIRF microscopy based *in vitro* system to study both AGO2 miRNA activity and the co-localization of AGO2 and KRAS (**CHAPTER 4**).

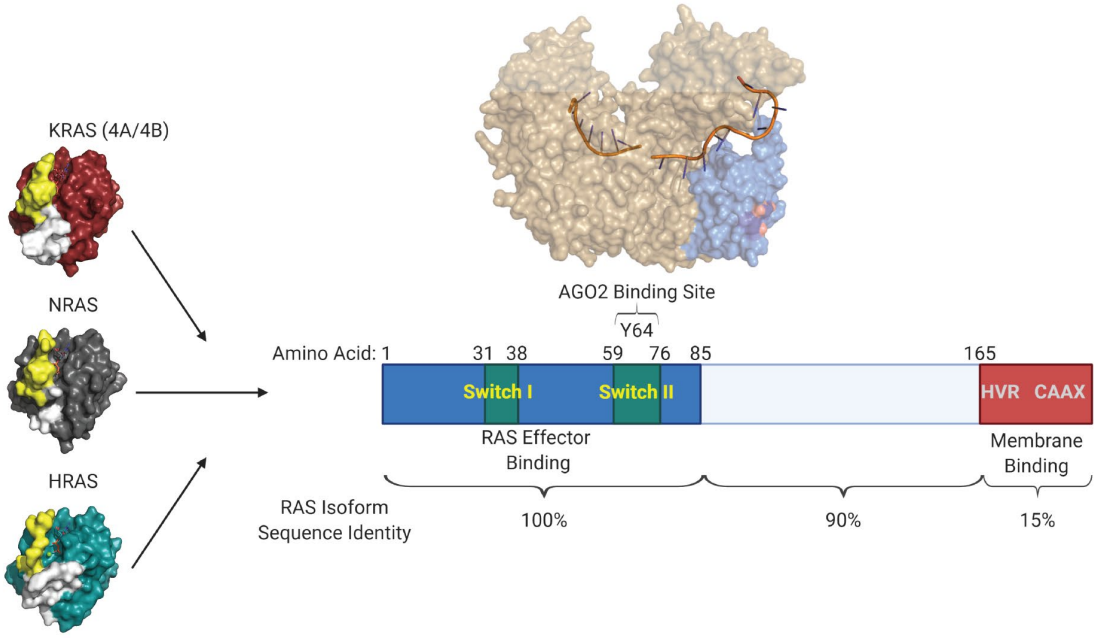

Figure 1.1: RAS Isoform Homology
The three RAS isoforms share nearly 100% sequence identity in the N-Terminal domain which contains the AGO2 binding site at Y64.

This figure was generated via BioRender

Protein Crystal Structures from Jessica Waninger

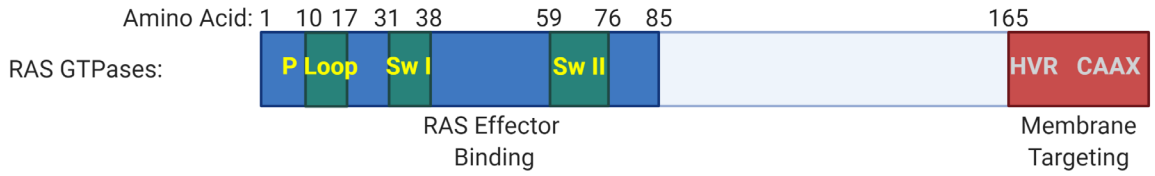

Figure 1.2: RAS Protein Functional Domains

The three RAS isoforms are all comprised of the same main functional domains. The N-terminal G-domain is shaded in blue and runs from amino acid (aa) 1-85. This region is primarily responsible for RAS GTPase activity and effector binding. The P-loop (phosphate binding loop; aa 10-17) is essential for nucleotide loading. The Switch I domain (aa 31-38) and Switch II domain (aa 59-76) are the main site of effector protein binding. The allosteric lobe (labeled in light blue; aa 85-165) plays some role in interaction between RAS proteins and the cell membrane. Finally, the C-terminal domain (shaded red above; starting at aa 165) of the RAS isoforms is the region of most sequence divergence. The hypervariable region (HVR) serves to anchor RAS to the inner plasma membrane following modifications (**Figure 1.5**).

This figure was generated via BioRender

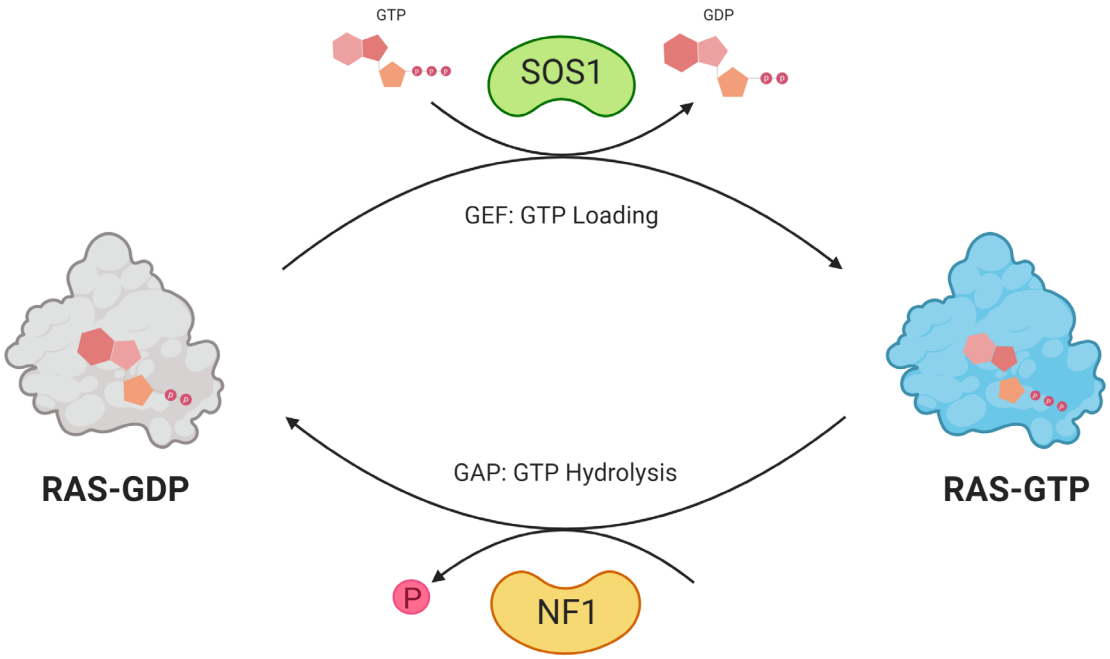

Figure 1.3: RAS GTPase Cycle
Thus RAS GTP/GDP cycling is primarily regulated by guanine nucleotide exchange factors (GEFs) and GTPase-activating proteins (GAPs). GEF proteins, such as SOS1, activate RAS by increasing the dissociation rate of GDP, leading to loading of GTP from the cell cytoplasm. In order to inactivate RAS-GTP signaling, GAP proteins, such as NF1, are required to promote GTP hydrolysis.

This figure was generated via BioRender

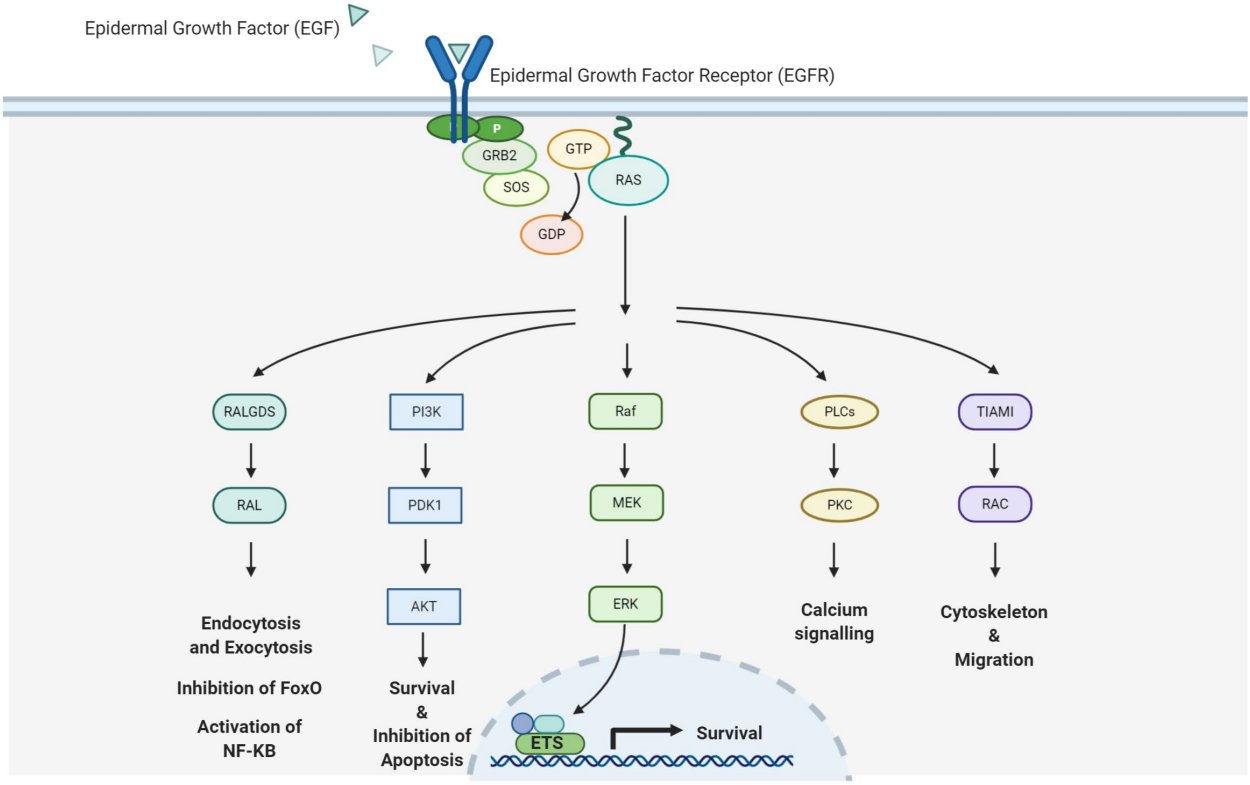

Figure 1.4: RAS Mediated Signaling Pathways

Upon RAS-GTP loading at the plasma membrane by SOS1, the switch I and switch II domains of RAS proteins undergo a conformational change allowing for interactions with their downstream effector partners. The figure above outlines some of the main signaling pathways downstream of RAS activation in human cells.

This figure was generated via BioRender

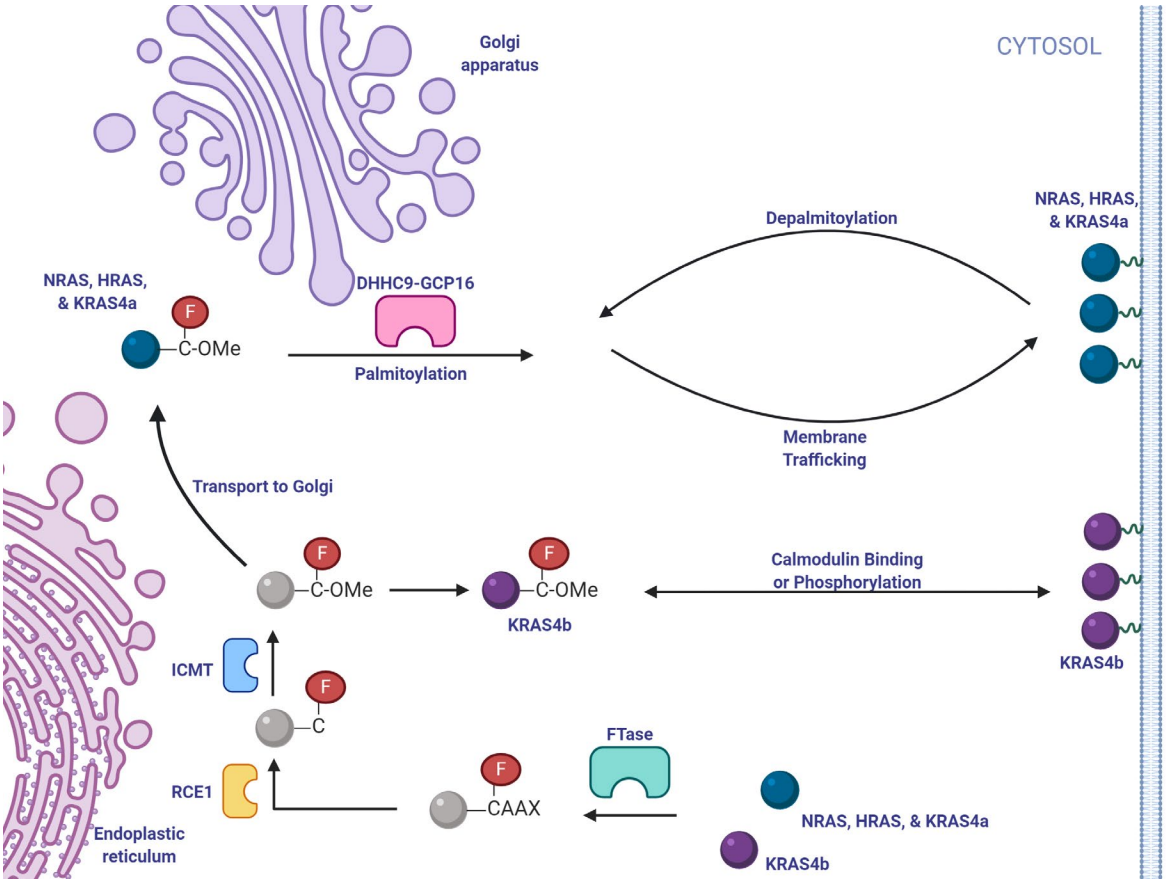

Figure 1.5: RAS Membrane Trafficking

Sequential modification of RAS C-terminal domain allows for trafficking to the plasma membrane. Following modification of the CAAX motif with Farneylstransferase (FTase), all RAS isoforms are transported to the Endoplasmic Reticulum where RCE1 and ICMT further modify the C-terminus. HRAS, NRAS, and KRAS4a are then transported to the Golgi Apparatus for palmitoylation by DHHC9-GCP16, allowing trafficking to the membrane. KRAS4b is transported directly to the plasma membrane via calmodulin binding or phosphorylation.

This figure was generated via BioRender

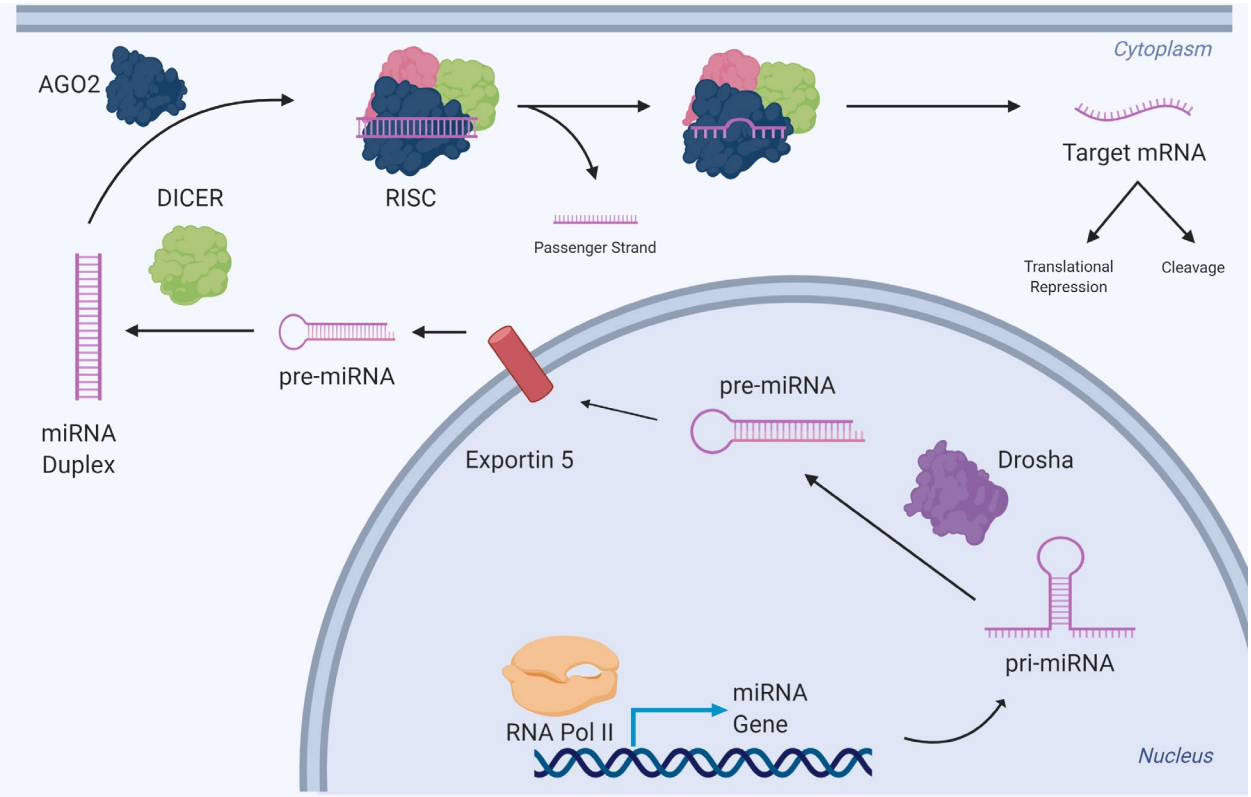

Figure 1.6: miRNA Biogenesis Pathway

MicroRNA genes are transcribed by RNA Pol II in the nucleus where transcripts form a hairpin stem-loop structure (pri-miRNA). The pri-miRNA is then processed by DROSHA and DGCR8 into a pre-miRNA which is then expored to the cytoplasm by Exportin 5. The pre-miRNA is then incorporated into RISC by DICER which cleaves both ends of the pre-miRNA, leaving a 20-22 nucleotide miRNA duplex. AGO2 then unwinds the duplex, ejecting the passenger strand. The RISC complex is then targeted by the miRNA guide strand to its target mRNA transcript where AGO2 mediates translational repression or cleavage.

This figure was generated via BioRender

References

1. Malumbres, M. and M. Barbacid, *RAS oncogenes: the first 30 years.* Nat Rev Cancer, 2003. **3**(6): p. 459-65.
2. Colicelli, J., *Human RAS superfamily proteins and related GTPases.* Sci STKE, 2004. **2004**(250): p. RE13.
3. Tsai, F.D., et al., *K-Ras4A splice variant is widely expressed in cancer and uses a hybrid membrane-targeting motif.* Proc Natl Acad Sci U S A, 2015. **112**(3): p. 779-84.
4. Hobbs, G.A., C.J. Der, and K.L. Rossman, *RAS isoforms and mutations in cancer at a glance.* J Cell Sci, 2016. **129**(7): p. 1287-92.
5. Pai, E.F., et al., *Structure of the guanine-nucleotide-binding domain of the Ha-ras oncogene product p21 in the triphosphate conformation.* Nature, 1989. **341**(6239): p. 209-14.
6. Harrison, R.A., et al., *Structural Dynamics in Ras and Related Proteins upon Nucleotide Switching.* J Mol Biol, 2016. **428**(23): p. 4723-4735.
7. Castellano, E. and E. Santos, *Functional specificity of ras isoforms: so similar but so different.* Genes Cancer, 2011. **2**(3): p. 216-31.
8. Parker, J.A. and C. Mattos, *The Ras-Membrane Interface: Isoform-specific Differences in The Catalytic Domain.* Mol Cancer Res, 2015. **13**(4): p. 595-603.
9. Abankwa, D., A.A. Gorfe, and J.F. Hancock, *Mechanisms of Ras membrane organization and signalling: Ras on a rocker.* Cell Cycle, 2008. **7**(17): p. 2667-73.
10. Clarke, S., *Protein isoprenylation and methylation at carboxyl-terminal cysteine residues.* Annu Rev Biochem, 1992. **61**: p. 355-86.
11. Kamata, T. and J.R. Feramisco, *Epidermal growth factor stimulates guanine nucleotide binding activity and phosphorylation of ras oncogene proteins.* Nature, 1984. **310**(5973): p. 147-50.
12. Satoh, T., et al., *Platelet-derived growth factor receptor mediates activation of ras through different signaling pathways in different cell types.* Mol Cell Biol, 1993. **13**(6): p. 3706-13.
13. Wennerberg, K., K.L. Rossman, and C.J. Der, *The Ras superfamily at a glance.* J Cell Sci, 2005. **118**(Pt 5): p. 843-6.
14. Bos, J.L., H. Rehmann, and A. Wittinghofer, *GEFs and GAPs: critical elements in the control of small G proteins.* Cell, 2007. **129**(5): p. 865-77.
15. Vetter, I.R. and A. Wittinghofer, *The guanine nucleotide-binding switch in three dimensions.* Science, 2001. **294**(5545): p. 1299-304.
16. Traut, T.W., *Physiological concentrations of purines and pyrimidines.* Mol Cell Biochem, 1994. **140**(1): p. 1-22.
17. Scheffzek, K., et al., *The Ras-RasGAP complex: structural basis for GTPase activation and its loss in oncogenic Ras mutants.* Science, 1997. **277**(5324): p. 333-8.
18. Oda, K., et al., *A comprehensive pathway map of epidermal growth factor receptor signaling.* Mol Syst Biol, 2005. **1**: p. 2005 0010.
19. Gale, N.W., et al., *Grb2 mediates the EGF-dependent activation of guanine nucleotide exchange on Ras.* Nature, 1993. **363**(6424): p. 88-92.
20. Fernandez-Medarde, A. and E. Santos, *Ras in cancer and developmental diseases.* Genes Cancer, 2011. **2**(3): p. 344-58.

21. Cox, A.D., et al., *Drugging the undruggable RAS: Mission possible?* Nat Rev Drug Discov, 2014. **13**(11): p. 828-51.
22. Prior, I.A., P.D. Lewis, and C. Mattos, *A comprehensive survey of Ras mutations in cancer.* Cancer Res, 2012. **72**(10): p. 2457-67.
23. Khan, A.Q., et al., *RAS-mediated oncogenic signaling pathways in human malignancies.* Semin Cancer Biol, 2019. **54**: p. 1-13.
24. Munoz-Maldonado, C., Y. Zimmer, and M. Medova, *A Comparative Analysis of Individual RAS Mutations in Cancer Biology.* Front Oncol, 2019. **9**: p. 1088.
25. Haigis, K.M., *KRAS Alleles: The Devil Is in the Detail.* Trends Cancer, 2017. **3**(10): p. 686-697.
26. Vojtek, A.B., S.M. Hollenberg, and J.A. Cooper, *Mammalian Ras interacts directly with the serine/threonine kinase Raf.* Cell, 1993. **74**(1): p. 205-14.
27. McCormick, F. and A. Wittinghofer, *Interactions between Ras proteins and their effectors.* Curr Opin Biotechnol, 1996. **7**(4): p. 449-56.
28. Leevers, S.J., H.F. Paterson, and C.J. Marshall, *Requirement for Ras in Raf activation is overcome by targeting Raf to the plasma membrane.* Nature, 1994. **369**(6479): p. 411-4.
29. Fey, D., et al., *The complexities and versatility of the RAS-to-ERK signalling system in normal and cancer cells.* Semin Cell Dev Biol, 2016. **58**: p. 96-107.
30. Pruitt, K. and C.J. Der, *Ras and Rho regulation of the cell cycle and oncogenesis.* Cancer Lett, 2001. **171**(1): p. 1-10.
31. Gupta, S., et al., *Binding of ras to phosphoinositide 3-kinase p110alpha is required for ras-driven tumorigenesis in mice.* Cell, 2007. **129**(5): p. 957-68.
32. Vanhaesebroeck, B., et al., *The emerging mechanisms of isoform-specific PI3K signalling.* Nat Rev Mol Cell Biol, 2010. **11**(5): p. 329-41.
33. Park, W.S., et al., *Comprehensive identification of PIP3-regulated PH domains from C. elegans to H. sapiens by model prediction and live imaging.* Mol Cell, 2008. **30**(3): p. 381-92.
34. Castellano, E. and J. Downward, *RAS Interaction with PI3K: More Than Just Another Effector Pathway.* Genes Cancer, 2011. **2**(3): p. 261-74.
35. Sheridan, C. and J. Downward, *Inhibiting the RAS-PI3K pathway in cancer therapy.* Enzymes, 2013. **34 Pt. B**: p. 107-36.
36. Downward, J., *Targeting RAS signalling pathways in cancer therapy.* Nat Rev Cancer, 2003. **3**(1): p. 11-22.
37. Hofer, F., et al., *Activated Ras interacts with the Ral guanine nucleotide dissociation stimulator.* Proc Natl Acad Sci U S A, 1994. **91**(23): p. 11089-93.
38. De Ruiter, N.D., B.M. Burgering, and J.L. Bos, *Regulation of the Forkhead transcription factor AFX by Ral-dependent phosphorylation of threonines 447 and 451.* Mol Cell Biol, 2001. **21**(23): p. 8225-35.
39. Bodemann, B.O. and M.A. White, *Ral GTPases and cancer: linchpin support of the tumorigenic platform.* Nat Rev Cancer, 2008. **8**(2): p. 133-40.
40. Henry, D.O., et al., *Ral GTPases contribute to regulation of cyclin D1 through activation of NF-kappaB.* Mol Cell Biol, 2000. **20**(21): p. 8084-92.
41. Lambert, J.M., et al., *Tiam1 mediates Ras activation of Rac by a PI(3)K-independent mechanism.* Nat Cell Biol, 2002. **4**(8): p. 621-5.
42. Harden, T.K., S.N. Hicks, and J. Sondek, *Phospholipase C isozymes as effectors of Ras superfamily GTPases.* J Lipid Res, 2009. **50 Suppl**: p. S243-8.

43. Furfine, E.S., et al., *Protein farnesyltransferase: kinetics of farnesyl pyrophosphate binding and product release.* Biochemistry, 1995. **34**(20): p. 6857-62.
44. Lane, K.T. and L.S. Beese, *Thematic review series: lipid posttranslational modifications. Structural biology of protein farnesyltransferase and geranylgeranyltransferase type I.* J Lipid Res, 2006. **47**(4): p. 681-99.
45. Boyartchuk, V.L., M.N. Ashby, and J. Rine, *Modulation of Ras and a-factor function by carboxyl-terminal proteolysis.* Science, 1997. **275**(5307): p. 1796-800.
46. Schlitzer, M., A. Winter-Vann, and P.J. Casey, *Non-peptidic, non-prenylic inhibitors of the prenyl protein-specific protease Rce1.* Bioorg Med Chem Lett, 2001. **11**(3): p. 425-7.
47. Swarthout, J.T., et al., *DHHC9 and GCP16 constitute a human protein fatty acyltransferase with specificity for H- and N-Ras.* J Biol Chem, 2005. **280**(35): p. 31141-8.
48. Shahinian, S. and J.R. Silvius, *Doubly-lipid-modified protein sequence motifs exhibit long-lived anchorage to lipid bilayer membranes.* Biochemistry, 1995. **34**(11): p. 3813-22.
49. Goodwin, J.S., et al., *Depalmitoylated Ras traffics to and from the Golgi complex via a nonvesicular pathway.* J Cell Biol, 2005. **170**(2): p. 261-72.
50. Hancock, J.F., H. Paterson, and C.J. Marshall, *A polybasic domain or palmitoylation is required in addition to the CAAX motif to localize p21ras to the plasma membrane.* Cell, 1990. **63**(1): p. 133-9.
51. Ahearn, I.M., et al., *Regulating the regulator: post-translational modification of RAS.* Nat Rev Mol Cell Biol, 2011. **13**(1): p. 39-51.
52. Land, H., L.F. Parada, and R.A. Weinberg, *Tumorigenic conversion of primary embryo fibroblasts requires at least two cooperating oncogenes.* Nature, 1983. **304**(5927): p. 596-602.
53. Newbold, R.F. and R.W. Overell, *Fibroblast immortality is a prerequisite for transformation by EJ c-Ha-ras oncogene.* Nature, 1983. **304**(5927): p. 648-51.
54. Balmain, A. and I.B. Pragnell, *Mouse skin carcinomas induced in vivo by chemical carcinogens have a transforming Harvey-ras oncogene.* Nature, 1983. **303**(5912): p. 72-4.
55. el-Deiry, W.S., et al., *WAF1, a potential mediator of p53 tumor suppression.* Cell, 1993. **75**(4): p. 817-25.
56. Trimarchi, J.M. and J.A. Lees, *Sibling rivalry in the E2F family.* Nat Rev Mol Cell Biol, 2002. **3**(1): p. 11-20.
57. Lin, A.W., et al., *Premature senescence involving p53 and p16 is activated in response to constitutive MEK/MAPK mitogenic signaling.* Genes Dev, 1998. **12**(19): p. 3008-19.
58. Hahn, W.C., et al., *Creation of human tumour cells with defined genetic elements.* Nature, 1999. **400**(6743): p. 464-8.
59. Irani, K., et al., *Mitogenic signaling mediated by oxidants in Ras-transformed fibroblasts.* Science, 1997. **275**(5306): p. 1649-52.
60. Woo, R.A. and R.Y. Poon, *Activated oncogenes promote and cooperate with chromosomal instability for neoplastic transformation.* Genes Dev, 2004. **18**(11): p. 1317-30.
61. Voncken, J.W., et al., *MAPKAP kinase 3pK phosphorylates and regulates chromatin association of the polycomb group protein Bmi1.* J Biol Chem, 2005. **280**(7): p. 5178-87.

62. Dolado, I., et al., *p38alpha MAP kinase as a sensor of reactive oxygen species in tumorigenesis.* Cancer Cell, 2007. **11**(2): p. 191-205.
63. Hruban, R.H., et al., *Progression model for pancreatic cancer.* Clin Cancer Res, 2000. **6**(8): p. 2969-72.
64. Kanda, M., et al., *Presence of somatic mutations in most early-stage pancreatic intraepithelial neoplasia.* Gastroenterology, 2012. **142**(4): p. 730-733 e9.
65. Fearon, E.R. and B. Vogelstein, *A genetic model for colorectal tumorigenesis.* Cell, 1990. **61**(5): p. 759-67.
66. Ostrem, J.M., et al., *K-Ras(G12C) inhibitors allosterically control GTP affinity and effector interactions.* Nature, 2013. **503**(7477): p. 548-51.
67. Janes, M.R., et al., *Targeting KRAS Mutant Cancers with a Covalent G12C-Specific Inhibitor.* Cell, 2018. **172**(3): p. 578-589 e17.
68. Reiss, Y., et al., *Inhibition of purified p21ras farnesyl:protein transferase by Cys-AAX tetrapeptides.* Cell, 1990. **62**(1): p. 81-8.
69. Whyte, D.B., et al., *K- and N-Ras are geranylgeranylated in cells treated with farnesyl protein transferase inhibitors.* J Biol Chem, 1997. **272**(22): p. 14459-64.
70. Liu, P., Y. Wang, and X. Li, *Targeting the untargetable KRAS in cancer therapy.* Acta Pharm Sin B, 2019. **9**(5): p. 871-879.
71. Fakih, M., et al., *Phase 1 study evaluating the safety, tolerability, pharmacokinetics (PK), and efficacy of AMG 510, a novel small molecule KRASG12C inhibitor, in advanced solid tumors.* Journal of Clinical Oncology, 2019. **37**(15_suppl): p. 3003-3003.
72. Biankin, A.V., et al., *Pancreatic cancer genomes reveal aberrations in axon guidance pathway genes.* Nature, 2012. **491**(7424): p. 399-405.
73. Rawla, P., T. Sunkara, and V. Gaduputi, *Epidemiology of Pancreatic Cancer: Global Trends, Etiology and Risk Factors.* World J Oncol, 2019. **10**(1): p. 10-27.
74. Guerra, C. and M. Barbacid, *Genetically engineered mouse models of pancreatic adenocarcinoma.* Mol Oncol, 2013. **7**(2): p. 232-47.
75. Bailey, J.M., et al., *p53 mutations cooperate with oncogenic Kras to promote adenocarcinoma from pancreatic ductal cells.* Oncogene, 2016. **35**(32): p. 4282-8.
76. von Figura, G., et al., *The chromatin regulator Brg1 suppresses formation of intraductal papillary mucinous neoplasm and pancreatic ductal adenocarcinoma.* Nat Cell Biol, 2014. **16**(3): p. 255-67.
77. Bryant, K.L., et al., *KRAS: feeding pancreatic cancer proliferation.* Trends Biochem Sci, 2014. **39**(2): p. 91-100.
78. Yachida, S. and C.A. Iacobuzio-Donahue, *Evolution and dynamics of pancreatic cancer progression.* Oncogene, 2013. **32**(45): p. 5253-60.
79. Jones, S., et al., *Core signaling pathways in human pancreatic cancers revealed by global genomic analyses.* Science, 2008. **321**(5897): p. 1801-6.
80. Mazur, P.K., et al., *Current methods in mouse models of pancreatic cancer.* Methods Mol Biol, 2015. **1267**: p. 185-215.
81. Hingorani, S.R., et al., *Preinvasive and invasive ductal pancreatic cancer and its early detection in the mouse.* Cancer Cell, 2003. **4**(6): p. 437-50.
82. Aguirre, A.J., et al., *Activated Kras and Ink4a/Arf deficiency cooperate to produce metastatic pancreatic ductal adenocarcinoma.* Genes Dev, 2003. **17**(24): p. 3112-26.

83. Hingorani, S.R., et al., *Trp53R172H and KrasG12D cooperate to promote chromosomal instability and widely metastatic pancreatic ductal adenocarcinoma in mice.* Cancer Cell, 2005. **7**(5): p. 469-83.
84. Lee, T.I. and R.A. Young, *Transcriptional regulation and its misregulation in disease.* Cell, 2013. **152**(6): p. 1237-51.
85. Klemm, S.L., Z. Shipony, and W.J. Greenleaf, *Chromatin accessibility and the regulatory epigenome.* Nat Rev Genet, 2019. **20**(4): p. 207-220.
86. Fire, A., et al., *Production of antisense RNA leads to effective and specific inhibition of gene expression in C. elegans muscle.* Development, 1991. **113**(2): p. 503-14.
87. Fire, A., et al., *Potent and specific genetic interference by double-stranded RNA in Caenorhabditis elegans.* Nature, 1998. **391**(6669): p. 806-11.
88. Bartel, D.P., *MicroRNAs: genomics, biogenesis, mechanism, and function.* Cell, 2004. **116**(2): p. 281-97.
89. Lee, R.C., R.L. Feinbaum, and V. Ambros, *The C. elegans heterochronic gene lin-4 encodes small RNAs with antisense complementarity to lin-14.* Cell, 1993. **75**(5): p. 843-54.
90. Lee, Y., et al., *MicroRNA genes are transcribed by RNA polymerase II.* EMBO J, 2004. **23**(20): p. 4051-60.
91. Zeng, Y., R. Yi, and B.R. Cullen, *Recognition and cleavage of primary microRNA precursors by the nuclear processing enzyme Drosha.* EMBO J, 2005. **24**(1): p. 138-48.
92. Han, J., et al., *Molecular basis for the recognition of primary microRNAs by the Drosha-DGCR8 complex.* Cell, 2006. **125**(5): p. 887-901.
93. Bohnsack, M.T., K. Czaplinski, and D. Gorlich, *Exportin 5 is a RanGTP-dependent dsRNA-binding protein that mediates nuclear export of pre-miRNAs.* RNA, 2004. **10**(2): p. 185-91.
94. Macfarlane, L.A. and P.R. Murphy, *MicroRNA: Biogenesis, Function and Role in Cancer.* Curr Genomics, 2010. **11**(7): p. 537-61.
95. Zhang, H., et al., *Human Dicer preferentially cleaves dsRNAs at their termini without a requirement for ATP.* EMBO J, 2002. **21**(21): p. 5875-85.
96. Schwarz, D.S., et al., *Asymmetry in the assembly of the RNAi enzyme complex.* Cell, 2003. **115**(2): p. 199-208.
97. Hutvagner, G. and M.J. Simard, *Argonaute proteins: key players in RNA silencing.* Nat Rev Mol Cell Biol, 2008. **9**(1): p. 22-32.
98. Matranga, C., et al., *Passenger-strand cleavage facilitates assembly of siRNA into Ago2-containing RNAi enzyme complexes.* Cell, 2005. **123**(4): p. 607-20.
99. Hock, J. and G. Meister, *The Argonaute protein family.* Genome Biol, 2008. **9**(2): p. 210.
100. Pratt, A.J. and I.J. MacRae, *The RNA-induced silencing complex: a versatile gene-silencing machine.* J Biol Chem, 2009. **284**(27): p. 17897-901.
101. Liu, J., et al., *Argonaute2 is the catalytic engine of mammalian RNAi.* Science, 2004. **305**(5689): p. 1437-41.
102. Kwak, P.B. and Y. Tomari, *The N domain of Argonaute drives duplex unwinding during RISC assembly.* Nat Struct Mol Biol, 2012. **19**(2): p. 145-51.
103. Yan, K.S., et al., *Structure and conserved RNA binding of the PAZ domain.* Nature, 2003. **426**(6965): p. 468-74.
104. Ma, J.B., et al., *Structural basis for 5'-end-specific recognition of guide RNA by the A. fulgidus Piwi protein.* Nature, 2005. **434**(7033): p. 666-70.

105. Kiriakidou, M., et al., *An mRNA m7G cap binding-like motif within human Ago2 represses translation.* Cell, 2007. **129**(6): p. 1141-51.
106. Song, J.J., et al., *Crystal structure of Argonaute and its implications for RISC slicer activity.* Science, 2004. **305**(5689): p. 1434-7.
107. Elkayam, E., et al., *The structure of human argonaute-2 in complex with miR-20a.* Cell, 2012. **150**(1): p. 100-10.
108. Humphreys, D.T., et al., *MicroRNAs control translation initiation by inhibiting eukaryotic initiation factor 4E/cap and poly(A) tail function.* Proc Natl Acad Sci U S A, 2005. **102**(47): p. 16961-6.
109. Thermann, R. and M.W. Hentze, *Drosophila miR2 induces pseudo-polysomes and inhibits translation initiation.* Nature, 2007. **447**(7146): p. 875-8.
110. Guhaniyogi, J. and G. Brewer, *Regulation of mRNA stability in mammalian cells.* Gene, 2001. **265**(1-2): p. 11-23.
111. Boeynaems, S., et al., *Protein Phase Separation: A New Phase in Cell Biology.* Trends Cell Biol, 2018. **28**(6): p. 420-435.
112. Brangwynne, C.P., et al., *Germline P granules are liquid droplets that localize by controlled dissolution/condensation.* Science, 2009. **324**(5935): p. 1729-32.
113. Molliex, A., et al., *Phase separation by low complexity domains promotes stress granule assembly and drives pathological fibrillization.* Cell, 2015. **163**(1): p. 123-33.
114. Eulalio, A., et al., *P-body formation is a consequence, not the cause, of RNA-mediated gene silencing.* Mol Cell Biol, 2007. **27**(11): p. 3970-81.
115. Detzer, A., et al., *Cell stress is related to re-localization of Argonaute 2 and to decreased RNA interference in human cells.* Nucleic Acids Res, 2011. **39**(7): p. 2727-41.
116. Liu, J., et al., *MicroRNA-dependent localization of targeted mRNAs to mammalian P-bodies.* Nat Cell Biol, 2005. **7**(7): p. 719-23.
117. Bashkirov, V.I., et al., *A mouse cytoplasmic exoribonuclease (mXRN1p) with preference for G4 tetraplex substrates.* J Cell Biol, 1997. **136**(4): p. 761-73.
118. Ingelfinger, D., et al., *The human LSm1-7 proteins colocalize with the mRNA-degrading enzymes Dcp1/2 and Xrnl in distinct cytoplasmic foci.* RNA, 2002. **8**(12): p. 1489-501.
119. Behm-Ansmant, I., et al., *mRNA degradation by miRNAs and GW182 requires both CCR4:NOT deadenylase and DCP1:DCP2 decapping complexes.* Genes Dev, 2006. **20**(14): p. 1885-98.
120. Pillai, R.S., et al., *Inhibition of translational initiation by Let-7 MicroRNA in human cells.* Science, 2005. **309**(5740): p. 1573-6.
121. Chen, C.Y., et al., *Ago-TNRC6 triggers microRNA-mediated decay by promoting two deadenylation steps.* Nat Struct Mol Biol, 2009. **16**(11): p. 1160-6.
122. Sheu-Gruttadauria, J. and I.J. MacRae, *Phase Transitions in the Assembly and Function of Human miRISC.* Cell, 2018. **173**(4): p. 946-957 e16.
123. Jakymiw, A., et al., *Disruption of GW bodies impairs mammalian RNA interference.* Nat Cell Biol, 2005. **7**(12): p. 1267-74.
124. Leung, A.K., J.M. Calabrese, and P.A. Sharp, *Quantitative analysis of Argonaute protein reveals microRNA-dependent localization to stress granules.* Proc Natl Acad Sci U S A, 2006. **103**(48): p. 18125-30.
125. Rudel, S., et al., *Phosphorylation of human Argonaute proteins affects small RNA binding.* Nucleic Acids Res, 2011. **39**(6): p. 2330-43.

126. Mazumder, A., et al., *A transient reversal of miRNA-mediated repression controls macrophage activation.* EMBO Rep, 2013. **14**(11): p. 1008-16.
127. Patranabis, S. and S.N. Bhattacharyya, *Phosphorylation of Ago2 and Subsequent Inactivation of let-7a RNP-Specific MicroRNAs Control Differentiation of Mammalian Sympathetic Neurons.* Mol Cell Biol, 2016. **36**(8): p. 1260-71.
128. McKenzie, A.J., et al., *KRAS-MEK Signaling Controls Ago2 Sorting into Exosomes.* Cell Rep, 2016. **15**(5): p. 978-987.
129. Zeng, Y., et al., *Phosphorylation of Argonaute 2 at serine-387 facilitates its localization to processing bodies.* Biochem J, 2008. **413**(3): p. 429-36.
130. Horman, S.R., et al., *Akt-mediated phosphorylation of argonaute 2 downregulates cleavage and upregulates translational repression of MicroRNA targets.* Mol Cell, 2013. **50**(3): p. 356-67.
131. Shen, J., et al., *EGFR modulates microRNA maturation in response to hypoxia through phosphorylation of AGO2.* Nature, 2013. **497**(7449): p. 383-7.
132. Gebert, L.F.R. and I.J. MacRae, *Regulation of microRNA function in animals.* Nat Rev Mol Cell Biol, 2019. **20**(1): p. 21-37.
133. Jee, D. and E.C. Lai, *Alteration of miRNA activity via context-specific modifications of Argonaute proteins.* Trends Cell Biol, 2014. **24**(9): p. 546-53.
134. Qi, H.H., et al., *Prolyl 4-hydroxylation regulates Argonaute 2 stability.* Nature, 2008. **455**(7211): p. 421-4.
135. Sahin, U., et al., *Sumoylation of human argonaute 2 at lysine-402 regulates its stability.* PLoS One, 2014. **9**(7): p. e102957.
136. Leung, A.K., et al., *Poly(ADP-ribose) regulates stress responses and microRNA activity in the cytoplasm.* Mol Cell, 2011. **42**(4): p. 489-99.
137. Ivey, K.N. and D. Srivastava, *microRNAs as Developmental Regulators.* Cold Spring Harb Perspect Biol, 2015. **7**(7): p. a008144.
138. Vienberg, S., et al., *MicroRNAs in metabolism.* Acta Physiol (Oxf), 2017. **219**(2): p. 346-361.
139. Colpaert, R.M.W. and M. Calore, *MicroRNAs in Cardiac Diseases.* Cells, 2019. **8**(7).
140. Cimmino, A., et al., *miR-15 and miR-16 induce apoptosis by targeting BCL2.* Proc Natl Acad Sci U S A, 2005. **102**(39): p. 13944-9.
141. Reinhart, B.J., et al., *The 21-nucleotide let-7 RNA regulates developmental timing in Caenorhabditis elegans.* Nature, 2000. **403**(6772): p. 901-6.
142. Boyerinas, B., et al., *The role of let-7 in cell differentiation and cancer.* Endocr Relat Cancer, 2010. **17**(1): p. F19-36.
143. Johnson, S.M., et al., *RAS is regulated by the let-7 microRNA family.* Cell, 2005. **120**(5): p. 635-47.
144. Xia, X.M., et al., *Clinical significance and the correlation of expression between Let-7 and K-ras in non-small cell lung cancer.* Oncol Lett, 2010. **1**(6): p. 1045-1047.
145. Lee, H., et al., *Biogenesis and regulation of the let-7 miRNAs and their functional implications.* Protein Cell, 2016. **7**(2): p. 100-13.
146. O'Donnell, K.A., et al., *c-Myc-regulated microRNAs modulate E2F1 expression.* Nature, 2005. **435**(7043): p. 839-43.
147. Sylvestre, Y., et al., *An E2F/miR-20a autoregulatory feedback loop.* J Biol Chem, 2007. **282**(4): p. 2135-43.

148. Osada, H. and T. Takahashi, *let-7 and miR-17-92: small-sized major players in lung cancer development.* Cancer Sci, 2011. **102**(1): p. 9-17.
149. Hamer, P.J., et al., *Production and characterization of anti-RAS p21 monoclonal antibodies.* Hybridoma, 1990. **9**(6): p. 573-87.
150. Shankar, S., et al., *KRAS Engages AGO2 to Enhance Cellular Transformation.* Cell Rep, 2016. **14**(6): p. 1448-1461.
151. Kersten, K., et al., *Genetically engineered mouse models in oncology research and cancer medicine.* EMBO Mol Med, 2017. **9**(2): p. 137-153.
152. Jackson, E.L., et al., *The differential effects of mutant p53 alleles on advanced murine lung cancer.* Cancer Res, 2005. **65**(22): p. 10280-8.
153. Powell, M.B., et al., *Hyperpigmentation and melanocytic hyperplasia in transgenic mice expressing the human T24 Ha-ras gene regulated by a mouse tyrosinase promoter.* Mol Carcinog, 1995. **12**(2): p. 82-90.
154. Chan, I.T. and D.G. Gilliland, *Oncogenic K-ras in mouse models of myeloproliferative disease and acute myeloid leukemia.* Cell Cycle, 2004. **3**(5): p. 536-7.
155. Karim, B.O. and D.L. Huso, *Mouse models for colorectal cancer.* Am J Cancer Res, 2013. **3**(3): p. 240-50.
156. Albanese, C., et al., *Recent advances in inducible expression in transgenic mice.* Semin Cell Dev Biol, 2002. **13**(2): p. 129-41.
157. Thai, K., et al., *KRAS AND AGO2 INTERACTION PROMOTE INITIATION OF PLASMABLASTIC LYMPHOMA USING AN IN VIVO MOUSE TRANSPLANT MODEL.* Hematological Oncology, 2017. **35**(S2): p. 155-155.

Chapter 2

An Essential Role for *Argonaute 2* in EGFR-KRAS Signaling in Pancreatic Cancer Development[1]

Abstract

Both KRAS and EGFR are essential mediators of pancreatic cancer development and interact with Argonaute 2 (AGO2) to perturb its function. Here, in a mouse model of mutant KRAS-driven pancreatic cancer, loss of *AGO2* allows precursor lesion (PanIN) formation yet prevents progression to pancreatic ductal adenocarcinoma (PDAC). Precursor lesions with *AGO2* ablation undergo oncogene-induced senescence with altered microRNA expression and EGFR/RAS signaling, bypassed by loss of *p53*. In mouse and human pancreatic tissues, PDAC progression is associated with increased plasma membrane localization of RAS/AGO2. Furthermore, phosphorylation of $AGO2^{Y393}$ disrupts both the wild-type and oncogenic KRAS-AGO2 interaction, albeit under different conditions. ARS-1620 (G12C-specific inhibitor) disrupts the $KRAS^{G12C}$-AGO2 interaction, suggesting that interaction can be pharmacologically targeted. Altogether, our study supports a biphasic model of pancreatic cancer development: an *AGO2*-independent early phase of PanIN formation reliant on EGFR-RAS signaling, and an *AGO2*-dependent phase wherein the mutant KRAS-AGO2 interaction is critical for PDAC progression.

[1] This chapter was previously accepted for publication as part of the following manuscript: Shankar S.*, Tien J.C.*, Siebenaler R.F.*, Chugh S.*, et al., An Essential Role for *Argonaute 2* in EGFR-KRAS Signaling in Pancreatic Cancer Development. *Nat Comm*, 2020. *These authors contributed equally

Introduction

KRAS mutations drive over 90% of pancreatic cancer, a disease with a dismal overall 5-year survival rate of only 9% [1]. Like all RAS GTPases, KRAS is a molecular switch that transduces extracellular mitogenic signals by cycling between an active GTP-bound and an inactive GDP-bound state. Proteins that regulate the nucleotide loading of RAS, like GTPase activating proteins (GAPs) or guanine exchange factors (GEFs), recruit RAS to the plasma membrane in response to activated growth factor receptors, such as EGFR [2, 3]. Recurrent oncogenic driver mutations in *RAS* result in the accumulation of its active GTP-bound form at the plasma membrane, leading to aberrant signaling [2, 3].

Genetically engineered mouse models (GEMMs) of pancreatic cancer were developed by expression of a single oncogenic $KRAS^{G12D}$ allele in the mouse exocrine pancreas. In this model, pre-invasive pancreatic intraepithelial (PanINs) lesions progress to pancreatic adenocarcinoma (PDAC) reflective of the human disease [4]. Use of such GEMMs has been instrumental in defining the key events that characterize PanIN development and PDAC progression [5, 6]. Of particular relevance is the observation that EGFR is essential for $KRAS^{G12D}$-driven PanIN development [7, 8]. However, the requirement for EGFR at the early stage of PanIN development has not translated to successful treatment [9], while directly targeting KRAS also remains a challenge [10].

Earlier, we identified a direct interaction between KRAS and Argonaute 2 (AGO2), independent of *KRAS* mutation status [11], which was required for oncogenic *KRAS*-driven cellular transformation. Interestingly, Shen et al. had previously shown that EGFR phosphorylates AGO2 at tyrosine 393 under hypoxic stress [12]. Here, we employed established mouse models of pancreatic cancer to determine the *in vivo* requirement of *AGO2* in pancreatic cancer development.

Our data show that oncogenic *KRAS*-initiated PanIN formation is reliant on EGFR and wild-type RAS signaling, independent of *AGO2*. Strikingly, however, we identify a critical dependence on *AGO2* for PanIN progression to PDAC, bypassed by loss of *p53*. While defining an essential role for *AGO2* in PDAC progression, we also further our understanding of how the KRAS-AGO2 interaction is regulated through EGFR activation. Disruption of the oncogenic KRAS-AGO2 association may, therefore, represent a point of therapeutic intervention to prevent pancreatic cancer progression.

Materials and Methods

Mouse strains

LSL-$KRAS^{G12D}$ [4] (Kras $^{LSL\text{-}G12D}$) and *p48Cre mice* [13] were obtained from Marina Pasca di Magliano, University of Michigan. Conditionally floxed *AGO2* [14] ($AGO2^{fl/fl}$) mice and $p53^{fl/+}$ mice were purchased from Jackson labs (Bar Harbor, Maine). PCR genotyping for $KRAS^{G12D}$*;p48Cre,* $p53^{fl/+}$, and *AGO2* alleles, from DNA isolated from mouse tails, was performed using standard methodology. To generate experimental and control mice, $AGO2^{fl/fl}$ *p48Cre*, and $KRAS^{G12D}$ lines were intercrossed to generate $AGO2^{fl/+}$*;p48Cre* and $KRAS^{G12D}$*;p48Cre* mice. These two lines were then intercrossed to generate the $AGO2^{fl/fl}$;$KRAS^{G12D}$*;p48Cre* experimental mice. Given that mice were maintained on a mixed background, littermate controls were systematically used in all experiments (sex ratio per cohort was balanced). All animals were housed in a pathogen-free environment, and all procedures were performed in accordance with requirements of the University of Michigan IACUC. Cre activation in acinar cells of pancreata of mice with mutant *KRAS* alleles was validated by genotyping using the $KRAS^{G12D}$ conditional PCR detailed in **Supplementary Table 2.3**.

Histology, immunohistochemistry, and immunofluorescence

Paraffin-embedded tissues from mice were processed using standard methodology. Details of the primary antibodies used for IHC are provided in **Supplementary Table 2.1**. Immunohistochemistry and immunofluorescence staining were performed using standard techniques. For immunofluorescence, slides were viewed using a Nikon 1A-B confocal microscope. To estimate co-localization of proteins, the Coloc2 program (ImageJ) was used to determine Pearson's coefficient. Cells within the PanIN/PDAC or metastatic regions (from mouse and human tissues), excluding the stromal compartment, were used to determine the extent of overlap. In panels with normal tissue shown in **Figure 2.5**, acinar cells were used for co-localization analyses. Average values over three different areas are shown.

Proximity Ligation Assay (PLA)

Cell lines were cultured in 8-well chamber slides. After the indicated treatment/stimulation, cells were fixed with 4% paraformaldehyde and then permeabilized using 0.1% Tween. Subsequent PLA staining was performed as per the protocol provided by the manufacturer (DUOlink kit, Millipore/Sigma). Mouse RAS10 and rabbit AGO2 antibodies, validated in this study, were used at 1:250 dilution to detect signals either alone or in combination. Negative controls were performed using either single antibody (**Supplementary Figure 2.16a**), Rasless MEFs (**Supplementary Figure 2.8d**), or tissue lacking AGO2 (**Figure 2.5d**). Images were obtained using the Nikon A1B inverted confocal microscope. For mouse tissue PLA, the paraffin-embedded sections were processed as for IF analysis. PLA was then performed using RAS10 or AGO2 antibodies, either alone or in combination, and imaged using the Nikon A1B confocal microscope.

Human TMA analysis

Pancreatic TMAs and frozen human tissue repositories were established by a pathologist (J.S.) and developed at the Tissue and Molecular Pathology Core in the Department of Pathology, University of Michigan, after IRB approval as described [15]. The Institutional Review Board at the University of Michigan approved the study (protocol number: HUM00098128). Patients with pancreas resections for pancreatitis, cystic neoplasms, or PDA from 2002 to 2015 at the University of Michigan Health System were included in the study. The electronic medical record was examined for clinical and demographic patient information. Date of surgery and date of last patient contact were recorded from the electronic medical record. Deaths were confirmed from the Social Security Death Index. Clinical staging was analyzed using the American Joint Committee on Cancer 8th edition staging system. For patients who received neoadjuvant treatment, clinical stage was analyzed based on pre-treatment tumor size, while pathological parameters of tumor size, grade, lymph node status, and peripancreatic, duodenal, and common bile duct extension were analyzed based on the post-treatment surgical specimen. All hematoxylin and eosin (H&E) slides were reviewed and diagnoses confirmed by a gastrointestinal pathologist (J.S.), and corresponding areas were carefully selected and marked. Duplicated 1 mm diameter adjacent tissue cores from the same lesion in a total of 311 patient tissue samples were selectively punched/extracted and transferred to recipient tissue array blocks. Five tissue microarrays (TMAs) were set up according to a standard protocol. H&E staining was performed on each TMA block using standard protocol, and unstained slides were prepared for immunohistochemical (IHC) staining and IHC scoring was performed by a pathologist (J.S.).

RNA in situ Hybridization (RNA-ISH)

RNA-ISH was performed to detect *Kras* mRNA on formalin-fixed paraffin-embedded (FFPE) tissue sections using the RNAscope 2.5 HD Brown kit (Advanced Cell Diagnostics, Newark, CA) and target probes against mouse *Kras* (412491). *Mm-Ubc* (mouse ubiquitin C) and *DapB* (Bacillus bacterial dihydrodipicolinate reductase) were used as positive and negative controls, respectively. FFPE tissue sections were baked for 1 hour at 60°C, deparaffinized in xylene twice for 5 minutes each, and dehydrated in 100% ethanol twice for 1 minute each, followed by air drying for 5 minutes. After hydrogen peroxide pre-treatment and target retrieval, tissue samples were permeabilized using Protease Plus and hybridized with the target probe in the HybEZ oven for 2 hours at 40°C. After two washes, the samples were processed for a series of signal amplification steps. Chromogenic detection was performed using DAB, counterstained with 50% Gill's Hematoxylin I (Fisher Scientific, Rochester, NY).

Quantitative RT-PCR

Pancreatic total RNA was isolated using the AllPrep DNA/RNA/miRNA Universal Kit (Qiagen). For quantitation of mRNA transcripts, RNA was extracted from the indicated samples, and cDNA was synthesized using the SuperScript III System according to the manufacturer's instructions (Invitrogen). Quantitative RT-PCR was conducted using primers detailed in **Supplementary Table 2.3** with SYBR Green Master Mix (Applied Biosystems) on the StepOne Real-Time PCR System (Applied Biosystems). Relative mRNA levels of the transcripts were normalized to the expression of the housekeeping gene *GAPDH*.

MiRNA expression profiles using qPCR of mouse miRnome panels

Pancreatic total RNA was isolated using AllPrep DNA/RNA/miRNA Universal Kit (Qiagen). 5 ng of total RNA from each sample was converted into cDNA using miRCURY™ LNA™ Universal RT microRNA PCR Universal cDNA Synthesis Kit II. Quantitative micro RT-PCR was performed using exiLENT SYBR Green master mix with microRNA ready to use PCR mix, Mouse&Rat panel I, V4.M (Exiqon, Cat # 203713) on ABI 7900HT Fast Real time PCR system (Applied Biosystems). Data were analyzed using GenEX ver 6 software.

Transcriptome analysis

mRNA was quantitated on the Illumina platform using the Riboerase library preparation protocol. Transcriptome data processing and quality control were performed using RSeQC package. Sequencing alignment was performed using splice aware aligner STAR with two pass alignment option using mm10 reference build. featureCounts from Rsubread package was used to get the count matrix for expression quantification. R-package edgeR DGEList object was used to import, organize, filter, and normalize the data by the method of trimmed mean of M-values (TMM) [16] using the calcNormFactors. This was followed by limma [17] and voom [18] analyses where default settings for the “voom” , ”lmFit”, “eBayes”, and “topTable” functions were used to assess differential gene expression. Finally, the fgsea package was used to perform gene set enrichment analysis. Software version details are: edgeR_3.28.0, limma_3.42.0, Rsubread_2.0.0 (featureCounts), RSeQC-2.6.4, STAR-2.7.3a.

Pancreatic tissue lysates and immunoblot analysis

Pancreata obtained from mice were homogenized in Mg^{2+}-containing lysis buffer. Clear lysates were separated using SDS-PAGE and processed for immunoblot analysis using standard methods. Primary antibodies used in the study are indicated in **Supplementary Table 2.1**. Particularly, Ras antibodies validated in a recent study [19] are also indicated. IMAGEJ (ImageJ-win64) was downloaded from https://imagej.net/Fiji/Downloads.

Isolation of pancreatic ductal organoids

Pancreatic ducts were isolated from the pancreas of 12-week old *KRAS^{G12D};p48Cre* and *AGO2$^{fl/fl}$;KRAS^{G12D};p48Cre* mice[39] by enzymatic digestion with 0.012% (w/v) collagenase XI (Sigma) and 0.012% (w/v) dispase (GIBCO) in DMEM media containing 1% FBS (GIBCO). Organoids were seeded in growth factor-reduced (GFR) Matrigel (BD). Organoid culture medium consisted of Advanced DMEM/F12 (Invitrogen), B27 (Invitrogen), 1.25 mM N-Acetylcysteine (Sigma), 10 nM gastrin (Sigma) and the following growth factors: 50 ng/ml EGF (Peprotech), 10% RSPO1-conditioned media (prepared in-house), 10% Noggin-conditioned media (prepared in-house [20]), 100 ng/ml FGF10 (Peprotech), and 10 mM nicotinamide (Sigma). For experiments, organoids were released from the Matrigel, mechanically disrupted into small fragments, and plated in fresh Matrigel. To enrich pancreatic ducts from tissues expressing oncogenic KRAS, no EGF was added to the base medium. Organoids were passaged at a 1:4–1:6 split ratio once per week for at least nine weeks to enrich $KRAS^{G12D}$ expressing organoids.

To carry out erlotinib treatment, organoid cultures were dissociated and split into equal parts and cultured in Matrigel for the indicated times. To collect untreated and treated samples,

organoids in Matrigel were enzymatically dissociated, collected, and washed prior to protein isolation.

RAS-GTP analysis

300-500 micrograms of indicated protein lysates were prepared from pancreatic ductal organoids or cell lines using Mg^{2+}-containing lysis buffer. RAF1-RBD agarose beads (Millipore) were used to pull down activated RAS-GTP[11]. The beads were washed and separated using SDS-PAGE and immunoblotted for the indicated proteins.

Plasmids

Full-length FH-*AGO2* constructs were obtained from Addgene (pIRESneo-FLAG/HA-AGO2 10822, PI:Thomas Tuschl). $AGO2^{Y393F}$ mutant construct was generated using the QuikChange II XL Site-Directed Mutagenesis Kit (Agilent) from the FH-*AGO2* plasmid described above using the primers detailed in **Supplementary Table 2.3**. DNA sequences were confirmed using Sanger sequencing at the University of Michigan Sequencing Core.

In vitro assay to measure KRAS-GTP levels

Purified catalytic domains of SOS1 (Cytoskeleton) and NF1 (Creative Biomart) were used to carry out nucleotide exchange and GTPase activity. Full-length KRAS and $KRAS^{G12V}$ were purified using bacterial expression at the University of Michigan Proteomic Core. AGO2 was purchased from Sino Biologicals. Halo tag protein was obtained from Promega. Purified components were added as indicated, and KRAS-GTP levels were estimated using the GTPase-GLO assay from Promega, following the manufacturer's instructions.

Cell culture, transfection, and EGF stimulation

All cell lines (detailed in **Supplementary Table 2.4**) were obtained from the American Type Culture Collection (ATCC) or as indicated. Cells were cultured following ATCC culture methods in media supplemented with the corresponding serum and antibiotics. Additionally, cells were routinely genotyped and tested bi-weekly for mycoplasma contamination. Only cells with the correct genotype and that were mycoplasma free were used for the experiments. For EGF stimulation, cells were grown to approximately 80% confluence and washed with PBS three times. Cells were incubated overnight (16 hr) in serum free media. EGF stimulation was performed for 5 minutes with 100 ng/µl of EGF (Gibco) at 37°C. After stimulation, cells were washed and protein lysates were prepared in K Buffer lysis buffer. For tyrosine kinase inhibition, cells were pre-treated with 15 µM of erlotinib for 1 hour prior to EGF stimulation, as described above.

HEK293 or MIA PaCa-2 cells were transfected with different *AGO2* constructs using Fugene HD (Promega) or Lipofectamine 3000 (Invitrogen) according to the manufacturer's protocols. For EGFR stimulation with transient *AGO2* construct overexpression, cells were transfected approximately 16 hours prior to overnight serum starvation and EGF stimulation.

RASless MEFs were a kind gift from the RAS Initiative. Details of how these cells were developed and their growth characteristics can be found at https://www.cancer.gov/research/key-initiatives/ras/ras-central/blog/2017/rasless-mefs-drug-screens.

Immunoprecipitation (IP) Analysis

For immunoprecipitation analysis, protein lysates were prepared in K Buffer (20 mM Tris pH 7.0, 5 mM EDTA, 150 mM NaCl, 1% Triton X100, 1 mM DTT, phosphatase inhibitors, and protease inhibitors). Typically,150-200 µg of protein lysates (RAS10 IP: 150 µg; AGO2 IP: 200 µg; KRAS

IP: 150 µg) were pre-cleared with 10 µl of Protein A/G agarose beads (Santa Cruz) for 1 hour. Pre-cleared lysates were incubated with 5-10 µg of the indicated primary antibodies targeting the protein of interest or with corresponding isotype controls overnight at 4°C. 30 µl of Protein A/G beads were then added to immune complexes and incubated for 1-3 hours at 4°C, spun, and washed in 150-300 mM NaCl containing K-buffer prior to separation of immunoprecipitates by SDS-PAGE. To determine the varying levels of KRAS expressed in different cells lines (with or without EGF stimulation), shown in **Figure 2.7**., pan RAS10 antibody was used for immunoprecipitation followed by immunoblot analysis using KRAS-specific SC-30 antibody.

β-galactosidase assay

β-galactosidase staining was performed using the Senescence β-Galactosidase Staining Kit #9860 (Cell Signaling) on 10 µM-thick frozen sections of mouse pancreas, as per the manufacturer's protocol.

Statistics and reproducibility

Reproducibility of results were ensured by 1) involving multiple members of the team to collect data, 2) analyzing pathologies with two independent pathologists, and 3) repeating cell line-based experiments at least twice. Many experiments were repeated by multiple members of the group.

Results

AGO2 loss allows pancreas development and PanIN formation

To investigate the role of *AGO2* in the development of pancreatic cancer *in vivo*, we employed the genetically engineered mouse model of pancreatic cancer initiated by a conditionally activated

allele of *KRAS* [4], *KRAS*$^{LSL\text{-}G12D/+}$ (KRAS^{G12D}, **Figure 2.1a**). Crossing *KRAS*^{G12D} mice with animals harboring *Cre* recombinase knocked into the pancreas-specific promoter, *p48* (*p48Cre*), yields *KRAS*^{G12D}*;p48Cre* mice that develop pancreatic intraepithelial neoplasia (PanINs) precursor lesions beginning around 8 weeks [4]. Over time, these PanINs progress to pancreatic ductal adenocarcinoma (PDAC) and develop metastases. Next, we generated transgenic mice with both *KRAS*^{G12D} and conditionally deleted allele(s) of *AGO2* [14] (**Figure 2.1a**). The resulting *KRAS*^{G12D}*;p48Cre* mice were either wild-type, heterozygous, or homozygous for the conditional allele of *AGO2* (hereafter referred to as *AGO2*$^{+/+}$*;KRAS*^{G12D}*;p48Cre*, *AGO2*$^{fl/+}$*;KRAS*^{G12D}*;p48Cre,* and *AGO2*$^{fl/fl}$*;KRAS*^{G12D}*;p48Cre,* respectively). Genomic PCR confirmed Cre-driven excision and recombination of the oncogenic *KRAS* allele [4] in pancreata from mice with *KRAS*^{G12D}*; p48Cre* alleles (**Supplementary Figure 2.1a**). Further, qRT-PCR analysis showed significant reduction in *AGO2* expression in *AGO2*$^{fl/fl}$*;KRAS*^{G12D}*;p48Cre* mice (**Supplementary Figure 2.1b**).

Histology of pancreata from mice with Cre-mediated *AGO2* ablation (*AGO2*$^{fl/fl}$; *p48Cre*) showed normal morphology (**Figure 2.1b**, left panels) with no differences in pancreatic weight compared to pancreata from *AGO2*$^{+/+}$;*p48Cre* mice (**Supplementary Figure 2.1c**). This suggests that loss of *AGO2* does not grossly interfere with pancreas development. Immunohistochemistry (IHC) with a monoclonal antibody specific to AGO2 (**Supplementary Figure 2.2**, **Supplementary Table 2.1**) showed minimal expression of AGO2 in the acinar cells of both *AGO2*$^{+/+}$;*p48Cre* and *AGO2*$^{fl/fl}$;*p48Cre* pancreata (**Figure 2.1b**, right panels). These data indicate a non-essential role for *AGO2* in the acinar cells during normal pancreatic development. However, expression of *KRAS*^{G12D} in the pancreatic acinar cells led to increased AGO2 expression in the PanINs as well as the surrounding stroma in 12-week old *AGO2*$^{+/+}$*;KRAS*^{G12D}*;p48Cre* mice (**Figure 2.1c**, top panels). Notably, we observed PanIN lesions in *AGO2*$^{fl/fl}$*;KRAS*^{G12D}*;p48Cre*

pancreata lacking *AGO2* expression (**Figure 2.1c**, lower panels) that were morphologically indistinguishable from those arising in *AGO2*$^{+/+}$;*KRAS*^{G12D};*p48Cre* mice. Further, PanINs from both *AGO2*$^{+/+}$;*KRAS*^{G12D};*p48Cre* and *AGO2*$^{fl/fl}$;*KRAS*^{G12D};*p48Cre* mice displayed high mucin content by Alcian blue staining [21] and similar gross weights of the pancreas, indicating indistinct phenotypes at 12-weeks (**Supplementary Figure 2.3a-b**).

AGO2 loss blocks PDAC progression and increases survival

Surprisingly, mice aged over 400 days showed significantly increased pancreatic weights in both the *AGO2*$^{+/+}$;*KRAS*^{G12D};*p48Cre* and *AGO2*$^{fl/+}$;*KRAS*^{G12D};*p48Cre* cohort compared to *AGO2*$^{fl/fl}$;*KRAS*^{G12D};*p48Cre* mice, suggestive of a higher tumor burden in mice with at least one functional allele of *AGO2* (**Figure 2.1d**). Histology of pancreata at the 400-day time point showed early/late PanIN lesions and some PDAC development in *AGO2*$^{+/+}$;*KRAS*^{G12D};*p48Cre* and *AGO2*$^{fl/+}$;*KRAS*^{G12D};*p48Cre* mice with a distribution consistent with those previously reported [8, 22]. However, in the *AGO2*$^{fl/fl}$;*KRAS*^{G12D};*p48Cre* mice, mostly early stage PanIN lesions were observed, strikingly, with no evidence of PDAC (**Figure 2.1e**). Occasionally, higher grade PanIN lesions were observed in *AGO2*$^{fl/fl}$;*KRAS*^{G12D};*p48Cre* pancreata, but these lesions invariably showed AGO2 expression (**Supplementary Figure 2.4a**), indicative of likely escape from Cre recombination, as has been previously noted in other contexts [8, 23].

To examine the effect of *AGO2* loss on tumor-free survival, a cohort of transgenic mice was monitored over 500 days. Twelve of 12 *AGO2*$^{+/+}$;*KRAS*^{G12D};*p48Cre* and 18 of 19 *AGO2*$^{fl/+}$;*KRAS*^{G12D};*p48Cre* mice died over a median of 406 and 414 days, respectively, typical for a murine model expressing *KRAS*^{G12D} in the pancreas [24, 25]. Remarkably, however, all mice with homozygous *AGO2* deficiency (*AGO2*$^{fl/fl}$;*KRAS*^{G12D};*p48Cre)* had survived at the 500 day cut-

off (**Figure 2.1f**). PDAC was observed in pancreata of all mice that expressed *AGO2*, but mice deficient for *AGO2* developed only early PanIN precursor lesions without progression to PDAC (**Figure 2.1g**). Necropsies of experimental mice revealed frequent metastases and abnormal pathologies [26] in the *AGO2*$^{+/+}$*;KRAS*^{G12D}*;p48Cre* and *AGO2*$^{fl/+}$*;KRAS*^{G12D}*;p48Cre* genotypes, but *AGO2*$^{fl/fl}$*;KRAS*^{G12D}*;p48Cre* mice rarely showed abnormal pathologies and were without PDAC or metastases (**Figure 2.1g**). Analyses of lungs with abnormal pathologies in two of the *AGO2*$^{fl/fl}$*;KRAS*^{G12D}*;p48Cre* mice (marked as gray boxes) showed a single benign lesion each, associated with AGO2 expression without indication of PDAC (**Supplementary Table 2.2, Supplementary Figure 2.4b**). One mouse of the *AGO2*$^{fl/fl}$*;KRAS*^{G12D}*;p48Cre* genotype developed a pancreatic cyst (without AGO2 expression), histologically resembling the mucinous cystic neoplasm, and survived for 368 days (**Supplementary Table 2.2, Supplementary Figure 2.4b**). Taken together, these data show that *AGO2* is not essential for normal pancreatic development or *KRAS*^{G12D}-driven PanIN formation. Notably, however, *AGO2* is indispensable for progression of PanINs to PDAC, despite the presence of other Argonaute proteins not deleted in this model with compensatory and overlapping RNAi functions.

PanINs with AGO2 loss undergo oncogene-induced senescence

Since precancerous lesions have been shown to undergo oncogene-induced senescence (OIS) in the pancreatic cancer mouse model [27], we performed OIS-associated β-galactosidase staining in pancreatic tissue sections of *AGO2*$^{+/+}$*;KRAS*^{G12D}*;p48Cre* and *AGO2*$^{fl/fl}$*;KRAS*^{G12D}*;p48Cre* mice. As shown in **Figure 2.2a-b**, PanINs of *AGO2*$^{fl/fl}$*;KRAS*^{G12D}*; p48Cre* mice showed a significant increase in senescence at the early time point that dramatically increased at 500 days compared to those with *AGO2* expression. Interestingly, immunoblot analysis of pancreatic tissues obtained

from *AGO2*$^{fl/fl}$;*KRAS*^{G12D};*p48Cre* mice revealed a significant increase in phospho-ERK levels compared to *AGO2*$^{+/+}$;*KRAS*^{G12D};*p48Cre* mice (which progress to PDAC), indicative of hyperactive MAPK signaling downstream of RAS in the absence of *AGO2* (**Figure 2.2c**). This striking observation resembles the effects of oncogenic *BRAF*^{V600E} in the pancreas [28]. Consistent with immunoblot analysis, phospho-ERK also showed strong and uniform IHC staining within PanINs in samples with *AGO2* ablation (**Supplementary Figure 2.5**). By contrast, phospho-ERK staining was not uniformly detected in the PDACs from *AGO2*$^{+/+}$;*KRAS*^{G12D};*p48Cre* mice. Thus, oncogenic *KRAS*-driven progression from PanIN to PDAC requires *AGO2* expression to block OIS in mice. We also observed OIS with high levels of phospho-ERK staining in PanINs from human pancreatic tissue (**Figure 2.2d**), suggesting that similar mechanisms may block PDAC development in the clinic.

Comparing immune profiles, we observed almost a 4-fold increase in infiltration of $CD8^+$ T lymphocytes and 20-fold increase in natural killer (NK) cells in pancreata lacking *AGO2*. No significant differences in the number of $CD4^+$ Th cells or $CD68^+$ macrophages were observed between genotypes (**Figure 2.2e**). It is interesting to note that $CD8^+$ T cells and NK cells share properties and interact to elicit potent cytotoxic activities [29]. Further, senescent PanINs lacking *AGO2* showed a marked increase in the NK cell population compared to PanINs of *AGO2*-expressing mice (**Figure 2.2f-g**) along the periphery and in close proximity to the PanIN lesions (**Figure 2.2h, Supplementary Figure 2.6**). Therefore, similar to other settings [30, 31], the senescent phenotype in our model supports NK cell engagement.

p53 loss bypasses the OIS associated with AGO2 ablation

Since p53 loss leads to evasion of senescence [32] and mutational inactivation of the *TP53* gene

has been observed in approximately 75% of PDAC patients [33], we determined the role of AGO2 in the context of p53 loss. For these studies, ablation of *AGO2* expression was carried out in the *Kras^{G12D};Trp53$^{fl/+}$;p48Cre* (KPC) mouse model. In these mice, Cre activation simultaneously activates *KRAS* and reduces *Trp53* levels. Tumor-free survival of chimeric mice with *AGO2$^{+/+}$;Kras^{G12D};Trp53$^{fl/+}$;p48Cre,* *AGO2$^{fl/+}$;Kras^{G12D};Trp53$^{fl/+}$;p48Cre*, and *AGO2$^{fl/fl}$;Kras^{G12D};Trp53$^{fl/+}$;p48Cre* genotypes was similar (**Figure 2.3a**). PDAC and metastatic spread were also similar in all genotypes (**Figure 2.3b**) despite efficient AGO2 ablation (**Figure 2.3c**). Thus, a requirement for *AGO2* in PDAC progression can be bypassed in a mouse model with *TP53* aberrations [32], considered a late event in the development of pancreatic cancer [34].

Membrane association of RAS and AGO2 in PDAC development

Having identified an essential role for *AGO2* in PDAC progression in mice, expression levels of AGO2 were next analyzed. Consistent with a role of *AGO2* in *KRAS*-driven oncogenesis in *AGO2$^{+/+}$;KRAS^{G12D};p48Cre* mice, IHC analysis showed increased levels of AGO2 in PDAC and metastatic tissues as compared to early PanIN lesions (**Figure 2.4a**). Transcript analysis in human pancreatic cancer suggested a significant increase in *AGO2* expression in PDAC compared to normal pancreas (**Supplementary Figure 2.7a**). To extend these observations at the protein level, we performed a systematic IHC analysis of a human pancreatic tissue microarray (TMA), comprising 44 duplicate pancreatic tissue cores, including PanIN, PDAC, and metastatic PDAC samples. AGO2 expression was remarkably higher in PDAC and metastatic PDAC cells compared to PanINs (**Figure 2.4b**), and this increase was statistically significant (**Figure 2.4c**). These data show that AGO2 protein levels are elevated with disease progression and suggest an important role for *AGO2* in pancreatic cancer development in humans.

Considering that RAS is known to localize to the plasma membrane [2, 35], we tested if RAS and the RAS-AGO2 interaction could be localized at the plasma membrane in the mouse models and human tissues. Since most commercial KRAS-specific antibodies have been shown to be unsuitable for IHC or immunofluorescence (IF) [19], we tested RAS10, a pan-RAS monoclonal antibody, and observed specific staining only in RAS expressing cells (**Figure 2.5a, Supplementary Figure 2.7b-c**). Surprisingly, relative to the surrounding normal tissue, IHC and IF analysis of mouse pancreatic tissues with this antibody detected high membranous RAS expression within the PanINs (**Figure 2.5b**). Pre-incubation of the antibody with RAS peptides spanning the antibody epitope abrogated RAS staining (**Figure 2.5c**). To corroborate the finding that RAS IHC and IF staining were primarily restricted to oncogenic KRAS-driven PanINs, we performed RNA *in situ* hybridization (RNA-ISH) using *KRAS*-targeted RNA probes (**Supplementary Figure 2.7d**). As shown in **Supplementary Figure 2.7e**, we observed *KRAS* transcripts restricted to the ducts of pancreatic lesions. The elevated *KRAS* transcript expression in PanINs is consistent with a recent study reporting increased oncogenic *KRAS* transcripts in engineered mouse models[36]. We also validated the AGO2 monoclonal antibody using pancreatic tissue from experimental mice (**Figure 2.5d, Supplementary Figure 2.2**).

Next, we assessed whether RAS and AGO2 co-localized in pancreatic tissues during PDAC progression. IF staining of normal acinar cells in the mouse pancreas displayed low and diffuse cytoplasmic staining of RAS and minimal expression of AGO2, with a low measure of co-staining pattern (Pearson's correlation for co-localization, PCC=0.1) (**Figure 2.5e**). Interestingly, as shown in **Figure 2.5e**, RAS expression increased in PanINs, which further increased in PDAC (**Supplementary Figure 2.7f**). In a parallel manner, AGO2 expression progressively increased in PanIN and PDAC tissues (**Supplementary Figure 2.7g**), with a concomitant increase in plasma

membrane localization and co-staining patterns with RAS (PanIN PCC=0.5; PDAC PCC=0.7). RAS staining could also be detected in the PanIN lesions of *AGO2*$^{fl/fl}$;*Kras*^{G12D};*p48Cre* mice (**Supplementary Figure 2.8a**). Localization of AGO2 to the plasma membrane was independently confirmed by analyzing co-localization with the membrane marker, E-cadherin (PCC=0.43; **Supplementary Figure 2.8b**). Furthermore, in pancreatic tissue obtained from normal mice treated with caerulein to induce pancreatitis [37], we observed wild-type RAS localization at the membrane without AGO2 co-staining (**Supplementary Figure 2.8c**). This suggests specificity of the RAS-AGO2 co-staining observed during oncogenic KRAS-driven PDAC development. Importantly, extending the IF analysis to human pancreatic tissues, we observed a similar pattern of localization of RAS and AGO2 with increased RAS-AGO2 co-staining signals at the plasma membrane associated with pancreatic cancer progression (PCC, normal to PDAC increased from 0.1 to 0.5, respectively) (**Figure 2.5f**).

For a direct assessment of the RAS-AGO2 interaction at single molecule resolution, we performed proximity ligation assays (PLA) [38, 39] using the RAS and AGO2 antibodies validated earlier (**Figure 2.5a, Supplementary Figure 2.2, 2.8d**). As shown in **Figure 2.5g**, PLA signals indicative of RAS-AGO2 interaction were observed at the plasma membrane within PanINs arising in *AGO2*$^{+/+}$;*KRAS*^{G12D};*p48Cre* but not in *AGO2*$^{fl/fl}$;*KRAS*^{G12D};*p48Cre* mice. This further corroborates the IF analyses and provides evidence of membranous RAS-AGO2 interaction. Together, these data indicate that during pancreatic cancer development, AGO2 localizes at the plasma membrane, the site of RAS activity [2, 35], and substantiates a role for *AGO2* in the progression of PanINs to PDAC. Interestingly, in the KPC model described above (**Figure 2.3c, Supplementary Figure 2.9a**), AGO2 expression also increased during PDAC progression in AGO2-sufficient pancreata (**Supplementary Figure 2.9b**). Significant overlapping membranous

signals for RAS and AGO2 (PCC=0.7) were observed in PDAC lesions from *AGO2*$^{+/+}$;*Kras*^{G12D};*Trp53*$^{fl/+}$;*p48Cre* mice (**Supplementary Figure 2.9c**).

AGO2 regulates expression of microRNAs that control OIS

Considering a central role for AGO2 in the RNAi pathway, we compared the microRNA expression profiles of pancreata from *AGO2*$^{+/+}$;*KRAS*^{G12D};*p48Cre* and *AGO2*$^{fl/flto}$;*KRAS*^{G12D};*p48Cre* mice at the 500-day time point. Among the small number of microRNAs that showed differential expression between the two genotypes, the miR-29 and miR-30 families of microRNAs were significantly downregulated in pancreata expressing *AGO2* (**Figure 2.6a, Supplementary Figure 2.10a**). Expression of this family of microRNAs was relatively upregulated within the PanINs lacking *AGO2*. These Rb-regulated microRNAs have been strongly associated with senescence [40], suggesting that their expression in the setting of *AGO2* loss contributes to the OIS phenotype. A similar pattern of regulation was observed for members of the tumor suppressive *let-7* family of microRNAs known to regulate cell proliferation [41] and differentiation [42]. On the other hand, oncogenic miR-21 was expressed to the same extent in the two genotypes. However, in the KPC model, downregulation of the miR-29, miR-30, and *let-7* microRNA families was independent of *AGO2* status (**Supplementary Figure 2.10b**), allowing for progression to PDAC even in the absence of *AGO2*.

Transcriptomic profiles of pancreata obtained from the two genotypes showed that the block in PDAC progression in *AGO2* loss was associated with reduced gene set enrichment scores for E2F targets, G2/M checkpoint controls, and canonical oncogenic KRAS signaling (**Figure 2.6b**, **Supplementary Figure 2.11**). Surprisingly, these transcriptional changes were accompanied with an increase in oxidative phosphorylation, considered conducive for PDAC development [43].

These data suggest a temporal requirement for *AGO2* for the biogenesis of select microRNAs to control PDAC progression.

The KRAS-AGO2 interaction limits RAS activation

Next, we sought to explore how AGO2 alters the EGFR-RAS signaling axis for two reasons: 1) EGFR has been shown to be essential for PanIN formation in the $KRAS^{G12D}$-driven pancreatic mouse model [7, 8, 44], and 2) EGFR activation has been shown to directly inhibit AGO2 function through phosphorylation of its tyrosine 393 residue [12]. Immunoblot analysis of pancreatic tissues from 12-week old mice with $AGO2^{+/+}$;$KRAS^{G12D}$;*p48Cre*, $AGO2^{fl/+}$;$KRAS^{G12D}$;*p48Cre*, and $AGO2^{fl/fl}$;$KRAS^{G12D}$;*p48Cre* genotypes showed a marked increase in AGO2 levels relative to normal pancreata (**Supplementary Figure 2.12a**) concordant with IF analysis (**Figure 2.5e**). Consistent with published studies [7, 8], total EGFR levels were also elevated in $KRAS^{G12D}$ mice irrespective of the *AGO2* genotype (**Supplementary Figure 2.12a**). However, in early PanINs initiated by oncogenic KRAS, significantly higher levels of phospho-EGFR (Y1068) were observed in pancreatic tissues of $AGO2^{fl/fl}$;$KRAS^{G12D}$;*p48Cre* mice (**Figure 2.6c, Supplementary Figure 2.12a-b**), indicating activated EGFR signaling in the absence of *AGO2* expression. IHC analysis confirmed the elevated phospho-EGFR levels observed in tissue lysates were restricted to PanIN lesions of $AGO2^{fl/fl}$;$KRAS^{G12D}$;*p48Cre* mice (**Figure 2.6d**). IHC of total EGFR showed no significant difference in expression in pancreatic tissues between genotypes (**Figure 2.6d, Supplementary Figure 2.13a-b**). As previously noted, irrespective of *AGO2* genotype, lesions from later time points showed a marked reduction in total EGFR levels [7, 8] in mice (and with disease progression in human tissue), further supporting the significance of EGFR signaling in the early stages of disease (**Supplementary Figure 2.13a,c**). Importantly, immunoblot analysis

showed that EGFR activation was accompanied with a remarkable increase in total RAS levels but not oncogenic $KRAS^{G12D}$ levels (**Figure 2.6c, Supplementary Figure 2.12**), raising an intriguing possibility that signaling in early stage PanINs is along the EGFR-wild-type RAS axis.

To investigate this further, we isolated pancreatic ducts from 12-week old *AGO2*$^{+/+}$*;KRAS*^{G12D}*;p48Cre* and *AGO2*$^{fl/fl}$*;KRAS*^{G12D}*;p48Cre* mice and cultured them as organoids [45] in the absence of EGF (**Supplementary Figure 2.14**). Immunoblot analysis showed increased levels of phospho-EGFR and total RAS in the organoids with *AGO2* loss, while $KRAS^{G12D}$ expression showed no change (**Figure 2.6e**), mirroring the observations from pancreatic tissue lysates. Given that AGO2 is a direct phosphorylation substrate of the EGFR kinase [12], our experiments define a reverse feedback up-regulation of phospho-EGFR via AGO2 [46-49].

To estimate the levels of activated wild-type RAS and oncogenic KRAS due to EGFR activation in *AGO2* loss, we performed the RAF-binding domain (RBD) assay using isoform specific antibodies. As shown in **Figure 2.6e**, significant increases in activated RAS were readily detected using pan-RAS and KRAS-specific antibodies. A modest increase in $KRAS^{G12D}$-GTP levels was also observed. These observations reveal that *AGO2* ablation activates EGFR signaling and results in increased GTP loading of both the wild-type and oncogenic KRAS.

Next, we monitored the extent of wild-type KRAS-GTP and $KRAS^{G12D}$-GTP levels upon treatment of the organoids with erlotinib. Remarkably, erlotinib treatment of organoids expressing *AGO2* showed an increase in $KRAS^{G12D}$-GTP levels. On the other hand, EGFR inhibition in *AGO2*-deficient organoids had no effect on the increased $KRAS^{G12D}$-GTP levels (**Figure 2.6f**). Conversely, in the absence of *AGO2*, EGFR inhibition dramatically reduced wild-type KRAS-GTP levels. The total KRAS-GTP levels in *AGO2*-sufficient organoids tracked with those of $KRAS^{G12D}$-GTP levels upon erlotinib treatment. These experiments clarify the role of AGO2 as a

regulator of KRAS activity. In its absence, both oncogenic and wild-type RAS forms are activated, yet unlike oncogenic KRAS, activated wild-type KRAS is sensitive to EGFR inhibition. Further, the activation of EGFR, wild-type KRAS, and downstream ERK, all remained sensitive to erlotinib treatment (**Figure 2.6f**).

To probe if *AGO2* loss activates wild-type RAS even in the absence of mutant KRAS, we performed immunoblot analysis and RAS activation assays using *AGO2*$^{-/-}$ MEFs that do not harbor any form of oncogenic RAS [50]. As shown in **Figure 2.6g**, *AGO2*$^{-/-}$ MEFs also exhibit increased phospho-EGFR and wild-type RAS levels along with elevated wild-type RAS-GTP levels, which were significantly reduced when rescued with *AGO2*. We then made stable lines expressing either vector, full-length wild-type AGO2, or RAS binding-deficient AGO2 (K112A/E114A) to interrogate the specific effects of the KRAS-AGO2 interaction on RAS signaling. As shown in **Figure 2.6h**, both wild-type AGO2 and AGO2$^{K112A/E114A}$ decreased phospho-EGFR activation. While the wild-type form of AGO2 limited RAS activation, the AGO2 mutant lacking RAS-binding residues sustained RAS activation. Further, increased pERK activation observed in the *AGO2*$^{-/-}$ MEFs could be rescued with AGO2 but not the RAS binding-deficient mutant (**Figure 2.6h**). Using diverse models, these data define AGO2 as a key regulator that limits KRAS activation and downstream effector engagement through its direct interaction with KRAS.

To further explore how AGO2 could regulate KRAS-GTP levels, we performed biochemical assays that monitor the levels of KRAS-GTP in the presence of known RAS regulators. Specifically, using purified catalytic domains of Neurofibromin 1-GAP and SOS1-GEF, we measured KRAS-GTP levels in the presence or absence of AGO2. As shown in **Figure 2.6i**, AGO2 had no effect on the intrinsic GTPase activity of KRAS and did not alter NF1-GAP activity on KRAS. However, SOS1-mediated nucleotide exchange on wild-type RAS was

significantly reduced in the presence of AGO2 (**Figure 2.6j**) in a dose-dependent manner (**Figure 2.6k**). In similar assays, oncogenic forms of KRAS were resistant to both GAP and GEF activity. Since both SOS and AGO2 compete for binding to the KRAS Switch II domain through Y64, our data predicts that the KRAS-AGO2 interaction limits wild-type RAS activation by competitively blocking SOS association (**Figure 2.9**). Thus, in addition to the microRNA and transcriptomic changes observed with *AGO2* ablation, loss of the KRAS-AGO2 interaction likely leads to increased ERK activation associated with the OIS phenotype.

AGO2^{Y393} phosphorylation disrupts the KRAS-AGO2 interaction

Considering that *AGO2* loss leads to increased signaling via EGFR and wild-type RAS through increased access of SOS to KRAS (**Figure 2.6j-k**), we posited that AGO2 binding to KRAS may also represent a rate limiting step in the activation of wild-type KRAS during growth factor stimulation. To explore this premise, we assayed for KRAS-AGO2 interaction across a panel of cell lines expressing wild-type or mutant *RAS* stimulated with EGF. Interestingly, EGF stimulation resulted in a dramatic decline in KRAS-AGO2 interaction in cells with wild-type *KRAS*, as observed in MCF-7, PC3, A375, and HeLa cells (**Figure 2.7a, Supplementary Figure 2.15a-b**). In contrast, EGF stimulation of cells harboring oncogenic *KRAS*, including A549 (*KRAS^{G12S}*), MIA PaCa-2 (*KRAS^{G12C}*), and Capan-1 (*KRAS^{G12V}*), retained binding of endogenous KRAS and AGO2 despite activation of the EGFR/MAPK/AKT pathway (**Figure 2.7b, Supplementary Figure 2.15c**). Disruption of the wild-type RAS-AGO2 interaction was also observed when HEK293 (wild-type *KRAS*) cells expressing FLAG-tagged AGO2 were stimulated with EGF; the interaction was rescued by treatment of cells with erlotinib (**Figure 2.7c**). This strongly suggests that EGFR kinase activity was critical for the disruption of the wild-type KRAS-AGO2 interaction. In

contrast, DLD-1 cells harboring mutant *KRAS*^{G13D} showed no loss of KRAS and AGO2 association either by EGF or erlotinib treatment (**Figure 2.7d**).

To test if the previously identified site of EGFR-mediated phosphorylation [12] on AGO2 at tyrosine 393 has a role in binding to KRAS, we analyzed the ability of a phosphorylation-deficient AGO2^{Y393F} mutant to bind RAS under different conditions. In HEK293 (wild-type *KRAS*) cells, EGF stimulation led to dissociation of wild-type AGO2 from RAS, but the AGO2^{Y393F} mutant continued to bind RAS with or without EGFR activation (**Figure 2.7e**), indicating that phosphorylation of this residue is critical for dissociation. Expression of these *AGO2* constructs in MIA PaCa-2 (*KRAS*^{G12S}) cells showed no discernible change in RAS binding upon EGFR activation (**Figure 2.7f**).

Next, we treated oncogenic KRAS-expressing cells with H_2O_2, known to inactivate tyrosine phosphatases by oxidation and, thus, activate EGFR [51]. In both H358 and Mia PaCa-2 cells expressing oncogenic KRAS, the KRAS-AGO2 interaction could be readily disrupted following H_2O_2 treatment (**Figure 2.7g-h**). This disruption was also found to be dependent on the Y393 phosphorylation site of AGO2, since mutant AGO2^{Y393F} remained recalcitrant to H_2O_2 treatment in Mia PaCa-2 cells (**Figure 2.7i**).

To track the localization of the RAS-AGO2 interaction upon growth factor activation, we performed PLA on cells expressing wild-type or mutant *KRAS*. The use of either RAS or AGO2 antibodies alone did not show signals for the RAS-AGO2 PLA (**Supplementary Figure 2.16a**). Interestingly, serum-starved PC3 cells showed increased membrane localization of both RAS and AGO2 proteins contributing to the increase in membrane-localized RAS-AGO2 PLA signals under these conditions (**Figure 2.7j**, upper panels). RAS-AGO2 interaction PLA signals were significantly reduced upon EGF stimulation and restored to levels observed under serum-sufficient

conditions. IF analyses also showed a similar pattern of RAS-AGO2 co-staining under these different culture conditions (**Supplementary Figure 2.16b**). A similar pattern of RAS-AGO2 interaction PLA signals was observed in wild-type *RAS* expressing MCF-7 cells (**Figure 2.7j**, panel I). In contrast, both HCT116 and H358 cells (**Figure 2.7j**, panels II and III), expressing oncogenic forms of *KRAS*, showed higher basal levels of RAS-AGO2 PLA signals compared to wild-type *RAS* expressing cells that remained consistent under different cell culture conditions. Combined, these data suggest that the wild-type KRAS-AGO2 interaction at the membrane is sensitive to EGF-stimulated phosphorylation of $AGO2^{Y393}$, while the oncogenic KRAS-AGO2 interaction is unaffected by ligand-activated EGFR. These data suggest that the Y393 phosphorylation site in AGO2 determines binding of both wild-type and oncogenic forms of KRAS; however, while AGO2 phosphorylation in wild-type RAS expressing cells can be achieved by EGF stimulation, mutant RAS-expressing cells require sustained EGFR activation through inhibition of tyrosine phosphatases.

ARS-1620 disrupts the oncogenic KRAS-AGO2 interaction

Finally, we tested if direct targeting of oncogenic KRAS could affect the endogenous mutant KRAS-AGO2 interaction. Interestingly, the mutant KRAS-AGO2 interaction was disrupted when H358 (**Figure 2.8a**) and MIA-PaCa-2 cells (**Figure 2.8b**), harboring $KRAS^{G12C}$ mutant alleles, were treated with ARS-1620 [52], a covalent G12C inhibitor. The disruption of endogenous $KRAS^{G12C}$-AGO2 interaction in these cells was concentration-dependent and reflects the differential sensitivities of the two cell lines to ARS-1620 [53]. In a similar assay, ARS-1620 treatment had no effect on the $KRAS^{G12D}$-AGO2 interaction in Panc 05.04 (**Figure 2.8c**) or Panc 10.05 cells (**Figure 2.8d**). Given that ARS-1620 binds an allosteric Switch II pocket (SW-IIP) [53]

on GDP-loaded $KRAS^{G12C}$, the disruption of $KRAS^{G12C}$-AGO2 binding provides orthogonal evidence that AGO2 makes contact with the Switch II region in KRAS. This data also proves that besides SOS, the easily detectable, endogenous membrane-bound $KRAS^{G12C}$-AGO2 interaction is an additional target of G12C inhibitors.

Discussion

Genetically engineered mouse models mirror the stepwise progression of human pancreatic cancer, starting with benign precursor lesions (PanINs) driven by mutant *KRAS* [25, 54, 55]. Here, a GEMM of *AGO2* loss delineates pancreatic cancer development into two distinct phases (**Figure 2.9**). The first phase of PanIN development is triggered by oncogenic *KRAS* and depends on EGFR-RAS mediated proliferation; this is followed by a second phase of PDAC progression that requires AGO2 expression to overcome OIS. While low-grade PanINs have been known to undergo senescence [27], our model represents the first instance where loss of a direct interactor of KRAS induces OIS to abrogate PDAC progression. Despite the increased presence of NK cells [56], the senescent cells are not cleared, allowing increased lifespan of mice lacking *AGO2*. Interestingly, the OIS phenotype is characterized by both the limited RNAi activity of AGO2 (to downregulate miRNAs that control cell proliferation/senescence, such as the *let-7* and miR-29/30 families [57-60]) and a concomitant increase in oncogenic and wild-type KRAS activity and downstream effector signaling. While the microRNA regulation may be a result of the complete lack of *AGO2* expression, the effects on RAS signaling can be attributed to the KRAS-AGO2 interaction. Notably, other members of the Argonaute family fail to compensate for these functions, reiterating the specific role of AGO2 in KRAS-driven pancreatic cancer. Since the

microRNAs identified here also regulate pancreatic autophagic process [61] and OIS [62], it will be interesting to determine the role of AGO2 in autophagy.

Through these studies, we show that AGO2 localized to the plasma membrane, a known site for KRAS activity but not RNA silencing activity [63-66]. Importantly, we show that AGO2 expression at the membrane increased during PDAC progression, both in mouse and human PDAC, highlighting membrane redistribution of AGO2 in clinical disease progression. Given that posttranscriptional regulation can involve dynamic polarization of mRNA targets[67], it will be interesting to understand the effects of AGO2 membrane localization on its RNAi function to control translation. Functionally, we find that p53 loss precludes a requirement for both *AGO2* and its RNAi activity, yet, like in the human tissues, RAS/AGO2 membrane localization is retained in this model. Since aberrations in *KRAS* and *p53* do not occur simultaneously, the mouse model with p53 loss represents a different etiology for PDAC progression and limits our understanding of the requirement of AGO2 in advanced disease states.

This study also reveals how EGFR activation allows fine-tuning of RAS signaling by disrupting the membrane RAS-AGO2 association under conditions of stress (starvation or presence of oncogenic KRAS). Interestingly, phosphorylation of AGO2 by EGFR simultaneously inhibits the last step of microRNA biogenesis [12] and activates RAS at the plasma membrane [68]. We observe that EGF stimulation is sufficient to disrupt the wild-type KRAS-AGO2 interaction, but disruption of the oncogenic KRAS-AGO2 interaction requires activation of the growth receptor through inhibition of cytosolic tyrosine phosphatases. However, under both of these conditions, interaction with KRAS is dependent on the Y393 phosphorylation status of AGO2. In fact, inhibition of tyrosine phosphatase PTP1B through oxidative stress has been shown to lead to accumulation of $AGO2^{Y393}$ in oncogenic RAS-expressing cells, leading to senescence

[69]. It is also intriguing that EGFR-mediated phosphorylation of AGO2^{Y393} disrupts KRAS binding in a manner reminiscent of AGO2-Dicer binding and renders AGO2 incapable of RNAi activity [12, 70]. While both KRAS and EGFR aberrations are mutually exclusive, both alter AGO2 RNAi function through distinct mechanisms [11].

Extending these observations to our mouse model, we predict that *AGO2* loss phenotypically mimics AGO2^{Y393} phosphorylation. During EGFR-dependent PanIN development (**Figure 2.9**), neither phosphorylated AGO2^{Y393} nor the setting of *AGO2* loss permits KRAS association, and this stage is, therefore, independent of AGO2. On the other hand, during progression to PDAC that is less reliant on EGFR, accumulation of AGO2^{Y393} in its non-phosphorylated form promotes KRAS binding which is essential for PDAC progression. Mouse models expressing only the RAS binding-deficient form of AGO2 will validate the biological role of the KRAS-AGO2 interaction.

Finally, we find that the G12C covalent inhibitor disrupts the mutant KRAS^{G12C}-AGO2 interaction. The inhibitor is known to covalently attach to cysteine residues and make contacts at the Switch II pocket. This binding has been shown to interfere with nucleotide exchange because of reduced SOS1-KRAS^{G12C} interaction [53]. Given that SOS and AGO2 compete for binding to the Switch II domain to regulate RAS-GTP levels, it is not surprising that AGO2 also fails to bind inhibitor-bound KRAS. Therefore, our data suggests that abrogation of the oncogenic KRAS-AGO2 association at the plasma membrane may represent a therapeutic opportunity for pancreatic cancer that warrants further investigation.

Figures

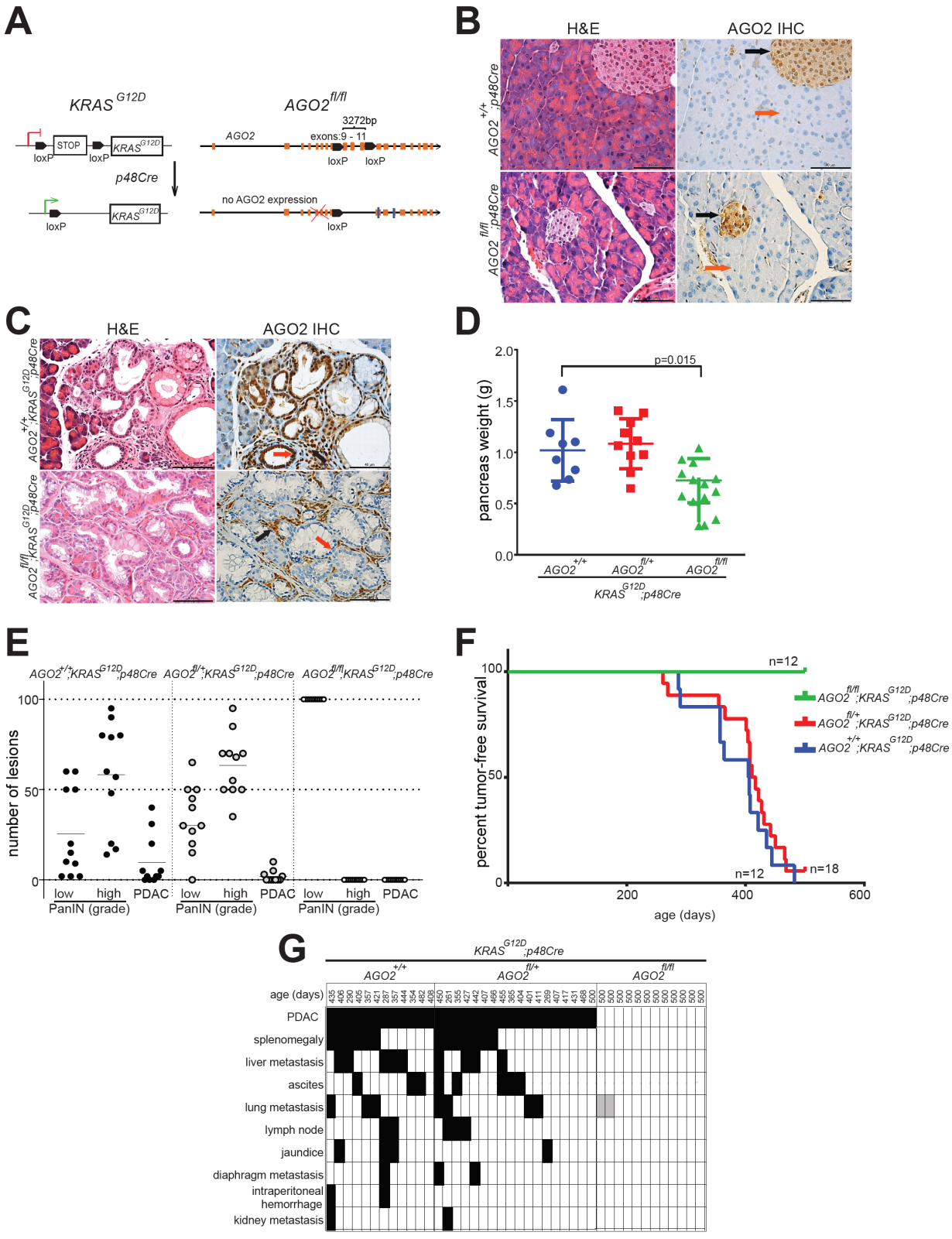
A
KRAS G12D
AGO2 fl/fl
STOP
loxP
KRASG12D
p48Cre
AGO2
3272bp
exons 9 - 11
no AGO2 expression
B
H&E
AGO2 IHC
AGO2+/+;p48Cre
AGO2fl/fl;p48Cre
C
H&E
AGO2 IHC
AGO2+/+;KRASG12D;p48Cre
AGO2fl/fl;KRASG12D;p48Cre
D
p=0.015
pancreas weight (g)
2.0
1.5
1.0
0.5
0.0
AGO2+/+
AGO2fl/+
AGO2fl/fl
KRASG12D;p48Cre
E
AGO2+/+;KRASG12D;p48Cre
AGO2fl/+;KRASG12D;p48Cre
AGO2fl/fl;KRASG12D;p48Cre
number of lesions
100
50
0
low
high
PDAC
PanIN (grade)
F
n=12
n=18
n=12
percent tumor-free survival
100
50
0
200
400
600
age (days)
AGO2fl/fl;KRASG12D;p48Cre
AGO2fl/+;KRASG12D;p48Cre
AGO2+/+;KRASG12D;p48Cre
G
KRASG12D;p48Cre
AGO2+/+
AGO2fl/+
AGO2fl/fl
age (days)
PDAC
splenomegaly
liver metastasis
ascites
lung metastasis
lymph node
jaundice
diaphragm metastasis
intraperitoneal hemorrhage
kidney metastasis

Figure 2.1 *AGO2* is essential for progression of precursor PanIN lesions to PDAC.
(A) Schematic of the conditionally activated endogenous alleles of $KRAS^{G12D}$ and *AGO2* used in the study to generate the $AGO2^{fl/fl}$;$KRAS^{G12D}$;*p48Cre* experimental mice.

(B) Representative images of H&E and AGO2 IHC analysis of pancreata obtained from $AGO2^{+/+}$;*p48Cre* and $AGO2^{fl/fl}$;*p48Cre* genotypes. Orange and black arrows indicate AGO2 expression in acinar cells and islets of Langerhans, respectively. Scale bar, 100 μm.

(C) Representative H&E and IHC analysis for AGO2 in pancreata obtained from 12-week old mice from the $AGO2^{+/+}$;$KRAS^{G12D}$;*p48Cre* and $AGO2^{fl/fl}$;$KRAS^{G12D}$;*p48Cre* genotypes. Orange and black arrows indicate AGO2 staining in the PanIN and stromal regions, respectively. Scale bar, 100 μm.

(D) Scatter plot showing the weight of pancreata obtained from 10 $AGO2^{+/+}$;$KRAS^{G12D}$;*p48Cre*, 17 $AGO2^{fl/+}$;$KRAS^{G12D}$;*p48Cre*, and 14 $AGO2^{fl/fl}$;$KRAS^{G12D}$;*p48Cre* mice aged over 400 days. Two sided t-test was performed to determine the P value and error bars are mean values +/- SEM.

(E) Histogram showing average number of early and late PanIN lesions observed in 11 mice each of $AGO2^{+/+}$;$KRAS^{G12D}$;*p48Cre*, $AGO2^{fl/+}$;$KRAS^{G12D}$;*p48Cre*, and $AGO2^{fl/fl}$;$KRAS^{G12D}$;*p48Cre* genotypes at 400 days. The number of early/ late PanINs and PDAC within pancreatic sections from each animal were counted as a percentage. For $AGO2^{fl/fl}$;$KRAS^{G12D}$;*p48Cre* mice, only lesions that do not express AGO2 have been included.

(F) Kaplan-Meier curve for tumor-free survival of $AGO2^{+/+}$;$KRAS^{G12D}$;*p48Cre*, $AGO2^{fl/+}$;$KRAS^{G12D}$;*p48Cre*, and $AGO2^{fl/fl}$; $KRAS^{G12D}$;*p48Cre* mice aged over 500 days. (G) Chart showing PDAC (within the pancreas), the different metastatic lesions, and abnormal pathologies (black boxes) observed in each mouse of the indicated genotypes aged over 500 days. Gray boxes in the $AGO2^{fl/fl}$;$KRAS^{G12D}$;*p48Cre* group indicate abnormal pathology observed at the indicated site and are addressed in further detail in Supplementary Figure 4. The number of mice indicated in this figure represent biologically independent individuals.

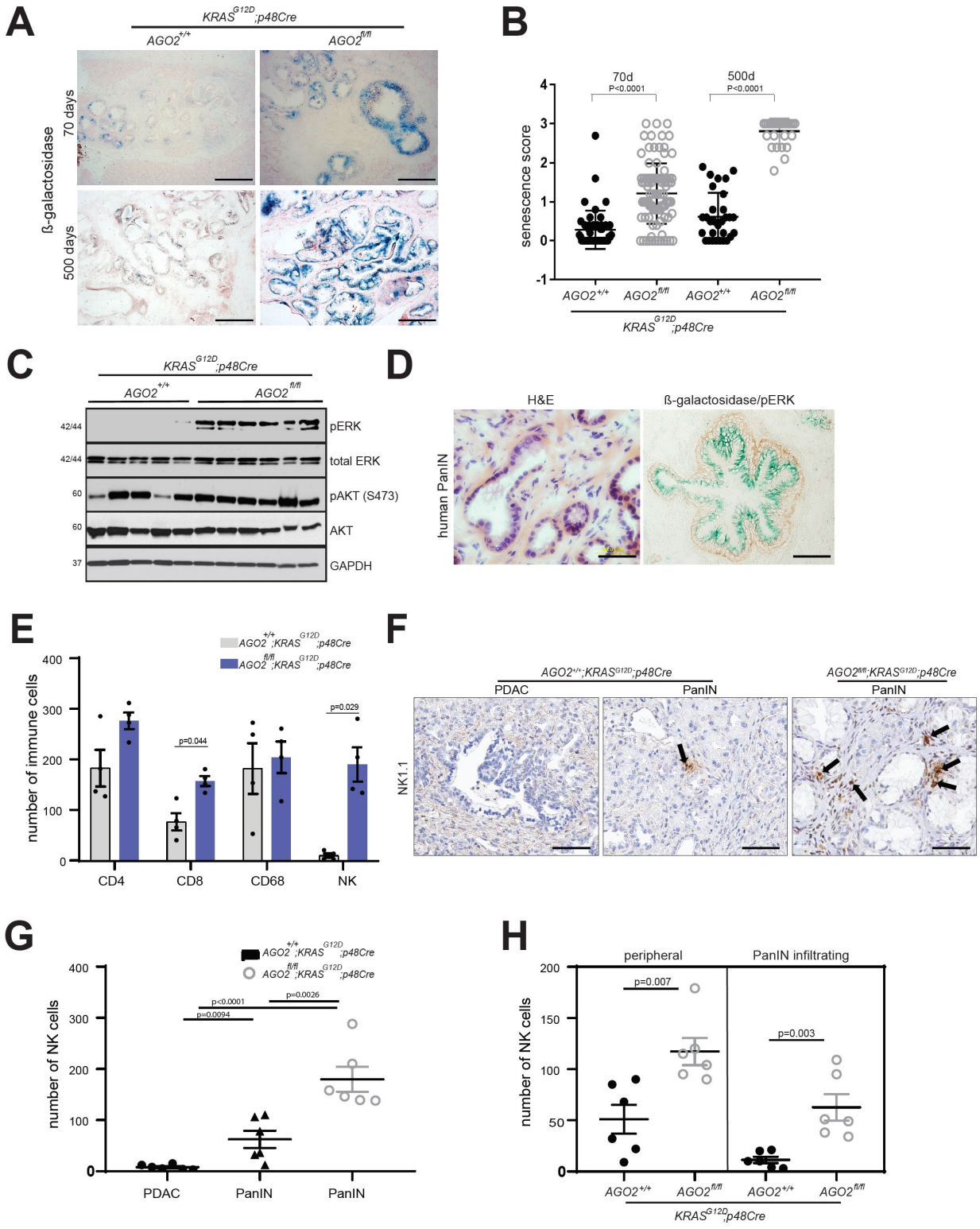

Figure 2.2 *AGO2* loss prevents PanIN to PDAC progression through OIS.
(A) β-galactosidase staining of pancreatic sections from *AGO2*$^{+/+}$;*KRAS*^{G12D};*p48Cre* and *AGO2*$^{fl/fl}$;*KRAS*^{G12D};*p48Cre* mice at 70- and 500-day time points. Scale bar, 100 μm.

(B) Scatter plot showing β-galactosidase staining in low grade PanINs. Data are from 47 PanINs from *AGO2*$^{+/+}$;*KRAS*^{G12D};*p48Cre* and 98 PanINs from *AGO2*$^{fl/fl}$;*KRAS*^{G12D};*p48Cre* from four individual mice at the 70- day time point and 30 PanINs from three individual mice at 500-day time points. Intensity of staining and percent cells within 30 low grade PanINs were used to determine the senescence score = intensity x percent positive cells. p values were determined using a two sided t-test. Data are presented as mean values +/- SEM.

(C) Immunoblot analysis of RAS-driven MAPK (indicated by pERK) and PI3K (indicated by pAKT) signaling from individual pancreata obtained from mice of the indicated genotypes, aged to 400 days. Numbers on the left indicate protein molecular weights in kDa.

(D) Representative images of H&E staining (left) and dual staining for β-galactosidase and phospho-ERK (right) in human pancreatic tissue with PanINs (representative staining of at least 10 PanINs from two patients). Scale bar, 40 μm.

(E) Immune profile of lesions from the indicated genotypes. 10 different pancreatic sections from four individual mice were assessed for the indicated IHC markers that distinguish immune cell populations. Significant p values are indicated and were determined using two tailed t-test.

(F) Representative images of NK1.1-positive NK cells surrounding PanIN and PDAC lesions within the indicated genotypes. Scale bar, 50 μm.

(G) Plot showing NK cell number in PanIN/PDAC lesions within the indicated genotypes. Pancreatic tissues from six mice were analyzed for NK1.1 IHC-positive NK cells. Two tailed t-test was used to determine p values.

(H) Scatter plot showing peripheral and PanIN infiltrating NK cell count from PanINs in the indicated genotypes. Counts were obtained from 10 consecutive fields from six mice at 20X magnification, and the indicated p values were determined using two tailed t-test. In relevant panels, data are presented as mean values +/- SEM.

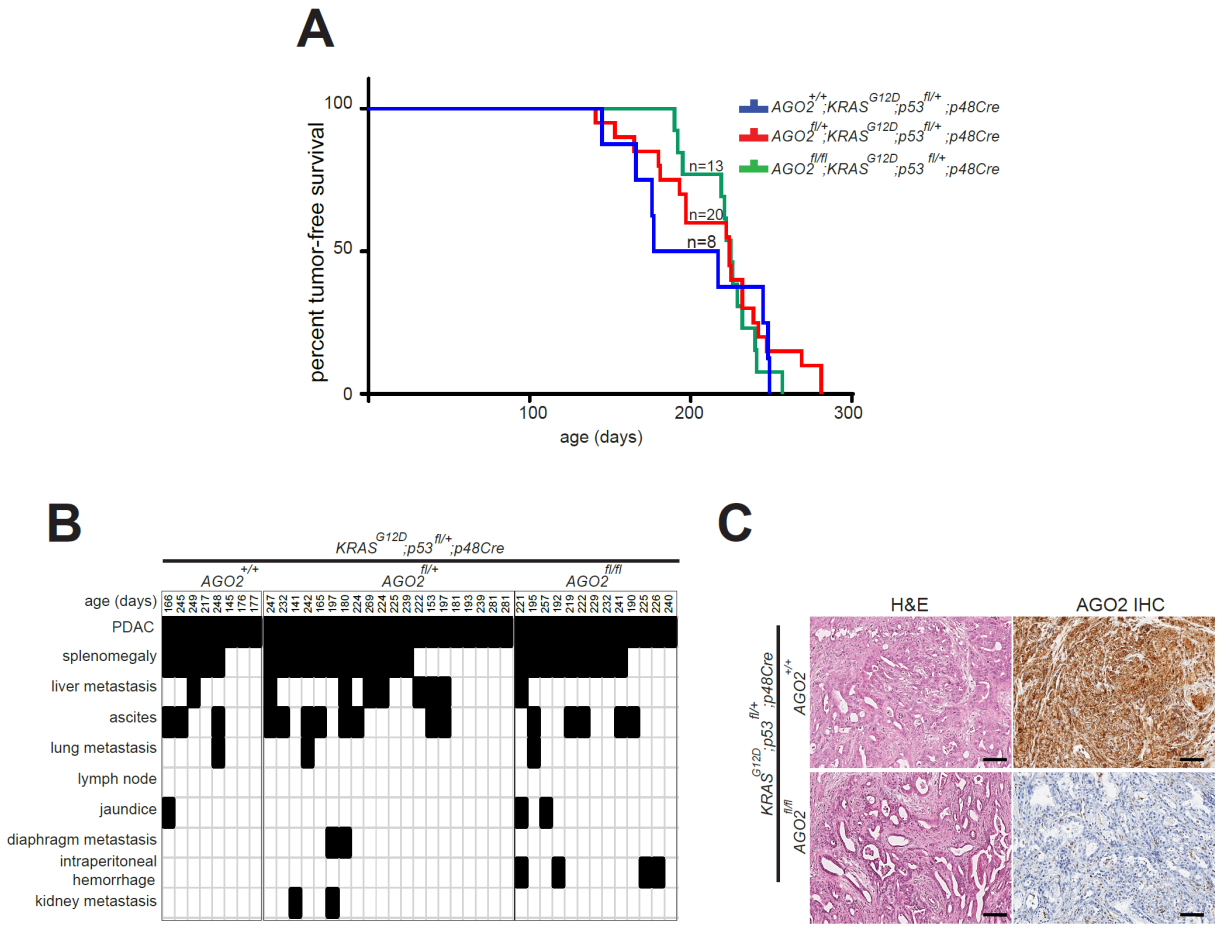

Figure 2.3 p53 loss bypasses requirement for *AGO2* during PDAC progression.
(A) Kaplan-Meier tumor-free survival of *Ago2*$^{+/+}$*;Kras*^{G12D}*;Trp53*$^{fl/+}$*;p48Cre,* Ago2$^{fl/+}$*;Kras*^{G12D}*;Trp53*$^{fl/+}$*;p48Cre*, and *Ago2*$^{fl/fl}$*;Kras*^{G12D}*;Trp53*$^{fl/+}$*;p48Cre* mice.

(B) Chart showing PDAC (within the pancreas), the different metastatic lesions, and abnormal pathologies (black boxes) observed in each mouse of the indicated genotypes.

(C) Representative H&E and AGO2 IHC in the indicated genotype. Scale bar, 100 μm.

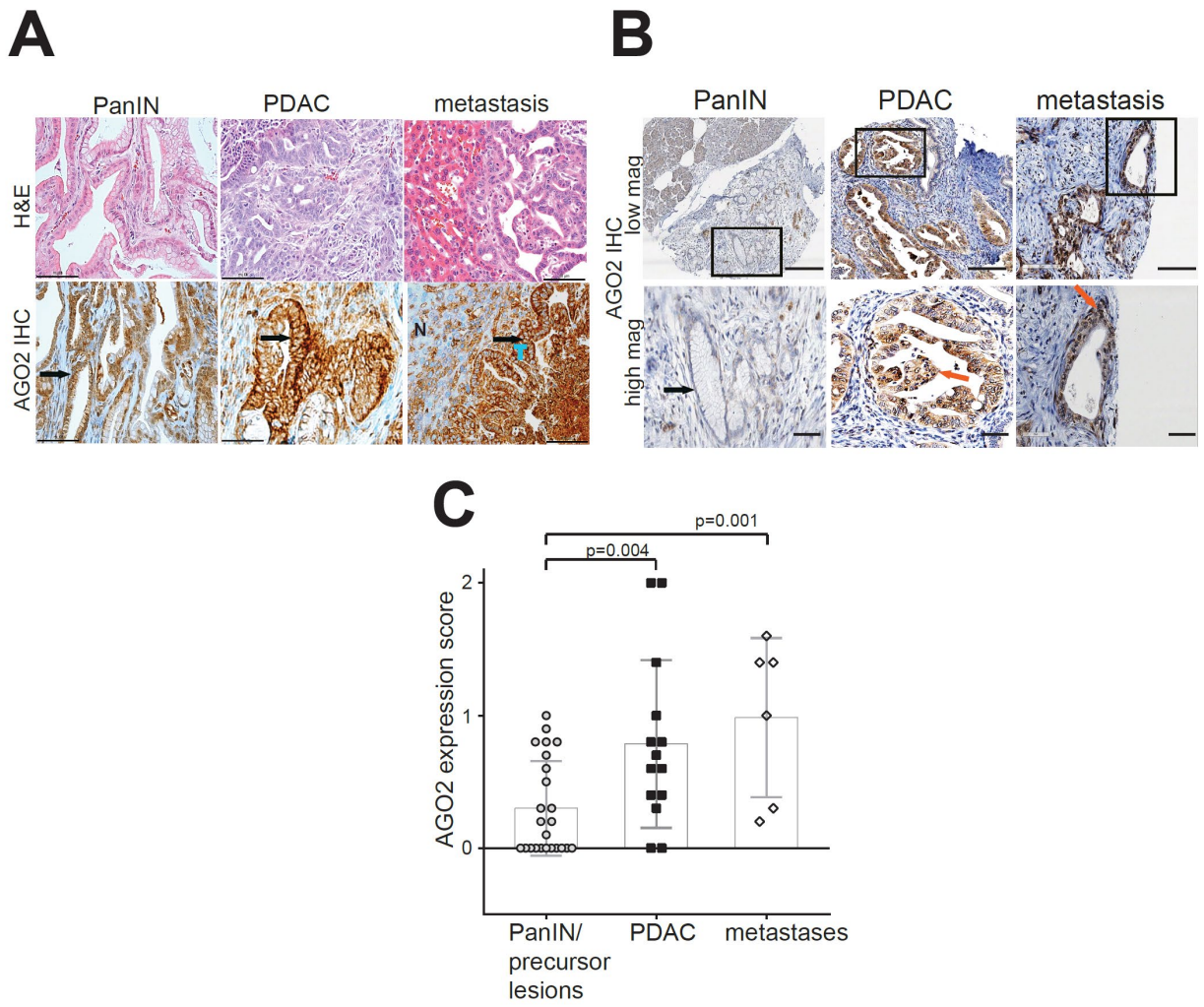

Figure 2.4 Increased AGO2 expression during mouse and human PDAC progression.
(A) Representative images of AGO2 IHC analysis within an individual *AGO2*$^{+/+}$;*KRAS*^{G12D};*p48Cre* mouse showing increased AGO2 expression in PDAC and metastasis compared to PanIN lesions. Arrows point to PanIN, PDAC, or metastatic PDAC in respective panels. In the metastasis panel, N=normal liver and T=tumor. Scale bar, 40 µm.

(B) Representative images of IHC analysis for AGO2 expression in human PDAC progression showing elevated AGO2 protein expression in PDAC and metastatic tissue. Lower panels show higher magnifications of areas marked in the upper panels. Scale bars in the top and bottom panels are 200 µm and 80 µm, respectively. Arrows point to PanIN and PDAC.

(C) Box and scatter plot showing AGO2 expression on a human tissue microarray (TMA) containing 44 human pancreatic tissue samples (24 precancerous, 14 PDAC, and six metastatic PDAC lesions), as determined by IHC analysis. Each sample was scored for intensity of stain and percent tumor cells staining for AGO2, and the final score = intensity x percent positive cells. p values were determined using a two sided t-test. Data are presented as mean values +/- SEM.

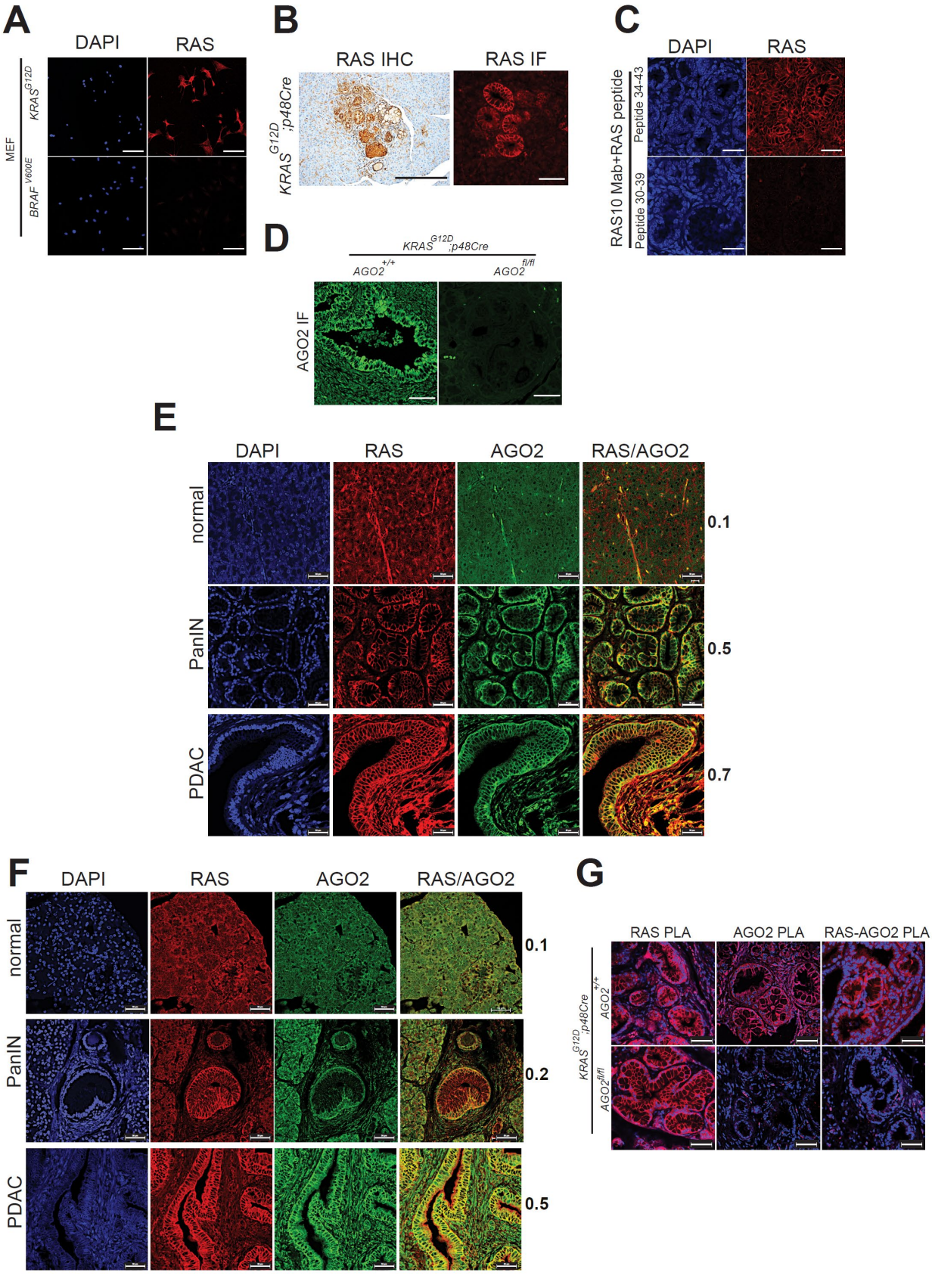
A
DAPI
RAS
MEF
KRASG12D
BRAFV600E
B
RAS IHC
RAS IF
KRASG12D;p48Cre
C
DAPI
RAS
RAS10 Mab+RAS peptide
Peptide 34-43
Peptide 30-39
D
KRASG12D;p48Cre
AGO2+/+
AGO2fl/fl
AGO2 IF
E
DAPI
RAS
AGO2
RAS/AGO2
normal
PanIN
PDAC
0.1
0.5
0.7
F
DAPI
RAS
AGO2
RAS/AGO2
normal
PanIN
PDAC
0.1
0.2
0.5
G
RAS PLA
AGO2 PLA
RAS-AGO2 PLA
KRASG12D;p48Cre
AGO2+/+
AGO2fl/fl

Figure 2.5 Increased membrane co-localization of RAS and AGO2 during PDAC progression.
(A) RAS10 (panRAS) antibody specificity for IHC and IF analyses was determined by staining RASless MEFs rescued by either oncogenic *KRAS* or $BRAF^{V600E}$. Scale bar, 100 μm.

(B) Membranous RAS staining in 10-week old PanINs of mouse tissues expressing oncogenic *KRAS* using either IHC (left) or IF (right). Scale bars, 50 μm.

(C) Peptide competition assay to demonstrate specificity of the RAS10 antibody in mouse tissues expressing oncogenic *KRAS*. Representative IF images using the RAS10 antibody pre-incubated with RAS peptide spanning the antibody epitope 30-39aa and control overlapping RAS peptide spanning 34-43aa. Scale bar, 50 μm.

(D) Representative images of AGO2 IF analysis in pancreatic tissues from $AGO2^{+/+}$;$KRAS^{G12D}$;*p48Cre* and $AGO2^{fl/fl}$;$KRAS^{G12D}$;*p48Cre* mice. Scale bar, 50 μm.

(E) Representative images of IF analysis for RAS and AGO2 through PDAC progression in the $AGO2^{+/+}$;$KRAS^{G12D}$;*p48Cre* mice. Scale bar, 50 μm.

(F) Representative images of IF analysis of human pancreatic tissue on a TMA showing co-localization of AGO2 and RAS in PanIN and PDAC cells. For (E) and (F), numbers adjacent to merged images indicate the Pearson's coefficient of co-localization (PCC) of RAS-AGO2 signals at the membranous regions (where 0 is no overlap and 1 is complete overlap). PCC was determined using co-localization signals of at least 50 cells in three distinct areas representative of normal acinar, PanIN, PDAC, or metastases. Scale bar, 50 μm.

(G) Representative images of Proximity Ligation Assay (PLA), performed to detect either RAS (RAS PLA) or AGO2 (AGO2 PLA) expression and the RAS-AGO2 interaction (RAS-AGO2 PLA) within PanIN lesions of $AGO2^{+/+}$;$KRAS^{G12D}$;*p48Cre* (upper panel) and $AGO2^{fl/fl}$;$KRAS^{G12D}$;*p48Cre* (lower panel) mice. PLA signals appear as red dots around DAPI stained nuclei in blue. Scale bar, 50 μm.

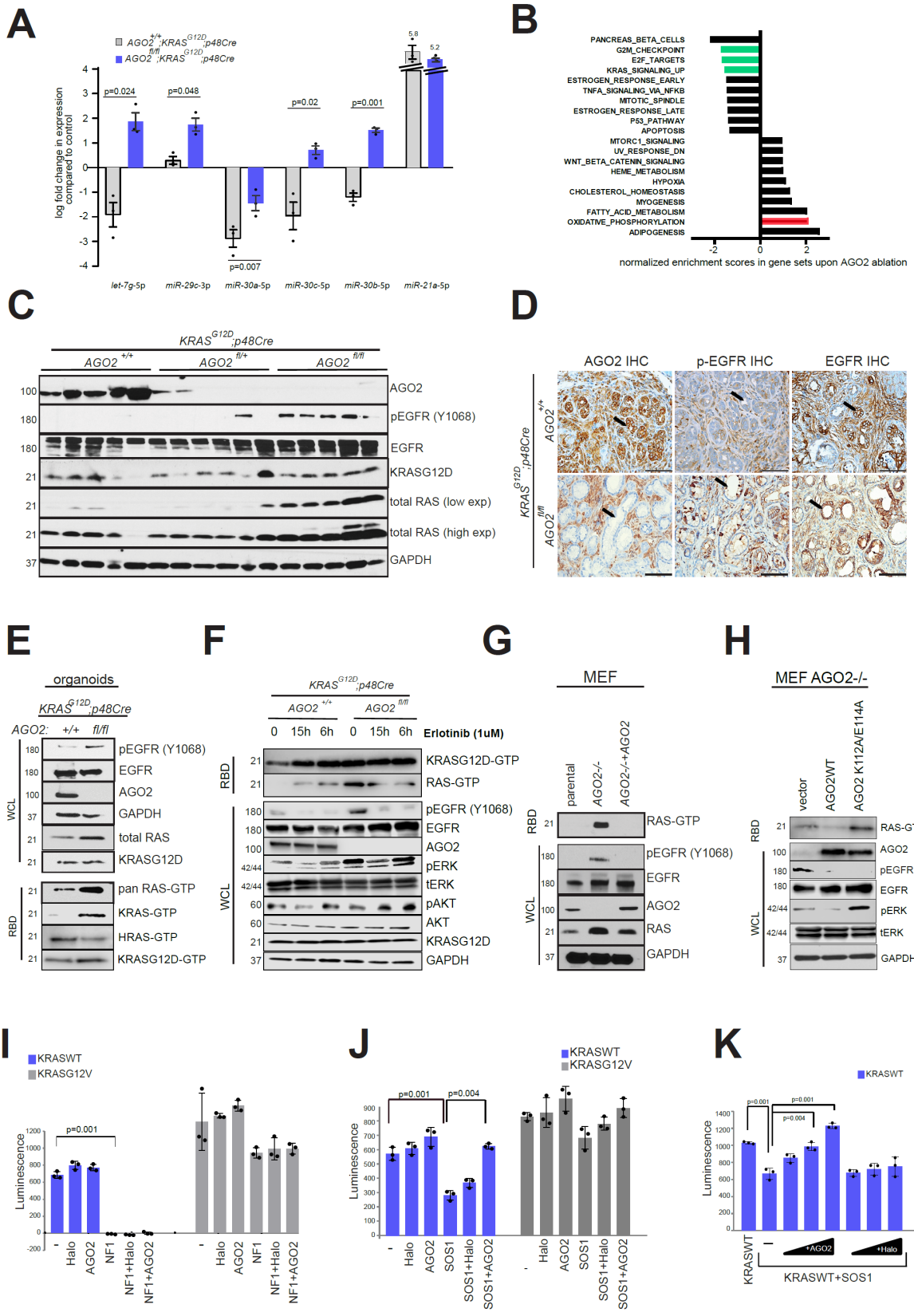
A
AGO2+/+;KRASG12D;p48Cre
AGO2fl/fl;KRASG12D;p48Cre
log fold change in expression compared to control
p=0.024
p=0.048
p=0.007
p=0.02
p=0.001
5.8
5.2
let-7g-5p
miR-29c-3p
miR-30a-5p
miR-30c-5p
miR-30b-5p
miR-21a-5p
B
PANCREAS_BETA_CELLS
G2M_CHECKPOINT
E2F_TARGETS
KRAS_SIGNALING_UP
ESTROGEN_RESPONSE_EARLY
TNFA_SIGNALING_VIA_NFKB
MITOTIC_SPINDLE
ESTROGEN_RESPONSE_LATE
P53_PATHWAY
APOPTOSIS
MTORC1_SIGNALING
UV_RESPONSE_DN
WNT_BETA_CATENIN_SIGNALING
HEME_METABOLISM
HYPOXIA
CHOLESTEROL_HOMEOSTASIS
MYOGENESIS
FATTY_ACID_METABOLISM
OXIDATIVE_PHOSPHORYLATION
ADIPOGENESIS
normalized enrichment scores in gene sets upon AGO2 ablation
C
KRASG12D;p48Cre
AGO2+/+
AGO2fl/+
AGO2fl/fl
AGO2
pEGFR (Y1068)
EGFR
KRASG12D
total RAS (low exp)
total RAS (high exp)
GAPDH
D
AGO2 IHC
p-EGFR IHC
EGFR IHC
KRASG12D;p48Cre
AGO2+/+
AGO2fl/fl
E
organoids
KRASG12D;p48Cre
AGO2: +/+ fl/fl
WCL
RBD
pEGFR (Y1068)
EGFR
AGO2
GAPDH
total RAS
KRASG12D
pan RAS-GTP
KRAS-GTP
HRAS-GTP
KRASG12D-GTP
F
KRASG12D;p48Cre
AGO2+/+
AGO2fl/fl
0 15h 6h 0 15h 6h Erlotinib (1uM)
RBD
WCL
KRASG12D-GTP
RAS-GTP
pEGFR (Y1068)
EGFR
AGO2
pERK
tERK
pAKT
AKT
KRASG12D
GAPDH
G
MEF
parental
AGO2-/-
AGO2-/-+AGO2
RBD
WCL
RAS-GTP
pEGFR (Y1068)
EGFR
AGO2
RAS
GAPDH
H
MEF AGO2-/-
vector
AGO2WT
AGO2 K112A/E114A
RBD
WCL
RAS-GTP
AGO2
pEGFR (Y1068)
EGFR
pERK
tERK
GAPDH
I
KRASWT
KRASG12V
Luminescence
p=0.001
-
Halo
AGO2
NF1
NF1+Halo
NF1+AGO2
J
KRASWT
KRASG12V
Luminescence
p=0.001
p=0.004
-
Halo
AGO2
SOS1
SOS1+Halo
SOS1+AGO2
K
KRASWT
Luminescence
p=0.001
p=0.001
p=0.004
KRASWT
+AGO2
+Halo
KRASWT+SOS1

Figure 2.6 AGO2 modulates microRNAs and limits RAS activation to control OIS.
(A) Plot showing relative expression of microRNAs from pancreata obtained from three mice from each of the indicated genotypes at the 500-day time point. Log fold change values were generated relative to microRNA expression in three *p48Cre* mice (used as reference). Two sided t-tests were performed to determine the P value and error bars are mean values +/- SEM.

(B) GSEA (Gene Set Enrichment Analysis) of transcriptional changes significantly enriched (FDR value <0.05) in pancreatic tissue. Green and red bars represent relevant gene sets discussed in the main text.

(C) Immunoblot analysis from individual pancreata obtained from 12-week old mice of the indicated genotypes.

(D) Representative images of IHC analysis in PanINs of 12-week old mice in the indicated genotypes. Arrows indicate PanINs. Scale bar, 100 μm.

(E) Immunoblot analysis of pancreatic ductal organoids obtained from 12-week old $AGO2^{+/+}$;$KRAS^{G12D}$;*p48Cre* and $AGO2^{fl/fl}$;$KRAS^{G12D}$;*p48Cre* mice. Total RAS-GTP was determined using the RAF binding assay (RBD) followed by immunoblotting with indicated antibodies.

(F) Immunoblot analysis of pancreatic organoids upon treatment with erlotinib at 6h and 12h time points.

(G) Immunoblot analysis of parental, *AGO2-/-*, and *AGO2-/-* + *AGO2* mouse embryonic fibroblasts (MEF). RAS-GTP levels were determined by the RAF binding assay.

(H) Immunoblot analysis of *AGO2-/-* MEFs stably expressing vector, wild-type AGO2, and $AGO2^{K112A/E114A}$.

(I) Full-length wild-type KRAS and $KRAS^{G12V}$ proteins were incubated with NF1-GTPase activating protein (GAP) or

(J) SOS1 (guanine exchange factor) in the presence or absence of AGO2, and the levels of free GTP were analyzed (as a luminescence-based readout for GTP hydrolysis). Halo protein was used as a control.

(K) Wild-type KRAS was incubated with SOS1 in the presence of increasing concentrations of either AGO2 or Halo protein prior to measurement of free GTP levels. Significance was assessed in I-K using Welch's two tailed test to determine p values. In relevant panels of this figure, data are presented as mean values +/- SEM. Numbers on the left of the immunoblots in this figure indicate protein molecular weights in kDa.

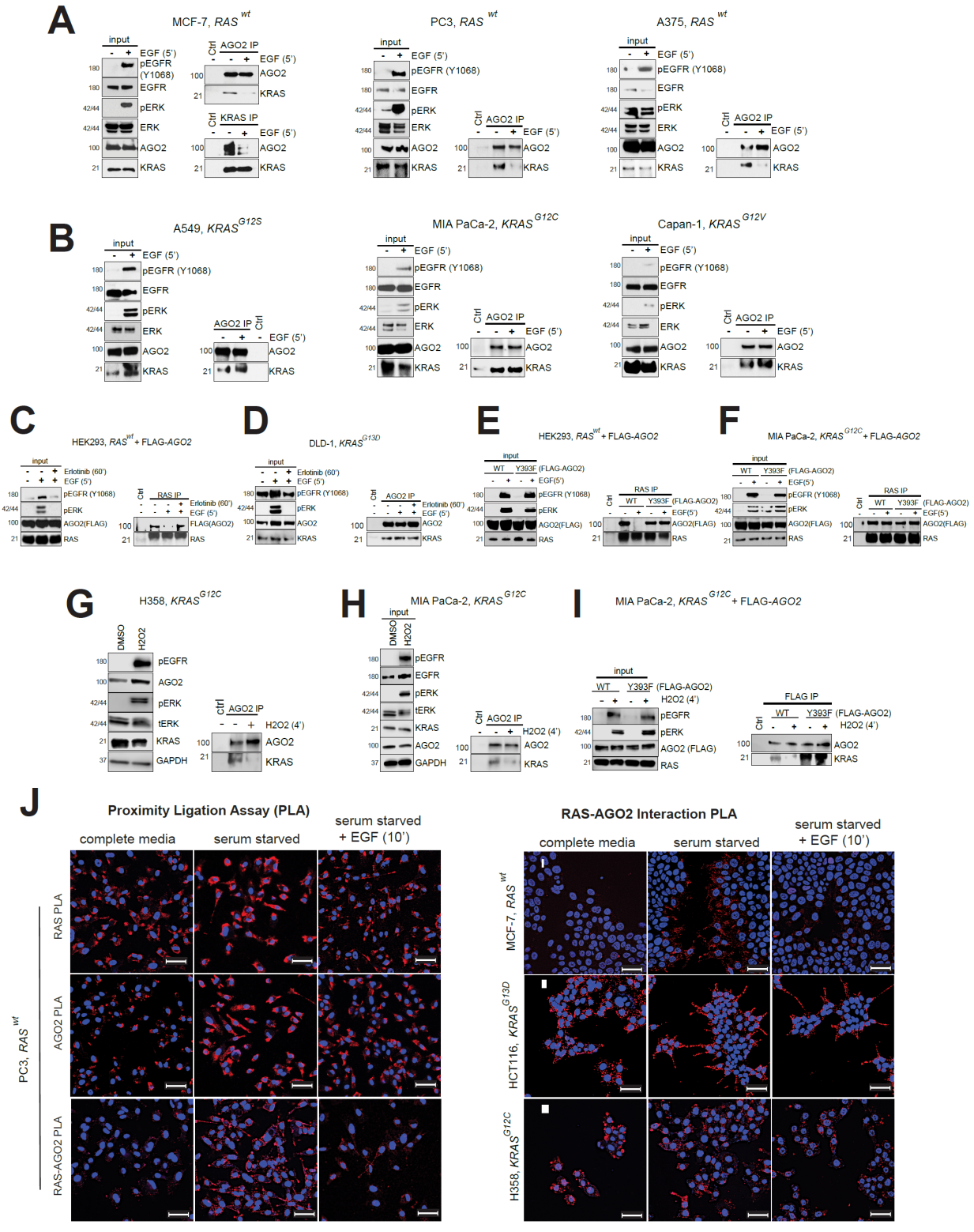

Figure 2.7 Phosphorylation of AGO2^{Y393} disrupts its interaction with KRAS.
(A) Immunoprecipitation (IP) of endogenous AGO2 upon EGF stimulation (5') in the indicated cancer cells expressing wild-type *RAS* followed by immunoblot analysis of KRAS. For MCF7

cells, endogenous co-IP analysis was performed using both AGO2 and KRAS-specific antibodies. For each cell line and panel in this figure, MAPK activation and levels of various proteins are shown as input blots.

(B) IP of endogenous AGO2 upon EGF stimulation (5'), in the indicated cancer cells harboring different *KRAS* mutations, followed by immunoblot analysis of KRAS.

(C) Co-IP and immunoblot analysis of RAS and AGO2 upon EGF stimulation of HEK293 (wild-type *KRAS*) cells expressing FLAG-AGO2 or

(D) DLD-1 ($KRAS^{G13D}$) cells in the presence or absence of erlotinib.

(E) EGF stimulation and RAS co-IP analysis in HEK293 (wild-type *KRAS*) and

(F) MIA PaCa-2 ($KRAS^{G12C}$) cells expressing FLAG-tagged *AGO2* (wild-type or Y393F). IP of endogenous AGO2 upon H_2O_2 treatment (4'), in

(G) H358 and

(H) MIA PaCa-2 cells harboring *KRAS* mutations, followed by immunoblot analysis of KRAS.

(I) H_2O_2 treatment and KRAS-AGO2 co-IP analysis in MIA PaCa-2 ($KRAS^{G12C}$) cells expressing FLAG-tagged *AGO2* (wild-type or Y393F). Numbers on the left of the immunoblots in this panel indicate protein molecular weights in kDa.

(J) Left panels, Representative images of single target (RAS or AGO2) and RAS-AGO2 interaction PLA in wild-type RAS expressing PC3 cells across the indicated cell culture conditions. Right panels, Representative images of PLA to detect RAS-AGO2 interaction in wild-type RAS expressing MCF-7 (panel I) and oncogenic KRAS expressing HCT116 (panel II) and H358 (panel III) cells grown in the indicated culture conditions. PLA signals appear as red dots around DAPI stained nuclei in blue. Scale bar, 50 μm.

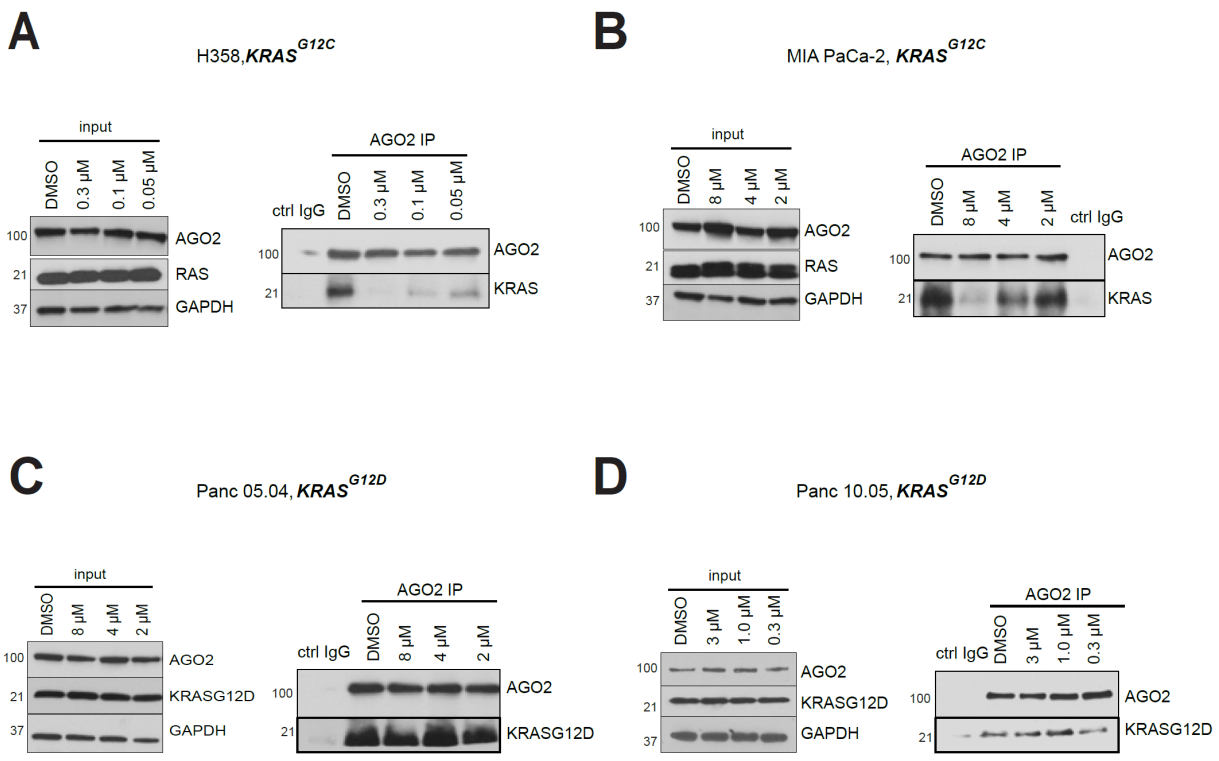

Figure 2.8 ARS-1620, a G12C-specific inhibitor, disrupts the KRAS^{G12C}-AGO2 interaction. (A) IP of endogenous AGO2 followed by immunoblot to detect KRAS in *KRAS^{G12C}* harboring H358 and

(B) MIA PaCa-2 cells treated with varying concentrations of ARS-1620 for three and nine hours, respectively.

(C and D) *KRAS^{G12D}* and wild-type *KRAS* harboring (C) Panc 05.04 and (D) Panc 10.05 cells, respectively, treated with ARS-1620 for 24h followed by AGO2 IP and immunoblot analysis of KRAS^{G12D} or KRAS. For each cell line, input blots for AGO2 and RAS are shown.

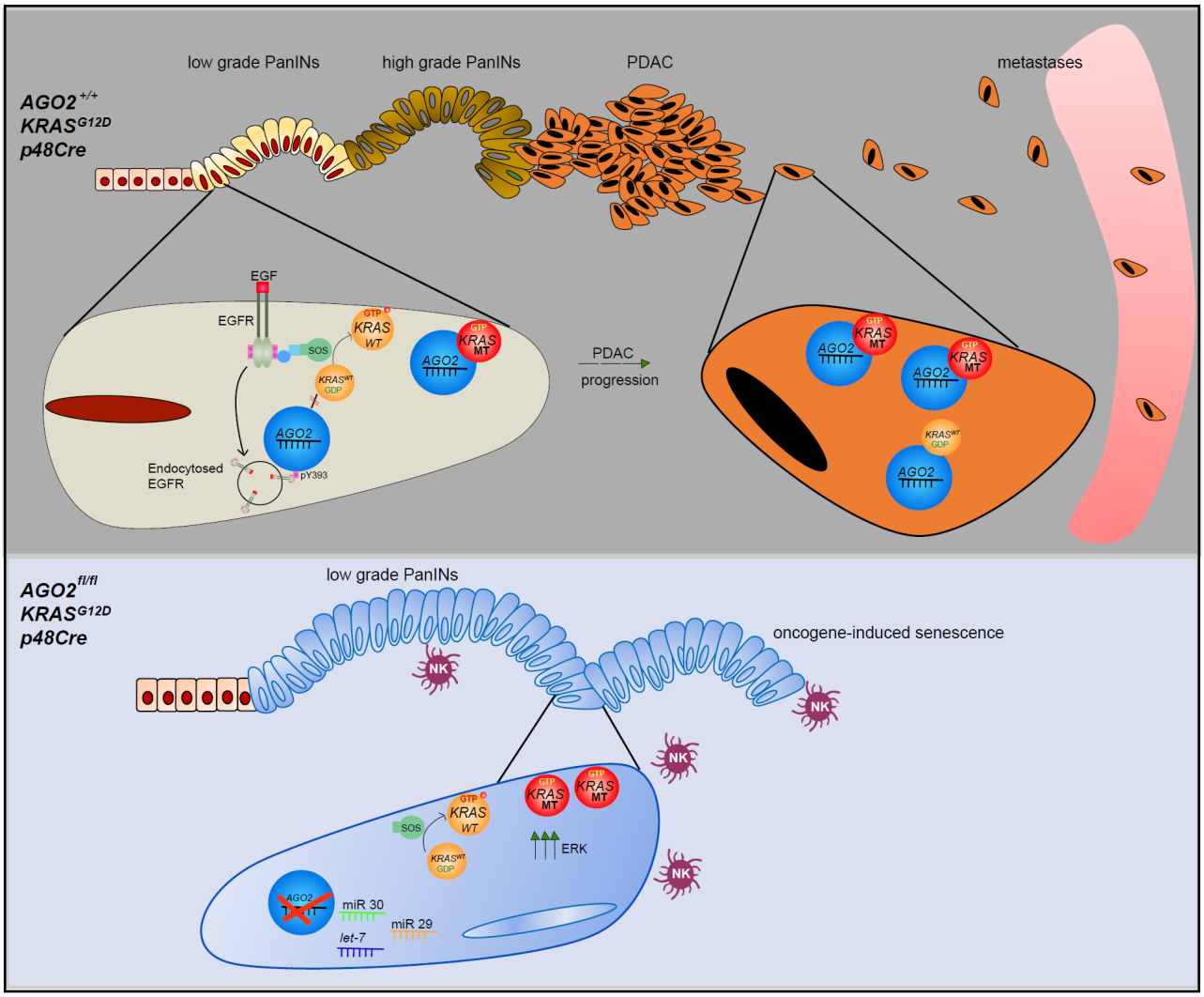

Figure 2.9. Schematic model showing the essential role of *AGO2* in PDAC progression. Expression of *KRAS*^{G12D} in normal pancreatic cells initiates low grade PanINs which progress to higher grade PanINs, PDAC, and metastases. PanIN formation requires EGFR that can phosphorylate AGO2 to disrupt the KRAS-AGO2 interaction and is, therefore, AGO2-independent. PDAC progression is associated with increased expression of KRAS and AGO2 at the membrane. *AGO2* ablation results in increased expression of microRNAs that regulate cell proliferation and senescence and also activates KRAS to promote oncogene-induced senescence. OIS due to *AGO2* loss prevents progression of low grade PanINs to PDAC and leads to infiltration by natural killer (NK) cells.

References

1. Siegel, R.L., K.D. Miller, and A. Jemal, *Cancer statistics, 2019.* CA Cancer J Clin, 2019. **69**(1): p. 7-34.
2. Simanshu, D.K., D.V. Nissley, and F. McCormick, *RAS Proteins and Their Regulators in Human Disease.* Cell, 2017. **170**(1): p. 17-33.
3. Pylayeva-Gupta, Y., E. Grabocka, and D. Bar-Sagi, *RAS oncogenes: weaving a tumorigenic web.* Nat Rev Cancer, 2011. **11**(11): p. 761-74.
4. Hingorani, S.R., et al., *Preinvasive and invasive ductal pancreatic cancer and its early detection in the mouse.* Cancer Cell, 2003. **4**(6): p. 437-50.
5. Herreros-Villanueva, M., et al., *Mouse models of pancreatic cancer.* World J Gastroenterol, 2012. **18**(12): p. 1286-94.
6. Drosten, M., C. Guerra, and M. Barbacid, *Genetically engineered mouse models of K-Ras-driven lung and pancreatic tumors: validation of therapeutic targets.* Cold Spring Harb Perspect Med, 2018. **8**(5): p. 1-18.
7. Ardito, C.M., et al., *EGF receptor is required for KRAS-induced pancreatic tumorigenesis.* Cancer Cell, 2012. **22**(3): p. 304-17.
8. Navas, C., et al., *EGF receptor signaling is essential for k-ras oncogene-driven pancreatic ductal adenocarcinoma.* Cancer Cell, 2012. **22**(3): p. 318-30.
9. Wang, J.P., et al., *Erlotinib is effective in pancreatic cancer with epidermal growth factor receptor mutations: a randomized, open-label, prospective trial.* Oncotarget, 2015. **6**(20): p. 18162-73.
10. McCormick, F., *KRAS as a therapeutic target.* Clin Cancer Res, 2015. **21**(8): p. 1797-801.
11. Shankar, S., et al., *KRAS Engages AGO2 to Enhance Cellular Transformation.* Cell Rep, 2016. **14**(6): p. 1448-1461.
12. Shen, J., et al., *EGFR modulates microRNA maturation in response to hypoxia through phosphorylation of AGO2.* Nature, 2013. **497**(7449): p. 383-7.
13. Kawaguchi, Y., et al., *The role of the transcriptional regulator Ptf1a in converting intestinal to pancreatic progenitors.* Nat Genet, 2002. **32**(1): p. 128-34.
14. O'Carroll, D., et al., *A Slicer-independent role for Argonaute 2 in hematopoiesis and the microRNA pathway.* Genes Dev, 2007. **21**(16): p. 1999-2004.
15. Ettel, M., et al., *Expression and prognostic value of NSD1 and SETD2 in pancreatic ductal adenocarcinoma and its precursor lesions.* Pathology, 2019. **51**(4): p. 392-398.
16. Robinson, M.D. and A. Oshlack, *A scaling normalization method for differential expression analysis of RNA-seq data.* Genome Biol, 2010. **11**(3): p. R25.
17. Smyth, G.K., *Linear models and empirical bayes methods for assessing differential expression in microarray experiments.* Stat Appl Genet Mol Biol, 2004. **3**: p. Article3.
18. Law, C.W., et al., *voom: Precision weights unlock linear model analysis tools for RNA-seq read counts.* Genome Biol, 2014. **15**(2): p. R29.
19. Waters, A.M., et al., *Evaluation of the selectivity and sensitivity of isoform- and mutation-specific RAS antibodies.* Sci Signal, 2017. **10**(498).
20. Heijmans, J., et al., *ER stress causes rapid loss of intestinal epithelial stemness through activation of the unfolded protein response.* Cell Rep, 2013. **3**(4): p. 1128-39.

21. Kopp, J.L., et al., *Identification of Sox9-dependent acinar-to-ductal reprogramming as the principal mechanism for initiation of pancreatic ductal adenocarcinoma.* Cancer Cell, 2012. **22**(6): p. 737-50.
22. Qiu, W., et al., *Disruption of p16 and activation of Kras in pancreas increase ductal adenocarcinoma formation and metastasis in vivo.* Oncotarget, 2011. **2**(11): p. 862-73.
23. Morris, J.P.t., et al., *Dicer regulates differentiation and viability during mouse pancreatic cancer initiation.* PLoS One, 2014. **9**(5): p. e95486.
24. Hingorani, S.R., et al., *Trp53R172H and KrasG12D cooperate to promote chromosomal instability and widely metastatic pancreatic ductal adenocarcinoma in mice.* Cancer Cell, 2005. **7**(5): p. 469-83.
25. Guerra, C. and M. Barbacid, *Genetically engineered mouse models of pancreatic adenocarcinoma.* Mol Oncol, 2013. **7**(2): p. 232-47.
26. Collins, M.A., et al., *Metastatic pancreatic cancer is dependent on oncogenic Kras in mice.* PLoS One, 2012. **7**(12): p. e49707.
27. Caldwell, M.E., et al., *Cellular features of senescence during the evolution of human and murine ductal pancreatic cancer.* Oncogene, 2012. **31**(12): p. 1599-608.
28. Collisson, E.A., et al., *A central role for RAF-->MEK-->ERK signaling in the genesis of pancreatic ductal adenocarcinoma.* Cancer Discov, 2012. **2**(8): p. 685-93.
29. Sun, J.C. and L.L. Lanier, *NK cell development, homeostasis and function: parallels with CD8(+) T cells.* Nat Rev Immunol, 2011. **11**(10): p. 645-57.
30. Krizhanovsky, V., et al., *Implications of cellular senescence in tissue damage response, tumor suppression, and stem cell biology.* Cold Spring Harb Symp Quant Biol, 2008. **73**: p. 513-22.
31. Krizhanovsky, V., et al., *Senescence of activated stellate cells limits liver fibrosis.* Cell, 2008. **134**(4): p. 657-67.
32. Morton, J.P., et al., *Mutant p53 drives metastasis and overcomes growth arrest/senescence in pancreatic cancer.* Proc Natl Acad Sci U S A, 2010. **107**(1): p. 246-51.
33. Jones, S., et al., *Core signaling pathways in human pancreatic cancers revealed by global genomic analyses.* Science, 2008. **321**(5897): p. 1801-6.
34. Maitra, A., et al., *Precursors to invasive pancreatic cancer.* Adv Anat Pathol, 2005. **12**(2): p. 81-91.
35. Schmick, M., et al., *KRas localizes to the plasma membrane by spatial cycles of solubilization, trapping and vesicular transport.* Cell, 2014. **157**(2): p. 459-471.
36. Chung, W.J., et al., *Kras mutant genetically engineered mouse models of human cancers are genomically heterogeneous.* Proc Natl Acad Sci U S A, 2017. **114**(51): p. E10947-E10955.
37. Halbrook, C.J., et al., *Mitogen-activated protein kinase kinase activity maintains acinar-to-ductal metaplasia and is required for organ regeneration in pancreatitis.* Cell Mol Gastroenterol Hepatol, 2017. **3**(1): p. 99-118.
38. Gullberg, M., et al., *Cytokine detection by antibody-based proximity ligation.* Proc Natl Acad Sci U S A, 2004. **101**(22): p. 8420-4.
39. Soderberg, O., et al., *Direct observation of individual endogenous protein complexes in situ by proximity ligation.* Nat Methods, 2006. **3**(12): p. 995-1000.
40. Martinez, I., et al., *miR-29 and miR-30 regulate B-Myb expression during cellular senescence.* Proc Natl Acad Sci U S A, 2011. **108**(2): p. 522-7.

41. Johnson, C.D., et al., *The let-7 microRNA represses cell proliferation pathways in human cells.* Cancer Res, 2007. **67**(16): p. 7713-22.
42. Patranabis, S. and S.N. Bhattacharyya, *Phosphorylation of Ago2 and Subsequent Inactivation of let-7a RNP-Specific MicroRNAs Control Differentiation of Mammalian Sympathetic Neurons.* Mol Cell Biol, 2016. **36**(8): p. 1260-71.
43. Ashton, T.M., et al., *Oxidative Phosphorylation as an Emerging Target in Cancer Therapy.* Clin Cancer Res, 2018. **24**(11): p. 2482-2490.
44. Siveke, J.T. and H.C. Crawford, *KRAS above and beyond - EGFR in pancreatic cancer.* Oncotarget, 2012. **3**(11): p. 1262-3.
45. Boj, S.F., et al., *Organoid models of human and mouse ductal pancreatic cancer.* Cell, 2015. **160**(1-2): p. 324-38.
46. Oda, K., et al., *A comprehensive pathway map of epidermal growth factor receptor signaling.* Mol Syst Biol, 2005. **1**: p. 1-17.
47. Lowenstein, E.J., et al., *The Sh2 and Sh3 Domain Containing Protein Grb2 Links Receptor Tyrosine Kinases to Ras Signaling.* Cell, 1992. **70**(3): p. 431-442.
48. Hayes, T.K. and C.J. Der, *Mutant and wild-type Ras: co-conspirators in cancer.* Cancer Discov, 2013. **3**(1): p. 24-26.
49. Young, A., D. Lou, and F. McCormick, *Oncogenic and wild-type Ras play divergent roles in the regulation of mitogen-activated protein kinase signaling.* Cancer Discov, 2013. **3**(1): p. 112-23.
50. Broderick, J.A., et al., *Argonaute protein identity and pairing geometry determine cooperativity in mammalian RNA silencing.* RNA, 2011. **17**(10): p. 1858-69.
51. Tan, X., et al., *Stress-Induced EGFR Trafficking: Mechanisms, Functions, and Therapeutic Implications.* Trends Cell Biol, 2016. **26**(5): p. 352-366.
52. Janes, M.R., et al., *Targeting KRAS mutant cancers with a covalent G12C-specific inhibitor.* Cell, 2018. **172**(3): p. 578-589.
53. Lito, P., et al., *Allele-specific inhibitors inactivate mutant KRAS G12C by a trapping mechanism.* Science, 2016. **351**(6273): p. 604-8.
54. Perez-Mancera, P.A., et al., *What we have learned about pancreatic cancer from mouse models.* Gastroenterology, 2012. **142**(5): p. 1079-92.
55. Gutmann, D.H., K. Hunter-Schaedle, and K.M. Shannon, *Harnessing preclinical mouse models to inform human clinical cancer trials.* J Clin Invest, 2006. **116**(4): p. 847-52.
56. Sagiv, A., et al., *Granule exocytosis mediates immune surveillance of senescent cells.* Oncogene, 2013. **32**(15): p. 1971-7.
57. Lyu, G., et al., *TGF-beta signaling alters H4K20me3 status via miR-29 and contributes to cellular senescence and cardiac aging.* Nat Commun, 2018. **9**(1): p. 2560.
58. Hu, Z., et al., *MicroRNA-29 induces cellular senescence in aging muscle through multiple signaling pathways.* Aging (Albany NY), 2014. **6**(3): p. 160-75.
59. Wang, X., et al., *Regulation of let-7 and its target oncogenes (Review).* Oncol Lett, 2012. **3**(5): p. 955-960.
60. Balzeau, J., et al., *The LIN28/let-7 Pathway in Cancer.* Front Genet, 2017. **8**: p. 31.
61. Kwon, J.J., et al., *Novel role of miR-29a in pancreatic cancer autophagy and its therapeutic potential.* Oncotarget, 2016. **7**(44): p. 71635-71650.
62. Dou, Z., et al., *Autophagy mediates degradation of nuclear lamina.* Nature, 2015. **527**(7576): p. 105-9.

63. Kourtidis, A. and P.Z. Anastasiadis, *Close encounters of the RNAi kind: the silencing life of the adherens junctions.* Curr Opin Cell Biol, 2018. **54**: p. 30-36.
64. Zeng, Y. and B.R. Cullen, *RNA interference in human cells is restricted to the cytoplasm.* RNA, 2002. **8**(7): p. 855-60.
65. Stalder, L., et al., *The rough endoplasmatic reticulum is a central nucleation site of siRNA-mediated RNA silencing.* EMBO J, 2013. **32**(8): p. 1115-27.
66. Gagnon, K.T., et al., *RNAi factors are present and active in human cell nuclei.* Cell Rep, 2014. **6**(1): p. 211-21.
67. Moor, A.E., et al., *Global mRNA polarization regulates translation efficiency in the intestinal epithelium.* Science, 2017. **357**(6357): p. 1299-1303.
68. Wee, P. and Z.X. Wang, *Epidermal growth factor receptor cell proliferation signaling pathways.* Cancers, 2017. **9**(5): p. 1-45.
69. Yang, M., et al., *Dephosphorylation of tyrosine 393 in argonaute 2 by protein tyrosine phosphatase 1B regulates gene silencing in oncogenic RAS-induced senescence.* Mol Cell, 2014. **55**(5): p. 782-90.
70. Jee, D. and E.C. Lai, *Alteration of miRNA activity via context-specific modifications of Argonaute proteins.* Trends Cell Biol, 2014. **24**(9): p. 546-53.

Chapter 3

Loss of AGO2 Induces Senescence Via PTP1B Inhibition in Mutant *HRAS* and *NRAS* Driven Cancers[2]

Abstract

Activating mutations in *RAS* GTPases drive nearly 30% of all human cancers. Here, we describe a novel role for Argonaute 2 (AGO2) in maintaining a proliferative state in mutant HRAS and NRAS driven cancers. We identified an endogenous interaction between AGO2 and RAS in both wild-type and mutant HRAS/NRAS cells. This binding was regulated through an EGFR signaling cascade in multiple cell lineages, and EGF stimulation specifically disrupted AGO2 interaction with wild-type but not mutant RAS via phosphorylation of AGO2-Y393. Knockdown of AGO2 led to a profound decrease in mutant HRAS/NRAS driven cell lines but not WT RAS cells. These cells demonstrated increased beta-galactosidase staining and induction of *TP53*, $p21^{WAF1/Cip1}$, and p16 expression, suggesting that decreased AGO2 expression is sufficient to induce senescence in mutant but not WT HRAS/NRAS cells. Furthermore, we observed an induction of reactive oxygen species following AGO2 knockdown which induced increased pEGFR and pERK signaling through inhibition of the PTP1B phosphatase. Loss AGO2 in mutant HRAS/NRAS cell lines also led to an inhibition of migration and metastasis in a zebrafish xenograft model. Taken together these results suggest that AGO2's interaction with mutant HRAS and NRAS plays a key role in

[2] This chapter is under submission for publication as part of the following manuscript: Siebenaler R.F., et al., Loss of AGO2 Induces Senescence Via PTP1B Inhibition in Mutant *HRAS* and *NRAS* Driven Cancers. *Neoplasia*, 2020.

mutant RAS driven proliferation and both mutant HRAS and NRAS depend on AGO2 to overcome senescence.

Introduction

RAS GTPases act as growth factor receptor-regulated molecular switches, modulating cellular growth, survival, and differentiation. RAS proteins cycle between through nucleotide loading of active GTP-bound and inactive GDP-bound states, and regulator proteins, such as GTPase activating proteins (GAPs) or guanine exchange factors (GEFs), promote nucleotide exchange at the plasma membrane under the control of EGFR and other growth factor receptors [1-4]. Activating mutations in *RAS* occur in over 30% of all cancers particularly, pancreatic, melanoma, myeloma, and colon cancers [2, 5, 6]. Oncogenic mutations in RAS inhibit intrinsic GTPase activity, leading to constitutively active RAS signaling independent of growth factor receptor control driving cell transformation [1, 2, 7]. Despite our understanding of the signaling events triggered by oncogenic RAS, targeting RAS clinically remains a particularly challenging prospect [3, 8].

With the goal of identifying novel partners and regulators of mutant RAS mediated oncogenesis, we recently probed a panel of human cancer cell lines for protein partners of RAS and identified an interaction between KRAS and Argonaute 2 (AGO2) [9], a key member of the RNA-induced silencing complex (RISC). Specifically, the Switch II domain of KRAS bound to the N-terminus of AGO2. While this interaction was observed in both wild-type (WT) and mutant KRAS expressing cell lines, we found that AGO2 was required for oncogenic *KRAS*-driven cellular transformation. AGO2's RISC activity and miRNA duplex unwinding was inhibited by interaction with mutant KRAS [9], suggesting that the RAS-AGO2 interaction plays a dynamic

role in promoting mutant KRAS driven cancer. Furthermore, we recently extended these initial observations in a mutant *Kras* driven mouse model of pancreatic ductal adenocarcinoma (PDAC) with co-knockout of Ago2 (Chapter 2). Loss of Ago2 lead to an increase in oncogene induced senescence (OIS) from an induction of wild-type (WT) RAS-GTP signaling. These findings suggest an important role for the AGO2-RAS interaction in promoting a RAS driven oncogenic state.

Mutations in *HRAS* and *NRAS* account for approximately 4% and 11% of all *RAS* driven cancers respectively [6], and despite the evidence for a functional role of mutant KRAS-AGO2 interaction in cellular transformation and proliferation, we did not examine the role of AGO2 in mutant *HRAS* or *NRAS* cancers. Considering the high level of amino acid homology between RAS isoforms, particularly in the Switch II domain [6], we predicted that AGO2 also interacted with the HRAS and NRAS isoforms. Here, we identify AGO2-HRAS and AGO2-NRAS interactions in both WT and mutant *RAS* cell lines, and we characterize an endogenous regulatory mechanism through EGFR for the association of RAS proteins and AGO2. In addition, we identify a requirement for AGO2 in mutant *HRAS* and *NRAS* driven cell proliferation. Following knockdown of AGO2, these cells became senescent and displayed upregulation of multiple senescence pathways including *TP53* (p53), $p21^{WAF1/Cip1}$ (p21), and $p16^{Ink4a}$ (CDKN2A; p16) [10, 11]. However, WT *RAS* cells did not demonstrate changes in proliferation or senescence upon AGO2 knockdown, suggesting that mutant *HRAS* and *NRAS* cells rely on AGO2 expression but not WT RAS driven cells. Decreased expression of AGO2 increased production of reactive oxygen species, leading to an inhibition of protein phosphatase PTP1B and increased levels of pEGFR. Finally, we find that loss of AGO2 inhibits the migratory and metastatic capacity of both mutant *HRAS* and *NRAS* cells. Taken together these results suggest that AGO2 interactions with mutant HRAS and

NRAS play a key role in mutant *RAS* driven proliferation, and both mutant HRAS and NRAS depend on AGO2 to overcome senescence.

Materials and Methods

Cell culture, transfection and EGF stimulation

All cell lines (detailed in **Supplemental Table 3.1**) were obtained from the American Type Culture Collection (ATCC) or DSMZ-German Collection of Microorganisms and Cell Cultures (DSMZ; Kasumi-2). Cells were cultured following ATCC culture methods in media supplemented with the corresponding serum and antibiotics. Additionally, cells were routinely genotyped and tested bi-weekly for mycoplasma contamination. For EGF stimulation, cells were grown to approximately 80% confluence and washed with PBS three times. Cells were incubated overnight (16 hours) in serum free media. EGF stimulation was performed for 5 minutes with 100 ng/µl of epidermal growth factor (Gibco) at 37°C. After stimulation, cells were washed and protein lysates were prepared in K Buffer lysis buffer.

U2OS were transfected with different *AGO2* constructs using Fugene HD (Promega) according to manufacturers' protocols. For EGFR stimulation with transient AGO2 construct overexpression, cells were transfected approximately 16 hours prior to overnight serum starvation and EGF stimulation.

Immunoprecipitation (IP) and Immunoblot Analysis

For IP analysis, protein lysates were prepared in K Buffer (20mM Tris pH 7.0, 5 mM EDTA, 150mM NaCl, 1% Triton X100, 1 mM DTT, phosphatase inhibitors, and protease inhibitors). Typically,150-200 µg of protein lysates (RAS10 IP: 150 µg; AGO2 IP: 200 µg; KRAS IP: 150

μg) were pre-cleared with 10 μl of Protein A/G agarose beads (Santa Cruz) for 1 hour. Pre-cleared lysates were incubated with 5-10 μg of the indicated primary antibodies targeting the protein of interest or with corresponding isotype controls overnight at 4°C. 30 μl of Protein A/G beads were then added to immune complexes and incubated for 1-3 hours at 4°C, spun, washed in 150-300 mM NaCl containing K Buffer prior to separation of immunoprecipitates by SDS PAGE (Full antibody list detailed in **Supplemental Table 3.2**).

Plasmids

Full length FH-*AGO2* constructs were obtained from Addgene (pIRESneo-FLAG/HA-AGO2 10822, PI:Thomas Tuschl). *AGO2Y*^{393F} mutant construct was generated using the QuikChange II XL Site-Directed Mutagenesis Kit (Agilent) from the FH-*AGO2* plasmid described above using the primers:

hAGO2_Y393F_Fwd 5'*AAATTCACGGACGAATGGATCTGTGTTGAAACTTGCAC*3'

hAGO2_Y393F_Rev 5'*GTGCAAGTTTCAACACAGATCCATTCGTCCGTGAATTT*3'.

DNA sequences were confirmed using Sanger sequencing at the University of Michigan Sequencing Core.

Proximity Ligation Assay (PLA)

U2OS, T24, and Mel-Juso cell lines were cultured on 8 well chamber slides and serum starved overnight. After indicated treatment/stimulation, cells were fixed with 4% paraformaldehyde, permeabilized using 0.1%Tween. Subsequent PLA staining was performed as per protocol provided by themanufacturer (DUOlink kit, Millipore/Sigma). Antibodies were validated for use in (**Chapter 2**). PLA was performed using RAS10 or AGO2 antibodies either alone or in

combination and imaged using Nikon A1B confocal microscope.

shRNA Viral Transduction and AGO2 Knockdown Assays

T24, Kasumi-2, Mel-Juso, SK-MEL-2, H1299, HeLa, and A375 cells were treated with two independent shRNAs in viral vectors (validated Mission shRNA lentiviral plasmids, Sigma) targeting AGO2 (TRCN0000011203 and TRCN0000007867). Cells were incubated at 37 °C in 5% CO_2 and were selected with puromycin over a period of 5 days.

PTP1B inhibition and siRNA Transfection

The Screen-Well Phosphatase Inhibitor Library (Enzolifesiences; BML-2834) was tested against NIH 3T3 AGO2$^{-/-}$ [9] at 10 mM concentration and dissolved in DMSO and treated for 16 hours. For hydrogen peroxide treatment, cells were treated in 4 mM H_2O_2 for 4 minutes. PTP1B siRNAs were obtained from Dharmacon.

Cellular Proliferation Assays

Following puromycin selection, AGO2 knockdown stable cell lines were measured for proliferation through IncuCyte. Approximately 25,000 cells were seeded in triplicate on 24-well plates and measured over a 4-5 day period. Confluence rate and standard deviation between replicates were measured on IncuCyte and calculated via Incucyte Zoom software. Kasumi-2 leukemia cell lines were manually counted via hemocytometer [12] in triplicate experiments, and results were analyzed in GraphPad Prism 8 for statistical significance.

β-galactosidase senescence assay

Following puromycin selection, AGO2 knockdown stable cell lines were seeded on a 6-well plate. β-galactosidase staining was performed using the Senescence β-Galactosidase Staining Kit #9860 (Cell Signaling) following the established protocol.

RAS-GTP pull down assay

Protein lysates were prepared from cell lines using Mg^{2+} containing lysis buffer. The RAS-RAF interaction was studied using the RBD agarose beads as per manufacturer's instructions (Millipore). Pull down assays were performed using the lysates from pancreatic ductal organoids and cell lines as indicated. The pull down of RAS by RBD agarose beads indicates the presence of active GTP-bound RAS interacting with RAF1.

Cellular Migration Assays

Following puromycin selection, AGO2 knockdown stable cell lines were seeded on a 24-well FluoroBlok plate (Corning) in triplicate. Cells were seeded in the upper chamber in serum free media with full serum media in the bottom chamber per the manufacturer's instructions. Cells were incubated approximately 24 hours at 37°C in 5% CO_2. Following migration assay, media was removed from the bottom chamber and cells were stained with CellTrace Calcein Green, AM (Invitrogen). Plates were read for fluorescent signal on Tecan Infinite M1000 Pro. Results were analyzed in GraphPad Prism 8 for statistical significance.

Zebrafish Xenograft Metastasis Assays

Wild type ABTL zebrafish were maintained according to standard protocols, and embryos were

generated by natural pairwise mating between ABTL zebrafish. These embryos are then raised at 28.5°C on a 14h light/10h dark cycle in a 100 mm petri dish containing aquarium water with methylene blue to prevent fungal growth.

GFP-expressing cells are resuspended in PBS at a concentration of 1×10^7 cells/ml. 48hr post fertilization wild-type embryos were manually dechorionated then anaesthetized using 0.04 mg/ml tricaine. Approximately 10 nl (approx. 100 cancer cells) of cell suspension were microinjected into the perivitelline space using a borosilliac micropipette tip with filament. Embryos were then returned to aquarium water and washed twice to remove tricaine, then moved to a 96 well plate with one embryo per well and kept at 35°C for the duration of the experiment.

All embryos were imaged at 24 hour intervals to follow metastatic dissemination of injected cells. For each condition, metastasis was visually assessed by counting the total number of distinct cellular foci in the body of the embryos.

All of the metastasis studies were terminated at 7 days post-fertilization in accordance with the approved embryo protocols. Embryos were either imaged directly in the 96 well plates or placed onto a concave glass slide to capture representative images using a fluorescent microscope (Olympus-IX71). For quantification, evidently distinct cell foci in the embryo body were counted 72 hours after the injections.

All experiments were done in approved University of Michigan fish facilities using protocols approved from the University of Michigan Institutional Animal Care and Use Committee (UM-IACUC). For all these experiments, relevant ethical regulations were carefully followed. No statistical methods were used to predetermine sample size for any of the cohort analyses or experiments. The experiments were not randomized and investigators were not blinded to allocation during experiments and outcome assessment unless otherwise stated.

Data availability statement: The datasets generated during and/or analyzed during the current study are available from the corresponding author upon reasonable request.

Results

Endogenous Interaction of AGO2 with HRAS and NRAS

Our previous work identified a novel interaction between KRAS and AGO2 in both WT and mutant *KRAS* cell lines across multiple cell lineages and cancers via co-immunoprecipitation followed by mass spectrometry (coIP MS) [9]. Importantly, AGO2 was found to directly interact with the switch II domain of KRAS through the Y64 residue. While nearly 85% of RAS driven cancers are KRAS mutants [6], HRAS and NRAS share approximately 82-90% of the amino acid sequence with KRAS [13] with the majority of variance occurring within the C-terminal region (**Figure 3.1a**). This hyperviarable region within the C-terminus of RAS accounts for differences in post-translational modifications between the isoforms [14], ultimately leading to varying membrane trafficking and signaling between them [15].

Considering the sequence homology between RAS isoforms is 100% identical within the Switch II region, we asked whether the interaction between AGO2 and HRAS/NRAS could be detected endogenously in human cancer cell lines. Using a pan-RAS antibody specific to the Switch I domain of RAS (RAS10 [16]), we performed coIPs across multiple cell lines expressing both WT and mutant HRAS/NRAS. Interaction with AGO2 was detected in all cell lines expressing either HRAS or NRAS, regardless of mutation status or cell lineage (**Figure 3.1b-c**). Together these results suggest that the AGO2-RAS interaction is consistent across RAS isoforms and mutation status of RAS.

EGFR activation disrupts wild-type RAS-AGO2 interaction but not mutant RAS-AGO2 interaction

Upon receptor tyrosine kinase activation, canonical regulators of RAS, such as the GEF and the GAP proteins, preferentially bind and determine the GDP/GTP bound status of wild-type RAS proteins. These regulators have reduced affinities to oncogenic forms of RAS [17], thereby resulting in constitutive GTP loading of mutant RAS. Recent studies demonstrated that EGFR directly binds and phosphorylates $AGO2^{Y393}$ under hypoxic conditions [18]. These findings prompted us to investigate the effect of EGFR activation on the AGO2-RAS interaction. Using an AGO2 specific antibody [19], We carried out RAS-AGO2 co-immunoprecipitation (co-IP) assays across a panel of cell lines expressing either *HRAS* or *NRAS* upon stimulation with EGF. While basal RAS and AGO2 binding was observed in all the cells, short term EGF stimulation abolished the wild-type HRAS-AGO2 interaction in HeLa and LNCaP cells that was observed using AGO2 antibodies for co-IP analysis (**Figure 3.2a**). Furthermore, short term EGF stimulation also disrupted the interaction of NRAS-AGO2 via AGO2 coIP in MCF7 and HEK293T cells expressing WT *NRAS* (**Figure 3.2b**).

EGFR signaling and cellular trafficking is known to be dysregulated in the presence of mutant *RAS* [20]. Considering the connection between EGFR and RAS signaling, we next asked if mutations in *HRAS* and *NRAS* could alter growth factor control of the AGO2-RAS interaction. Interestingly, EGF stimulation in cells harboring oncogenic HRAS, including T24 [21] ($HRAS^{G12V}$) and Hs578T ($HRAS^{G12D}$) retained binding of endogenous HRAS and AGO2, despite activation of the EGFR/MAPK pathway (**Figure 3.2c**). This was further corroborated in a panel of mutant NRAS cell lines, including Mel-Juso [22] ($NRAS^{Q61L}$) and H1299 [23] ($NRAS^{Q61K}$), which also showed resistance to EGFR regulation of AGO2-NRAS interaction (**Figure 3.2d**). This suggests that the mutant HRAS-AGO2 and mutant NRAS-AGO2 associations are unaffected by

growth factor activation. Together, these observations represent an intriguing difference in the regulation of the RAS-AGO2 interaction between wild-type and mutant *HRAS* and *NRAS* that may indicate an important mechanistic difference between the regulation of WT and oncogenic forms of RAS.

Previous studies have identified multiple phosphorylation sites in AGO2, including Y529, S387, and Y393 [24], that have been mechanistically associated with AGO2 miRNA binding [25], localization [26], and interactions [27], respectively. To test if the previously identified phosphorylation of AGO2 at tyrosine 393 by EGFR [18] has a role in binding to RAS, we tested the ability of a phosphorylation-deficient $AGO2^{Y393F}$ mutant to bind RAS under different conditions. In U2OS [28] (RAS^{WT}) cells, EGF stimulation led to dissociation of wild-type AGO2 from RAS, but the $AGO2^{Y393F}$ mutant continued to bind RAS with or without EGFR activation (**Figure 3.2e**). Together, these data suggest that the wild-type RAS-AGO2 interaction is sensitive to EGFR mediated phosphorylation of $AGO2^{Y393}$ while the oncogenic HRAS or NRAS interaction with AGO2 is resistant to EGFR activation.

To further confirm the disruption of AGO2-RAS interaction and track the localization of these proteins following growth factor activation, we performed proximity ligation assays (PLA) on a subset of the cells tested above expressing either WT (U2OS) or mutant HRAS/NRAS (T24 and Mel-Juso). Our previous work in **Chapter 2** identified that WT AGO2-KRAS was disrupted upon EGF stimulation via IP immunoblot and PLA. This was again confirmed in the U2OS (WT RAS) cell line that saw a remarkable loss of AGO2-RAS co-localization following EGF stimulation via PLA (**Figure 3.2f**). Additionally, both mutant HRAS (T24) and mutant NRAS (Mel-Juso) cells demonstrated continued interaction via PLA of AGO2-RAS despite EGFR activation (**Figure 3.2f**). These results corroborate our co-IP analysis, that the mutant RAS-AGO2

interaction is resistant to EGF stimulation, suggesting that mutant HRAS and NRAS are able to escape endogenous interaction of AGO2-RAS binding.

AGO2 interaction is essential for mutant HRAS and NRAS driven cell proliferation

Considering ubiquity of AGO2 interaction with both WT and mutant RAS, we next asked if AGO2 played a role promoting growth in oncogenic HRAS and NRAS cancer. Using two independent shRNAs targeting AGO2, we generated stable transduced cell lines in a variety of mutant HRAS and NRAS driven cell lines. As expected, knockdown of AGO2 led to a profound reduction in cell proliferation in a mutant $HRAS^{G12V}$ driven urinary bladder carcinoma cell line [21] (T24) and a $HRAS^{G13V}$ driven acute lymphocytic leukemia cell line [29] (Kasumi-2) compared to a matched non-targeting control shRNAs (**Figure 3.3a**). Additionally, two mutant *NRAS* driven melanoma cell lines [22, 30] (Mel-Juso; $NRAS^{Q61L}$, and SK-MEL-2; $NRAS^{Q61H}$) demonstrated marked growth reduction following loss of AGO2 (**Figure 3.3b**). This reduced proliferation potential following AGO2 knockdown suggest that AGO2 acts to promote and maintain oncogenic HRAS and NRAS proliferation in mutant RAS driven cells.

Our previous work on the interaction of AGO2 and KRAS demonstrated that *KRAS* independent cell lines were resistant to loss of AGO2[9]. Knockdown of AGO2 expression in the WT RAS cell line, HeLa, did not alter cell proliferation (**Figure 3.3c**). Interestingly, this was also seen in the melanoma cell line A375 [31] that harbors the $BRAF^{V600E}$ mutation exhibiting a constitutively activated ERK/MAPK pathway, independent of RAS mutation (**Fig. 3.3c**). These results suggest that mutant HRAS and NRAS dependence on AGO2 is unrelated to constitutive MAPK signaling, but rather, a requirement for AGO2-RAS interaction in these cells.

Loss of AGO2 promotes senescence in mutant HRAS and NRAS driven cells through induction of senescence pathways

RAS genes play a central role in the regulation of the cell cycle through mitogenic MAPK signaling, promoting cell proliferation and survival [32]. In order to better understand the effects of AGO2 loss on mutant RAS cells, we next asked if decreased cell proliferation was due to an induction of cellular senescence. Following stable AGO2 knockdown, we performed β-galactosidase staining [33] in the cell line panel described above. β-galactosidase staining is considered a strong biomarker for cellular senescence associated with the build-up in lysosomes [34]. Both mutant *HRAS* (T24) and mutant *NRAS* (Mel-Juso) driven cell lines displayed a significant increase in the number of β-galactosidase positive cells (**Figure 3.4a**). Furthermore, cells displayed morphologic changes consistent with cellular senescence such as increased size, flat appearance, and nucleus changes [35] (**Supplemental Figure 3.1**). These results suggest that the loss of AGO2 led to the induction of senescence in these cells. Additionally, cell lines (HeLa and A375) expressing WT RAS did not lead to an increased level of β-galactosidase staining (**Figure 3.4b**) in keeping with their continued proliferation following AGO2 knockdown.

Senescence is regulated via multiple pathways within cells converging in part on activation of tumor suppressor pathways p53/p21 and p16 [36]. Cellular senescence has been connected to multiple forms of stress including DNA damage [37], oncogene induced senescence [38], replicative senescence [39], and others. While senescence is controlled by a complex set of signaling events and pathways [36], induction of p21 and p16 proteins work to inhibit progression through the cell-cycle via inhibition of cyclin-dependent kinase phosphorylation of Retinoblastoma (Rb) proteins. Activation of Rb via hypophosphorylation leads to cell cycle arrest in G1 phase, inducing cellular senescence [40]. Mutations in *RAS* genes are well known to drive

cell cycle arrest in a process known as oncogene-induced senescence when introduced to primary fibroblast cells [38]. Considering the observed increase in β-galactosidase staining following AGO2 loss, we asked whether these known senescence pathways were activated in our mutant *HRAS* and *NRAS* driven cell lines. Immunoblot analysis of these cells displayed a marked increase in p53, p21, and p16 proteins in AGO2 knockdown cells compared to their non-targeting controls (**Figure 3.4c; Supplemental Figure 3.2**). These two pathways have long been known to be upregulated following $HRAS^{G12V}$ overexpressed in primary rodent fibroblast cells [38], suggesting that AGO2 may play a role in suppressing oncogene induced senescence in transformed cells. Together our results demonstrate that loss of AGO2 is sufficient to induce senescence and arrest cell proliferation via an induction of p53/p21 and p16 senescence pathways.

Since mutations or loss of the *TP53* gene leads to evasion of senescence and other tumor suppressor functions in the progression of multiple tumor types [41-43], we asked if p53 loss could overcome the observed necessity for AGO2 in mutant *NRAS* driven cancers. We selected a non-small cell lung cancer mutant NRAS cell line, H1299 [44], that is *TP53* null. Whereas knockdown of AGO2 was sufficient to decrease proliferation and induce senescence in our previously tested cell lines, H1299 cells did not demonstrate a sensitivity to AGO2 loss, maintaining normal growth and negative β-galactosidase staining (**Supplemental Figure 3.2**) despite expression of mutant NRAS. These findings suggest that AGO2 is a requirement for mutant *HRAS* and *NRAS* driven tumor growth that can be circumvented through the loss of *TP53* expression in these cells.

Loss of AGO2 Promotes Inactivation of PTP1B and EGFR Activation Feedforward Loop

Since AGO2 loss led to an induction of senescence in mutant *HRAS* and *NRAS* driven cells, we next asked if loss of AGO2 could promote hyperactivation of downstream RAS signaling, resulting

in an oncogene induced senescence. Our previous work in a genetically engineered mouse model of *KRAS* driven pancreatic ductal adenocarcinoma (PDAC) demonstrated that AGO2 can partially inhibit KRAS interaction with SOS1. Guanine exchange factors (GEFs), like SOS1, play an important role in the activation of WT RAS by promoting the release of GDP, ultimately leading to the loading of GTP into RAS [45]. Our *in vitro* data demonstrating this inhibition of KRAS-SOS1 activity was confirmed *in vivo* where AGO2 loss lead to an increase in RAS-GTP loading in both WT RAS mouse embryonic fibroblast (MEF) cells and PDAC PanIN organoid cell culture (**Chapter 2**). Confirming this observation, we tested an AGO2 null NIH3T3 mouse fibroblast cell line and found a similar induction of RAS-GTP compared to parental controls (**Figure 3.5a**).

Interestingly, we did not initially observe an increase in pEGFR in our NIH3T3 AGO2 null cells as we had previously seen in our PDAC model (**Chapter 2**). Previous studies observed a deactivation of the protein phosphatase PTP1B via oxidation by reactive oxygen species (ROS) in senescent fibroblasts following the overexpression of mutant $HRAS^{G12V}$ [46]. Additionally, loss of PTP1B activity led to the phosphorylation of $AGO2^{Y393}$ increasing p21 expression through inhibition of AGO2 RNAi function, ultimately leading to senescence. Reactive oxygen species (ROS) are well known product of mutant RAS protein mitogenic signaling [47, 48]. We asked if treatment with ROS, like H_2O_2, may play a role in inhibiting phosphatases in our mutant *HRAS* and *NRAS* cell lines following loss of AGO2. As EGFR phosphorylation is a known target of PTP1B [49] and other AGO2 null fibroblasts show activation of pEGFR (**Supplemental Figure 3.3**), we treated our NIH3T3 AGO2 knockout cell lines with H_2O_2. Following ROS treatment, there was a strong induction of pEGFR-Y1068 (**Figure 3.5b**). This residue is known to recruit RAS activators like GRB2 and SOS1 in human cells [50], accounting for downstream activation of WT RAS in this cell line (**Figure 3.5a**). Considering PTP1B is deactivated by ROS, we next

asked if targeted inhibition of this phosphatase could induce similar activation of Y1068-EGFR *in vitro*. Using a phosphatase inhibitor panel, we saw a large induction of pEGFR-Y1068 in NIH3T3 AGO2$^{-/-}$ cells treated with inhibitors known to target PTP1B (**Figure 3.5c-d**), including MSI-1436 [51] and orthovanadate [52]. Finally, we performed an siRNA knockdown of PTP1B in NIH3T3 cells and saw a similar induction of pEGFR-Y1068 confirming this residue is activated upon loss of PTP1B activity (**Figure 3.5e**).

Since our mutant *HRAS* (T24) and *NRAS* (Mel-Juso) cell lines saw strong induction of senescence upon loss of AGO2, we next explored whether pEGFR-Y1068 could be activated downstream in our knockdown cell lines. Following immunoblotting, we observed not only an increase in pEGFR-Y1068 but also increased levels of pERK (**Figure 3.5f**). These results suggest an induction of RAS-GTP signaling following AGO2 loss similar to what we have observed *in vivo* in our PDAC mouse model and *in vitro* with purified proteins (**Chapter 2**). In addition, we observed a strong increase in production of ROS following AGO2 knockdown (**Figure 3.5g**) supporting our earlier observations that inhibition of PTP1B led to an induction of pEGFR and RAS signaling. Together these results suggest an important new mechanism for the induction of oncogene induced senescence (OIS) in mutant *RAS* driven cells following the loss of AGO2. As we have previously seen (**Chapter 2; Figure 3.6a**), the loss of AGO2 leads to the induction of WT RAS activation by increasing SOS1-RAS GEF activity. This increase in RAS-GTP levels leads to the hyperactivation of downstream signaling pathways such as pERK, ultimately resulting in OIS. Our results here suggest a second, feedforward pathway that is activated upon AGO2 loss (**Figure 3.6b**). As increased SOS1 activation of WT RAS increases mitogenic signaling, ROS production increases following AGO2 loss (**Figure 3.5g**). H_2O_2 and other ROS in turn inactivate PTP1B, causing the accumulation of active pEGFR-Y1068 (**Figure 3.5b-e**). This increased

pEGFR feeds directly into further activating WT RAS and downstream MAPK signaling (**Figure 3.5f**), further promoting oncogene induced senescence in these cells (**Figure 3.4**).

AGO2 interaction promotes cell migration and metastasis in mutant HRAS and NRAS cells

In addition to their role in mitogenic signaling, oncogenic mutations in RAS have been shown to play an important role in the migratory and invasive capacity of transformed cells [53]. Additionally, senescent cells have been previously shown to have a mixed role in the promotion of migration and metastasis in cancer cells. While senescence has been linked to an inhibition of cytoskeletal changes required for migration [54], senescent cells within the stroma have been linked to the induction of motility and migration via increased senescence-associated secretory phenotype (SASP) signaling [55]. Considering the important role of RAS mutations in inducing cellular invasion and metastasis, we asked if knockdown of AGO2 played any role in the migratory capacity of mutant *HRAS* and *NRAS* cells. Using an *in vitro* FluoroBlok transwell migration system (Corning), we placed equal numbers of serum starved cells from our stable AGO2-KD cell lines (T24 (*HRAS*), Mel-Juso (*NRAS*), and HeLa (RAS^{WT})) in the upper chamber with full serum media in the lower chamber. After overnight incubation, cells were stained with calcein green and read for total migration. T24 and Mel-Juso cells with stable AGO2 knockdown demonstrated reduced capacity to migrate compared to their matched non-targeting controls (**Figure 3.7a**). However, WT RAS stable cell line (HeLa) saw no difference in relative number of migratory cells between AGO2 knockdown and control conditions (**Figure 3.7a**).

In order to better assess the role of AGO2 in promoting tumor invasion, we employed an *in vivo* zebrafish cellular metastasis model previously described (**Figure 3.7b**) [56], providing a fast and accurate method to assess invasive and metastatic potential. AGO2 stable knockdown

cells were dyed and injected into the yoke sac of zebrafish embryos, and metastatic foci in the zebrafish body and tail were counted 48 hours after injection. In keeping with our previous results, AGO2 knockdown impaired mutant *HRAS* (T24) and *NRAS* (Mel-Juso) driven cancer cell line ability to metastasize into the tail of zebrafish embryos (**Figure 3.7c**); likewise, HeLa cells expressing WT RAS demonstrated similar levels of metastatic foci between groups (**Figure 3.7d**). This loss in migratory and metastatic potential following AGO2 knockdown may be due to pleotropic effects including induction of senescence or altered miRNA expression and activity. Future studies will be necessary to fully elucidate the mechanistic role AGO2 loss plas in promoting migration and invasion in mutant *HRAS* and *NRAS* driven cells.

Discussion

Following the recent identification of the KRAS-AGO2 interaction [9], here we identify the endogenous interaction of both HRAS-AGO2 and NRAS-AGO2. Mutations in *RAS* are found in many human cancers, and while mutations in *KRAS* represent the majority of human cases, *HRAS* and *NRAS* mutations are common in a wide variety of tumors including melanoma, head and neck tumors, and multiple leukemia types [6]. While the different RAS isoforms function through the same downstream effector pathways, they have functionally distinct membrane localization and subcellular trafficking [15]. Our initial studies identifying the interaction of KRAS-AGO2 also found an inhibition of mutant *KRAS* driven cell proliferation upon loss of AGO2 [9]. However, loss of AGO2 did not lead to an induction of senescence in these cell lines, suggesting a potential functional difference between KRAS and HRAS/NRAS's interaction with AGO2. The reliance of mutant RAS on AGO2 binding appears unique to these cells considering that WT RAS cells were also unperturbed by the knockdown of AGO2 cells. These results suggest that while all *RAS* driven

cancer cells may be dependent on AGO2 binding, the various RAS isoforms differ in their specific reliance on their interaction with RAS to maintain an oncogenic state.

Stimulation of EGFR leads to the disruption of the wild-type RAS-AGO2 interaction across different cell lineages and cancer cell lines. Oncogenic HRAS and NRAS, however, are resistant to this disruption. Our study thus uncovers an important mechanistic difference between wild-type and oncogenic HRAS and NRAS in their interaction with AGO2 and suggests functional relevance. Our data also show that EGFR-mediated phosphorylation of $AGO2^{Y393}$ disrupts wild-type RAS binding. This event both regulates WT-RAS interaction with AGO2 and inhibits microRNA processing [18]. Furthermore, this result confirms our earlier observation that the interaction of AGO2-KRAS was also regulated by EGFR (**Chapter 2**). Recent work by other groups has also found that mutant KRAS promotes phosphorylation of $AGO2^{S387}$ through MAPK signaling, leading to alteration of miRNA maturation and exosome sorting [26]. These results suggest that EGFR-RAS-MAPK signaling play an important role in regulating AGO2 biology within normal cellular physiology and tumor biology.

Our results suggest an important role for AGO2 in the maintenance of cancer proliferation stimulated by oncogenic driver mutations in *HRAS* and *NRAS*. Recent studies have demonstrated that AGO2 is upregulated in bladder transitional cell carcinoma tumors compared to normal bladder. Furthermore, higher expression of AGO2 was correlated with higher tumor grade, metastasis, and lower overall survival time in patients [57], suggesting that AGO2 plays an important role in the aggressiveness of these tumors. Importantly, our results corroborate an important role for AGO2 in these tumors as the mutant $HRAS^{G12V}$ cell line, T24, is of a transitional cell carcinoma background [21]. However, other studies have seen a decrease in AGO2 expression in melanoma compared to normal skin tissues. Importantly, AGO2 expression was seen to decrease

with increasing severity of tumors as cell lines derived from primary tumors demonstrated higher AGO2 protein expression than metastatic cells [58]. These results may suggest that AGO2 may play a dynamic role in promoting tumor development, proliferation, and survival that may depend on not only *RAS* mutational status but also tumor cell lineage or tumor stage/grade.

Interestingly, AGO2 has previously been linked to oncogene induced senescence driven by $HRAS^{G12V}$ in fibroblasts. Phosphorylation of $AGO2^{Y393}$ led to increased p21 expression and senescence following the inactivation of protein phosphatase PTP1B [46]. Our model suggests that phosphorylation of Y393-AGO2 leads to the disruption of HRAS-AGO2 and NRAS-AGO2 interaction (**Figure 2**). Additionally, the loss of AGO2 inhibits mutant *HRAS* and *NRAS* growth in part through induction of senescent pathways like p53 and p21 (**Figure 3.4**). Finally, the loss of AGO2 leads to the production of ROS causing the inactivation of PTP1B and the induction of a pEGFR-RAS-ERK feedforward loop (**Figure 3.5 and 3.6**). This observed oncogene induced senescence (OIS) pathway suggests that the continued binding of RAS and AGO2 is, in part, required to prevent senescence that can be overcome through loss of AGO2 expression. Furthermore, our observation of resistance to EGFR phosphorylation of AGO2 in the setting of mutant *HRAS* or *NRAS* may be the result of additional dysregulation of protein phosphatases such as PTP1B, leading to promotion of RAS-AGO2 binding. Our work in a $Kras^{G12D}$ mouse model of PDAC (**Chapter 2**), broadly identified the Ago2-Kras interaction as necessary for the prevention of OIS and progression from PanIN lesion to PDAC; however, loss of p53 in a parallel model escaped the requirement for Ago2. Similarly, we observed a resistance to AGO2-KD in mutant *NRAS* cells in a p53 null background. As many mutant RAS driven cancers also have loss of p53 or other senescence mediators, it is possible that RAS's reliance on AGO2 is limited to early stages of cancer development. Further exploration of this complex interaction may uncover additional

mechanisms of regulation of mutant RAS biology through its interaction with AGO2. Overall, our findings suggest that RAS-AGO2 interaction may play a broad role in maintaining a progrowth state and preventing senescence in mutant *HRAS* and *NRAS* driven cells.

Despite recent progress in targeting specific mutations of *KRAS* [59], few treatment options remain available to target *RAS* clinically. Taken together, our study finds a novel role for AGO2 as a regulator of cellular proliferation, senescence, and migration/metastasis in mutant *HRAS* and *NRAS* driven cancers. A greater understanding of this RAS-AGO2 interaction in human cancer may inform possible future clinical targeting of mutant RAS.

Figures

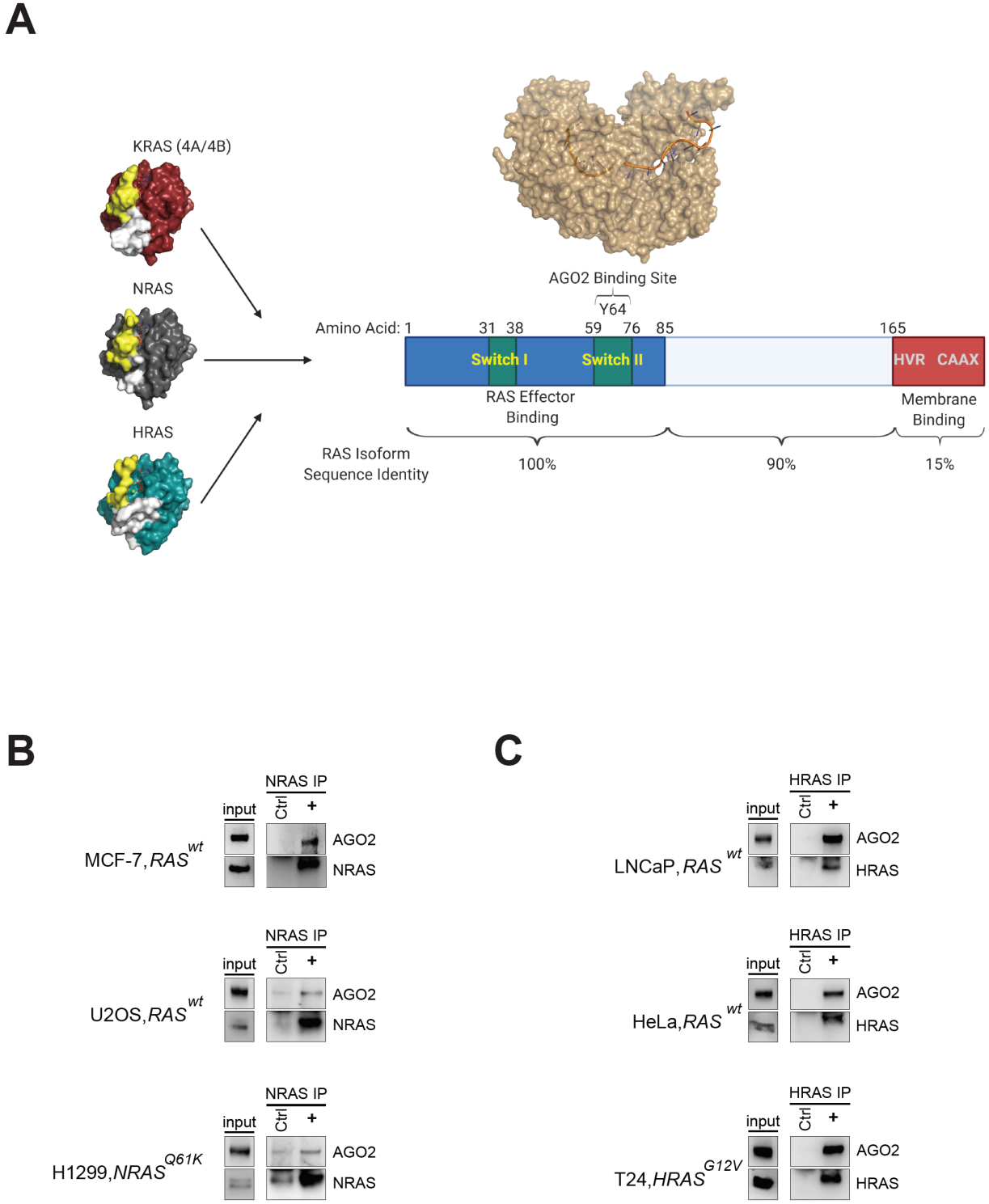

Figure 3.1 Interaction of AGO2 with HRAS and NRAS.
(A) Amino acid homology between different RAS isoforms show 100% amino acid conservation at the Switch II domain where AGO2 binds KRAS.
(B-C) Immunoprecipitation (IP) of endogenous AGO2 or RAS from a panel of benign and cancer cell lines with differing expression of WT or mutant HRAS (B) and NRAS (C).

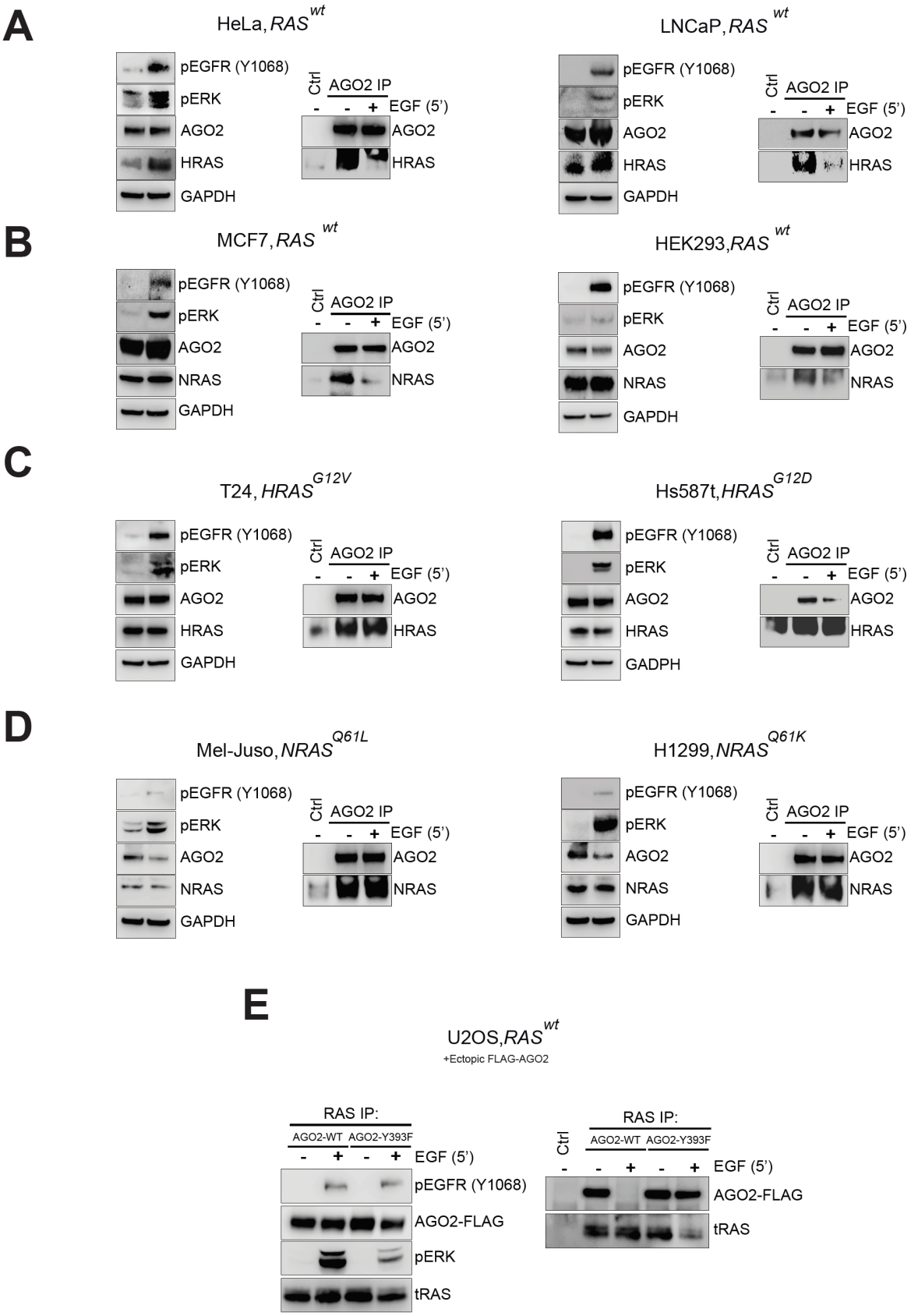
A
HeLa, RAS wt
pEGFR (Y1068)
pERK
AGO2
HRAS
GAPDH
Ctrl
AGO2 IP
- - + EGF (5')
AGO2
HRAS
LNCaP, RAS wt
pEGFR (Y1068)
pERK
AGO2
HRAS
GAPDH
Ctrl
AGO2 IP
- - + EGF (5')
AGO2
HRAS
B
MCF7, RAS wt
pEGFR (Y1068)
pERK
AGO2
NRAS
GAPDH
Ctrl
AGO2 IP
- - + EGF (5')
AGO2
NRAS
HEK293, RAS wt
pEGFR (Y1068)
pERK
AGO2
NRAS
GAPDH
Ctrl
AGO2 IP
- - + EGF (5')
AGO2
NRAS
C
T24, HRAS G12V
pEGFR (Y1068)
pERK
AGO2
HRAS
GAPDH
Ctrl
AGO2 IP
- - + EGF (5')
AGO2
HRAS
Hs587t, HRAS G12D
pEGFR (Y1068)
pERK
AGO2
HRAS
GADPH
Ctrl
AGO2 IP
- - + EGF (5')
AGO2
HRAS
D
Mel-Juso, NRAS Q61L
pEGFR (Y1068)
pERK
AGO2
NRAS
GAPDH
Ctrl
AGO2 IP
- - + EGF (5')
AGO2
NRAS
H1299, NRAS Q61K
pEGFR (Y1068)
pERK
AGO2
NRAS
GAPDH
Ctrl
AGO2 IP
- - + EGF (5')
AGO2
NRAS
E
U2OS, RAS wt
+Ectopic FLAG-AGO2
RAS IP:
AGO2-WT AGO2-Y393F
- + - + EGF (5')
pEGFR (Y1068)
AGO2-FLAG
pERK
tRAS
RAS IP:
Ctrl
AGO2-WT AGO2-Y393F
- - + - + EGF (5')
AGO2-FLAG
tRAS

F

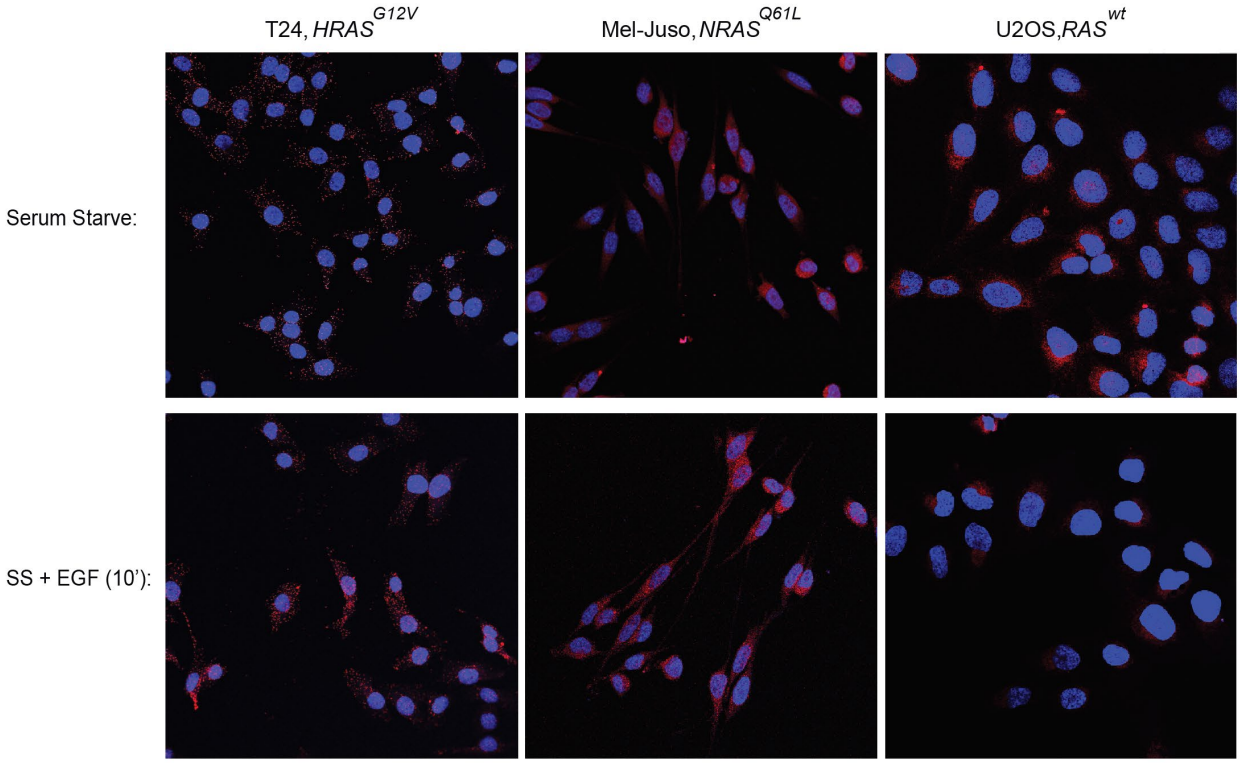

Figure 3.2 EGF stimulation disrupts wild-type HRAS-AGO2 and NRAS-AGO2 interaction across multiple cell lineages while mutant RAS-AGO2 interaction is recalcitrant to EGFR activation.

(A-B) Immunoprecipitation (IP) of endogenous AGO2 upon EGF stimulation (5') in HeLa, LNCaP, MCF7, and Hek293T cell lines expressing wild-type RAS followed by immunoblot analysis of HRAS (A) or NRAS (B).

(C) Co-IP of endogenous AGO2 following EGF stimulation (5') in T24 and Hs578T cancer cells harboring different *HRAS* mutations, followed by immunoblot analysis of HRAS.

(D) Co-IP of endogenous AGO2 in Mel-Juso and H1299 cells with different *NRAS* mutations.

(E) EGF stimulation and RAS co-IP analysis in U2OS (RAS^{WT}) cells expressing FLAG-tagged *AGO2* (WT and Y393F).

(F) For each cell line, MAPK activation and levels of various proteins are shown as input blots. PLA of U2OS, T24, and Mel-Juso following overnight serum starvation followed by EGF stimulation (10').

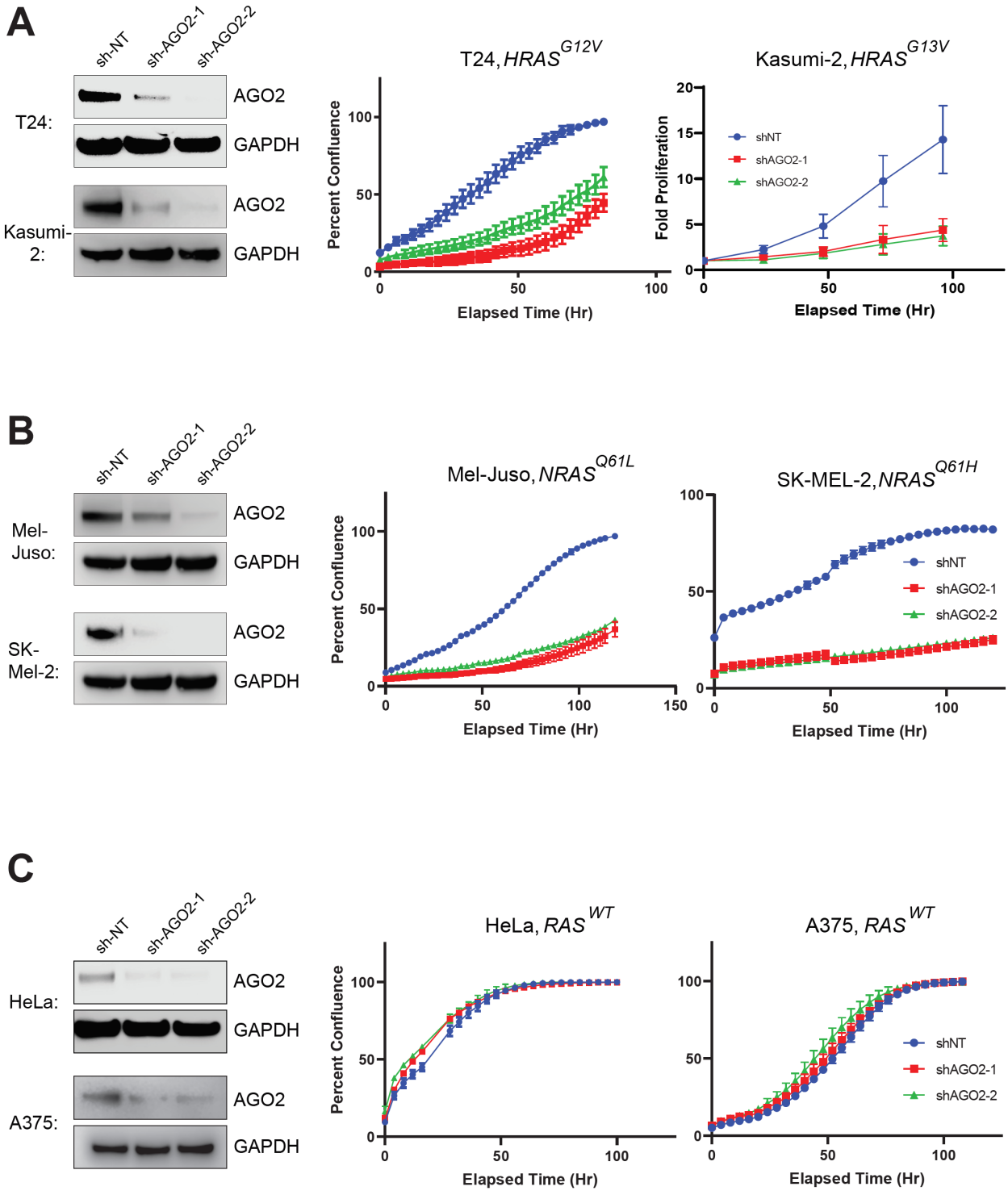

Figure 3.3 AGO2 knockdown inhibits proliferation in mutant *HRAS* and *NRAS* but not WT *RAS* cell lines.

(A) Immunoblot confirmation of AGO2 knockdown following stable transduction of shRNA transcripts and matched cell proliferation overtime in $HRAS^{G12V}$ mutant T24 bladder cancer and $HRAS^{G13V}$ mutant Kasumi-2 ALL cell line.

Figure 3.3 Continued
(B) Matched immunoblot and cell proliferation for *NRAS* mutant melanoma cell lines Mel-Juso and SK-MEL-2.
(C) WT *RAS* cell line (HeLa and A375) with matched cell growth and immunoblot confirmation of AGO2 loss.

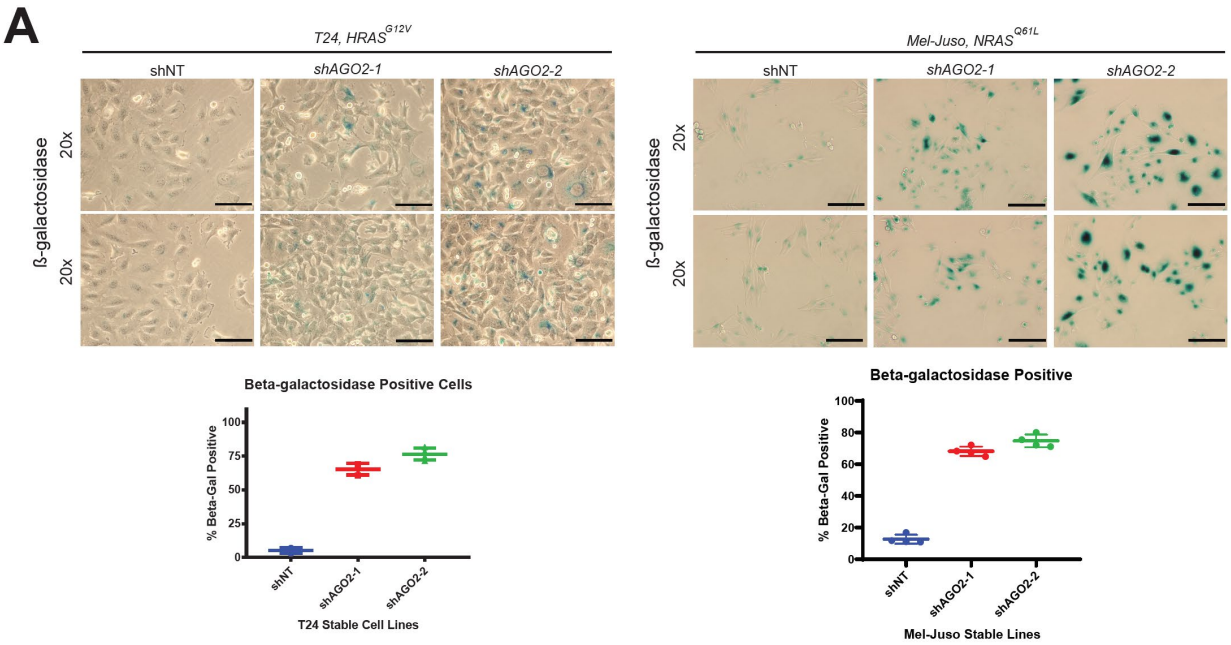
A
T24, HRAS G12V
shNT
shAGO2-1
shAGO2-2
ß-galactosidase
20x
20x
Beta-galactosidase Positive Cells
% Beta-Gal Positive
100
75
50
25
0
shNT
shAGO2-1
shAGO2-2
T24 Stable Cell Lines
Mel-Juso, NRAS Q61L
Beta-galactosidase Positive
% Beta-Gal Positive
100
80
60
40
20
0
Mel-Juso Stable Lines

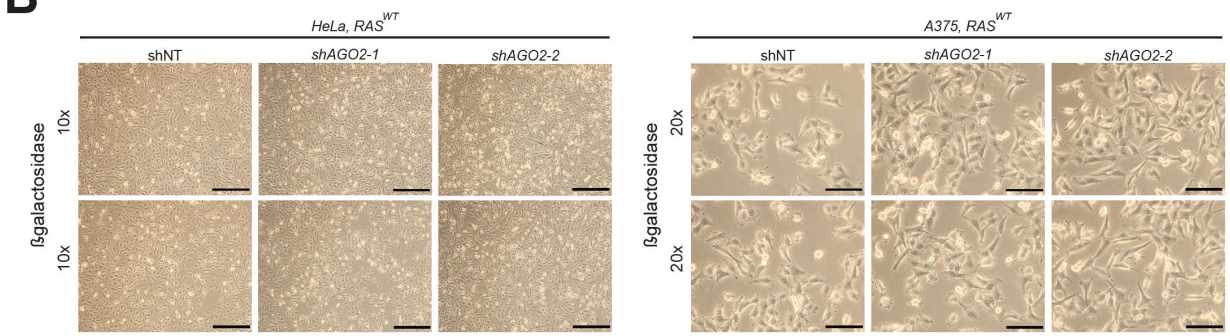
B
HeLa, RAS WT
shNT
shAGO2-1
shAGO2-2
ßgalactosidase
10x
10x
A375, RAS WT
20x
20x

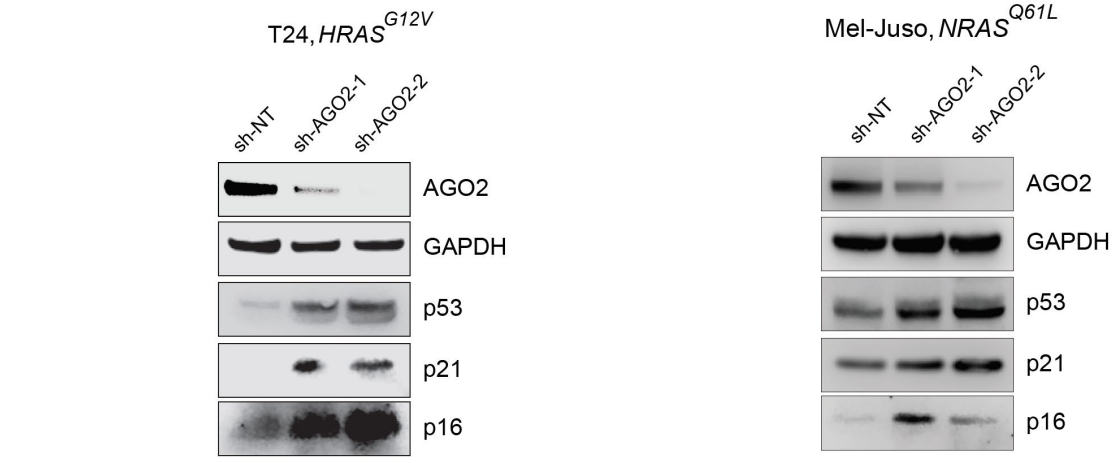
C
T24, HRAS G12V
sh-NT
sh-AGO2-1
sh-AGO2-2
AGO2
GAPDH
p53
p21
p16
Mel-Juso, NRAS Q61L

Figure 3.4 Loss of AGO2 induces senescence in mutant *HRAS* and *NRAS* cell lines.
(A) Representative images following β-galactosidase staining of T24 ($HRAS^{G12V}$) and Mel-Juso ($NRAS^{Q61L}$) from stably transduced AGO2 knockdown cell lines (images at 20x). Matched scatter plot showing percent β-galactosidase staining in an average of 5 images from each condition.

(B) β-galactosidase staining of WT RAS cell lines following stable knockdown of AGO2 (HeLa, 10x; A375, 20).

(C) Immunoblot blot analysis of senescence markers (p53, p21, and p16) in stable AGO2 knockdown T24 ($HRAS^{G12V}$) and Mel-Juso ($NRAS^{Q61L}$) cells.

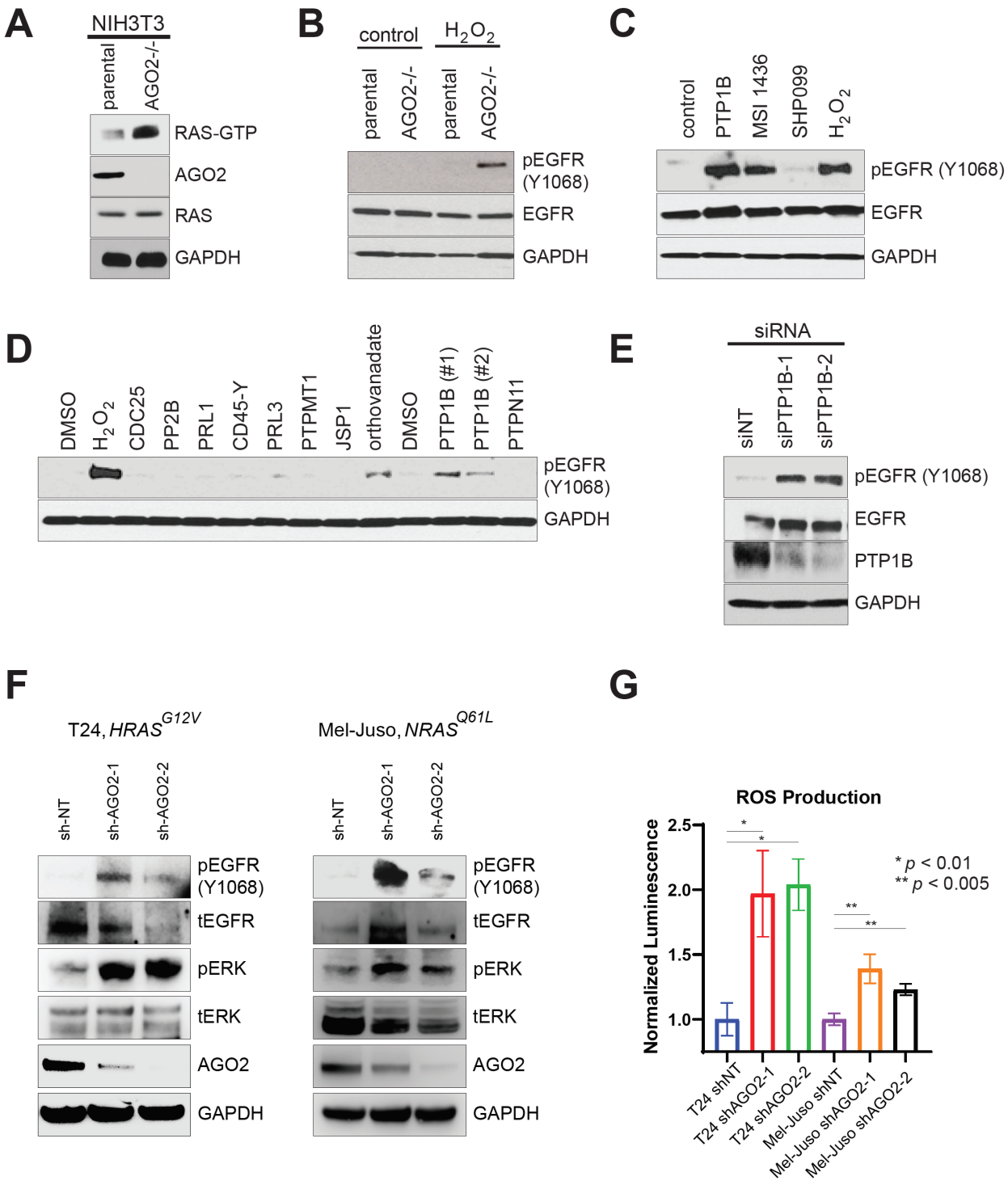

Figure 3.5 AGO2 increases production of ROS, inducing a feedforward loop activating EGFR-RAS-ERK signaling via inhibition of PTP1B.

(A) Representative immunoblot analysis of NIH3T3 AGO2-/- mouse fibroblasts for induction of RAS-GTP following loss of AGO2.

Figure 3.5 continued
(B) Increased pEGFR (Y1068) upon treatment with hydrogen peroxide for 4 minutes in NIH3T3 AGO2-/- cells (B).

(C-D) Immunoblot analysis of pEGFR (Y1068) upon treatment with various phosphatase inhibitors in NIH3T3 AGO2-/- cells.

(E) Knockdown of PTP1B using two independent siRNA followed by immunoblot analysis to assess EGFR and pEGFR (Y1068) levels.

(F) Immunoblot blot analysis of pERK and pEGFR induction in stable AGO2 knockdown T24 (*HRAS*^{G12V}) and Mel-Juso (*NRAS*^{Q61L}) cells.

(G) Normalized ROS production in T24 and Mel-Juso shAGO2 knockdown cell lines.

A

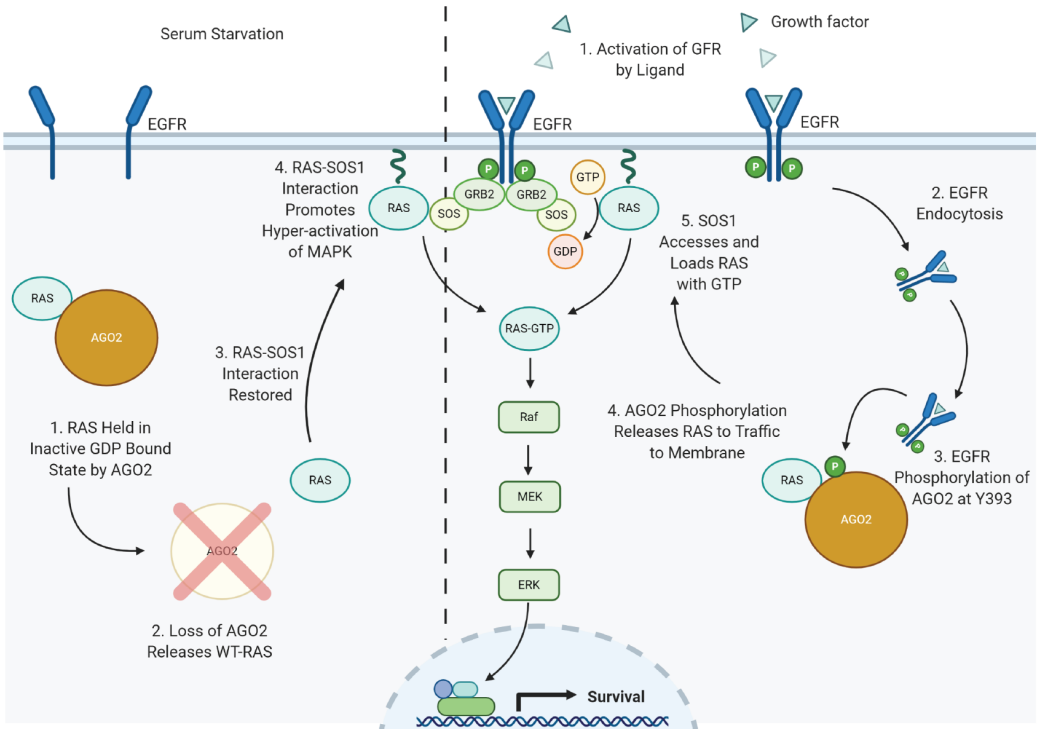
Serum Starvation
Growth factor
1. Activation of GFR by Ligand
EGFR
EGFR
EGFR
4. RAS-SOS1 Interaction Promotes Hyper-activation of MAPK
GRB2
GRB2
SOS
SOS
GTP
GDP
RAS
RAS
5. SOS1 Accesses and Loads RAS with GTP
2. EGFR Endocytosis
RAS
AGO2
3. RAS-SOS1 Interaction Restored
RAS-GTP
Raf
MEK
ERK
4. AGO2 Phosphorylation Releases RAS to Traffic to Membrane
3. EGFR Phosphorylation of AGO2 at Y393
1. RAS Held in Inactive GDP Bound State by AGO2
RAS
AGO2
2. Loss of AGO2 Releases WT-RAS
Survival

B

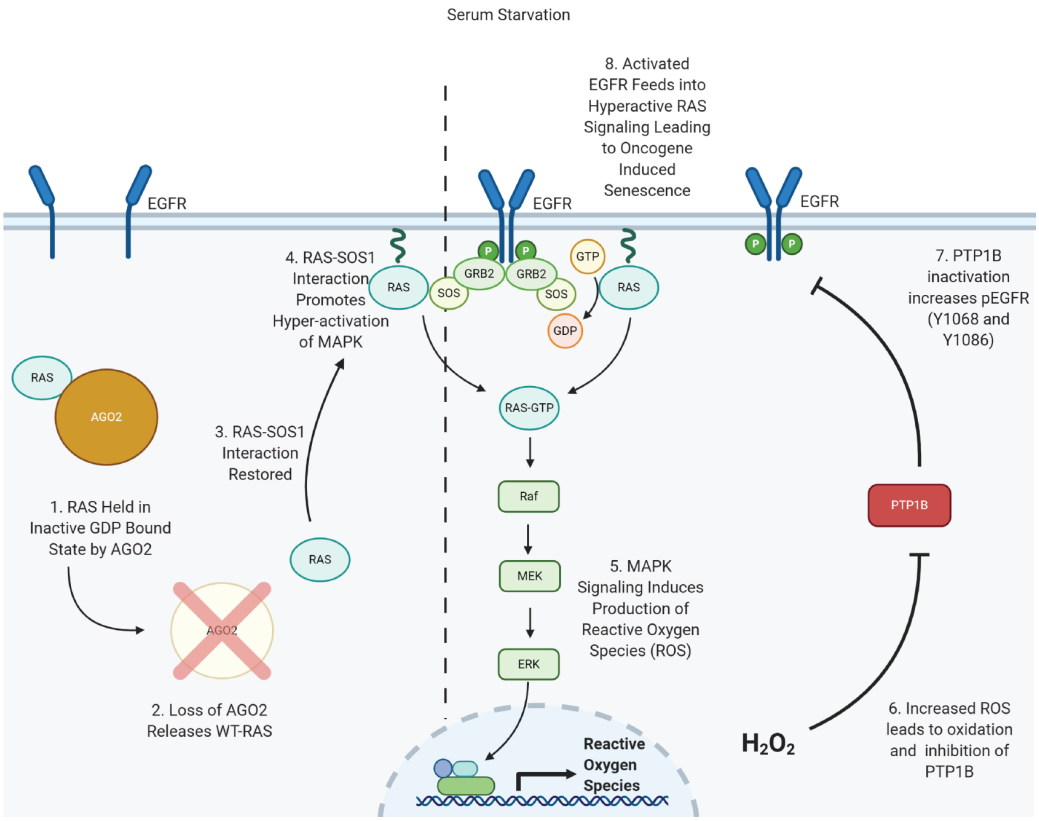
Serum Starvation
8. Activated EGFR Feeds into Hyperactive RAS Signaling Leading to Oncogene Induced Senescence
EGFR
EGFR
EGFR
4. RAS-SOS1 Interaction Promotes Hyper-activation of MAPK
GRB2
GRB2
SOS
SOS
GTP
GDP
RAS
RAS
7. PTP1B inactivation increases pEGFR (Y1068 and Y1086)
RAS
AGO2
3. RAS-SOS1 Interaction Restored
RAS-GTP
Raf
PTP1B
MEK
5. MAPK Signaling Induces Production of Reactive Oxygen Species (ROS)
ERK
1. RAS Held in Inactive GDP Bound State by AGO2
RAS
AGO2
2. Loss of AGO2 Releases WT-RAS
Reactive Oxygen Species
H_2O_2
6. Increased ROS leads to oxidation and inhibition of PTP1B

Figure 3.6 Models for induction of senescence following AGO2 loss in mutant *RAS* cells.
(A) A model for RAS-GTP activation upon AGO2 loss: 1. RAS interaction with SOS1 is inhibited by AGO2-RAS binding, 2. Loss of AGO2 releases WT-RAS, and 3. RAS-SOS1 interaction is restored, leading to 4. Increased activation of MAPK in mutant RAS cells.

(B) The hyperactivation of RAS leads to 5. An increase in Reactive Oxygen Species (ROS), 6. The increased ROS oxidizes and inhibits PTP1B phosphatase activity, 7. Leading to an increase in pEGFR (Y1068), which in turn 8. Feeds forward into the activation of WT RAS leading to OIS.

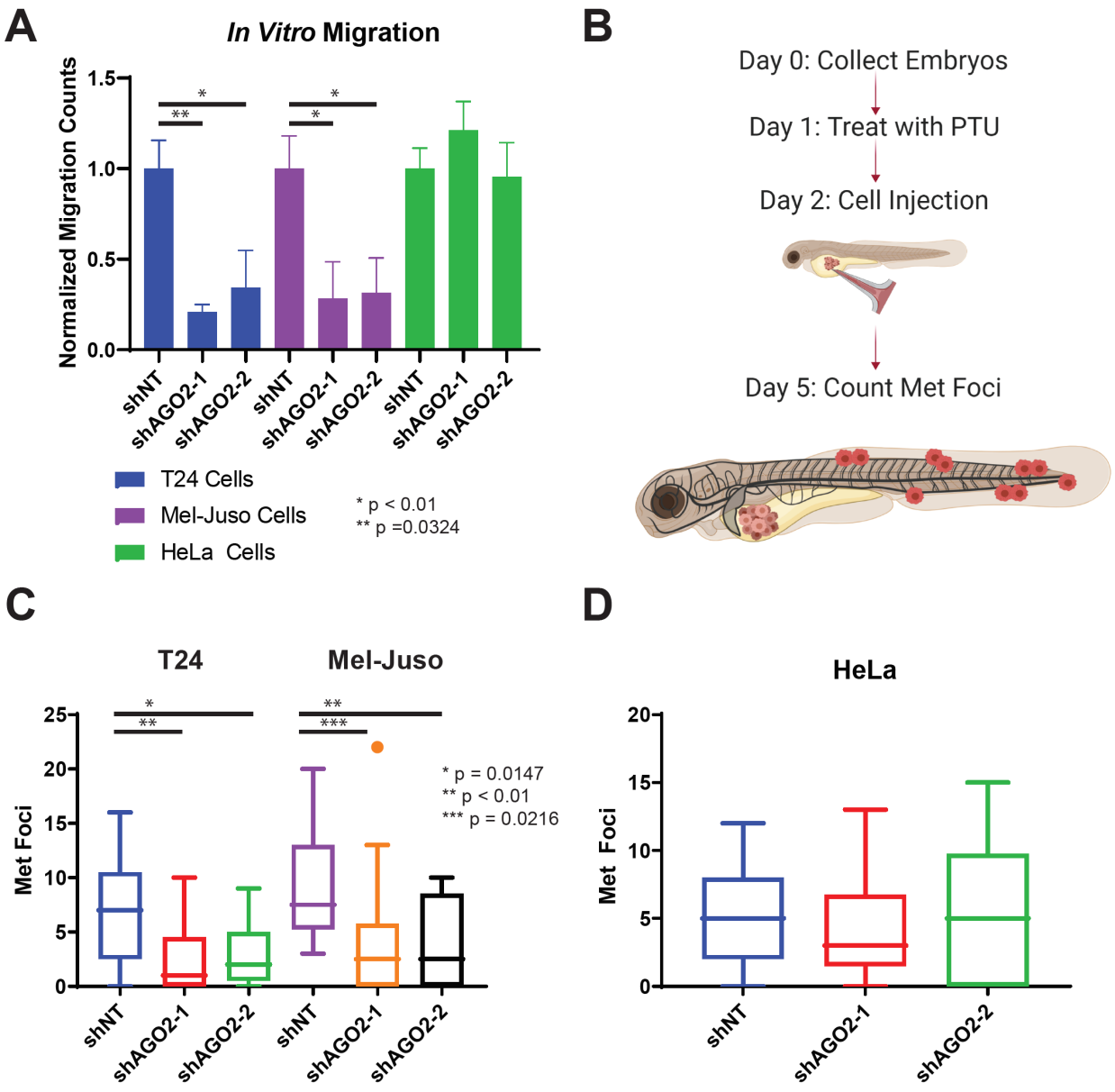

Figure 3.7 AGO2 promotes migration and metastasis in mutant *HRAS* and *NRAS* driven cell lines.

(A) Normalized migration signal of HeLa (RAS^{WT}), T24 ($HRAS^{G12V}$), and Mel-Juso ($NRAS^{Q61L}$) from stably transduced AGO2 knockdown cell lines in the *in vitro* FluoroBlok transwell migration system (Corning).

(B) Model of zebrafish xenograft assay protocol.

(C-D) Average of total metastatic foci from HeLa (RAS^{WT}), T24 ($HRAS^{G12V}$), and Mel-Juso ($NRAS^{Q61L}$) stable AGO2 knockdown cell lines.

References

1. Simanshu, D.K., D.V. Nissley, and F. McCormick, *RAS Proteins and Their Regulators in Human Disease.* Cell, 2017. **170**(1): p. 17-33.
2. Pylayeva-Gupta, Y., E. Grabocka, and D. Bar-Sagi, *RAS oncogenes: weaving a tumorigenic web.* Nat Rev Cancer, 2011. **11**(11): p. 761-74.
3. Stephen, A.G., et al., *Dragging ras back in the ring.* Cancer Cell, 2014. **25**(3): p. 272-81.
4. Cox, A.D. and C.J. Der, *Ras history: The saga continues.* Small GTPases, 2010. **1**(1): p. 2-27.
5. Kleeff, J., et al., *Pancreatic cancer.* Nat Rev Dis Primers, 2016. **2**: p. 16022.
6. Hobbs, G.A., C.J. Der, and K.L. Rossman, *RAS isoforms and mutations in cancer at a glance.* J Cell Sci, 2016. **129**(7): p. 1287-92.
7. Rajalingam, K., et al., *Ras oncogenes and their downstream targets.* Biochim Biophys Acta, 2007. **1773**(8): p. 1177-95.
8. McCormick, F., *KRAS as a Therapeutic Target.* Clin Cancer Res, 2015. **21**(8): p. 1797-801.
9. Shankar, S., et al., *KRAS Engages AGO2 to Enhance Cellular Transformation.* Cell Rep, 2016. **14**(6): p. 1448-1461.
10. Deng, C., et al., *Mice lacking p21CIP1/WAF1 undergo normal development, but are defective in G1 checkpoint control.* Cell, 1995. **82**(4): p. 675-84.
11. Romagosa, C., et al., *p16(Ink4a) overexpression in cancer: a tumor suppressor gene associated with senescence and high-grade tumors.* Oncogene, 2011. **30**(18): p. 2087-97.
12. Green, M.R. and J. Sambrook, *Estimation of Cell Number by Hemocytometry Counting.* Cold Spring Harb Protoc, 2019. **2019**(11): p. pdb prot097980.
13. Zhou, B., C.J. Der, and A.D. Cox, *The role of wild type RAS isoforms in cancer.* Semin Cell Dev Biol, 2016. **58**: p. 60-9.
14. Hancock, J.F., et al., *All ras proteins are polyisoprenylated but only some are palmitoylated.* Cell, 1989. **57**(7): p. 1167-77.
15. Hancock, J.F., *Ras proteins: different signals from different locations.* Nat Rev Mol Cell Biol, 2003. **4**(5): p. 373-84.
16. Cheng, C.M., et al., *Compartmentalized Ras proteins transform NIH 3T3 cells with different efficiencies.* Mol Cell Biol, 2011. **31**(5): p. 983-97.
17. Munoz-Maldonado, C., Y. Zimmer, and M. Medova, *A Comparative Analysis of Individual RAS Mutations in Cancer Biology.* Front Oncol, 2019. **9**: p. 1088.
18. Shen, J., et al., *EGFR modulates microRNA maturation in response to hypoxia through phosphorylation of AGO2.* Nature, 2013. **497**(7449): p. 383-7.
19. Rudel, S., et al., *A multifunctional human Argonaute2-specific monoclonal antibody.* RNA, 2008. **14**(6): p. 1244-53.
20. van Houdt, W.J., et al., *Oncogenic KRAS desensitizes colorectal tumor cells to epidermal growth factor receptor inhibition and activation.* Neoplasia, 2010. **12**(6): p. 443-52.
21. Reddy, E.P., et al., *A point mutation is responsible for the acquisition of transforming properties by the T24 human bladder carcinoma oncogene.* Nature, 1982. **300**(5888): p. 149-52.

22. Tsao, H., et al., *Relative reciprocity of NRAS and PTEN/MMAC1 alterations in cutaneous melanoma cell lines.* Cancer Res, 2000. **60**(7): p. 1800-4.
23. Ohashi, K., et al., *Characteristics of lung cancers harboring NRAS mutations.* Clin Cancer Res, 2013. **19**(9): p. 2584-91.
24. Lopez-Orozco, J., et al., *Functional analyses of phosphorylation events in human Argonaute 2.* RNA, 2015. **21**(12): p. 2030-8.
25. Rudel, S., et al., *Phosphorylation of human Argonaute proteins affects small RNA binding.* Nucleic Acids Res, 2011. **39**(6): p. 2330-43.
26. McKenzie, A.J., et al., *KRAS-MEK Signaling Controls Ago2 Sorting into Exosomes.* Cell Rep, 2016. **15**(5): p. 978-987.
27. Jee, D. and E.C. Lai, *Alteration of miRNA activity via context-specific modifications of Argonaute proteins.* Trends Cell Biol, 2014. **24**(9): p. 546-53.
28. Ottaviano, L., et al., *Molecular characterization of commonly used cell lines for bone tumor research: a trans-European EuroBoNet effort.* Genes Chromosomes Cancer, 2010. **49**(1): p. 40-51.
29. Duchartre, Y., et al., *Effects of CD49d-targeted antisense-oligonucleotide on alpha4 integrin expression and function of acute lymphoblastic leukemia cells: Results of in vitro and in vivo studies.* PLoS One, 2017. **12**(11): p. e0187684.
30. Vogel, C.J., et al., *Cooperative induction of apoptosis in NRAS mutant melanoma by inhibition of MEK and ROCK.* Pigment Cell Melanoma Res, 2015. **28**(3): p. 307-17.
31. Tanami, H., et al., *Involvement of overexpressed wild-type BRAF in the growth of malignant melanoma cell lines.* Oncogene, 2004. **23**(54): p. 8796-804.
32. Macaluso, M., et al., *Ras family genes: an interesting link between cell cycle and cancer.* J Cell Physiol, 2002. **192**(2): p. 125-30.
33. Dimri, G.P., et al., *A biomarker that identifies senescent human cells in culture and in aging skin in vivo.* Proc Natl Acad Sci U S A, 1995. **92**(20): p. 9363-7.
34. Lee, B.Y., et al., *Senescence-associated beta-galactosidase is lysosomal beta-galactosidase.* Aging Cell, 2006. **5**(2): p. 187-95.
35. Kuilman, T., et al., *The essence of senescence.* Genes Dev, 2010. **24**(22): p. 2463-79.
36. Lee, S. and J.S. Lee, *Cellular senescence: a promising strategy for cancer therapy.* BMB Rep, 2019. **52**(1): p. 35-41.
37. d'Adda di Fagagna, F., et al., *A DNA damage checkpoint response in telomere-initiated senescence.* Nature, 2003. **426**(6963): p. 194-8.
38. Serrano, M., et al., *Oncogenic ras provokes premature cell senescence associated with accumulation of p53 and p16INK4a.* Cell, 1997. **88**(5): p. 593-602.
39. Hayflick, L. and P.S. Moorhead, *The serial cultivation of human diploid cell strains.* Exp Cell Res, 1961. **25**: p. 585-621.
40. Chicas, A., et al., *Dissecting the unique role of the retinoblastoma tumor suppressor during cellular senescence.* Cancer Cell, 2010. **17**(4): p. 376-87.
41. Morton, J.P., et al., *Mutant p53 drives metastasis and overcomes growth arrest/senescence in pancreatic cancer.* Proc Natl Acad Sci U S A, 2010. **107**(1): p. 246-51.
42. Xue, W., et al., *Senescence and tumour clearance is triggered by p53 restoration in murine liver carcinomas.* Nature, 2007. **445**(7128): p. 656-60.
43. Symonds, H., et al., *p53-dependent apoptosis suppresses tumor growth and progression in vivo.* Cell, 1994. **78**(4): p. 703-11.

44. Lin, D.L. and C. Chang, *p53 is a mediator for radiation-repressed human TR2 orphan receptor expression in MCF-7 cells, a new pathway from tumor suppressor to member of the steroid receptor superfamily.* J Biol Chem, 1996. **271**(25): p. 14649-52.
45. Vetter, I.R. and A. Wittinghofer, *The guanine nucleotide-binding switch in three dimensions.* Science, 2001. **294**(5545): p. 1299-304.
46. Yang, M., et al., *Dephosphorylation of tyrosine 393 in argonaute 2 by protein tyrosine phosphatase 1B regulates gene silencing in oncogenic RAS-induced senescence.* Mol Cell, 2014. **55**(5): p. 782-90.
47. Lee, A.C., et al., *Ras proteins induce senescence by altering the intracellular levels of reactive oxygen species.* J Biol Chem, 1999. **274**(12): p. 7936-40.
48. Ogrunc, M., et al., *Oncogene-induced reactive oxygen species fuel hyperproliferation and DNA damage response activation.* Cell Death Differ, 2014. **21**(6): p. 998-1012.
49. Ishino, Y., et al., *Protein tyrosine phosphatase-1B (PTP1B) helps regulate EGF-induced stimulation of S-phase entry in human corneal endothelial cells.* Mol Vis, 2008. **14**: p. 61-70.
50. Yamaoka, T., et al., *Specific epidermal growth factor receptor autophosphorylation sites promote mouse colon epithelial cell chemotaxis and restitution.* Am J Physiol Gastrointest Liver Physiol, 2011. **301**(2): p. G368-76.
51. Smith, A.M., et al., *The protein tyrosine phosphatase 1B inhibitor MSI-1436 stimulates regeneration of heart and multiple other tissues.* NPJ Regen Med, 2017. **2**: p. 4.
52. Kumar, S., et al., *Attenuation of hyperhomocysteinemia induced vascular dementia by sodium orthovanadate perhaps via PTP1B: Pertinent downstream outcomes.* Behav Brain Res, 2019. **364**: p. 29-40.
53. Castellano, E., et al., *RAS signalling through PI3-Kinase controls cell migration via modulation of Reelin expression.* Nat Commun, 2016. **7**: p. 11245.
54. Moujaber, O., et al., *Cellular senescence is associated with reorganization of the microtubule cytoskeleton.* Cell Mol Life Sci, 2019. **76**(6): p. 1169-1183.
55. Aifuwa, I., et al., *Senescent stromal cells induce cancer cell migration via inhibition of RhoA/ROCK/myosin-based cell contractility.* Oncotarget, 2015. **6**(31): p. 30516-31.
56. Teng, Y., et al., *Evaluating human cancer cell metastasis in zebrafish.* BMC Cancer, 2013. **13**: p. 453.
57. Yang, F.Q., et al., *Argonaute 2 is up-regulated in tissues of urothelial carcinoma of bladder.* Int J Clin Exp Pathol, 2014. **7**(1): p. 340-7.
58. Voller, D., et al., *Strong reduction of AGO2 expression in melanoma and cellular consequences.* Br J Cancer, 2013. **109**(12): p. 3116-24.
59. Ostrem, J.M., et al., *K-Ras(G12C) inhibitors allosterically control GTP affinity and effector interactions.* Nature, 2013. **503**(7477): p. 548-51.

Chapter 4

A Single-Molecule Tool Box for the Study of AGO2-RAS Interaction

Abstract

Here we present Single-Molecule Toolbox for the use of studying AGO2's interaction with KRAS and other RISC members. Using an *in vitro* translation (IVT) system, we over-expressed Halo and SNAP tagged AGO2 and KRAS in a HeLa based cell extract system. We studied the *in vitro* activity of AGO2 demonstrating a requirement for the presence of RISC members for targeted mRNA cleavage. Additionally, we found GTP-loaded KRAS inhibited AGO2 targeted cleavage *in vitro*, suggesting further functional relevance for this interaction in mutant *KRAS* driven cancers. Using a single-molecule (SM) assay with total internal reflection fluorescence (TIRF), we also observed the interaction of Halo-AGO2 and SNAP-KRAS at a single molecule resolution demonstrating their binding in 1 to 1 stoichiometry. Finally, we observed that IVT generated AGO2 formed higher order clusters *in vitro* that could be disrupted via RNase treatment. This Single-Molecule Toolbox represents a new tool to aid in the study of the biochemistry of AGO2 and its interaction with KRAS.

Introduction

In recent decades, the field of fluorescent microscopy has greatly expanded its scope and resolution within both live cells and *in vitro* protein samples. The use of single-molecule (SM) microscopy

has uncovered the dynamic, biochemical relationships of many cellular processes including DNA replication, cell division, cellular trafficking, cell receptor biology, signal transduction, and many other aspects of cellular biology [1]. Unlike many traditional cellular and molecular biology techniques which analyze the cell as a whole, SM microscopy provides a means to study the biochemical properties of individual proteins such as AGO2 or RAS.

Cellular control of post transcriptional gene expression is an important mechanism by which cells alter the abundance of mRNA transcripts under specific stimuli. RNA interference (RNAi) is one of the primary routes of control in which double stranded RNA is processed and targeted by RNA Induced Silencing Complex (RISC) proteins, like AGO2, to a complementary mRNA transcript [2-4]. In recent years, an appreciation for the role of phase separation or phase transition in biological processes, including RNAi, has increased significantly [5-7]. AGO2 and RISC complex members (like TRNC6) in particular have been shown to form higher order complexes in order to accelerate the deadenylation and translational repression of target mRNA [8]. However, it remains unclear what specific role this phase transition plays in RNAi and what the minimal RISC components are required for generating these phase separated particles.

Following the identification of a novel interaction between AGO2 and KRAS [9], our understanding of this interaction and its importance in normal and cancer cell biology has expanded considerably. Ago2 was shown to be essential in the development of pancreatic ductal adenocarcinoma (PDAC) in a $KRAS^{G12D}$ driven mouse model by preventing oncogene induced senescence (OIS) and allowing transition from early to late PanIN precursor lesions (**Chapter 2**). In addition, we found that not only did AGO2 interact with the other RAS isoforms (HRAS and NRAS), but we also demonstrated that AGO2 plays a critical role in the proliferation of cancers driven by mutations in these isoforms (**Chapter 3**). Despite our growing understanding of the

interaction of AGO2 and RAS proteins, our knowledge of their precise biochemistry remains elusive. Specifically, mutant KRAS has been shown to inhibit AGO2 miRNA duplex unwinding [9], but it is unclear whether this inhibition is due to a direct inhibition due to RAS binding on AGO2's N-terminal domain, alteration of AGO2 interaction with RISC members, changes in AGO2 subcellular localization, or some combination of the above. Additionally, we have previously shown that AGO2 blocks KRAS interaction with guanine nucleotide exchange factors (GEFs) like SOS1 (**Chapter 2**), but the precise stoichiometry and kinetics of these dynamic interactions are unclear.

With the goal of better studying the biochemical relationship between AGO2 and its binding partners such as RISC members or RAS proteins, we have developed an *in vitro* Single-Molecule Tool Box. Utilizing a HeLa lysate *in vitro* translation (IVT) system, we are able to generate specific human proteins with functional enzymatic tags (HaloTag [10] and SNAP-Tag [11]), allowing for the fluorescent labeling for single molecule visualization via total internal reflection fluorescence (TIRF) microscopy. Here we present our development of this SM tool box and begin to describe the biochemical relationship of AGO2-RAS and AGO2 with RISC members.

Methods

In Vitro Translation and Protein Concentration Estimation

Proteins of interest were cloned into the pT7-CFE1 (ThermoFisher) plasmid with the desired HaloTag or SNAP-tag. Following the generation of our *in vitro* expression plasmid library, we used the 1-Step Human Coupled IVT kit (ThermoFisher; Cat. Number 88882). For each IVT reaction, the manufacturer's protocol was followed by adding HeLa lysate, accessory proteins, reaction mixture, and specific pT77-CFE plasmid to a microcentrifuge tube and incubating at 30°C

for 4 hours. Utilizing this system, we were able to generate a panel of plasmids for the over expression of multiple recombinant human RISC proteins including AGO2, TRBP, TRNC6A, and DICER. Furthermore, we generated a panel comprising each of the three RAS isoforms for expression in the pT7-CFE backbone. Expression of target protein was confirmed via immunoblot.

For downstream applications, the protein concentrations of over expressed IVT products were estimated. Briefly, a standard dilution immunoblot of a purified HaloTag (Promega) or SNAP-Tag (NEB) with a known concentration was run with the matching IVT over-expression. This process can also be accomplished with purified proteins lacking a specific tag. Using ImageJ software densitometry analysis, the IVT product concentration was estimated comparing to the signal of known purified proteins.

In Vitro HaloTag and SNAP-Tag Labeling

Multiple enzyme based tags have been developed to provide a flexible platform to study a given protein. Amongst these are the HaloTag (33 kDa tag developed from a mutant *Rhodococcus* dehalogenase enzyme) and the SNAP-tag (19 kDa tag developed from an O^6-alkylguanine-DNA-alkyltransferase mutant human enzyme). In both cases, these tags bind and react to a specific ligand-linker in an irreversible process [11, 12]. This allows for the development of multiple functional groups conjugated to the Halo or SNAP ligand which can be used based on specific experimental needs such as live cell imaging or protein purification [13].

Following the concentration estimation of HeLa IVT protein products, the HaloTag and SNAP-Tags were labeled for downstream applications. Each tagged protein was incubated in a specific buffer with a specific substrate dye at a 1:2 mole ratio. HaloTag Jenalia Fluor (JF) dyes (JF549 and JF646 (Promega)) were mixed with IVT protein in a Hepes-NaCl buffer (500 mM

Hepes, 1.5 M NaCl, 10 mM DTT). SNAP-Cell SiR (NEB) dyes were mixed with SNAP-Tag IVT proteins in 1x PBS with 10 mM DTT. Labeling was conducted at 37°C for 30 minutes followed by rotation at room temperature for 1 hour. The protein mixtures were then rotated at 4°C overnight. Halo and SNAP substrates and labeled proteins were protected from ambient light throughout labeling procedure.

After overnight incubation with their specific dye, the tagged proteins were run on an SDS-PAGE gel with a dye dilution curve to assess labeling efficiency for downstream applications (**Supplemental Figure 4.2a**). Gels were imaged using a Typhoon Variable Mode Imager to visualize the specific fluorophore chosen. To assess binding of labeled proteins, he tagged proteins were mixed in approximately equal molar concentrations for 1 hour at room temperature and Co-IP'ed with HaloTag antibody and visualized as described above (**Supplemental Figure 4.2b**).

In Vitro AGO2 Cleavage Reporter Assay

In vitro translated AGO2 and other RNAi proteins of interest were incubated with either a non-targeting (NT) control or Firefly Luciferase (FL) targeted siRNA duplex (100 nM) allowing suitable loading into AGO2/RISC at 4°C for 15 minutes. Renilla Luciferase (RL) was used as an internal control between reaction samples. Following the addition of FL and RL mRNA (with 5'-cap and Poly-A tail) in a 10:1 ratio (50mM/5mM), the reaction mixtures were incubated at 37°C for 1-1.5 hours for targeted cleavage of FL mRNA. The samples are then incubated in a Wheat Germ Extract (WGE; Promega) allowing for efficient translation of FL and RL proteins. Using the Dual-Glo (Promega) luciferase assay, FL and RL luminescence signals were read on a luminometer (GloMax, Promega). A normalized FL/RL signal ratio was then calculated comparing NT control and FL siRNA signal levels to assess efficiency of target FL cleavage.

For AGO2-KRAS *in vitro* cleavage assay (**Supplemental Figure 4.3**), HeLa lysate IVT over expression was used to generate AGO2 and KRAS (WT and G12V) for use in these assays. KRAS IVT mixtures were then loaded with various nucleotides (GDP and GTP) to control for differences due to KRAS GTP vs GDP binding state. Additionally, the ATP (not loaded by KRAS) and GTPγS (a non-hydrolyzable GTP analog) nucleotides were used as controls, and both BSA and GFP were used in place of KRAS as non-interacting controls.

Single Molecule Microscopy Slide Preparation

In brief, quartz slides were prepared with 2 holes for the assembly of the flow chamber. After previous usage, flow chamber slides were cleaned by first boiling in water and cleaned with razor to remove old epoxy and coverslip. Slides were then sonicated in Alconox solution (ThermoFisher) for 1 hour in a coplin jar. Following rinsing in Milli-Q (MQ) water, slides were again sonicated in 1M KOH for 20 min and rinsed with MQ water. Slides were flamed with torch to remove any other impurities and then boiled in Piranha solution (90 ml ddH_2O, 20 ml NH_4OH, and 20 ml 35% H_2O_2) for 30 minutes. After Piranha treatment, slides were rinsed with MQ water and dried with nitrogen. Slides were then treated with APTES (3-aminopropyltriethoxysilane) to undergo aminosilylation allowing proteins to bind to the slide downstream. Slides were placed in acetone and 2 ml APTES in a coplin jar and incubated for 20 min followed by 1 mi sonication and an additional incubation for 10 min.

Following the cleaning and initial steps prepping the quartz slides, they were then coated with mPEG-Biotin to assist in the binding of streptavidin on the day of imaging. Briefly, slides were washed with MQ water and nitrogen dried following aminosilylation. Biotin-PEG and mPEG powders were prepared in a PEGylation buffer (0.1 M sodium bicarbonate) and centrifuged for 1

min at 10,000 rpm to remove bubbles. Slides were then oriented in an empty pipette tip holder with water in the bottom chamber. The PEG solution (70 ul) was then added to the slide surface and a 24x30 mm glass cover slip (Fisher) was placed on top taking care to remove any bubbles introduced. Note that the cover slip was treated in the same method described above starting with the aminosilylation step. Slides were placed in a dark drawer and incubated for 2-3 hours or overnight. After incubation with mPEG-Biotin, the slides were treated with were treated with Sulfo-DST to assist in cross-linking PEG to the slide. Slides were again washed in MQ water and dried with nitrogen. The DST solution was produced by dissolving 12 mg of DST into 1 M sodium bicarbonate. Following removal of solution bubbles, 70 ul of DST solution was added to each slide with a cover slip placed on top (note cover slip orientation to same treated side must be maintained). Slides were incubated for 30 minutes, rinsed with MQ water, and dried with nitrogen gas.

Finally, a chamber was then constructed by adding two pieces of double sided tape in a diagonal fashion flanking the two slide holes. The treated cover slip was then placed down with care not to pull on and off. Epoxy was used to seal the chamber and allowed to dry at room temperature. Plastic tubing was added to the two slide holes (using trimmed pipette tips as a scaffold) for inlet and outlet, thus generating a flow chamber by which to analyze our single molecules. Completed slides were then stored in a dark, dry place until use.

Single Molecule Imaging

Using a custom built total internal reflection fluorescence (TIRF) microscope, we were able to visualize individual molecules of Halo-AGO2 or SNAP-KRAS. In more traditional wide-field microscopy, samples are visualized via a light source directly passing through the sample. This

ultimately leads to high levels of fluorescent background, as many fluorophores outside of the plane of view are excited [14]. TIRF microscopy overcomes these limitations by exciting a small region under 100-150 nm. Briefly, this is achieved by reflecting light at an incident angle within a high refractive index medium into a lower refractive medium, leading to total reflection within the higher medium. This generates an evanescent wave which can excite fluorophores only in a thin region greatly reducing the background noise generated [15, 16]. As we only wish to observe single molecules, TIRF provides the ideal platform with which to analyze signal from individual proteins with minimal background noise.

Our high resolution, single molecule analysis via TIRF required the development of a flow chamber slide suitable for our imaging needs (**Figure 4.2a**). In order to monitor a given protein, each slide is treated as needed for downstream single molecule analysis and an antibody based scaffold can be assembled to capture any given protein of interest in a sandwich assay (**Figure 4.2b**). This sandwich assay provides multiple advantages for the study of single molecule interactions. We further prepared our slides assembled as described above for the SM sandwich assay. A HEPES buffered saline (HBS) buffer was used throughout to wash the slide with care given with each solution to not introduce bubbles into the flow chamber. Following an initial clearing with 200 ul of 1x HBS buffer (20 mM HEPES-KOH pH 7.4, 135 mM NaCl, 5 mM KCl, 1 mM $MgCl_2$), a second wash with 200 ul of 0.1% Tween 20 detergent dissolved in 1x HBS buffer was incubated in the flow chamber for 10 min at room temperature (RT). Another clearing step with 1x HBS buffer was followed by a 10 min incubation in 0.2 mg/ml streptavidin. The slide was again cleared with 1x HBS buffer and incubated in 200 ul of Protein G Biotin (20 ug/ml) for 10 minutes. Finally, the slide was cleared with 1x HBS buffer and incubated in Halo monoclonal primary antibody (Promega; G9211) diluted 1:100 in HBS buffer for 10 minutes. Following this

final wash, each slide was imaged to generate a background signal. As each slide contains some level of background noise, these images provide a signal control. As our IVT extracts and over expression proteins still retain all endogenous HeLa lysate proteins, the capture of HaloTag or SNAP-Tag proteins via a specific antibody sandwich allows one to stringently wash not only the extraneous HeLa lysate proteins but also the remaining unbound fluorescent dye. These wash steps greatly reduce background, allowing for a higher level of specific fluorescent signal.

After completing slide preparation, HaloTag and SNAP-Tag labeled proteins were prepared in a series of dilution steps for addition to slides. In brief, dilutions of 1/1000, 1/750, 1/500, 1/250, and 1/100 were prepared depending on the initial concentration of a particular IVT preparation. Each protein dilution was prepared in a similar loading solution (0.1% base Tween 20 in 1x HBS buffer) containing 2 mM trolox, 50 μM protocatechiuc acid (PCA), and 50 nM protocatechuate dehydrogenase (PCD) as oxygen scavengers. As above, protein dilution samples were incubated on slides for 10 min to allow binding of HaloTag to antibody, followed by a quick wash with 1x HBS. Additionally, a No Protein wash in the oxygen scavenging solution described above was used for a final slide wash before imaging on TIRF microscope.

In Vitro RNase Treatment

For our analysis of AGO2 forming higher order complexes, 10 ul of Halo-AGO2 IVT extract was incubated with 5 ul of RNase cocktail (ThermoFisher; AM2286) for 15 min at 37°C. Control, non-treated Halo-AGO2 was incubated in 1x HBS in the same ratio to maintain the concentration of AGO2. Protein dilutions of the Halo-AGO2 extracts were adjusted to match the Halo-Tag alone controls when loaded on slide.

Results

In Vitro Translation for Tagged-Human Protein Expression

In order to study the complex biochemical properties of the AGO2-RAS interaction, we set out to develop a robust set of *in vitro* tools which would allow deeper analysis with faithful reproduction of AGO2 and RAS biology. While purified proteins provide a means to obtain large levels of any protein of interest to facilitate easy study of protein structure, biochemical properties, and function, it is a time and skill intensive process [17]. Cell free expression (CFE) systems have been commercially developed in both bacterial and mammalian backgrounds and are a faster alternative to producing high levels of any protein of interest *in vitro* [18, 19]. With the goal of producing a panel of multiple AGO2 and K/H/NRAS mutants for both single molecule imaging and *in vitro* biochemical functional studies, we selected the HeLa extract based 1-Step Human Couple *In Vtiro* Translation (IVT) kit (ThermoFisher), which produces high levels of specific proteins in four hours. These constructs allow for the specific overexpression of their target protein with little background (**Supplemental Figure 4.1a**).

Fusion protein tags for recombinant proteins have been available for decades with many potential experimental uses including affinity purification (eg His or FLAG tags) [20], identification of protein binding partners (eg TurboID) [21], and fluorescent imaging (eg GFP or YFP tags) [22]. While individual protein tags are ideal for typically a single experimental function, they are typically ill suited for other functions. In order to circumvent the limitations of single function protein tags, we selected the HaloTag and SNAP-tag based enzymatic tags for their versatility in labeling, surface binding ligands (biotin), and ease of use in both live cell and *in vitro* systems. While green fluorescent protein (GFP) and similar fluorescent protein tags are useful in confocal microscopy to visualize proteins and cellular structures, they are limited in intensity of

signal, stability/photobleaching, and color options compared to many organic dye fluorophores [23-25]. Multiple commercial HaloTag and SNAP-tag ligand dyes are currently available allowing the specific connection of a high signal organic fluorophore to a tagged protein of interest, including the SNAP-Cell SiR (NEB) [26] and Jenalia Fluor (JF) dyes: JF549 and JF646 (Promega) [27].

Since each IVT reaction produces a varying level of target protein, concentrations of each protein must be estimated before downstream reactions to ensure consistent levels between experiments. Using commercially purified HaloTag (Promega) and SNAP-Tag (NEB) proteins of a known concentration, an immunoblot based dilution curve was generated to compare with the IVT generated proteins (**Supplemental Figure 4.1b**). While this estimation does not produce an exact measurement of IVT protein concentration, it ensures that proteins are within an acceptable range of variance in subsequent experiments. We ensured that there was no background protein-protein interaction detected between HaloTag and SNAP-tag via Co-immunoprecipitation (Co-IP; **Supplemental Figure 4.1c**). Furthermore, neither of these tags was found to interact with endogenous expression of either AGO2 or RAS.

Analyzing in Vitro RNA Induced Silencing Complex Activity

The functional role of the Argonaute protein family has been extensively studied in the literature, and AGO2's binding partners and RNA interference activity within the cell is well characterized. We set out to utilize a Firefly luciferase (FL) and Renilla luciferase (RL) [28] based Dual-Glo (Promega) reporter assay that is suitable *in vitro* and *in vivo* (**Figure 4.1a**). Using this assay, we asked what RNA Induced Silencing Complex (RISC) members were necessary for full AGO2 mediated RNAi. As expected, HeLa cell lines displayed almost complete loss of FL signal

following the addition of siRNA transcript targeting the FL mRNA compared to the control non-targeting (NT) siRNA (**Figure 4.1b**). While *in vivo* assays provide an important view into many cellular processes, *in vitro* assays utilizing purified or IVT proteins are more suitable for biochemical analysis. In order to better study the biochemical properties of AGO2 and its various RISC binding partners, we adapted the FL/RL reporter assay to an *in vitro* system. Surprisingly, purified AGO2 did not display any cleavage of FL mRNA when incubated with the target siRNA (**Figure 4.1b**).

Importantly, these reaction mixtures did not contain any other human proteins in RISC, suggesting that AGO2's RNAi activity was in part reliant on these binding partners *in vitro*. We next tested the cleavage ability of human AGO2 (hAGO2) derived through over expression in a bacterial IVT system (PURExpress; NEB). While this hAGO2 IVT protein displayed some enhanced ability to cleave FL mRNA, it was still minimal compared to HeLa *in vivo* activity. These results suggested that while bacterial RISC components were able to enhance AGO2 cleavage, hAGO2 may require all of its human RISC partners for normal activity *in vitro*. Using the HeLa IVT kit described earlier, we next asked if the HeLa lysate reagents retained any basal RNAi activity. Following the addition of siRNA transcript targeting FL, the HeLa cell extract displayed approximately 20-25% reduction in FL signal compared NT controls. However, the IVT over expression of AGO2 produced a nearly complete loss of FL, similar to levels seen *in vivo* in HeLa cells (**Figure 4.1b**). These results suggest that human AGO2 requires the presence of RISC members found in the HeLa IVT mixture in order to mediate full RNAi *in vitro*, and that the over expression of AGO2 can drive this cleavage assay further.

To further probe the *in vitro* requirement for RISC members in AGO2 mediated RNAi, we next tested the ability of IVT generated proteins to mediate miRNA translational repression.

Unlike siRNAs which typically are designed to be fully complementary to their target mRNA transcript, miRNAs often contain non-matching base pairs, leading to translational repression of target mRNA [29]. Utilizing a miRNA targeting FL, we conducted our reporter assay in the presence of multiple RISC members over expressed in the HeLa IVT mixture. AGO2, DICER, TRBP, and TRNC6A IVT alone did not produce sizeable repression of FL via targeted miRNA (**Figure 4.1c**), despite the presence of endogenous AGO2 within the HeLa lysate. However, the combination of all three RISC member IVTs with AGO2 IVT led to substantial repression of FL with targeted miRNA. Thus, AGO2 requires high expression of multiple RISC components *in vitro* in order to faithfully repress targeted mRNA transcripts through miRNAs.

We next ensured that our Halo-AGO2 tagged proteins could still recapitulate AGO2 RNAi activity. As seen previously, HeLa lysate could suppress FL signal by approximately 20%, and Halo-AGO2 achieved over 80% loss of FL signal with targeted siRNA demonstrating that the HaloTag did not alter AGO2 function (**Figure 4.1d**). We also set out to assess the ability of our *in vitro* cleavage assay to recapitulate known AGO2 mutation phenotypes. The Y529 residue of the MID domain has previously been established as crucial for 5'-end binding of miRNA transcripts, and phosphorylation of this tyrosine is known to block miRNA binding. Mutation at this site to a phosphomimetic glutamate (Y529E) produces a negative charge within the 5' binding site and has previously been shown to reduce siRNA mediated cleavage in transfected HeLa cells [30]. After adjusting concentrations of IVT over expression mixtures, mutant Y529E was compared to WT Halo-AGO2 in the FL/RL reporter cleavage assay described above. While WT Halo-AGO2 protein was able to reduce FL signal by approximately 75%, Y529E Halo-AGO2 saw minimal reduction of signal similar to the basal HeLa IVT mixture (**Figure 4.1e**), indicating that the observed signal reduction was likely do to endogenous WT AGO2 within the HeLa lysate. The "slicer" activity of

AGO2 is known to reside within the PIWI domain and the catalytic triad of D597, D669, and H807 [31]. Specifically, the D597A and D669A mutations are known to be catalytically dead despite continued binding of miRNA or siRNA transcripts [32]. Our Halo-AGO2 D669A IVT mixture displayed a similar reduction in AGO2 activity again resembling levels seen in the basal HeLa IVT mixture (**Figure 4.1e**).

Labeling Halo-AGO2 with Fluorescent Dyes

As both Halo-AGO2 and siRNA transcripts could be fluorescently labeled for future single-molecule imaging, we asked if the labeling process could alter RNAi activity. Using the method described above, Halo-AGO2 was loaded with JF549 dye (Promega), and proper labeling of Halo-AGO2 was confirmed via fluorescent SDS-PAGE gel (**Supplemental Figure 4.2a**). To further credential our Halo-AGO2 and SNAP-KRAS IVT proteins, we assessed their established binding affinity following labeling with their specific fluorescent dyes (SNAP 647-SiR; Halo JF549). As expected, WT Halo-AGO2 and WT SNAP-KRAS were able to interact following labeling and Co-IP together. Additionally, the Y64G mutant SNAP-KRAS was unable to interact with WT Halo-AGO2 and little fluorescent signal was seen following resolution on an SDS-PAGE gel in the Cy5 channel (**Supplemental Figure 4.2b**), confirming our previous observations [9].

Since the dying process dilutes the IVT mixture, a non-labeled Halo-AGO2 control was processed in parallel with DMSO added in place of dye. While the dying process diluted the IVT sample and lowered Halo-AGO2 activity *in vitro*, there was no difference observed between the non-labeled control and the JF549 labeled Halo-AGO2 (**Figure 4.1f**). Together these results indicate our IVT based AGO2 toolbox is fully functional *in vitro* and recapitulates known RNAi biology faithfully. Furthermore, we demonstrated that AGO2 requires additional RISC members

found in the HeLa lysate that are required for normal siRNA mediated cleavage and miRNA translational repression.

Single Molecule Analysis of AGO2-KRAS Interaction

The AGO2-KRAS interaction is readily observable *in vitro* via immunoprecipitation and *in vivo* through confocal microscopy as seen in earlier chapters. However, neither of these techniques provides a suitable means to assess the stoichiometry of AGO2-KRAS. In order to better study the interaction of AGO2 and RAS proteins *in vitro*, we set out to extend our toolbox to assess protein-protein interactions at a single molecule resolution.

Given our desire to study the interaction of AGO2 and KRAS at a single molecule level, we selected our Halo-AGO2 and SNAP-KRAS clones generated in the sections above. Not only do these provide with an easy method to generate high levels of IVT over expression of each protein, but they also are easily labeled with high intensity fluorescent dyes. Following the labeling of Halo-AGO2 (JF549; Promega) and SNAP-KRAS (SiR-A647; NEB), a set of flow chamber slides were prepped for single molecule analysis via TIRF microscopy (**Figure 4.2a**). Following the addition of both Protein A/G-biotin and primary Halo antibody, JF549-Halo-AGO2 was added to the slide in varying concentrations (**Figure 4.2b**). The number of Halo-AGO2 spots observed increased in a concentration dependent manner with Halo-Antibody and Protein A/G-biotin compared to the no Protein A/G controls (**Figure 4.2c**). To assess the ability of KRAS to interact with AGO2, we next added A647-SNAP-KRAS with increasing concentrations and only observed binding upon incubation with Halo-AGO2 and Halo antibody (**Figure 4.2d**).

This suggests that SNAP-KRAS is able to bind to the slide only in the presence of Halo-AGO2, as no SNAP primary antibody was added to the slide. Further analysis of the spots on these

interaction slides revealed that approximately 30% of each Halo-AGO2 spot was associated with a SNAP-KRAS spot and vice versa (**Figure 4.2e**). This suggests that a reasonable number of SNAP-KRAS spots may bind to the slide in a spurious, non-specific manner. As SNAP-KRAS only was found to bind after the addition of Halo-AGO2, it is possible that the stepwise addition of each protein IVT mixture leads to an accumulation of non-specific proteins crashing out of solution onto the slide surface, leading to increased SNAP-KRAS interactions on the surface; however, this possibility remains open to further investigation.

For downstream analysis of AGO2-KRAS interaction, only co-localizing spots (representing true AGO2-KRAS binding) were analyzed for stoichiometric study. In co-localizing pairs of Halo-AGO2 and SNAP-KRAS, the intensity of each spot was calculated and plotted as number of AGO2 molecules vs number of KRAS molecules (**Figure 4.2e**). In general, there was a 1:1 stoichiometry observed between spots of Halo-AGO2 and SNAP-KRAS indicating that each of these proteins bound a single partner. Furthermore, as the majority of spots analyzed were multimers containing multiple AGO2 and KRAS proteins, our results suggest that AGO2 and KRAS may cluster together in multiple protein complexes *in vitro*.

Assessing the Role of the AGO2-KRAS Interaction on RNAi Activity in Vitro

Following the development of our SM *in vitro* AGO2-KRAS binding assay, we next asked what the role KRAS may play in AGO2 RNAi activity. In *Shankar et al*, mutant KRAS was found to inhibit the unwinding of a dual labeled *Let-7a* siRNA transcript injected into various cell lines [9]. KRAS binds to AGO2's N-terminal domain which is known to play a role in the unwinding of siRNA and miRNA duplex [33]. However, these *in vivo* assays do not elucidate whether the

inhibition from mutant KRAS is due to the direct interaction with AGO2 or whether the cellular conditions within cells expressing these mutations somehow alter RNAi activity.

In order to understand the role that direct interaction between AGO2 and KRAS plays in RNAi, we utilized the *in vitro* AGO2 cleavage assay described above. Both basal HeLa IVT lysate and AGO2 IVT over expression reactions demonstrated normal cleavage levels, when incubated with BSA or GFP (regardless of nucleotide loading) with AGO2 IVT displaying higher levels of siRNA mediated FL loss (**Supplemental Figure 4.3a**). Next the basal IVT extract and AGO2 IVT over-expressions were incubated with WT KRAS and four nucleotide conditions (ATP, GDP, GTP, and GTPγS). Interestingly in both IVT samples, GTPγS loaded KRAS saw a significant inhibition of FL cleavage (**Supplemental Figure 4.3b**). Loading of GTP itself had a moderate reduction in AGO2 RNAi function, likely due to WT KRAS intrinsic GTP hydrolysis leading to conversion to KRAS-GDP. Finally, the addition of mutant KRAS to AGO2 IVT saw a large reduction in both GTP and GTPγS conditions (**Supplemental Figure 4.3c**), as $KRAS^{G12V}$ lacks intrinsic GTPase activity. These results suggest that GTP loaded KRAS is sufficient to inhibit AGO2 siRNA mediated cleavage *in vitro*; however, some RNAi activity was retained in all of these conditions suggesting that the previous inhibition of AGO2 duplex unwinding by mutant KRAS observed [9] may have a more complex role *in vivo*. These assays remain to be completed at a SM resolution to fully elucidate the biochemical properties of AGO2-KRAS interaction and its functional role in AGO2 RNAi activity.

Single Molecule Assessment of AGO2 Phase Transition and Higher Order Complexes

Following our study of AGO2-KRAS interaction using single molecule TIRF, we noted a high number of Halo-JF549-AGO2 multimers and clusters on the slide. These clusters were surprising

given that labeled Halo-tag (Halo-JF549) controls did not exhibit these clusters *in vitro* (**Supplemental Figure 4.4a**). Since labeled Halo-AGO2 IVT mixtures are functional *in vitro*, we hypothesized that this clustering was due to higher order complex formation within the RISC complex. Following RNase treatment, the number of Halo-JF549-AGO2 clusters greatly dispersed on the slide (**Supplemental Figure 4.4a**). Deeper analysis of these single molecule spots demonstrated that Halo-JF549-AGO2 had far less spots per field of view (FoV) than the Halo-JF549 tag alone, and following RNase treatment, the number of Halo-JF549-AGO2 spots/FoV increased to levels seen with the tag alone (**Supplemental Figure 4.4b**). Interestingly, when spots between these three groups were analyzed for the number of total molecules/FoV, non-treated Halo-JF549-AGO2 had similar total molecules to the other conditions (**Supplemental Figure 4.4c**), suggesting that Halo-JF549-AGO2 was clustering in higher order complexes *in vitro* that was disrupted upon RNase treatment. Further analysis of these groups indicated that while Halo-tag and RNase treated Halo-AGO2 primarily formed monomers on the surface, non-treated Halo-AGO2 primarily formed groups with greater than three molecules (**Supplemental Figure 4.4d**). These results indicate that AGO2 is at least partially reliant on RNA to form higher order clusters. However, future work will be necessary to elucidate the role of KRAS and other RISC members in the formation of these complexes both *in vitro* and *in vivo*.

Discussion

In this chapter, we have developed a single molecule toolbox to study the biochemical properties of AGO2 and its binding partners such as KRAS. Utilizing a HeLa IVT system, we can efficiently generate any number of functional human proteins *in vitro*. Through HaloTag and SNAP-Tags labeling with fluorescent dyes, we are able to visualize high resolution single molecules via total

internal reflection fluorescence (TIRF) microscopy. This platform represents a novel toolbox by which to study the biochemical properties of AGO2's interaction with RISC members and binding partners like KRAS. Here we have shown that AGO2 requires the presence of other RISC members to mediated siRNA and miRNA targeted cleavage of target mRNA transcripts. Additionally, IVT proteins are able to faithfully recapitulate known RNAi activity of both WT and various mutant forms of AGO2 *in vitro* (**Figure 4.1**). In addition, our SM sandwich assay confirmed the interaction of Halo-AGO2 and SNAP-KRAS in a 1:1 stoichiometry (**Figure 4.2**), and in keeping with previous observations [9], mutant KRAS and GTP-loaded WT KRAS are able to partially inhibit AGO2 RNAi function *in vitro* (**Supplemental Figure 4.3**). Finally, we demonstrated that Halo-AGO2 forms higher order complexes *in vitro* that can be disrupted with RNase treatment (**Supplemental Figure 4.4**).

Previous studies have identified TRNC6 (GW182) as a central component of the RISC and P bodies within cells [34], and recent work, demonstrated that the tryptophan binding region of AGO2 recognizes specific residues within TRNC6. The interaction of AGO2 and TRNC6 led to the phase separation of these proteins both *in vitro* and *in vivo*, acting to promote the deadenylation of target mRNA through accelerated miRNA RISC activity [8]. In our SM studies with Halo-AGO2, we were initially surprised to observe areas of high density signal when incubated on our flow chamber slides (**Supplemental Figure 4.4**). These observations were in contrast to the expected single molecule distribution observed with HaloTag alone, and they suggest that IVT Halo-AGO2 may form higher order complexes *in vitro*. This would not be surprising as the HeLa IVT extract contains all endogenous human RISC members. Furthermore, treatment with RNase disrupted these complexes, greatly reducing the stoichiometry of Halo-AGO2 spots observed. This observation suggests that RNA transcripts play a key role in producing these higher order clusters,

but it is unclear whether this process is driven by mRNA or miRNA sequences. Future studies will probe whether the addition of synthetic RNAs of different sizes can recapitulate these phase separated particles through these *in vitro* SM stoichiometry assays. It remains unclear the extent to which specific AGO2 functional domains and point mutations could disrupt this process *in vitro* with point mutations such as AGO2-D669A (catalytically dead) or AGO2-ΔN-Domain constructs. Additionally, it remains to be seen if these higher order complexes can be altered by the addition of RISC members (TRNC6 specifically) or the addition of KRAS.

In this study, we have recapitulated the AGO2-KRAS interaction *in vitro* at a single molecule level. Our results show that AGO2 and RAS bind in a 1:1 stoichiometry. While we are unable to confirm whether the AGO2-RAS is a direct interaction in this system do to the presence of other proteins within the HeLa IVT extract, SNAP-KRAS's requirement for Halo-AGO2 to bind to the HaloTag antibody treated slide further support the establishment of this interaction either as a direct binding event or as a part of a larger complex. Additionally, the *in vitro* cleavage assays demonstrate that GTP loaded KRAS at least partially inhibits AGO2 RNAi activity. This finding is in keeping with the known ability for AGO2 to prevent miRNA unwinding *in vivo* [9]. However, it is unclear the exact mechanism by which this inhibition occurs. One hypothesis is that AGO2-KRAS binding disrupts RISC phase separation, thereby partially inhibiting AGO2 RNAi activity. Likewise, it may be possible that KRAS preferentially shifts AGO2 to different compartments of the cell away from RISC members. Our previous studies in a mouse model of pancreatic ductal adenocarcinoma (PDAC) showed that AGO2-KRAS co-localization at the plasma membrane increased with severity of PDAC progression (**Chapter 2**). Thus, AGO2 may be sequestered by mutant KRAS *in vivo* away from other binding partners, hampering miRNA binding and/or targeting.

This SM toolbox provides a platform by which to interrogate these biochemical questions regarding the AGO2-KRAS interaction. The addition of Halo-AGO2 and SNAP-KRAS with labeled miRNA and target mRNA transcripts could be conducted a multi-colored SM assay. This could elucidate whether specific SNAP-KRAS mutants are sufficient to alter miRNA loading into AGO2, targeting of AGO2 to mRNA transcripts, or preventing the formation of higher order complexes *in vitro*. While we have already demonstrated faithful loading of labeled miRNA *in vitro* with little background (data not shown), these questions remain open for future exploration.

Finally, this SM toolbox is not restricted to smaller scale biochemical experiments. As the precise protein crystal structure of AGO2-KRAS interaction remains elusive, it has been difficult to approach small molecule methods to disrupt the binding of these proteins. Our SM platform could be modified to potentially screen potential small molecule inhibitors on a medium to higher throughput scale. The disruption of AGO2-KRAS would be apparent following incubation with various compounds, and while such an experiment may require the development of different flow chambers or specific assay conditions, it illustrates the versatility that this SM toolbox provides for the study of biochemical interactions such as AGO2-KRAS.

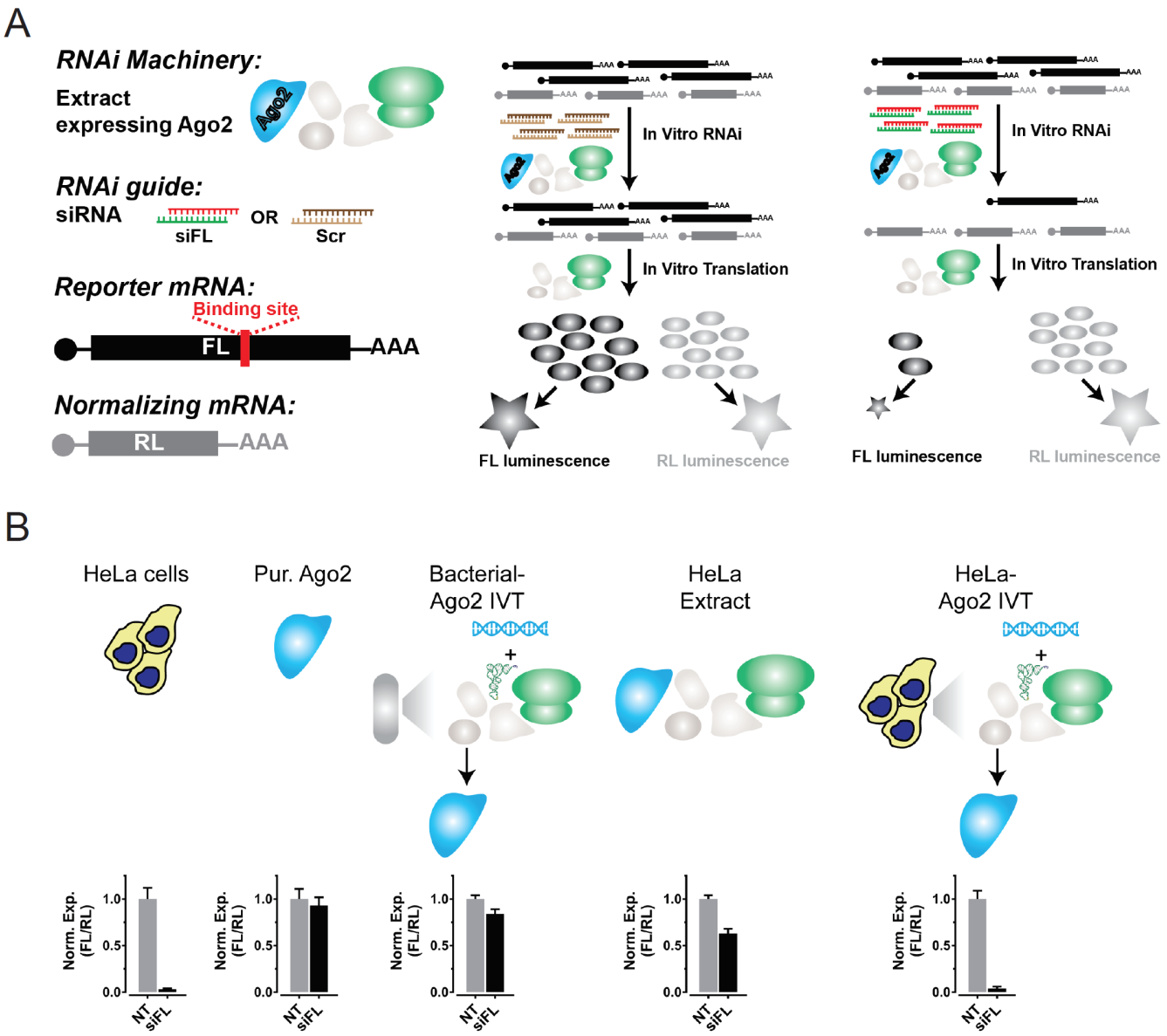

Figure 4.1 *In Vitro* AGO2 RNAi Activity Requires RISC Member Proteins

(A) Overview of *in vitro* AGO2 FL/RL siRNA mediated cleavage assay

(B) Comparison of RNAi activity between HeLa cells, purified AGO2, bacterial IVT AGO2, HeLa extract, and HeLa IVT AGO2 Overexpression

(C) Comparison of miRNA activity between the conditions in 4.1b, HeLa IVT DICER, HeLa IVT TRBP, HeLa IVT TNRC6A, and a mixture of AGO2 IVT with RISC members

(D) HaloTag addition to AGO2 does not hinder IVT generated RNAi activity

(E) Halo-AGO2 point mutations Y529E and D669A inhibit RNAi activity

(F) Labeling of HaloTag does not inhibit AGO2 function. Compared to a mock diluted non-labeled Halo-AGO2 to account for dilution during HaloTag dye labeling process

Figure 4.1 Continued

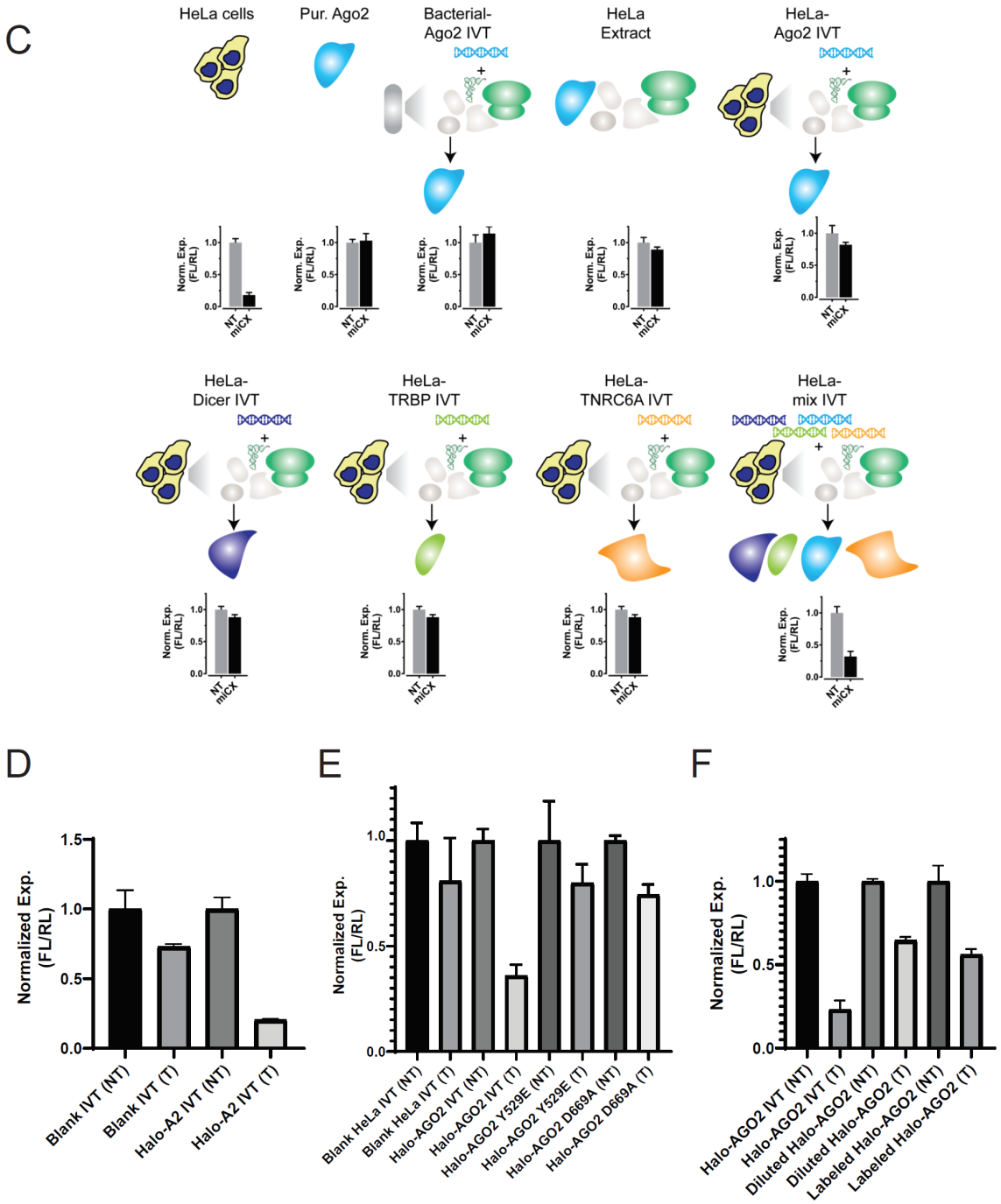

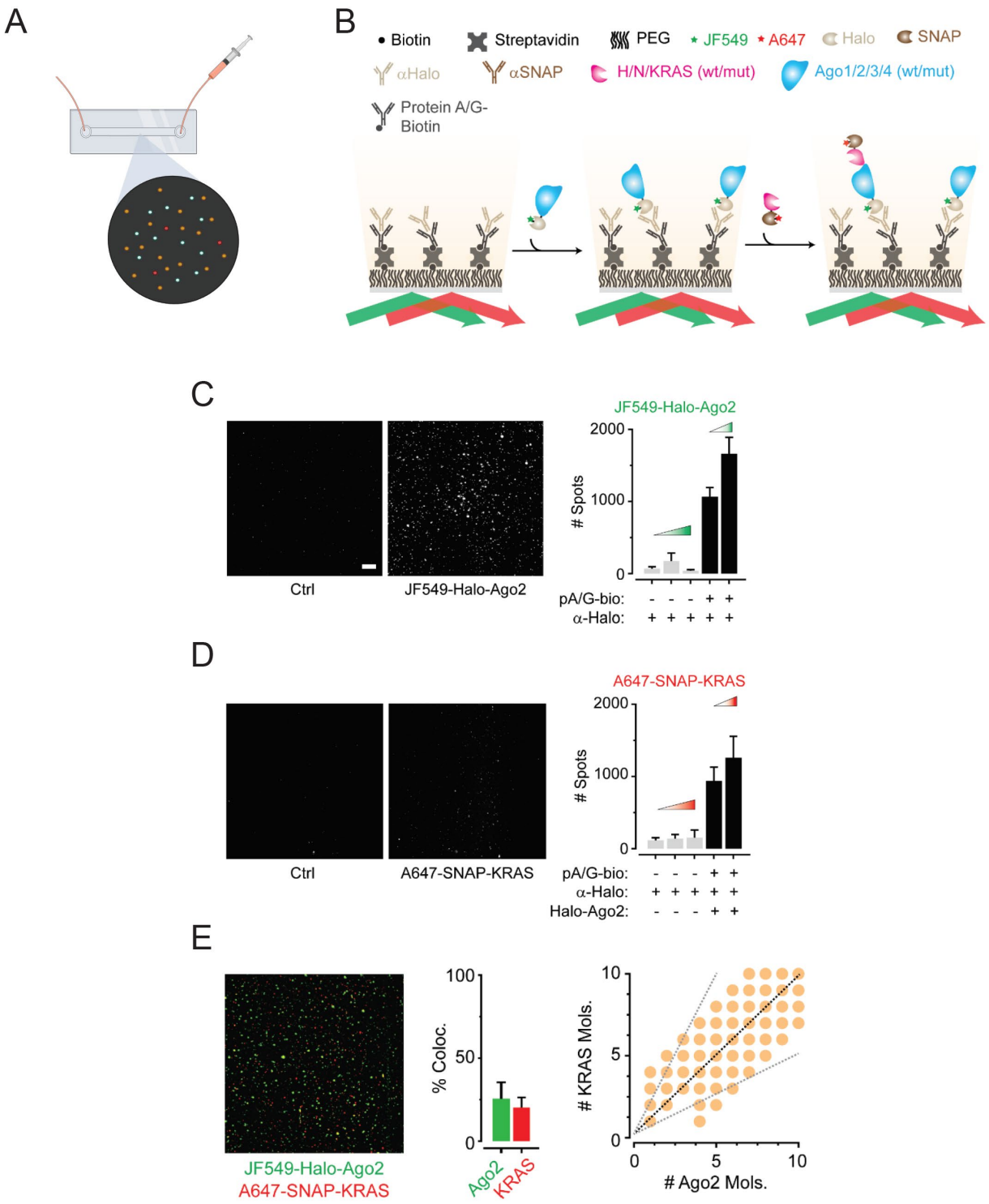

Figure 4.2 *In Vitro* Single Molecule Assay of Halo-AGO2 and SNAP-KRAS Interaction
(A) Model of SM Slide Flow Chamber

Figure 4.2 Continued
(B) Model of sandwich assay for SM interaction assay
(C) Single molecule analysis of JF549-Halo-AGO2 comparing full Halo antibody sandwich with no protein A/G-biotin control
(D) Single molecule analysis of A647-SNAP-KRAS with Halo-AGO2 co-incubation comparing full Halo antibody sandwich with no protein A/G-biotin control
(E) Co-localization of Halo-AGO2 and SNAP-KRAS with stoichiometry analysis

References

1. Shashkova, S. and M.C. Leake, *Single-molecule fluorescence microscopy review: shedding new light on old problems.* Biosci Rep, 2017. **37**(4).
2. Fire, A., et al., *Potent and specific genetic interference by double-stranded RNA in Caenorhabditis elegans.* Nature, 1998. **391**(6669): p. 806-11.
3. Bartel, D.P., *MicroRNAs: genomics, biogenesis, mechanism, and function.* Cell, 2004. **116**(2): p. 281-97.
4. Macfarlane, L.A. and P.R. Murphy, *MicroRNA: Biogenesis, Function and Role in Cancer.* Curr Genomics, 2010. **11**(7): p. 537-61.
5. Shin, Y. and C.P. Brangwynne, *Liquid phase condensation in cell physiology and disease.* Science, 2017. **357**(6357).
6. Brangwynne, C.P., et al., *Germline P granules are liquid droplets that localize by controlled dissolution/condensation.* Science, 2009. **324**(5935): p. 1729-32.
7. Molliex, A., et al., *Phase separation by low complexity domains promotes stress granule assembly and drives pathological fibrillization.* Cell, 2015. **163**(1): p. 123-33.
8. Sheu-Gruttadauria, J. and I.J. MacRae, *Phase Transitions in the Assembly and Function of Human miRISC.* Cell, 2018. **173**(4): p. 946-957 e16.
9. Shankar, S., et al., *KRAS Engages AGO2 to Enhance Cellular Transformation.* Cell Rep, 2016. **14**(6): p. 1448-1461.
10. England, C.G., H. Luo, and W. Cai, *HaloTag technology: a versatile platform for biomedical applications.* Bioconjug Chem, 2015. **26**(6): p. 975-86.
11. Cole, N.B., *Site-specific protein labeling with SNAP-tags.* Curr Protoc Protein Sci, 2013. **73**: p. 30 1 1-30 1 16.
12. Los, G.V., et al., *HaloTag: a novel protein labeling technology for cell imaging and protein analysis.* ACS Chem Biol, 2008. **3**(6): p. 373-82.
13. Urh, M. and M. Rosenberg, *HaloTag, a Platform Technology for Protein Analysis.* Curr Chem Genomics, 2012. **6**: p. 72-8.
14. Tokunaga, M., et al., *Single molecule imaging of fluorophores and enzymatic reactions achieved by objective-type total internal reflection fluorescence microscopy.* Biochem Biophys Res Commun, 1997. **235**(1): p. 47-53.
15. Mattheyses, A.L., S.M. Simon, and J.Z. Rappoport, *Imaging with total internal reflection fluorescence microscopy for the cell biologist.* J Cell Sci, 2010. **123**(Pt 21): p. 3621-8.
16. Howard, G.C., W.E. Brown, and M. Auer, *Imaging life : biological systems from atoms to tissues*. xii, 459 pages.
17. Young, C.L., Z.T. Britton, and A.S. Robinson, *Recombinant protein expression and purification: a comprehensive review of affinity tags and microbial applications.* Biotechnol J, 2012. **7**(5): p. 620-34.
18. Wang, S., et al., *Simultaneous monitoring of transcription and translation in mammalian cell-free expression in bulk and in cell-sized droplets.* Synth Biol (Oxf), 2018. **3**(1): p. ysy005.
19. Mikami, S., T. Kobayashi, and H. Imataka, *Cell-free protein synthesis systems with extracts from cultured human cells.* Methods Mol Biol, 2010. **607**: p. 43-52.
20. Terpe, K., *Overview of tag protein fusions: from molecular and biochemical fundamentals to commercial systems.* Appl Microbiol Biotechnol, 2003. **60**(5): p. 523-33.

21. Branon, T.C., et al., *Efficient proximity labeling in living cells and organisms with TurboID.* Nat Biotechnol, 2018. **36**(9): p. 880-887.
22. Zhang, J., et al., *Creating new fluorescent probes for cell biology.* Nat Rev Mol Cell Biol, 2002. **3**(12): p. 906-18.
23. Fernandez-Suarez, M. and A.Y. Ting, *Fluorescent probes for super-resolution imaging in living cells.* Nat Rev Mol Cell Biol, 2008. **9**(12): p. 929-43.
24. Cranfill, P.J., et al., *Quantitative assessment of fluorescent proteins.* Nat Methods, 2016. **13**(7): p. 557-62.
25. Kremers, G.J., et al., *Fluorescent proteins at a glance.* J Cell Sci, 2011. **124**(Pt 2): p. 157-60.
26. Remenyi, R., R. Li, and M. Harris, *On-demand Labeling of SNAP-tagged Viral Protein for Pulse-Chase Imaging, Quench-Pulse-Chase Imaging, and Nanoscopy-based Inspection of Cell Lysates.* Bio Protoc, 2019. **9**(4).
27. Grimm, J.B., et al., *Synthesis of Janelia Fluor HaloTag and SNAP-Tag Ligands and Their Use in Cellular Imaging Experiments.* Methods Mol Biol, 2017. **1663**: p. 179-188.
28. Siebring-van Olst, E. and V.W. van Beusechem, *High-Throughput Firefly Luciferase Reporter Assays.* Methods Mol Biol, 2018. **1755**: p. 19-29.
29. Hock, J. and G. Meister, *The Argonaute protein family.* Genome Biol, 2008. **9**(2): p. 210.
30. Rudel, S., et al., *Phosphorylation of human Argonaute proteins affects small RNA binding.* Nucleic Acids Res, 2011. **39**(6): p. 2330-43.
31. Elkayam, E., et al., *The structure of human argonaute-2 in complex with miR-20a.* Cell, 2012. **150**(1): p. 100-10.
32. Liu, J., et al., *Argonaute2 is the catalytic engine of mammalian RNAi.* Science, 2004. **305**(5689): p. 1437-41.
33. Kwak, P.B. and Y. Tomari, *The N domain of Argonaute drives duplex unwinding during RISC assembly.* Nat Struct Mol Biol, 2012. **19**(2): p. 145-51.
34. Liu, J., et al., *MicroRNA-dependent localization of targeted mRNAs to mammalian P-bodies.* Nat Cell Biol, 2005. **7**(7): p. 719-23.

Chapter 5

Discussion and Future Directions

Summary of This Study

Since the identification of the *RAS* gene family as oncogenes in the early 1980s, much progress has been made in characterizing their role in promoting the formation and survival of many tumors. Mutations in *RAS* genes are found in nearly a third of human cancers, and they are considered drivers of some of the most aggressive and deadly tumor types, including pancreatic, melanoma, lung, and colorectal [1, 2]. Recent advancements in targeting specific mutations in $KRAS^{G12C}$ have opened new possibilities for developing novel therapeutic interventions for *RAS* [3, 4]. Here we have described an essential role for AGO2 in the development of mutant *KRAS* driven pancreatic ductal adenocarcinoma (PDAC) and in the prevention of senescence in mutant *HRAS* and *NRAS* cancers. Furthermore, we developed a toolbox for the study of protein-protein interactions at a single molecule resolution such as AGO2 and KRAS.

Following the Chinnaiyan lab's discovery of a novel interaction between AGO2 and KRAS, we developed a conditional mouse model of PDAC with activation of $Kras^{LSL\text{-}G12D}$ and knockout of $Ago2^{fl/fl}$ (**Chapter 2**). Loss of Ago2 led to a profound increase in survival and an arrest of mutant *Kras* cells in low grade PanIN precursor lesions. These lesions exhibited increased levels of EGFR-RAS-MAPK signaling activating WT-RAS, ultimately leading to oncogene induced senescence (OIS) blocking progression to high grade PanINs. We also observed a marked increase

in NK cell infiltration into PanINs in the AGO2 null background significant for their known role in surveillance of senescent tissues [5]. Additionally, we uncovered a novel mechanism of EGFR mediated disruption of AGO2-KRAS through phosphorylation of AGO2-Y393 which is hindered in mutant *KRAS* cells. Interestingly, the observed arrest following loss of Ago2 in early stage PanIN lesions was overcome by the accompanied loss of *Trp53* with mice developing PDAC and showing similar survival to those expressing Ago2. These GEMMs uncovered an important role for AGO2 in the development of pancreatic ductal adenocarcinoma demonstrating a requirement for AGO2-KRAS interaction for progression from low- to high-grade PanIN lesions.

We next extended these observations to assess the role of AGO2 in *HRAS* and *NRAS* driven cancers (**Chapter 3**). As the three isoforms of RAS share nearly 100% amino acid identity within the Switch II domain, we found that AGO2 interacted with both HRAS and NRAS across multiple human cell lines. We further corroborated our observation that EGFR phosphorylation of AGO2-Y393 is sufficient to disrupt AGO2-HRAS and AGO2-NRAS interaction. Following the knockdown of AGO2 in mutant *HRAS* and *NRAS* driven cell lines, we saw a profound reduction in proliferation and migration capacity. These changes were accompanied by increased oncogene induced senescence (via β-galactosidase staining) and expression of *p53, p21,* and *p16*. Similar to our PDAC mouse model in **Chapter 2**, we observed that loss of AGO2 in these cell lines had increased levels of pEGFR and pERK through induction of reactive species, like H_2O_2, causing the inactivation of the protein phosphatase PTP1B. This hyperactivation of EGFR-RAS-ERK following AGO2 loss leads to the observed oncogene induced senescence (OIS), and the inactivation of PTP1B represents a potential important player in AGO2-RAS promotion of oncogensis.

Finally, we set out to develop a Single Molecule (SM) Toolbox for the biochemical study of protein-protein interactions such as AGO2-KRAS or AGO2-RISC members (**Chapter 4**). Using a HeLa extract based *in vitro* translation (IVT) system, we were able to quickly generate multiple proteins of interest with functional tags such as HaloTag and SNAP-Tag. We demonstrated that AGO2's siRNA and miRNA targeted cleavage capacity *in vitro* is reliant upon the presence of other RISC members such as TRBP, TRNC6, and DICER. Furthermore, we observed that single molecules of IVT generated Halo-AGO2 formed higher order complexes that could be dispersed upon treatment with RNase. While these could be partially reconstituted with the addition of RISC members, RNA was necessary for full formation of these complexes. Our *in vitro* assays, also revealed that GTP loaded KRAS (WT and G12V) was able to at least partially inhibit AGO2-siRNA mediated cleavage of targeted mRNA transcripts. This was in keeping with the Chinnaiyan lab's previous observation that mutant KRAS cell lines exhibited an inhibition of AGO2 unwinding of exogenous miRNAs. Finally, we utilized our single molecule IVT assay to observe the *in vitro* binding of Halo-AGO2 and SNAP-KRAS in a 1:1 ratio. Together, the development of this SM Toolbox is able to faithfully recapitulate functional protein interactions *in vitro* and represents an exciting opportunity to further study AGO2 and its interacting partners like KRAS.

Unexplored Areas in This Study and Future Directions

Our studies have demonstrated that AGO2 plays a vital role in multiple mutant *RAS* driven cancer types to prevent the development of OIS, and we have confirmed *in vitro* that the interaction of AGO2-KRAS not only occurs but also has functional relevance inhibiting both AGO2 RNAi activity and KRAS GTP-loading from guanine exchange factors (GEF) like SOS1. However,

despite these data, many questions remain as to the role of AGO2-RAS interaction in both normal physiology and cancer biology.

Temporal Requirement for AGO2 in Mutant RAS Driven Cancers

Our genetically engineered mouse model (GEMM) of PDAC in **Chapter 2**, supported the notion that mutant *KRAS* drives the development PDAC in two phases. The first phase is initiated and driven by mutation in *KRAS* leading to the formation of low-grade PanIN lesions. Previous studies have shown this is dependent upon EGFR-RAS signaling [6], but we identified a second phase of development which requires AGO2-KRAS interaction to further progress from early to late PanIN and eventually PDAC. This was further corroborated in our mutant *HRAS* and *NRAS* studies in **Chapter 3**, where loss of AGO2 also led to OIS and loss of proliferation. Together, these results represent an exciting prospect for the reliance of mutant *RAS* genes on continued interaction with AGO2 to initiate and maintain RAS driven oncogenic growth.

However, the loss of *Trp53* in our PDAC GEMM (KPC mice) exhibited an escape from the OIS phenotype, and the knockdown of AGO2 in a *TP53* null, *NRAS* mutant cell line failed to halt growth as well. These findings suggest that the requirement for AGO2 in *RAS* mutant cells is at least partially dependent upon intact senescence proteins like *p53*. Many human cancers, including PDAC, are known to acquire mutations in *p53*, *p16*, and other senescence mediators [7]. During the progression from low-grade to high-grade PanIN lesions, the accumulation of mutations in tumor suppressors is well documented in human tumors [8]. Our model has simultaneous loss of *Trp53* and activation of $Kras^{G12V}$, as opposed to human tumors where inactivation or loss of p53 occurs after the oncogenic activation of *KRAS*. Thus, it is unclear if AGO2 is simply required for the early transition to higher grade PanINs or if AGO2 plays a broader

role in the maintenance of oncogenic growth outside of this phase. We observed increased AGO2 expression with increasing severity of disease in both our mouse model and samples from human PDAC and metastatic disease suggesting that high AGO2 levels may play a role in more aggressive stages of disease.

In order to better understand the role of AGO2 following the development of PDAC or another GEMM tumor, future studies could utilize a dual-recombinase system to allow temporal control of AGO2 loss following activation of oncogenic *KRAS* in a PDAC GEMM. Flippase (FLP) is a recombinase from *S. cerevisiae* which recombines DNA between FRT sites, similarly to Cre-loxP sites [9]. By using such a dual-recombinase system, one could achieve $Kras^{G12D}$ activation and loss of *Ago2* as temporally separate events. These GEMMs already exist to study PDAC with sequential genetic events. A *Pdx1-Flp*; $FSF\text{-}Kras^{G12D/+}$; $FSF\text{-}R26^{CAG\text{-}CreERT2/+}$; $Trp53^{lox/lox}$ GEMM allows for the simultaneous activation of $Kras^{G12D}$ and expression of a tamoxifen-inducible Cre-recombinase ($CreER^{T2}$), thus p53 loss can occur downstream of KRAS oncogenic activation [10]. A similar mouse model could be used to observe a more stepwise approach to AGO2 loss in the development of PDAC. Simultaneous loss of AGO2 with KRAS activation could be followed with tamoxifen induced loss of p53 to observe if OIS escape still occurs, or AGO2 loss could be induced after establishment of a tumor to assess its ability to overcome an established tumor with either KRAS activation alone or with p53 loss/inactivation.

A better understanding of the temporal requirements for AGO2 in the development and survival of RAS driven cancers is essential. TP53 is mutated in approximately 75% of pancreatic cancer [11]. Furthermore, other senescence mediators such as p16 (*CDKN2A*) are mutated in over 90% of pancreatic tumors and are generally considered to be an earlier event than p53 [12]. Just as *Trp53* loss contributes to faster development of PDAC in GEMM, the loss of *Cdkn2a* also leads

to accelerated, metastatic PDAC in mice driven by $KRAS^{G12D}$ [13]. As both p53 and p16 ultimately act as mediators of senescence leading to the inhibition of cyclin-dependent kinases and allow pRB repression of E2F transcription factors, it remains to be seen if p16 loss could also escape oncogene induced senescence upon Ago2 loss as seen in the KPC mice. Further elucidation of the requirements for AGO2 in pancreatic cancer temporally, genetically, and biochemically may be essential to any potential/future therapeutic targeting of AGO2-RAS in human cancers.

Regulation of AGO2-RAS Interaction

Our results in **Chapters 2** and **3** established phosphorylation of AGO2 at Y393 by epidermal growth factor (EGFR) as a key event in the regulation of AGO2 binding to WT RAS proteins. This regulation was partially inhibited by the expression of mutant RAS isoforms; however, this inhibitory block can be overcome by stronger activation of EGFR-AGO2 interaction through treatment with H_2O_2 (**Figure 2.7g-i**) [14, 15]. There are many other post-translational modifications of AGO2 that have previously been identified to alter its function. It is possible that some of these events may play a role in regulating AGO2-RAS interaction in either normal physiology or cancer biology.

For instance, phosphorylation at the S387 residue of AGO2 has been previously shown to increase localization to P-bodies [16]. It recently was connected to inhibition of AGO2 and miRNA sorting into exosomes downstream of mutant KRAS signaling [17]. It is unclear whether these observations are dependent or independent of AGO2-RAS interaction. Likewise, post-translational modifications of WT or mutant RAS may promote or inhibit its interaction with AGO2. The Y64 residue of KRAS was previously identified as the AGO2 binding site [18]. This tyrosine is part of the Switch II domain and is also a critical binding site for SOS1 [19]. Our results in **Chapter 2**

confirm that AGO2 and SOS1 compete for KRAS binding where AGO2 inhibited SOS1 GEF activity *in vitro*. Recent studies have shown that KRAS can be phosphorylated downstream of Src kinase at Y32 and Y64, inhibiting interaction with SOS1 and reduces RAS downstream signaling [20]. This event may also impair RAS interaction with AGO2 and suggests that the AGO2-RAS interaction may be under the dynamic control of multiple cellular pathways. Further study will be necessary to comprehend the level of endogenous control of AGO2-RAS interaction and may uncover potential sites and methods of disrupting this interaction in mutant RAS driven cancers.

The Role of AGO2 in Different Tissue Lineages and RAS Isoforms

Despite their high level of homology and shared downstream signaling effecter pathways, the *RAS* isoforms display preference for specific tissue lineages when driving oncogenic growth. Additionally, the different RAS proteins differ in their C-terminal hypervariable region (HVR), which plays an important role in membrane localization [21]. Even within the same tumor lineage, mutations in the different RAS isoforms can lead to different downstream phenotypes. For example, genetically engineered mouse models of colorectal cancer with $KRAS^{G12D}$ displayed increased proliferation and differentiation defects in an APC deficient background, while $NRAS^{G12D}$ mutations were associated with decreased apoptosis [22]. This highlights the differing abilities of the *RAS* genes to promote cancer even within the same tissue background. While the data presented in this dissertation show that all three RAS isoforms share in their endogenous interaction with AGO2, it is not yet clear if the AGO2-RAS interaction shares the same biological role in all *RAS* driven cancers or tissue lineages.

The loss of AGO2 in mutant *HRAS* and *NRAS* driven cell lines promoted OIS in part through the deactivation of PTP1B phosphatase and hyperactivation of pEGFR and pERK

(**Chapter 3**). While our mouse model of PDAC observed a similar phenotype with AGO2 knockdown (**Chapter 2**), we were unable to detect changes in PTP1B when investigating senescent PanIN lesions (data not shown). Importantly, inactivation of PTP1B in *HRAS* and *NRAS* driven cells was observed downstream of increased reactive oxygen species (ROS) production (**Figure 3.5**). Mutant *HRAS* and *NRAS* have both previously been associated with an induction of ROS through induction of NADPH-oxidase via MAPK-ERK signaling [23-25]. *KRAS* is known to promote the removal of ROS following oncogenic activation and activating antioxidant enzymes like Mn-superoxide dismutase [26, 27]. The Chinnaiyan Lab's own observations in knocking down AGO2 in *KRAS* mutant cell lines led to cell death but did not produce senescence [18]. These differences in behavior between different *RAS* mutant cell lines suggest that while all isoforms may rely upon association with AGO2, the particular mechanism may be isoform specific. Further inquiry will be necessary to fully elucidate the full role of AGO2-RAS interaction across *KRAS*, *HRAS*, and *NRAS* mutant cancers.

There may be many lineage specific effects of AGO2 loss even among *KRAS* mutant cancers. Preliminary studies from the Chinnaiyan lab have explored the role of AGO2-KRAS interaction in a tamoxifen inducible Cre-recombinase under the control of CCSP (Clara cell secretory protein; lung specific promoter [28]) $Trp53^{fl/fl}$; $LSL\text{-}Kras^{G12D/+}$; $Ago2^{fl/fl}$; *CCSP-CreERT*. As in our PDAC model (**Chapter 2**), mice with loss of Ago2 displayed a lower number of gross nodules and lower staged adenocarcinoma. However, unlike our previous models, loss of Ago2 was associated with a decrease in downstream pErk levels by IHC (Data not shown). While more extensive characterization of this mechanism remains, these preliminary data suggest that mutant RAS dependence on AGO2 may be cell lineage and context dependent relying on different downstream signaling pathways in different tumor types. Furthermore, it is possible that mutations

in RAS may be independent of AGO2 in certain tumor types. Thus, a more in-depth investigation of the role of AGO2-RAS interaction across human cancer types is needed to fully understand its requirement in the development and survival of many different tumors.

The Role AGO2-RAS Interaction in RNA Interference

As AGO2 is the central component of the RNA induced silencing complex (RISC), its direct interaction with RAS proteins remains an open area of inquiry to fully elucidate the functional role of their binding. KRAS binds to the N-terminal or wedge-domain of AGO2 which has previously been shown to play a vital role in unwinding of miRNA or siRNA duplexes before full assembly of RISC [29]. The Chinnaiyan lab previously observed an inhibition of *let-7* unwinding in cell lines expressing mutant copies of *KRAS* [18]. As RAS mRNA is a major target of *let-7* miRNAs [30], the binding of mutant KRAS to AGO2 may act to suppress this regulation during transformation, leading to increased levels of RAS within the cell. The *in vitro* results presented in **Chapter 4** corroborate this finding. We found that incubation of AGO2 with GTP-loaded KRAS inhibited siRNA mediated cleavage *in vitro* (**Supplemental Figure 4.3**), suggesting that active RAS binding is responsible for at least partially inhibiting RISC activity. In our PDAC mouse *in vivo* study, we observed an up-regulation of specific miRNA transcripts following knockout of AGO2 in mice expressing mutant $KRAS^{G12D}$ (**Figure 2.6a**). Members of the *let-7* family were up-regulated following AGO2 loss. We also detected increased expression of the miR-29 and miR-30 families, which are regulated through retinoblastoma and up-regulated in senescence [31]. However, it is unclear why the loss of AGO2 induces the upregulation of these specific miRNAs, and future studies will be required to fully elucidate this mechanism. While these data suggest a

functional role for AGO2-RAS interaction on RISC activity, the exact mechanism for the differential regulatory role for WT vs mutant RAS remains unclear.

One potential clue to the mechanistic role of mutant RAS alteration of AGO2 RNAi activity may be alterations in AGO2 subcellular localization. In our PDAC mouse model, we observed that not only did AGO2 expression increase with severity of disease (**Figure 2.4**), but we also saw an enrichment of co-localization of AGO2-RAS at the plasma membrane with PDAC progression (**Figure 2.5**). As RISC activity primarily occurs within the cytoplasm of the cell and not the plasma membrane [32, 33], these alterations in AGO2 localization may provide some insight into the mechanism for the observed inhibition of AGO2 with mutant KRAS. If mutant RAS sequesters AGO2 at the plasma membrane away from other RISC members, it is possible that this mechanism partially explains the inhibition of AGO2 observed.

Moreover, AGO2 and RISC members are known to interact within P-bodies of the cytoplasm [34], and recent *in vitro* work has demonstrated an important role for these aggregates and the RISC protein TNRC6 (GW182) in phase separation, leading to an acceleration of miRNA mediated deadenylation [35]. Our SM Toolbox described in **Chapter 4** also detected the assembly of higher order complexes that appear to depend on both RNA and RISC members (**Supplemental Figure 4.4**). It remains to be seen if these complexes are necessary for full AGO2 mediated RNAi *in vitro*. Furthermore, it is possible that AGO2's interaction with RAS proteins could play a role in disrupting the formation of RISC. We plan to further probe this line of questioning *in vitro* with the SM Toolbox described above. In addition, it is not fully clear why only mutant KRAS is able to inhibit AGO2 miRNA processing. Our *in vitro* data suggests that potentially GTP-loaded KRAS is able to inhibit regardless of WT or mutant status. Interaction with specific KRAS mutants may disrupt the formation of these higher order AGO2 complexes *in vitro*, or KRAS may alter AGO2's

ability to bind miRNA and target mRNA transcripts. Both of these hypotheses can be tested at a single molecule level with labeled miRNAs and mRNAs.

Modifications of AGO2 such as phosphorylation of Y393 have been associated with alterations in the ability to process specific long-loop miRNAs by altering interactions with DICER [14]. It is possible that mutant RAS interaction with AGO2 may shift preference to different miRNA families based on precursor loop structures. Alternatively, the AGO2-RAS interaction may inhibit or enrich targeting of miRNAs to specific mRNA lengths or structure. These questions remain for testing using our *in vitro* SM assay systems.

In addition to its use studying AGO2 and its interactions with RISC members and RAS, our SM toolbox is a versatile platform that could be used to study many different protein-protein interactions *in vitro*. As generation of specific purified proteins is an often labor intensive and costly option for biochemical inquiry, our *in vitro* translation (IVT) based SM system described in **Chapter 4** may be an attractive option for studying other protein-protein biochemical studies outside of AGO2 and its binding partners.

Potential for Clinical Targeting of the AGO2-RAS Interaction

For many years, *RAS* mutations haven been deemed clinically untargetable, and since these mutations frequently occur in some of the highest mortality cancers, lack of targeted therapies toward *RAS* genes has left a gap in our clinical arsenal against these cancers. RAS proteins lack a readily available site for small molecule inhibitors to bind, making direct targeting unattractive for years [36]. Secondary means of blunting RAS, such as targeting of downstream signaling, targeting membrane localization, or RNA interference, have been hampered by off-target effects, toxicity, and/or escape mechanisms from secondary pathways [37]. Despite these many setbacks,

recent work has developed a new class of inhibitors directly targeting $KRAS^{G12C}$ mutations. These inhibitors take advantage of the unique structural properties of G12C mutants which retain some level of intrinsic GTP hydrolysis [38]. By binding to a Switch II domain pocket unique to G12C mutants, these inhibitors lock mutant KRAS in a GDP bound state [4].

While these new inhibitors give some hope for future targeting of RAS clinically, other point mutations in *RAS* genes may not be amenable to similar strategies. The results of this dissertation provide some evidence that mutant RAS proteins are at least partially reliant on interaction with AGO2 to promote the development of PDAC (**Chapter 2**) and maintain a proliferative state in mutant *HRAS* and *NRAS* cell lines (**Chapter 3**). Furthermore, we observed that the $KRAS^{G12C}$ inhibitor (ARS-1620 [4]) was able to inhibit AGO2-KRAS association in cells expressing that specific point mutation (**Figure 2.8**). As these inhibitors are known to bind to the Switch II domain of KRAS and disrupt interaction with SOS1, our results suggest that AGO2-KRAS interaction is also inhibited. Additional research is required to fully elucidate if this AGO2 disruption is of functional relevance in $KRAS^{G12C}$ mutant cancers. While our previous work has suggested that AGO2's binding to mutant RAS can lead to an inhibition of RNAi activity, it would be interesting to probe whether these inhibitors can restore AGO2 function. Recent work has described the phosphorylation of Y64 on RAS by Src as important for reducing downstream signaling of RAS; furthermore, the authors describe the phosphatase SHP2 as a negative regulator of this event. Thus, targeting of SHP2 or other similar phosphatases targeting RAS-Y64 or even AGO2-Y393 could represent a more orthogonal approach to disrupting the interaction of AGO2-RAS in cancer. However, more biochemical and molecular studies will be necessary to evaluate the efficacy of such an approach. Our SM Toolbox described in **Chapter 4** would provide a prime

method for this study *in vitro*, and could further shed light on potential biochemical properties of these inhibitors.

The Chinnaiyan lab's work in describing the AGO2-RAS interaction has demonstrated an important role for this binding event in the development and survival of multiple *RAS* mutant cells and cancer models. Current efforts in the lab are underway to co-crystallize AGO2 and mutant $KRAS^{G12V}$ to assess any regions or pockets that may be utilized to develop targeted small molecules. In recent years, small molecule or peptide based inhibition of protein-protein interactions (PPIs) have been used to disrupt a plethora of different targets, like BET inhibitors [39]. While these methods may be of interest in the future, the necessity for structural knowledge of AGO2-RAS interaction hampers our current usage. However, our SM Toolbox might allow for screening of many small molecule peptides in a medium-high throughput fashion. The current flow chamber used would not be fully amenable to screening for disruption of AGO2-RAS; nevertheless, it could be used to develop a screening method to simultaneously assess the binding of AGO2-RAS with many different molecules similar to the Nucleic Acid Programmable Protein Array (NAPPA) [40]. These assays and technologies will require future research and validation, but represent promising opportunities to further study this interaction *in vitro*.

While AGO2-RAS may be an attractive clinical target, our results also suggest that loss of tumor suppressors and senescence mediators like p53 may provide an escape from the requirement for AGO2. As mutations in p53 and other senescence genes like p16 are commonly mutated in PDAC and other *RAS* driven cancers [40], targeting AGO2-RAS interaction may be limited clinically. For instance, EGFR has also been demonstrated to be essential to early PDAC tumor formation in a genetically engineered mouse model of PDAC [6], but targeting of EGFR has had limited clinical efficacy as patients commonly develop resistance after a few months of therapy

[41]. It is possible that targeting AGO2-KRAS interaction in PDAC may sensitize cancerous cells to other therapeutic targets via a combination therapy regimen. Despite this caveat, targeting AGO2-RAS interaction might still provide some clinical benefit to patients, even if it is limited by temporal efficacy and/or specific tumor mutation profile. Thus, further preclinical and molecular characterization will be required to fully elucidate the therapeutic potential of the AGO2 and RAS interaction.

References

1. Fernandez-Medarde, A. and E. Santos, *Ras in cancer and developmental diseases.* Genes Cancer, 2011. **2**(3): p. 344-58.
2. Cox, A.D., et al., *Drugging the undruggable RAS: Mission possible?* Nat Rev Drug Discov, 2014. **13**(11): p. 828-51.
3. Ostrem, J.M., et al., *K-Ras(G12C) inhibitors allosterically control GTP affinity and effector interactions.* Nature, 2013. **503**(7477): p. 548-51.
4. Janes, M.R., et al., *Targeting KRAS Mutant Cancers with a Covalent G12C-Specific Inhibitor.* Cell, 2018. **172**(3): p. 578-589 e17.
5. Sagiv, A., et al., *Granule exocytosis mediates immune surveillance of senescent cells.* Oncogene, 2013. **32**(15): p. 1971-7.
6. Navas, C., et al., *EGF receptor signaling is essential for k-ras oncogene-driven pancreatic ductal adenocarcinoma.* Cancer Cell, 2012. **22**(3): p. 318-30.
7. Bryant, K.L., et al., *KRAS: feeding pancreatic cancer proliferation.* Trends Biochem Sci, 2014. **39**(2): p. 91-100.
8. Hruban, R.H., et al., *Progression model for pancreatic cancer.* Clin Cancer Res, 2000. **6**(8): p. 2969-72.
9. Maetzig, T. and A. Schambach, *Development of Inducible Molecular Switches Based on All-in-One Lentiviral Vectors Equipped with Drug Controlled FLP Recombinase.* Methods Mol Biol, 2016. **1448**: p. 23-39.
10. Schonhuber, N., et al., *A next-generation dual-recombinase system for time- and host-specific targeting of pancreatic cancer.* Nat Med, 2014. **20**(11): p. 1340-1347.
11. Jones, S., et al., *Core signaling pathways in human pancreatic cancers revealed by global genomic analyses.* Science, 2008. **321**(5897): p. 1801-6.
12. Schutte, M., et al., *Abrogation of the Rb/p16 tumor-suppressive pathway in virtually all pancreatic carcinomas.* Cancer Res, 1997. **57**(15): p. 3126-30.
13. Aguirre, A.J., et al., *Activated Kras and Ink4a/Arf deficiency cooperate to produce metastatic pancreatic ductal adenocarcinoma.* Genes Dev, 2003. **17**(24): p. 3112-26.
14. Shen, J., et al., *EGFR modulates microRNA maturation in response to hypoxia through phosphorylation of AGO2.* Nature, 2013. **497**(7449): p. 383-7.
15. Yang, M., et al., *Dephosphorylation of tyrosine 393 in argonaute 2 by protein tyrosine phosphatase 1B regulates gene silencing in oncogenic RAS-induced senescence.* Mol Cell, 2014. **55**(5): p. 782-90.
16. Zeng, Y., et al., *Phosphorylation of Argonaute 2 at serine-387 facilitates its localization to processing bodies.* Biochem J, 2008. **413**(3): p. 429-36.
17. McKenzie, A.J., et al., *KRAS-MEK Signaling Controls Ago2 Sorting into Exosomes.* Cell Rep, 2016. **15**(5): p. 978-987.
18. Shankar, S., et al., *KRAS Engages AGO2 to Enhance Cellular Transformation.* Cell Rep, 2016. **14**(6): p. 1448-1461.
19. Sondermann, H., et al., *Structural analysis of autoinhibition in the Ras activator Son of sevenless.* Cell, 2004. **119**(3): p. 393-405.
20. Kano, Y., et al., *Tyrosyl phosphorylation of KRAS stalls GTPase cycle via alteration of switch I and II conformation.* Nat Commun, 2019. **10**(1): p. 224.

21. Clarke, S., *Protein isoprenylation and methylation at carboxyl-terminal cysteine residues.* Annu Rev Biochem, 1992. **61**: p. 355-86.
22. Haigis, K.M., et al., *Differential effects of oncogenic K-Ras and N-Ras on proliferation, differentiation and tumor progression in the colon.* Nat Genet, 2008. **40**(5): p. 600-8.
23. Seru, R., et al., *HaRas activates the NADPH oxidase complex in human neuroblastoma cells via extracellular signal-regulated kinase 1/2 pathway.* J Neurochem, 2004. **91**(3): p. 613-22.
24. Hole, P.S., et al., *Ras-induced reactive oxygen species promote growth factor-independent proliferation in human CD34+ hematopoietic progenitor cells.* Blood, 2010. **115**(6): p. 1238-46.
25. Yang, J.Q., et al., *Superoxide generation in v-Ha-ras-transduced human keratinocyte HaCaT cells.* Mol Carcinog, 1999. **26**(3): p. 180-8.
26. Recktenwald, C.V., et al., *Altered detoxification status and increased resistance to oxidative stress by K-ras transformation.* Cancer Res, 2008. **68**(24): p. 10086-93.
27. Santillo, M., et al., *Opposing functions of Ki- and Ha-Ras genes in the regulation of redox signals.* Curr Biol, 2001. **11**(8): p. 614-9.
28. Li, H., et al., *Cre-mediated recombination in mouse Clara cells.* Genesis, 2008. **46**(6): p. 300-7.
29. Kwak, P.B. and Y. Tomari, *The N domain of Argonaute drives duplex unwinding during RISC assembly.* Nat Struct Mol Biol, 2012. **19**(2): p. 145-51.
30. Diederichs, S. and D.A. Haber, *Dual role for argonautes in microRNA processing and posttranscriptional regulation of microRNA expression.* Cell, 2007. **131**(6): p. 1097-108.
31. Martinez, I., et al., *miR-29 and miR-30 regulate B-Myb expression during cellular senescence.* Proc Natl Acad Sci U S A, 2011. **108**(2): p. 522-7.
32. Zeng, Y. and B.R. Cullen, *RNA interference in human cells is restricted to the cytoplasm.* RNA, 2002. **8**(7): p. 855-60.
33. Stalder, L., et al., *The rough endoplasmatic reticulum is a central nucleation site of siRNA-mediated RNA silencing.* EMBO J, 2013. **32**(8): p. 1115-27.
34. Liu, J., et al., *MicroRNA-dependent localization of targeted mRNAs to mammalian P-bodies.* Nat Cell Biol, 2005. **7**(7): p. 719-23.
35. Sheu-Gruttadauria, J. and I.J. MacRae, *Phase Transitions in the Assembly and Function of Human miRISC.* Cell, 2018. **173**(4): p. 946-957 e16.
36. Kessler, D., et al., *Drugging an undruggable pocket on KRAS.* Proc Natl Acad Sci U S A, 2019. **116**(32): p. 15823-15829.
37. Stalnecker, C.A. and C.J. Der, *RAS, wanted dead or alive: Advances in targeting RAS mutant cancers.* Sci Signal, 2020. **13**(624).
38. Hunter, J.C., et al., *Biochemical and Structural Analysis of Common Cancer-Associated KRAS Mutations.* Mol Cancer Res, 2015. **13**(9): p. 1325-35.
39. Arkin, M.R., Y. Tang, and J.A. Wells, *Small-molecule inhibitors of protein-protein interactions: progressing toward the reality.* Chem Biol, 2014. **21**(9): p. 1102-14.
40. Miersch, S. and J. LaBaer, *Nucleic Acid programmable protein arrays: versatile tools for array-based functional protein studies.* Curr Protoc Protein Sci, 2011. **Chapter 27**: p. Unit27 2.
41. Malumbres, M. and M. Barbacid, *RAS oncogenes: the first 30 years.* Nat Rev Cancer, 2003. **3**(6): p. 459-65.

Appendices

Supplemental Figure 2.1

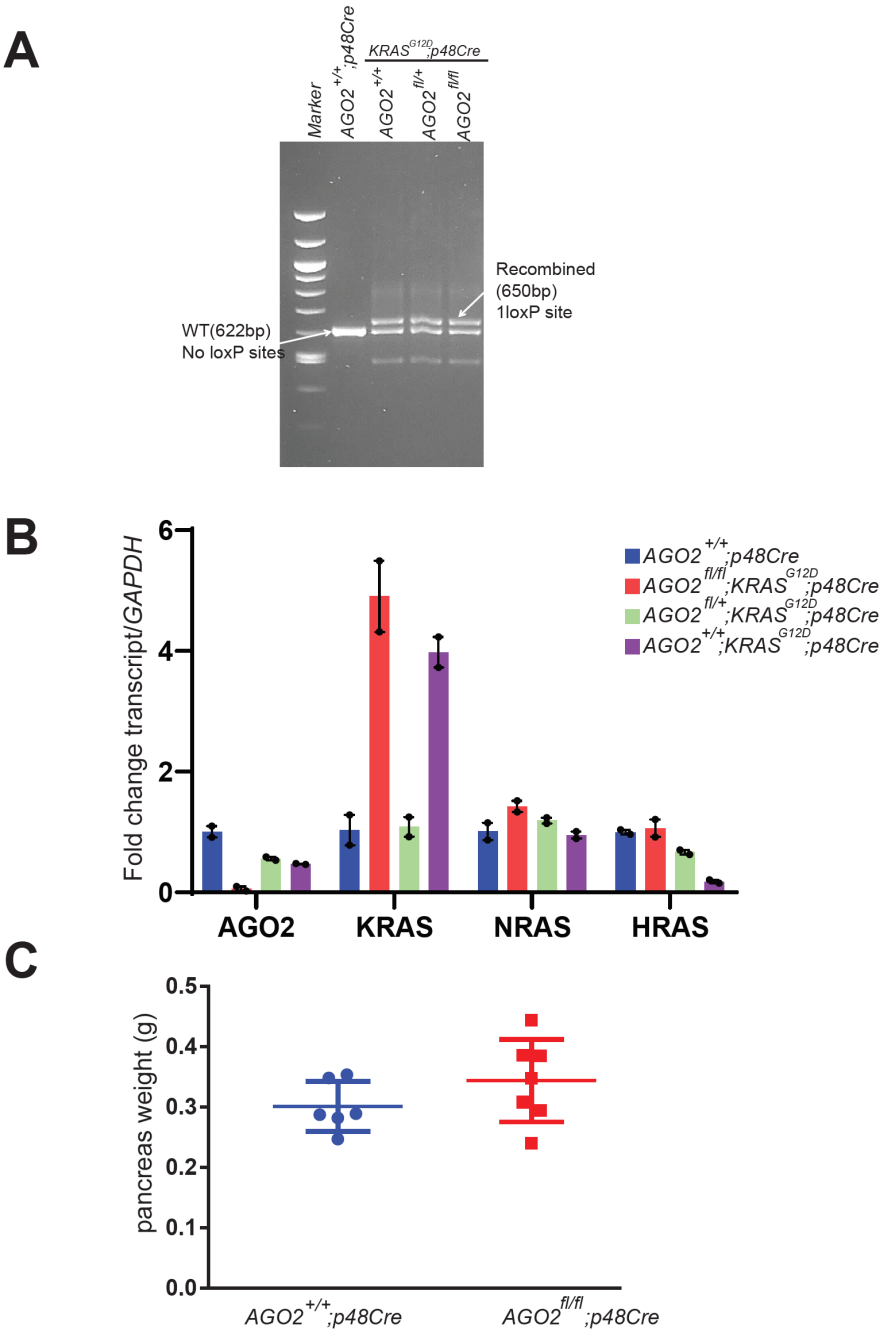

Supplementary Figure 1: **Cre activation in the pancreatic cancer mouse model.** (A) Genomic DNA analysis from the pancreata of the indicated genotypes showing recombined alleles in the LSL-*KRAS* model. (B) RT-qPCR analysis for different transcripts from one 10 week old mouse pancreata of each of the indicated genotypes. Further validations of AGO2 knockout efficiency were performed using IB/IF. Error bars indicate mean values +/- SEM of technical replicates (C) Scatter plot showing the weight of pancreata obtained from 6 *AGO2*$^{+/+}$;*KRAS*^{G12D};*Cre* and 7 *AGO2*$^{fl/fl}$;*KRAS*^{G12D};*Cre* mice of the indicated genotypes at 12 weeks of age. Data are presented as mean values +/- SEM.

Supplemental Figure 2.2

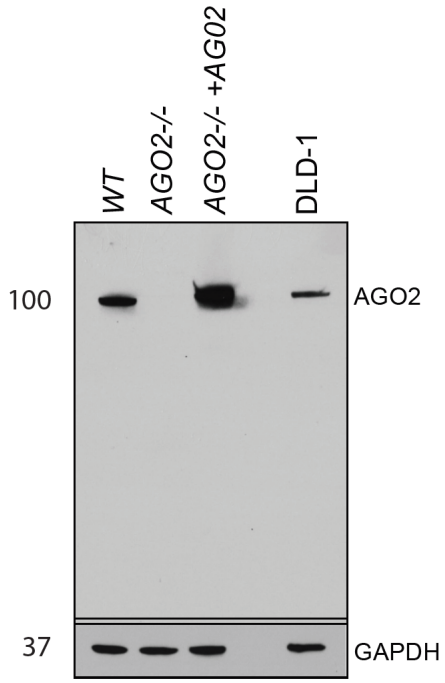

Supplementary Figure 2: **Specificity of AGO2 monoclonal antibody.** Western blot analysis of AGO2-/- mouse embryonic fibroblasts and human colon cancer cells using a monoclonal antibody to AGO2 to confirm specificity of the antibody prior to use in immunohistochemistry (IHC) and immunofluorescence (IF). Further details are provided in **Supplementary Table 1**. Numbers on the left indicate molecular weight in kDa.

Supplemental Figure 2.3

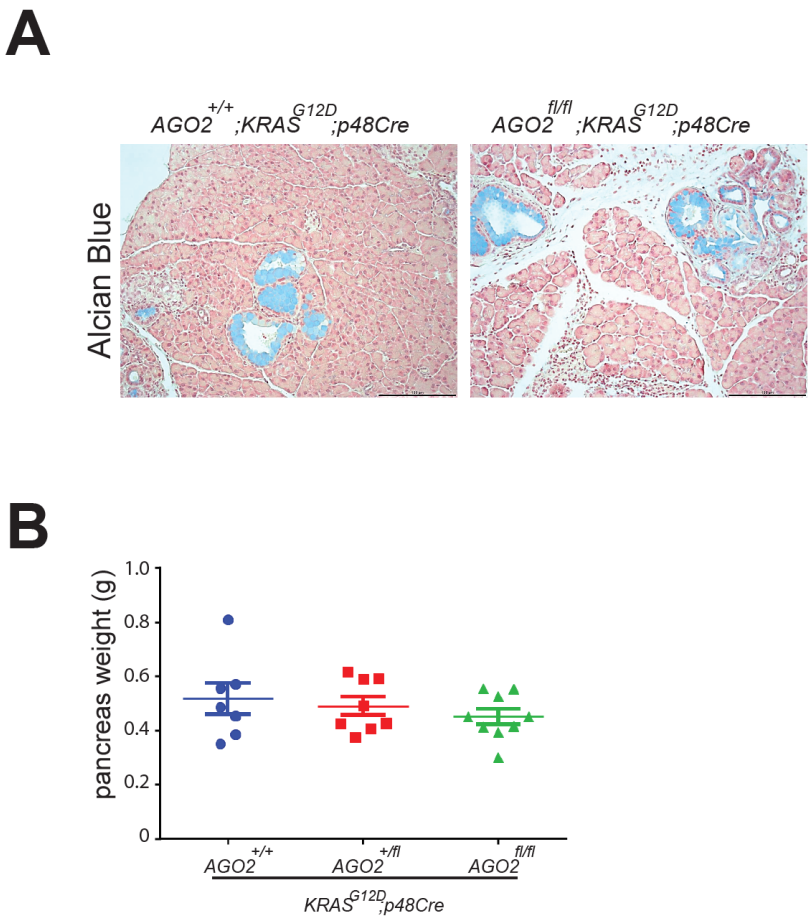

Supplementary Figure 3: **PanINs observed in *AGO2$^{+/+}$;KRAS^{G12D};p48Cre* and *AGO2$^{fl/fl}$;KRAS^{G12D};p48Cre* are similar.** (A) Alcian Blue (mucin) staining of PanINs of the indicated genotypes Scale bar represents 100 μm. (B) Scatter plot showing the weight of pancreata obtained from 8 mice of Ago2$^{+/+}$;*Kras^{G12D};Trp53$^{fl/+}$;p48Cre,* 20 of Ago2$^{fl/+}$;*Kras^{G12D};Trp53$^{fl/+}$;p48Cre*, and 13 of *Ago2$^{fl/fl}$;Kras^{G12D};Trp53$^{fl/+}$;p48Cre* genotype at 12 weeks of age. Data are presented as mean values +/- SEM.

Supplemental Figure 2.4

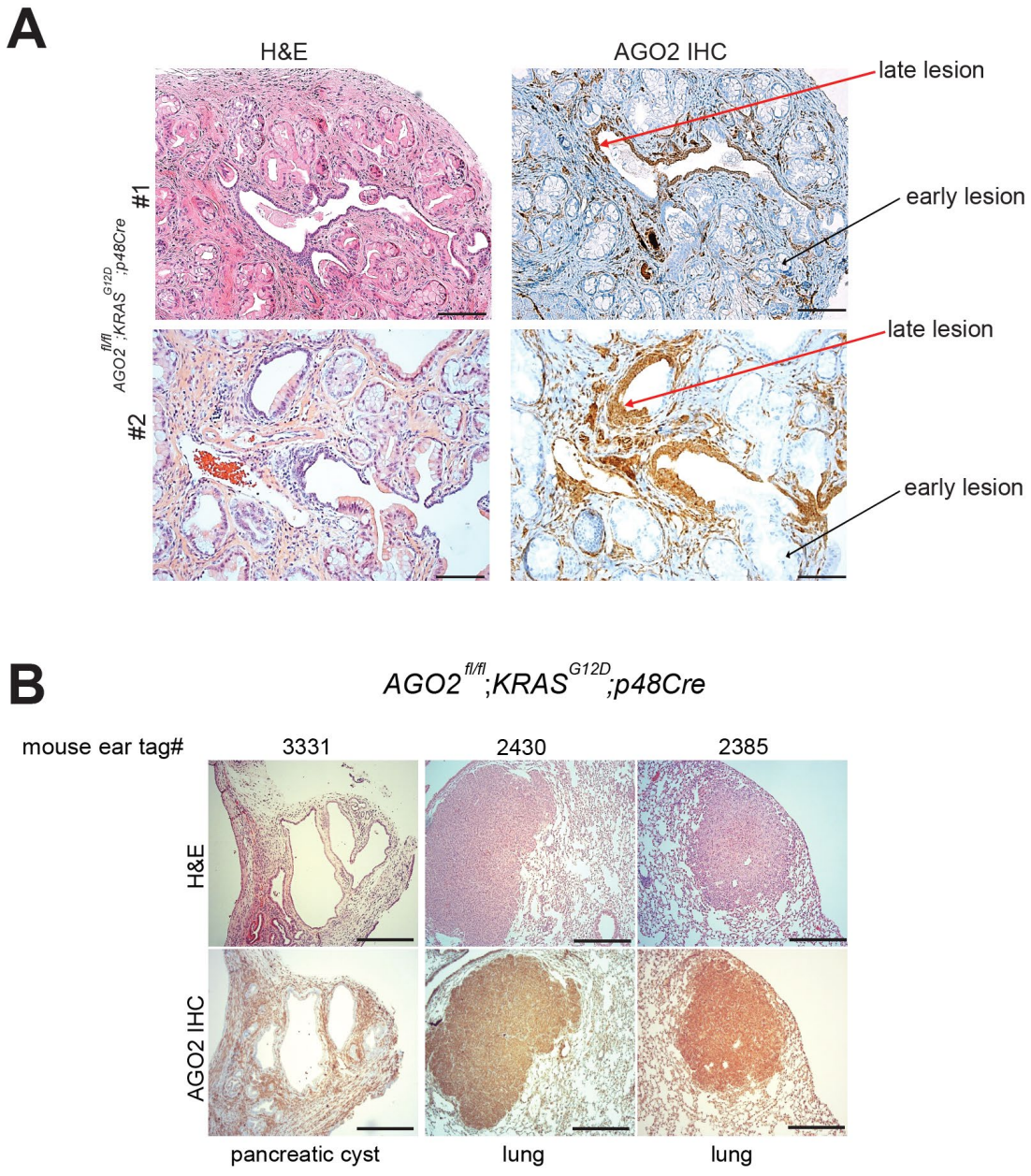

Supplementary Figure 4: Leaky expression and abnormal pathologies in pancreatic tissue with *AGO2* ablation. (A) Representative images of H&E and AGO2 IHC from two animals of the *AGO2*$^{fl/fl}$*;KRAS*^{G12D}*;p48Cre* cohort showing AGO2 expression in the late lesions. Scale bar represents 100 μm and 40 μm for upper and lower panels, respectively. (B) H&E and AGO2 IHC analysis of abnormal pancreas and lungs from the *AGO2*$^{fl/fl}$*;KRAS*^{G12D}*;p48Cre* mouse cohort (further detailed in **Supplementary Table 2**). Scale bar, 100 μm and 40 μm for low and high magnification, respectively.

Supplemental Figure 2.5

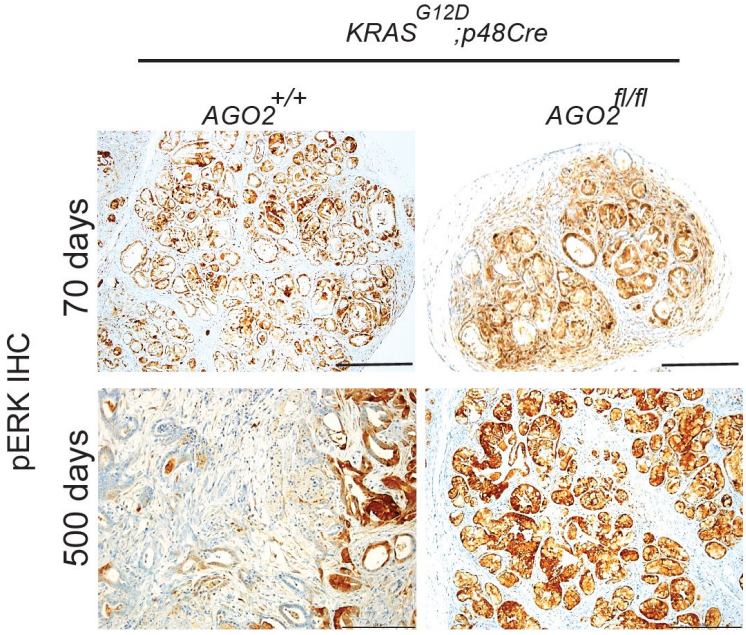

Supplementary Figure 5. High phosphoERK levels in PanINs of *AGO2$^{fl/fl}$;KRAS^{G12D};p48Cre* mice and increased AGO2 mRNA expression in human pancreatic cancer. (A) Representative images of phosphoERK IHC staining of pancreatic tissues from the indicated genotypes during PDAC progression. Scale bar is 100μm**.** Note the inconsistent staining pattern of phosphoERK in PDAC tissue of *AGO2$^{+/+}$; KRAS^{G12D};p48Cre* genotype at 500 day time point.

Supplemental Figure 2.6

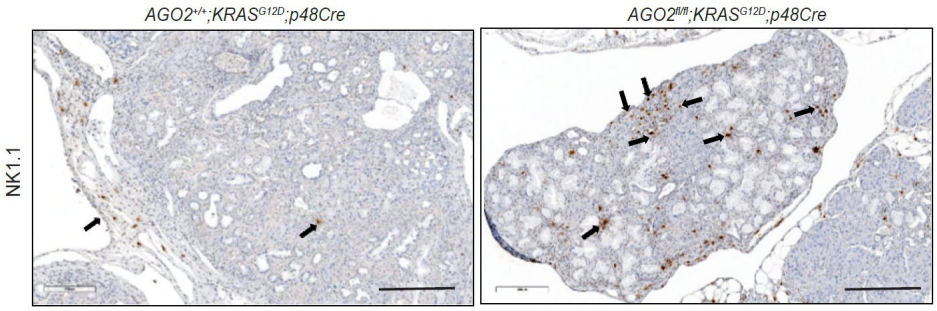

Supplementary Figure 6: Increased NK cell infiltration in the PanIN lesions of *AGO2$_{fl/fl}$;KRAS$_{G12D}$;p48Cre* mice compared to PanINs of *AGO2$_{+/+}$; KRAS$_{G12D}$;p48Cre*. Scale bar is 100μm

Supplemental Figure 2.7

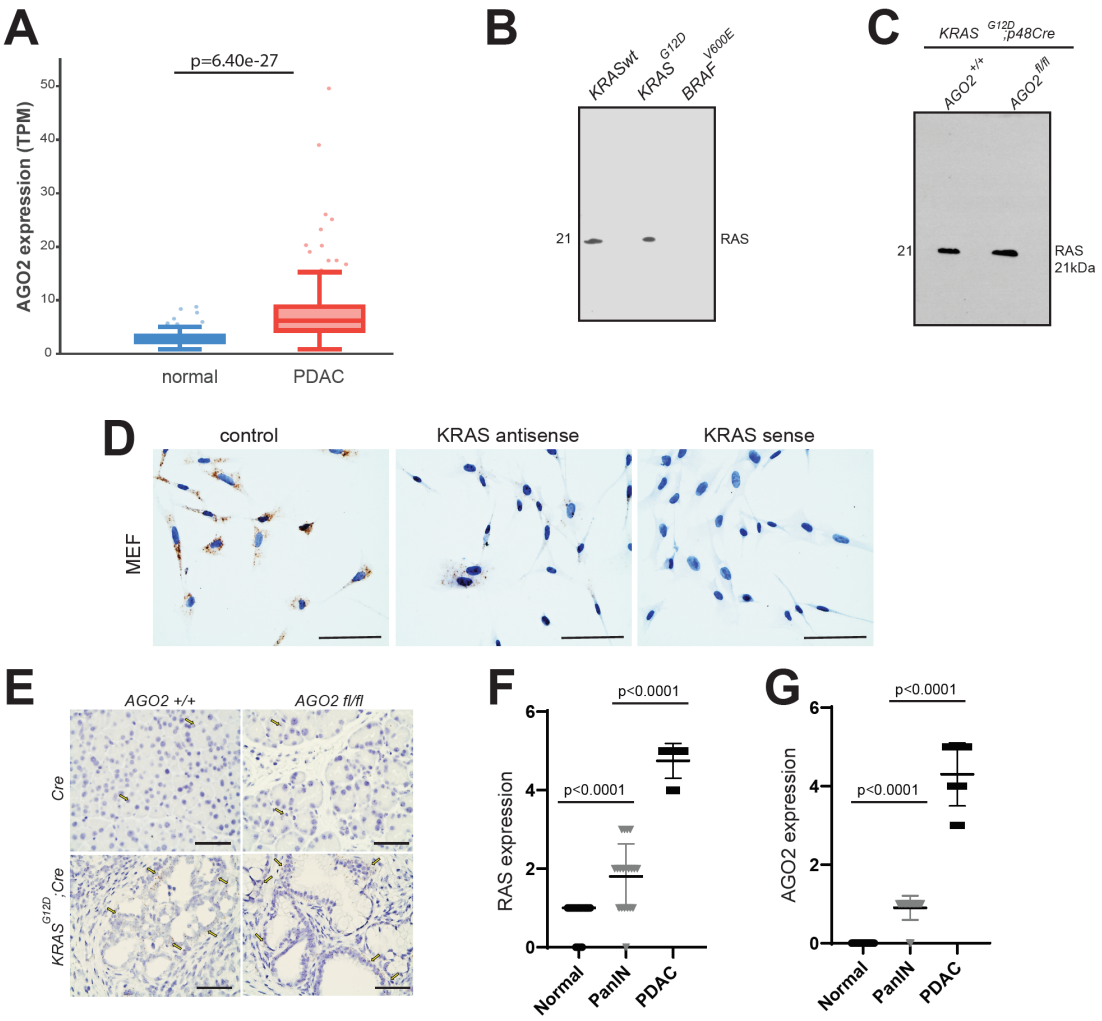

Supplementary Figure 7. Specificity of RAS10 Mab and KRAS/RAS expression in various models. (A) Levels of AGO2 mRNA transcripts in pancreatic adenocarcinoma in the TCGA dataset compared to levels in normal pancreatic tissue (obtained from GTEX dataset https://gtexportal.org/home). Transcripts from 198 normal and 178 human pancreatic cancer tissues are represented. The minima, median, maxima for normal is 0.657, 2.503, 8.567 and for pancreatic cancer is 1.151, 6.494, 49.839, respectively. The lower and upper quartile for normal is 1.9845 and 3.17075 and for cancer, 4.63675 and 9.11525 respectively. P-value was determined using two sided t-test. TPM: Transcripts per kilobase million. Specificity of the RAS10 antibody confirmed immunoblot analysis of Rasless MEFs rescued using various KRAS constructs (B) and mouse pancreas expressing oncogenic KRAS (C). Numbers on the left of the blots in (B) and (C) are molecular weights in kDa. Note that complete blots are shown to demonstrate the presence of a single band at 21kDa. Further details are provided in Table 1. (D) MEFs were assessed for KRAS RNA expression using RNA ISH. KRAS antisense and sense probes were used as positive and negative controls respectively. Scale bar represents 50 µm. (E) Representative images of KRAS RNA-ISH on pancreatic tissues from normal and *AGO2*$^{fl/fl}$ animals (top panels) and oncogenic KRAS expressing *AGO2*$^{+/+}$;*KRAS*^{G12D};*Cre* and *AGO2*$^{fl/fl}$;*KRAS*^{G12D};*Cre* mice (lower panels). Scale bar, 50µm. (F) Box plot quantitating RAS or (G) AGO2 expression levels in PanINs and PDAC. 3 individual mice were used and 20 PanINs/PDAC were assessed. For (F) and (G) Expression values range from 0-5 where 0 is for no expression and 5 is for maximum expression. Unpaired two sided t-test was performed to determine the p-values and data are presented as mean values +/- SEM.

Supplemental Figure 2.8

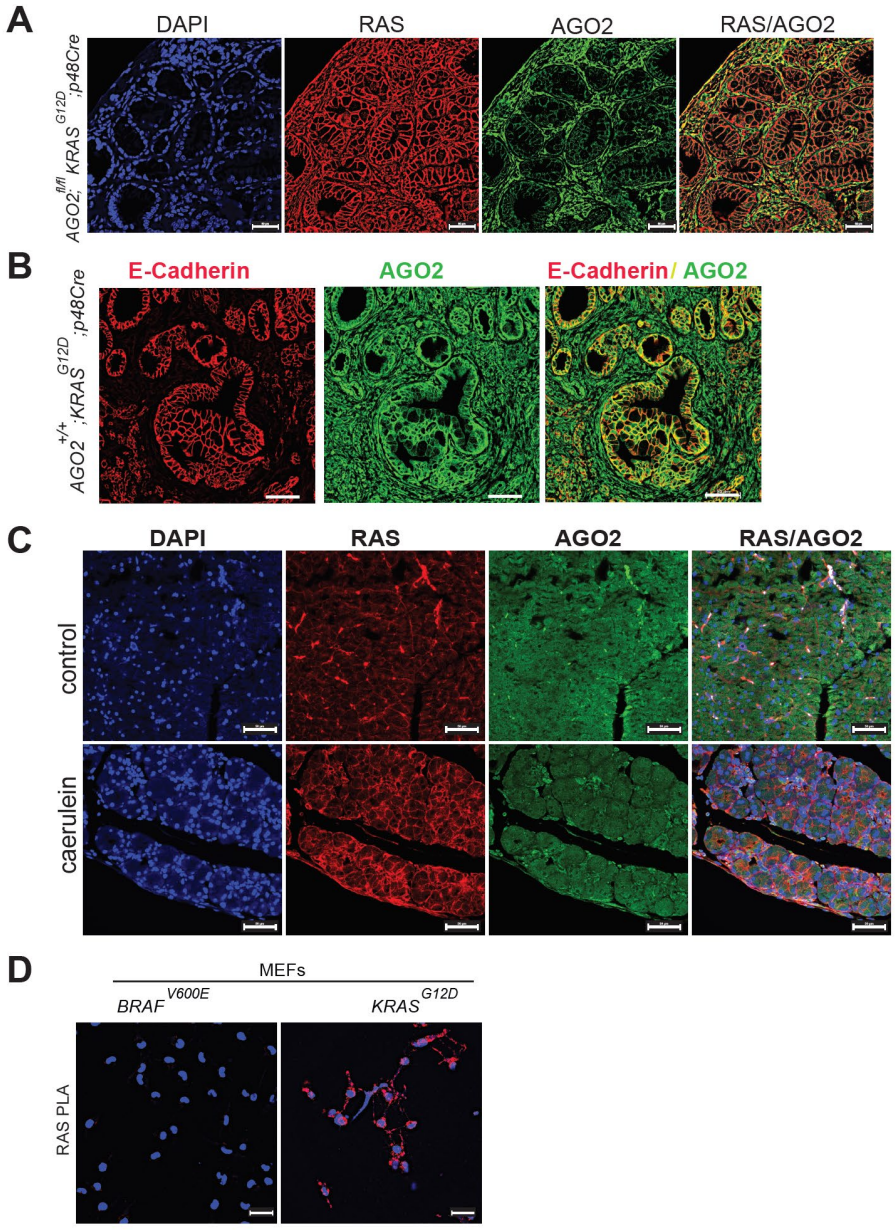

Supplementary Figure 8. Immunofluorescence (IF) and proximity ligation assay (PLA) using RAS and AGO2 antibodies. (A) RAS IF staining in *AGO2*$^{fl/fl}$;*KRAS*^{G12D};*Cre* PanINs at 400days. Scale bar, 50 μm. (B) Membrane localization of AGO2 demonstrated by AGO2/E-Cadherin co-localization signals in early PanIN lesions of *AGO2*$^{+/+}$;*KRAS*^{G12D};*Cre* mice. E-Cadherin is used as a plasma membrane marker, Scale bar, 50μm. (C) Representative images of RAS and AGO2 immunofluorescence staining on pancreatic tissue from normal mice after treatment with caerulein to induce pancreatitis. Scale bar, 50μm (D) Validation of RAS10 antibody for RAS Proximity ligation assay (PLA) detection in RASless MEFs expressing either *KRAS*^{G12D} or *BRAF*^{V600E}. Scale bar, 50 μm.

Supplemental Figure 2.9

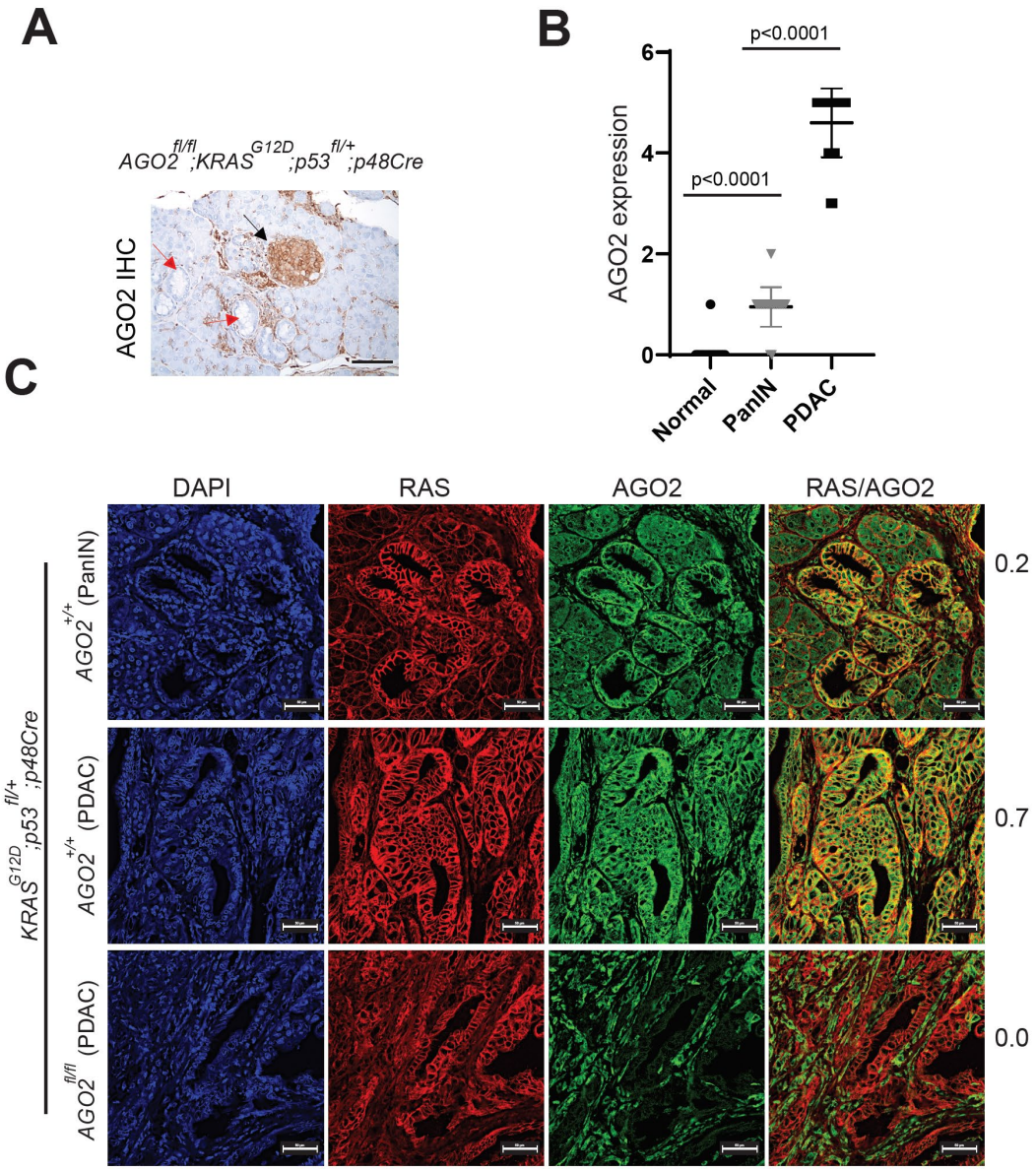

Supplementary Figure 9: IHC and IF staining of RAS/AGO2 in the pancreatic tissue of the KPC model. (A) AGO2 IHC in pancreatic tissue of *Ago2*$^{fl/fl}$;*Kras*^{G12D};*Trp53*$^{fl/+}$;*p48Cre*. Red and black arrows indicate the PanIN lesions and the islets of Langerhans. Scale bar, 50μm (B) Box plot quantitating AGO2 expression levels in PanINs and PDAC. Pancreatic tissue from three individual mice and 20 PanINs/PDAC lesions were assessed. Expression values range from 0-5 where 0 is for no expression and 5 is for maximum expression. Unpaired two sided t-test was performed to determine the p-value. Data are presented as mean values +/- SEM. (C) Representative images of IF analysis for RAS and AGO2 through PDAC progression in the *AGO2*$^{+/+}$;*KRAS*^{G12D}; *Trp53*$^{fl/+}$;*p48Cre* mice. Numbers adjacent to merged images indicate the Pearson's coefficient of co-localization (PCC) of RAS-AGO2 signals at the membranous regions (where 0 is no overlap and 1 is complete overlap). PCC was determined using co-localization signals of at least 50 cells in three distinct areas representative of normal acinar, PanIN or PDAC. Scale bar, 50 μm.

Supplemental Figure 2.10

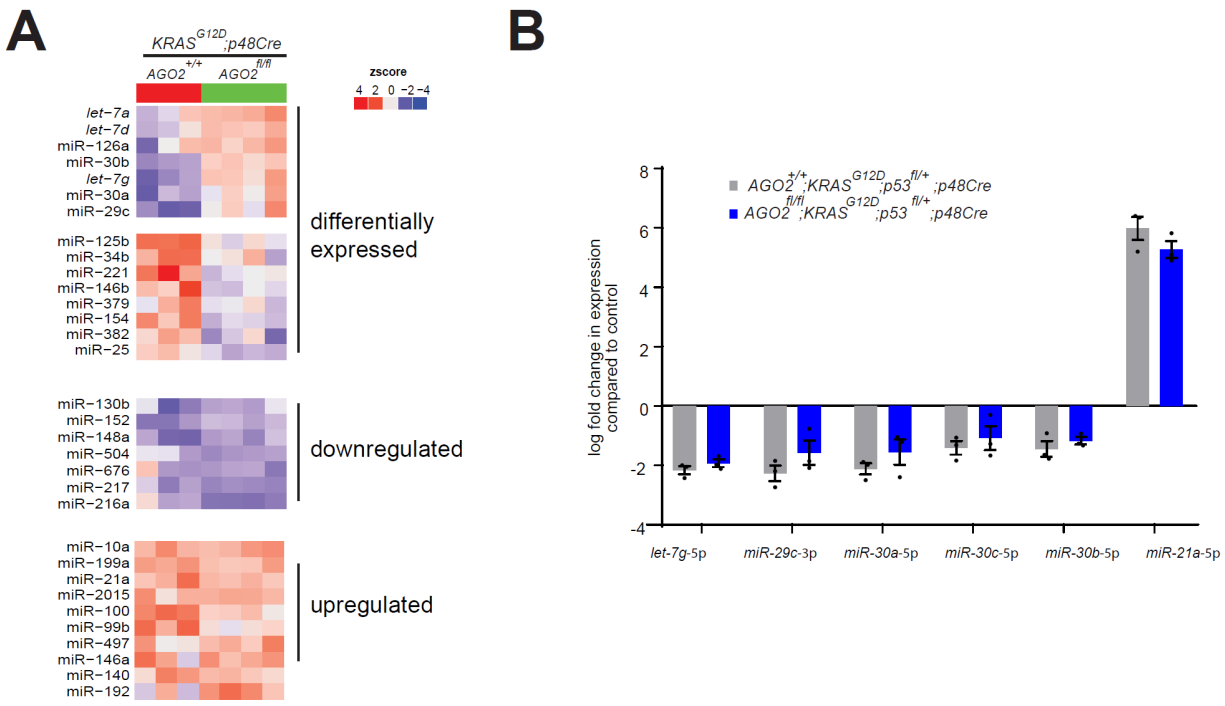

Supplementary Figure 10. microRNA expression changes due to AGO2 loss. (A) Heatmap analysis of the top 50 differentially expressed, upregulated and downregulated microRNAs in the indicated genotypes at the 500 day time point. microRNAs were quantitated using Exiqon qPCR. Log-transformed miRNA measurements were then centered on mean and divided by standard deviation across samples (z-score). Heatmaps were plotted using the R-package Complex Heatmap. (B) Relative quantitation of select microRNAs in pancreatic tissue obtained from 3 mice each from the indicated genotypes of the KPC model. In A and B expression was relative to expression of these microRNAs in pancreatic tissue obtained from mice expressing *p48Cre* alone. P-values are indicated in the graph and data are presented as mean values +/- SEM.

Supplemental Figure 2.11

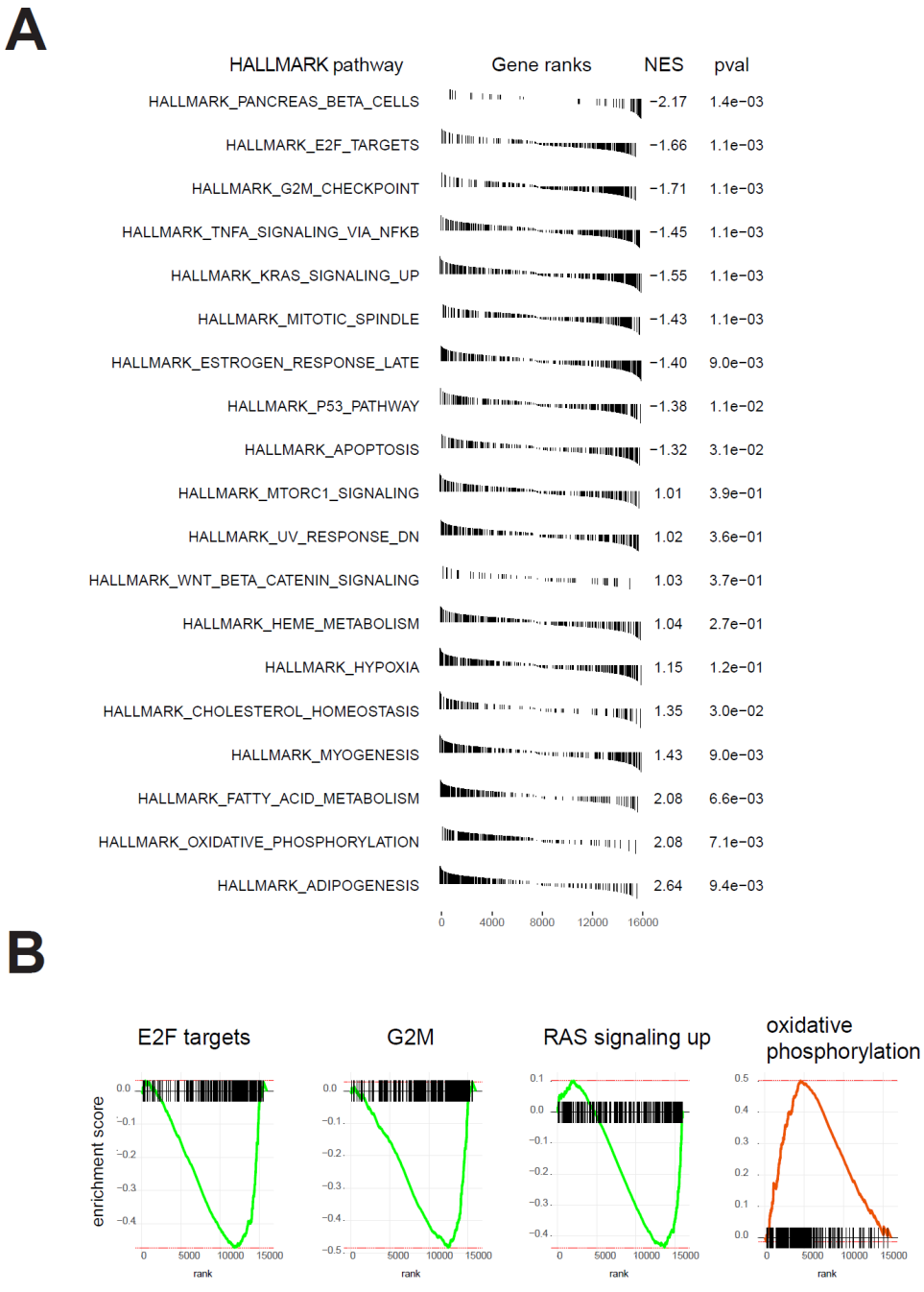

Supplementary Figure 11. Block in PDAC progression due to AGO2 loss is associated with significantly altered transcriptome. (A) GSEA analysis for all the significantly altered HALLMARK gene sets in pancreatic tissue of *AGO2*$^{fl/fl}$*;KRAS*^{G12D}*;p48Cre* mice compared to *AGO2*$^{+/+}$*; KRAS*^{G12D}*;p48Cre* mice. (B) GSEA plots for select data sets.

Supplemental Figure 2.12

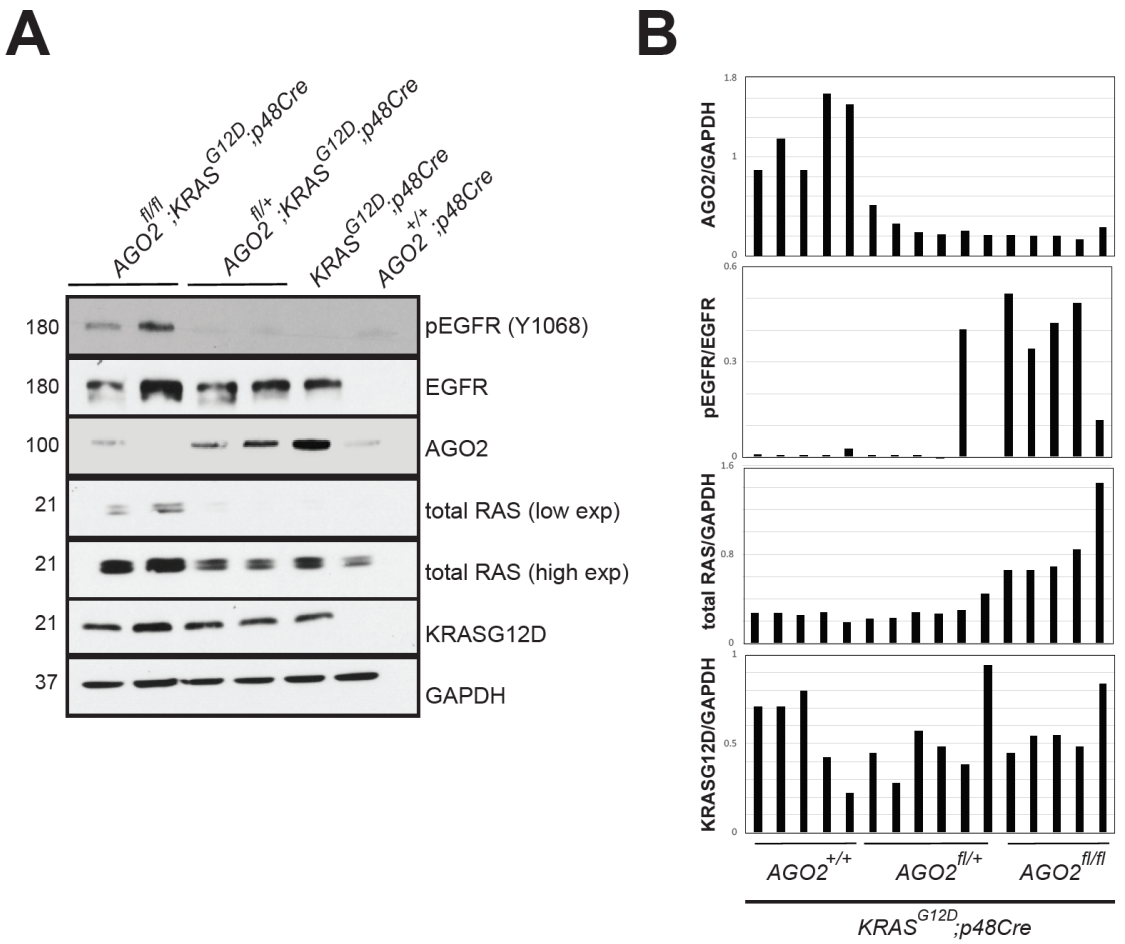

Supplementary Figure 12: AGO2 loss activates EGFR/wild type RAS signaling. Immunoblot analysis (A) and quantitation (B) of AGO2 and associated RAS signaling molecules from individual pancreas obtained from 12 week old mice obtained from 16 individual mice of the indicated genotypes. ImageJ software was employed quantitation and arbitrary values were determined with respect to GAPDH expression in the sample. For pEGFR, EGFR expression was used for comparison instead of GAPDH. Numbers on the left of the blots in (A) are protein molecular weights in kDa.

Supplemental Figure 2.13

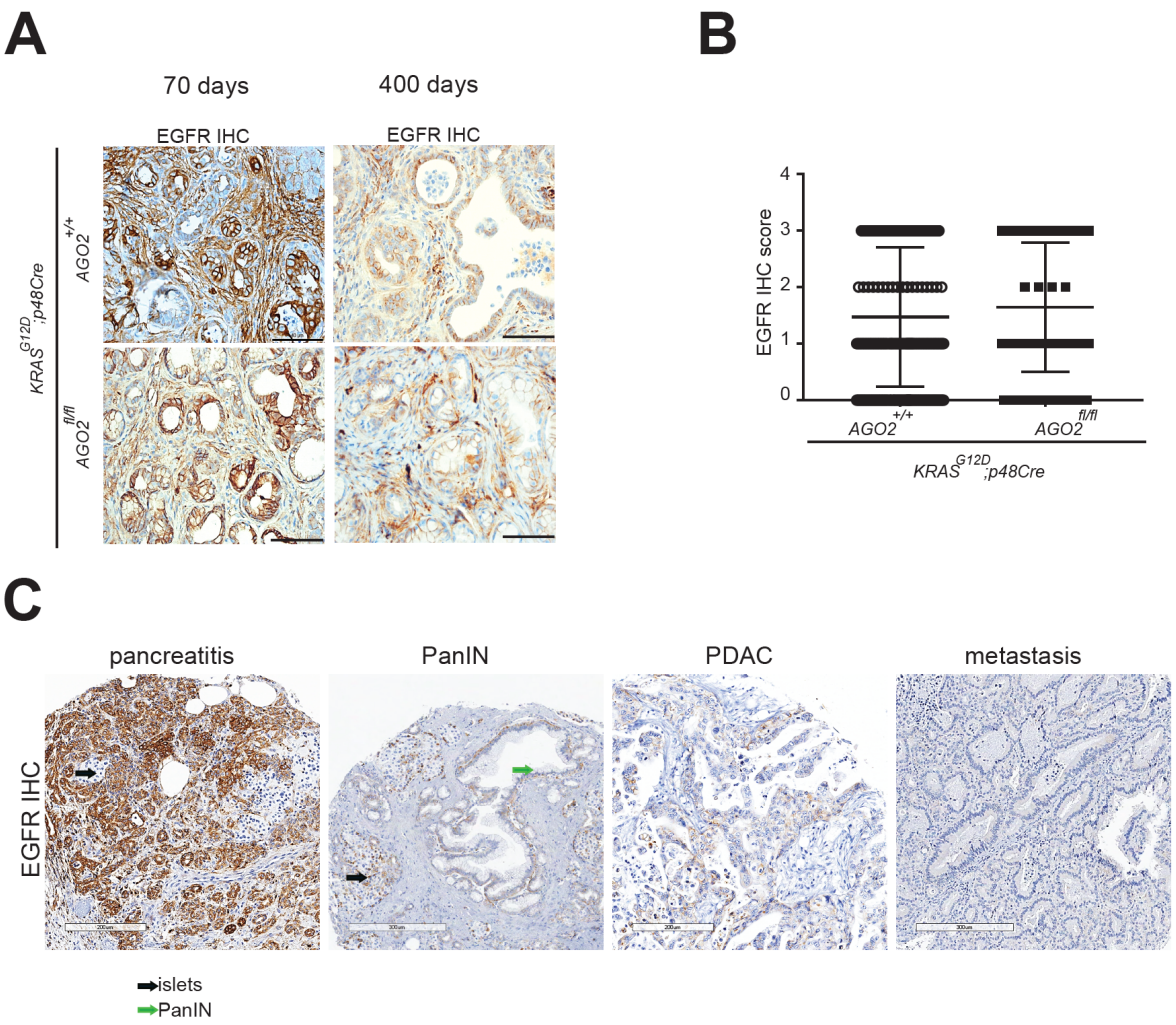

Supplementary Figure 13. EGFR expression is reduced during pancreatic cancer progression. (A). Representative images of EGFR IHC of pancreatic tissue from *AGO2*$^{+/+}$*; KRAS*^{G12D}*;p48Cre* and *AGO2*$^{fl/fl}$*;KRAS*^{G12D}*;p48Cre* mice at 70 or 400-day time points. Scale bar is 100μm (B) Box plot quantitating total EGFR levels in pancreas obtained from the indicated genotypes at 70 day time point. 300 PanINs from three mice pancreata were assessed for EGFR expression and intensity was given a value between 0-3, where 0 is considered no expression and 3 is high expression. EGFR expression score= Intensity of EGFR expression* number of PanINs. Two tailed t-test was performed and p value was determined to be 0.072. Data are presented as mean values +/- SEM. (C) Representative images of EGFR IHC on a human pancreatic tissue microarray through disease progression. Scale bar is 300μm.

Supplemental Figure 2.14

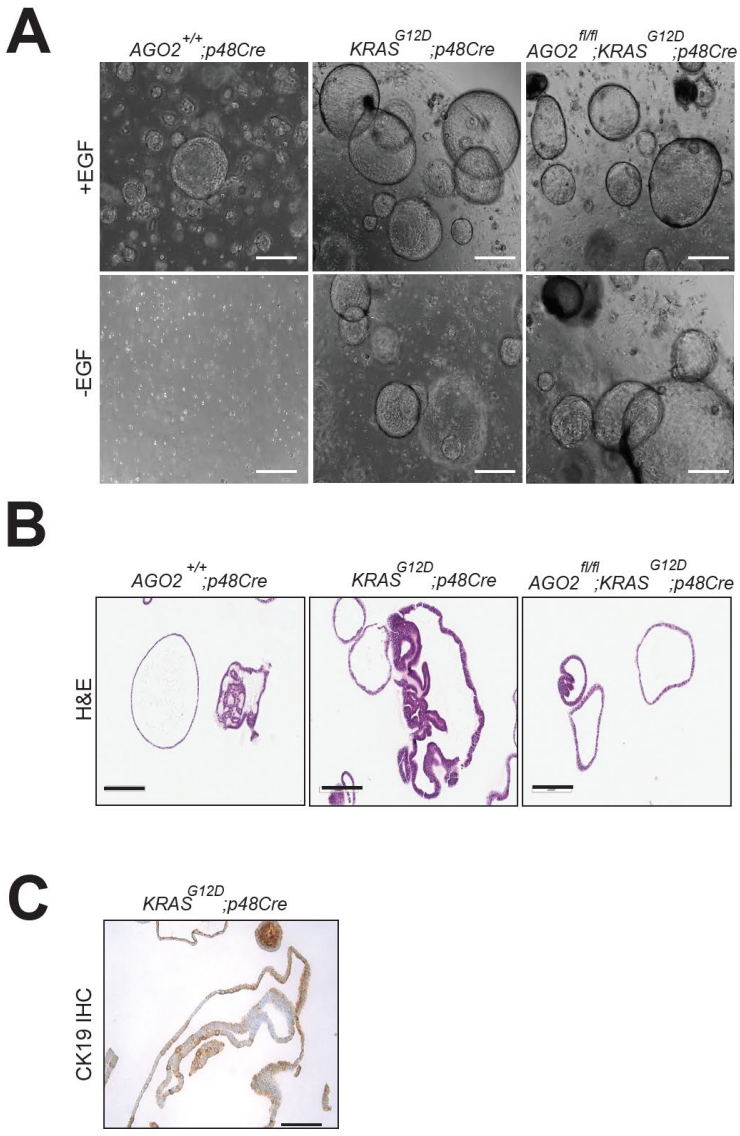

Supplementary Figure 14. Characterization of pancreatic ductal organoids obtained from 12 week old *AGO2$^{+/+}$;KRAS^{G12D};p48Cre* and *AGO2$^{fl/fl}$;KRAS^{G12D};p48Cre* mice. (A) Light microscopic images of mouse pancreatic ductal organoids obtained from the indicated genotypes and cultured in the presence or absence of EGF. (B) H&E staining of pancreatic ductal organoids. Scale bar,200μm (C) CK19 (ductal marker) IHC staining of pancreatic ducts isolated from *KRAS^{G12D};p48Cre* mouse. Scale bar, 100μm.

Supplemental Figure 2.15

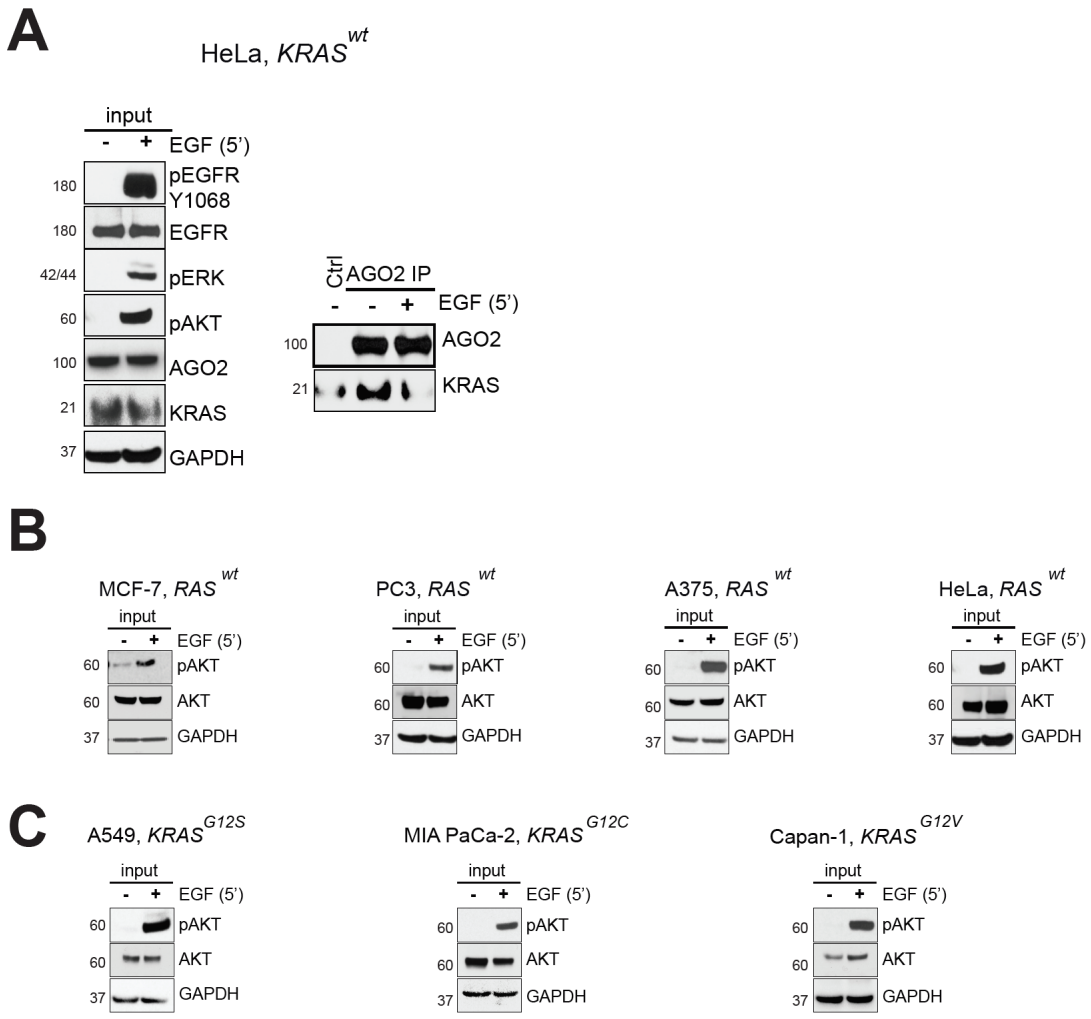

Supplementary Figure 15. EGF stimulation disrupts wild-type KRAS-AGO2 interaction (A) IP of endogenous AGO2 upon EGF stimulation (5'), in HeLa (*KRAS*^{wt}) cells followed by immunoblot analysis of KRAS. Input blots on the left show MAPK activation and levels of various proteins. Input blots show Akt activation upon EGF stimulation in *KRAS*^{wt} cells (B) or *KRAS*^{mt} cells (C) assessed in **Figure 7**. Numbers on the left of the immunoblots in this figure are protein molecular weights in kDa.

Supplemental Figure 2.16

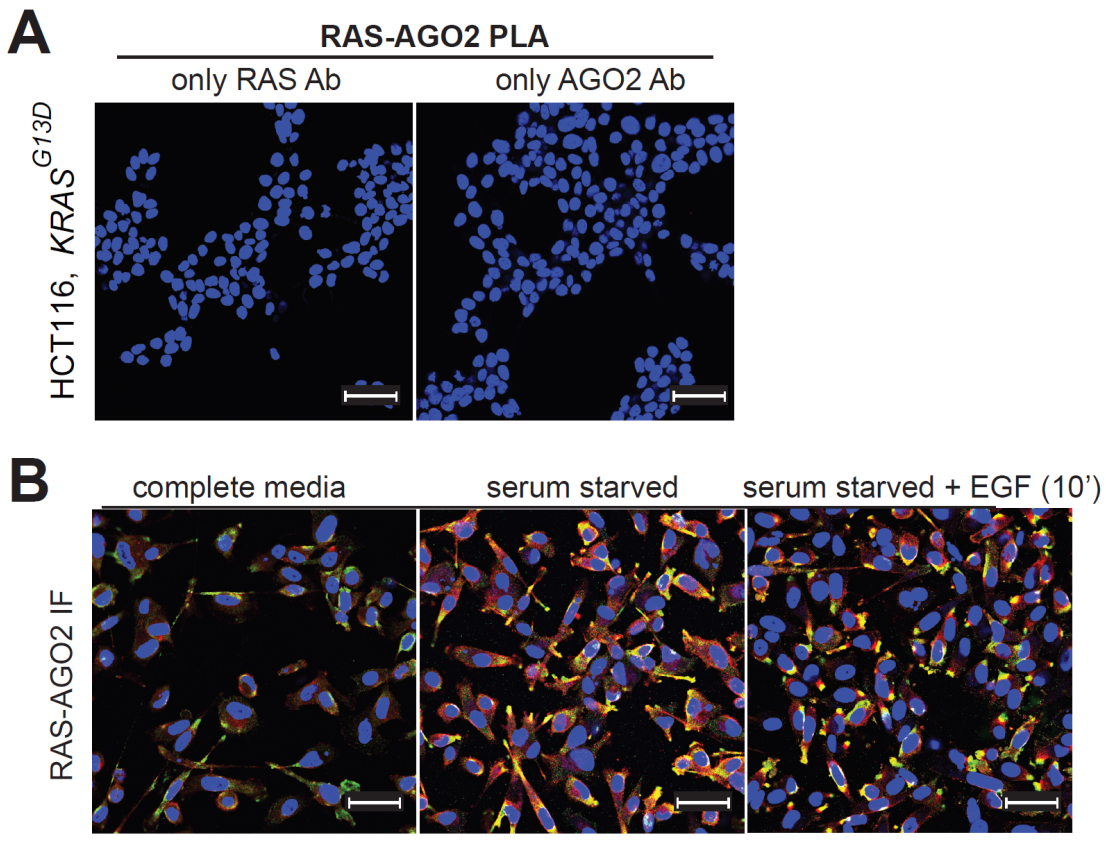

Supplementary Figure 16: Validation of RAS-AGO2 PLA in cell line models. (A) Control RAS-AGO2 PLA performed on HCT116 cells using either RAS or AGO2 antibody. (B) Representative images of RAS/AGO2 immunofluorescence in PC3 (*KRAS*^{wt}) cells grown under indicated conditions. Confocal images were taken under identical settings across all cell culture conditions. Scale bar, 50 μm.

Supplemental Table 2.1

Table 1: Antibodies used in the study

#	Antibody	Vendor	Catalog Number	Application	Specificity
1	Anti-Ras clone 10 (RAS10)	Millipore	05-516	IP (4ug), IB (1:1000), PLA (1:250)	Hu and Ms
2	K-Ras-2B Antibody (C-19)	Santa Cruz	sc-521	IP (4ug))	Hu
3	K-Ras monoclonal Ab	Santa Cruz	sc-30	IB (1:200)	human, mouse
4	RAS (G12D Mutant Specific) DH87	Cell Signaling	14429S	IB (1:1000)	human
5	KRAS (3B10-2F2)	Sigma- aldrich	WH0003845M1	IB (1:1000)	Human
6	HRAS- specific Antibody	Proteintech	18295-1-AP	IB (1:1000)	Human, mouse, rat
7	AGO2, 11A9	Sigma	SAB4200085	IP (10ug) ,IB (1:1000)	human
8	AGO2 EIF2C2	Sino Biologicals	50683-R036	IB (1:2000), IHC (1:100), PLA (1:200)	human
9	Anti- EGFR (phospho Y1092)	Abcam	ab40815 (EP774Y)	IHC (1:100)	human, mouse
10	Phospho-EGF Receptor (Y1068)	Cell Signaling	2234S	IB (1:1000)	human, mouse
11	Phospho-p44/42 MAPK (Erk 1/2)	Cell Signaling	4376	IB (1:1000)	human, mouse
12	ERK1(K-23)	Santa Cruz	sc-94	IB (1:500)	human, mouse, rat
13	Total p44/42 MAPK (Erk 1/2)	Cell Signaling	9102	IB (1:1000)	human, mouse
14	EGFR Antibody	Abcam	ab52894 (EP38Y)	IB (1:1000),IHC (1:50)	human, mouse, rat
15	EGFR(1005)	Santa Cruz	sc-03	IB (1:500)	human, mouse, rat
16	Anti-FLAG antibody	Sigma	F7425	IP (4ug), IB (1:1000)	human, mouse
17	Phospho-Akt S473	Cell Signaling	4060S	IB (1:1000)	human,mouse
18	AKT (pan) - C67E7	Cell Signaling	4691	IB (1:1000)	human,mouse
19	Anti-Cytokeratin 19 antibody	Abcam	ab133496	IHC (1:1000)	mouse
20	E-cadherin (36)	Ventana Roche	790-4497	IF (1:100)	Mouse
21	Nk1.1 (PK136)	Invitrogen	MA1-70100	IHC (1:100)	Mouse
22	anti-CD4 (SP35)	Ventana	790-4423	IHC (1:100)	Mouse
23	anti-CD68 (KP-1)	Ventana	790-2931	IHC (1:100)	Mouse
24	anti-CD8 (SP57)	Ventana	790-4460	IHC (1:100)	Mouse
25	Anti-Cytokeratin 19 antibody	Abcam	ab133496	IHC (1:500)	mouse
26	GAPDH- HRP	Cell Signaling	3683	IB (1:5000)	human, mouse
27	Normal mouse IgG	Santa Cruz	sc-2025	Isotype Control IP	mouse
28	Normal Rat IgG	Abcam	ab18450	Isotype Control IP	rat
29	Normal Rabbit IgG	Millipore	12-370	Isotype Control IP	rabbit

IP: Immunoprecipitation; IB: Immunoblot; IHC: Immunohistochemistry; PLA: Proximity Ligation Assay

Supplemental Table 2.2

Table 2: **Cases in *KRAS*^{G12D};*AGO2fl/fl;p48Cre* cohort with abnormal pathologies or death prior to 500 day time point**

Ear tag#	3331	2430	2385
Age (days)	368	500	500
Liver			
Ascites			
Lungs			
Diaphragm			
Hemorrhage			
Lymph nodes			
Kidneys			
Jaundice			
Enlarged Spleen			
Pathological Evaluation			
PDAC	no anaplastic PDAC or PDAC	no PDAC	no PDAC
Pancreas	low grade PanINs and cyst	only low grade PanIN	only low grade PanIN
AGO2 expression in pancreas	No AGO2 expression in the cyst or PanINs	no AGO2 expression in early PanINs	no AGO2 expression in early PanINs
Pancreatic Cyst	Yes	No cyst	No cyst
Further comment/ other pathology	resembles mucinous cystic neoplasm	likely benign lesion in lung, unknown origin	likely benign lesion in lung, unknown origin
AGO2 expression in mets?	n/a	AGO2 expressed in benign lung lesion	AGO2 expressed in benign lung lesion
Cause of Death	unknown	not dead before 500 days	not dead before 500 days

Supplemental Table 2.3

Table 3: Primers used in the study

I)

Transcript	Primer Sequence
m*HRAS*_Fwd	*5' GCTTCCTCTGTGTATTTGCCA 3'*
m*HRAS*_Rev	*5' CTTTCACCCGCTTGATCTGC 3'*
m*KRAS*_Fwd	*5' GTTAGCTCCAGTGCCCCAAT 3'*
m*KRAS*_Rev	*5' ATTCCCTAGGTCAGCGCAAC 3'*
m*NRAS*_Fwd	*5'ACTGGCCAAGAGTTACGGAA 3'*
m*NRAS*_Rev	*5' TGGCGTATCTCCCTTACCAG 3'*
m*AGO2*_Fwd	*5'GATCGCCAAGAGGAGATCAG3'*
m*AGO2*_Rev	*5'GCCTCCCAGTTTGACATTGA3'*
m*GAPDH*_Fwd	*5' AAGGTCATCCCAGAGCTGAA 3'*
m*GAPDH*_Rev	*5' CTGCTTCACCACCTTCTTGA 3'*
hAGO2 ORF Fwd	*5' ATCAACGTCAAGCTGGGAGG 3'*
hAGO2 ORF Rev	*5' GTGACGTCTGCTCCCAGAAA 3'*

II) *KRAS*^{G12D} conditional PCR primers 1) 5' *gtc ttt ccc cag cac agt gc* 3', 2) 5' *ctc ttg cct acg cca cca gct c* 3', and 3) 5' *agc tag cca cca tgg ctt gag taa gtc tgc a* 3' according to the Tyler Jacks lab protocol described in detail at

https://jacks-lab.mit.edu/protocols/genotyping/kras_cond

Supplemental Table 2.4

Number	Cell Line	Source	Tissue	Type	*KRAS* or *AGO2* status	From
1	PC3	Human	Prostate	Cancer	*KRAS* WT	ATCC
2	MCF7	Human	Breast	Cancer	*KRAS* WT	ATCC
3	A375	Human	Melanoma	Cancer	*KRAS* WT	ATCC
4	A549	Human	Lung	Cancer	*KRAS* G12S	ATCC
5	MIA PaCa-2	Human	Pancreas	Cancer	*KRAS* G12C	ATCC
6	CAPAN-1	Human	Pancreas	Cancer	*KRAS* G12V	ATCC
7	DLD-1 (MUT/WT)	Human	Colorectal	Cancer	*KRAS* G13D	ATCC
8	H358	Human	Lung	Cancer	*KRAS* G12C	ATCC
9	HCT116	Human	Colorectal	Cancer	*KRAS* G13D	ATCC
10	PANC-1	Human	Pancreas	Cancer	*KRAS* G12D	ATCC
11	Panc 05.04	Human	Pancreas	Cancer	*KRAS* G12C	ATCC
12	Panc 10.05	Human	Pancreas	Cancer	*KRAS* G12C	ATCC
13	HEK293FT	Human	Embryonic kidney	Benign	*KRAS* WT	ATCC
14	MEF,parental	Mouse	Embryonic fibroblast	Benign	*KRAS* WT	Zamore lab (PMID: 21878547)
15	*AGO2* MEF-/-	Mouse	Embryonic fibroblast	Benign	*AGO2* knockout	Zamore lab (PMID: 21878547)
16	*AGO2* MEF-/-+*AGO2*	Mouse	Embryonic fibroblast	Benign	*AGO2* knockout overexpressing *AGO2*	Zamore lab (PMID: 21878547)
17	Rasless MEFs	Mouse	Embryonic fibroblast	Benign	RAS deficient	The RAS Initiative https://www.cancer.gov/research/key-initiatives/ras/outreach/reference-reagents

Supplemental Figure 3.1

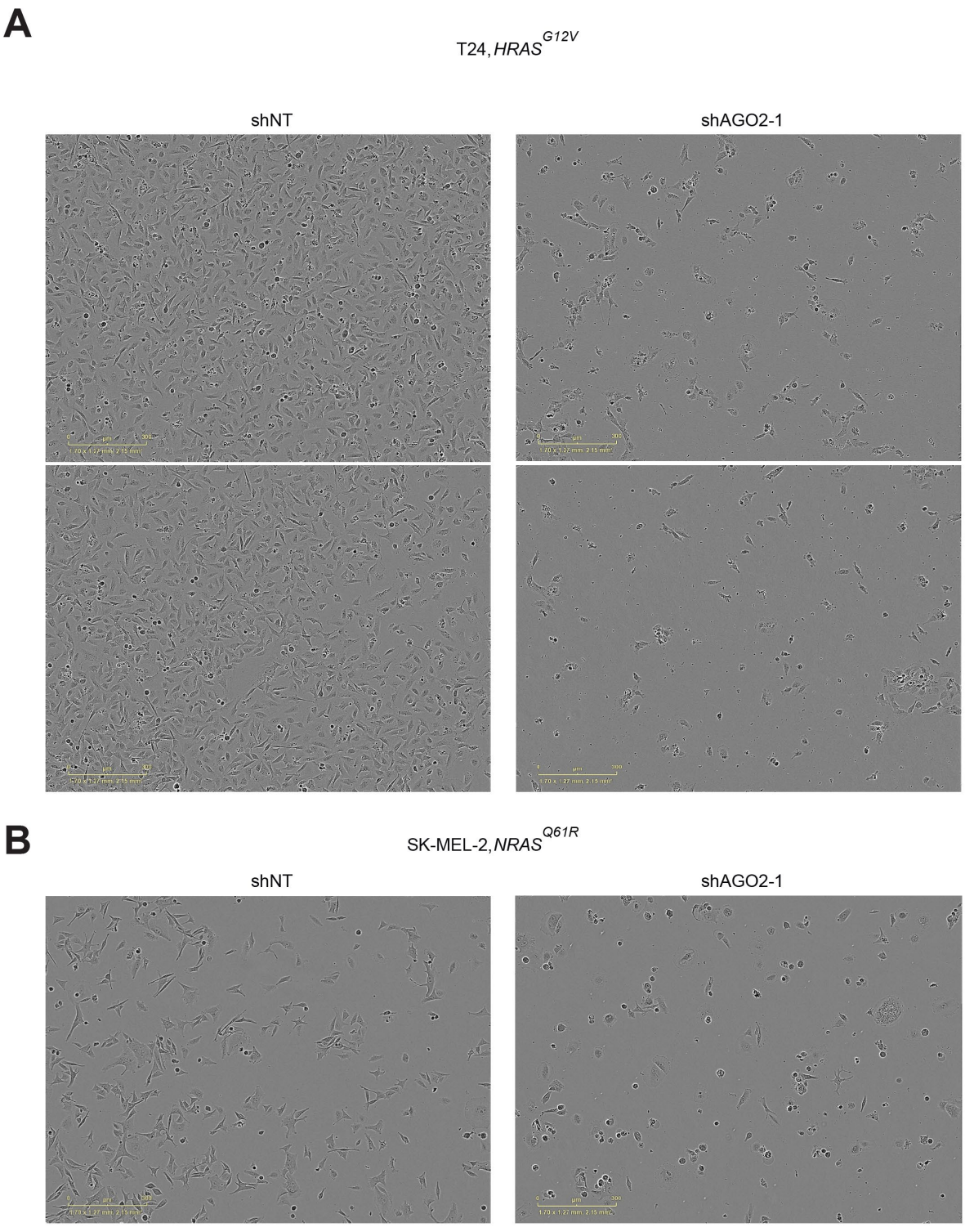

Supplemental Figure 3.1 Cell Morphology Changes Following AGO2 Knockdown
(A) T24 shNT vs shAGO2 morphology
(B) SK-MEL-2 shNT vs shAGO2 morphology

Supplemental Figure 3.2

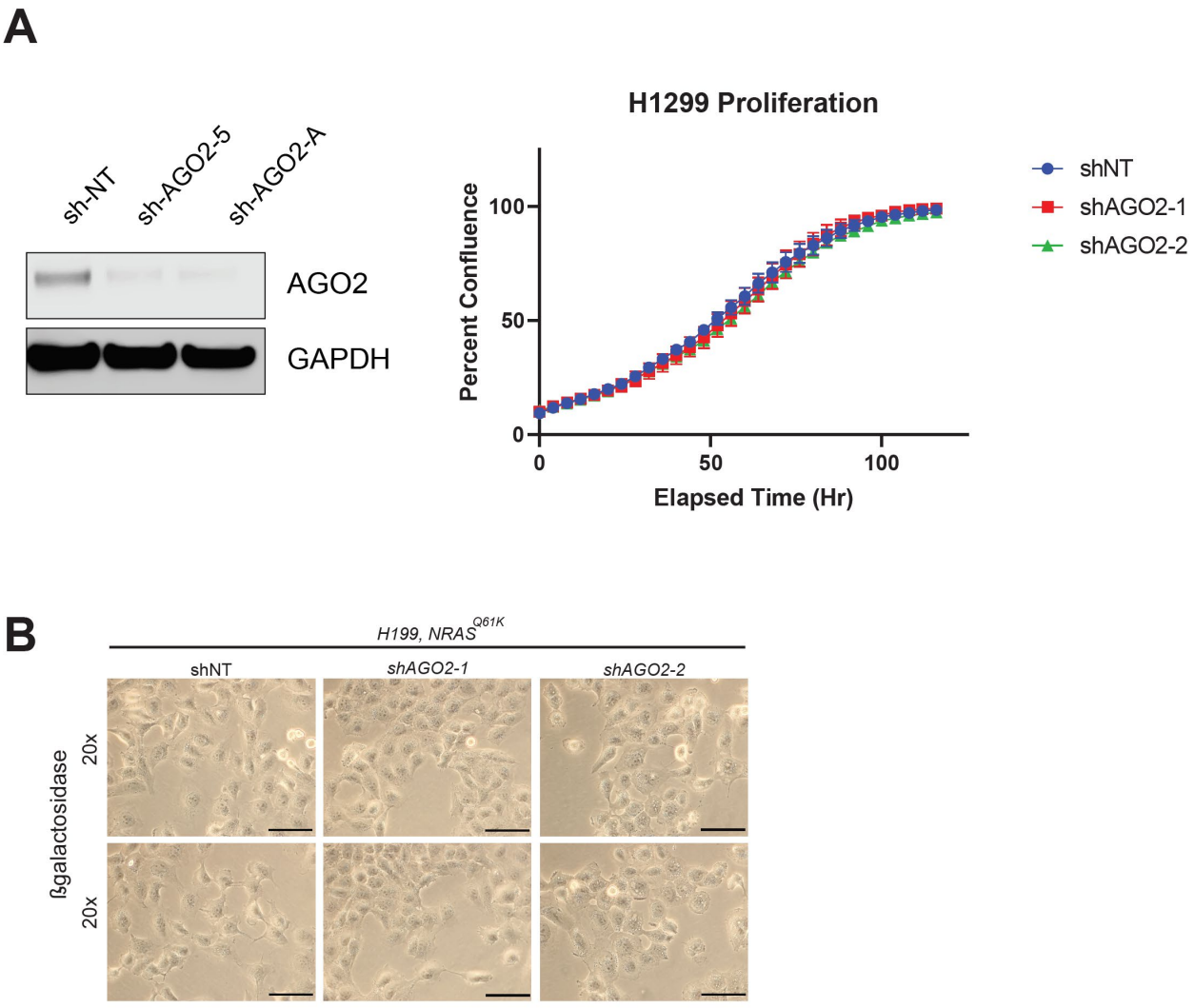

Supplemental Figure 3.2 p53 Null Cell Line is Unaffected by AGO2 Loss
(A) Western blot confirmation of AGO2 Knockdown in H1299 cell line with no change in proliferation

(B) Beta-Gal staining in H1299 cell line following AGO2 knockdown

Supplemental Figure 3.3

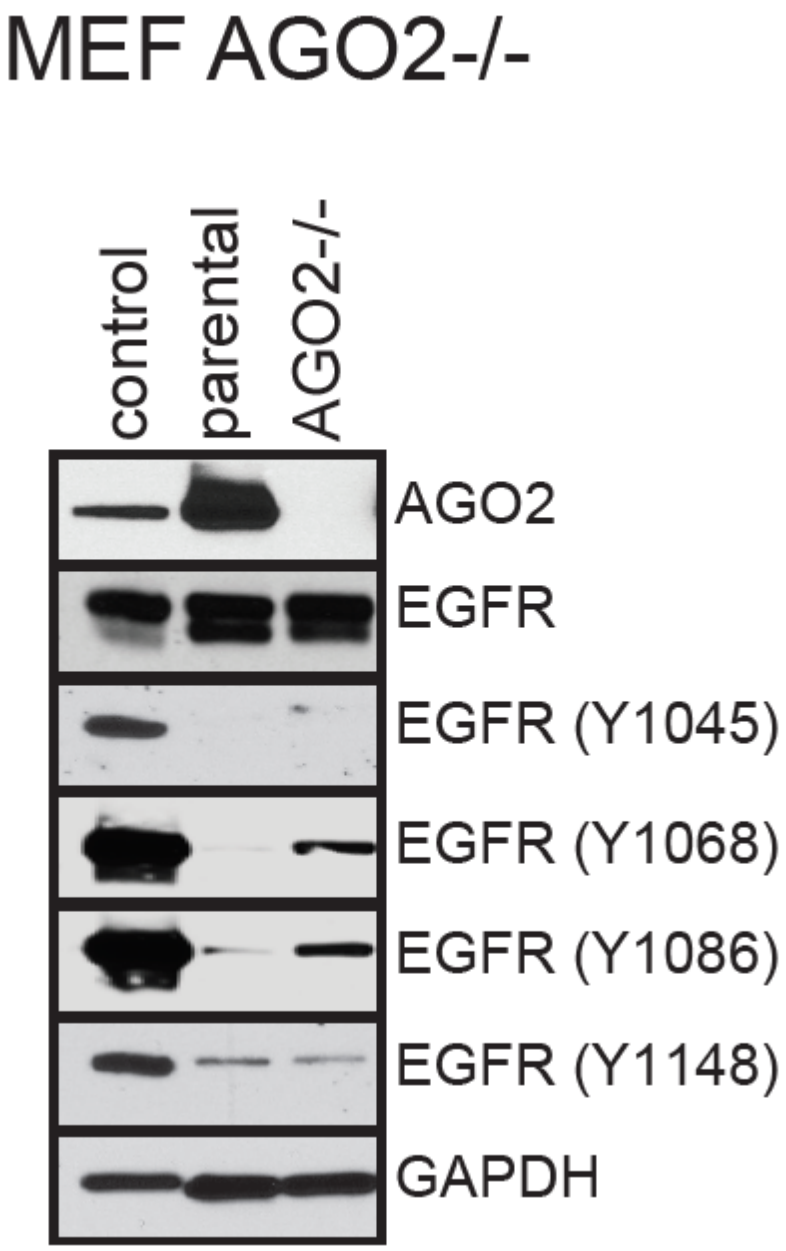

Supplemental Figure 3.3 Both EGFR Y1068 and Y1086 residues are activated in AGO2-/- MEFs

Immunoblot analysis of various EGFR tyrosine phosphorylation residues in different MEFs. A431 lung cancer cells are used as control since these cells demonstrate activated EGFR residues at multiple tyrosine phosphorylation sites and therefore used as positive control for immunoblot.

Supplemental Table 3.1: Cell Lines Utilized in Study

Number	Cell Line	Source	Tissue	Type	*RAS Status*
1	HEK293	Human	Embryonic Kidney	Benign	*RAS WT*
2	MCF-7	Human	Breast	Cancer	*RAS WT*
3	HeLa	Human	Cervix	Cancer	*RAS WT*
4	A375	Human	Skin Melanoma	Cancer	*RAS WT*
5	LNCaP	Human	Prostate	Cancer	*RAS WT*
6	U2OS	Human	Osteosarcoma	Cancer	*RAS WT*
7	T24	Human	Bladder	Cancer	*HRAS-G12V*
8	Kasumi-2	Human	ALL	Cancer	*HRAS-G13V*
9	Hs587t	Human	Breast	Cancer	*HRAS-G12D*
10	Mel-Juso	Human	Skin Melanoma	Cancer	*NRAS-Q61L*
11	SK-Mel-2	Human	Skin Melanoma	Cancer	*NRAS-Q61H*
12	MOLT4	Human	AML	Cancer	*NRAS-G12C*
13	H1299	Human	Lung	Cancer	*NRAS-Q61K*

Supplemental Table 3.2: Antibodies used for Immunoprecipitation and Immunobloting

#	Antibody	Vendor	Catalog Number	Application	Specificity	RAS Validation
1	Anti-Ras clone 10 (RAS10)	Millipore	05-516	IP, IB, PLA	Hu and Ms	Waters et al., 2017
2	HRAS	Proteintech	18295–1-AP	IB	Hu and Ms	Waters et al., 2017
3	NRAS	Santa Cruz	sc-31	IB	Hu and Ms	Waters et al., 2017
4	AGO2, 11A9	Sigma	SAB4200085	IP	Hu	N/A
5	AGO2 EIF2C2	Sino Biologicals	11079-T36	IB, PLA	Hu	N/A
6	Phospho-EGF Receptor (Tyr1068)	Cell Signaling	2234S	IB	Hu and Ms	N/A
7	EGFR Antibody	Millipore	06-847	IB	Hu	N/A
8	EGFR Antibody (A-10)	Santa Cruz	sc-373746	IB	Hu and Ms	N/A
9	p44/42 MAPK (Erk1/2)	Cell Signaling	9102S	IB	Hu	N/A
10	Phospho-p44/42 MAPK (Erk 1/2)	Cell Signaling	4376	IB	Hu and Ms	N/A
11	Anti-p53	Sigma	P8999-200UL	IB	Hu	N/A
12	p16 INK4A (D7C1M)	Cell Signaling	80772S	IB	Hu	N/A
13	p21 Waf1/Cip1 (12D1)	Cell Signaling	2947S	IB	Hu	N/A
14	GAPDH-HRP	Cell Signaling	3683	IB	Hu and Ms	N/A
15	PTP1B / PTPN1	Sino Biologicals	10304-RP02-100	IB	Hu	N/A
16	GAPDH-HRP	Cell Signaling	3683	IB	Hu and Ms	N/A
17	Normal Mouse IgG	Santa Cruz	sc-2025	Isotype Control IP	Ms	N/A
18	Normal Rat IgG	Abcam	ab18450	Isotype Control IP	Rt	N/A
19	Normal Rabbit IgG	Millipore	12-370	Isotype Control IP	Rb	N/A

IP: Immunoprecipitation; IB: Immunoblot; Hu: Human; Ms: Mouse; Rt: Rat; Rb: Rabbit; PLA: Proximity Ligation Assay

Supplemental Figure 4.1

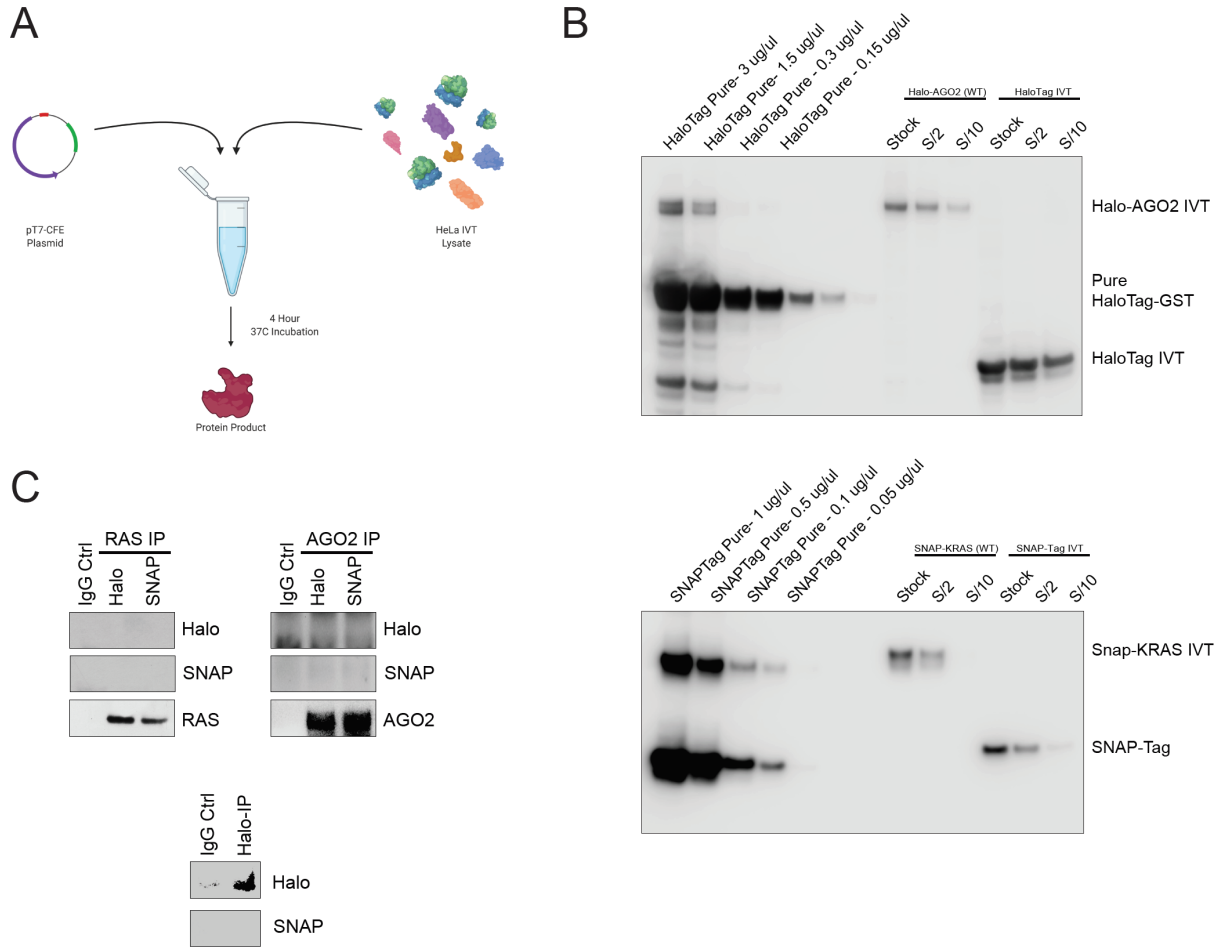

Supplemental Figure 4.1 Validation and Concentration Estimation of IVT Proteins
(A) HeLa *In Vitro* Translation System Model

(B) Concentration estimation of IVT products. A dilution curve of purified HaloTag (Promega) and SNAP-Tag (NEB) were compared to a dilution curve of IVT generated Halo-AGO2, HaloTag, SNAP-KRAS, and SNAP-Tag to estimate concentration of target protein generated during IVT reaction.

(C) Co-IP of HaloTag and SNAP-Tag with endogenous RAS, endogenous AGO2, and each other to confirm no binding.

Supplemental Figure 4.2

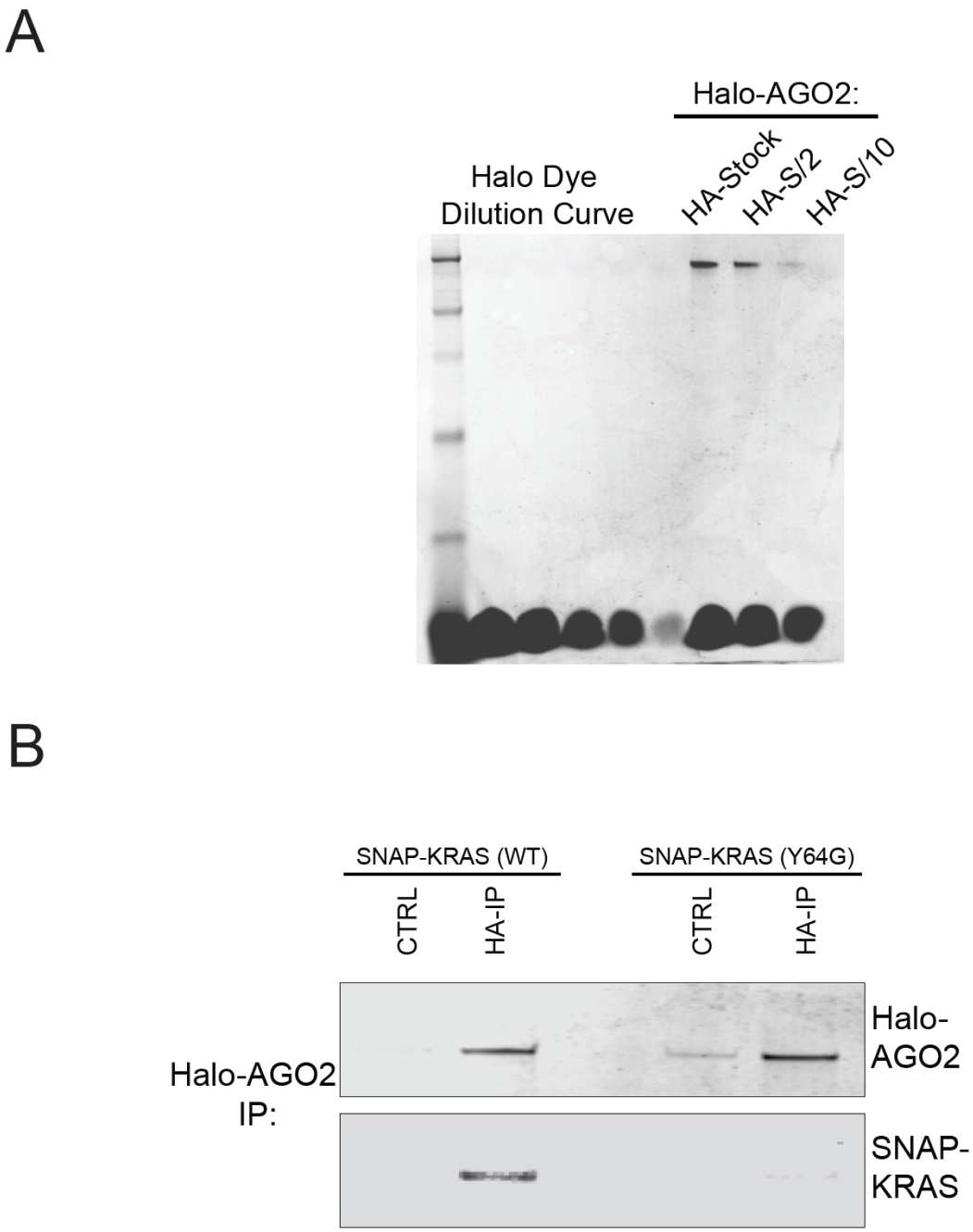

Supplemental Figure 4.2 Confirmation of Halo-Tag Labeling and Fluorescent Co-IP
(A) Confirmation of Halo-AGO2 vs dilution curve of Halo-Tag dye

(B) Co-IP of labeled Halo-AGO2 and SNAP-KRAS. Only WT KRAS binds with AGO2 and Y64G mutant shows no binding.

Supplemental Figure 4.3

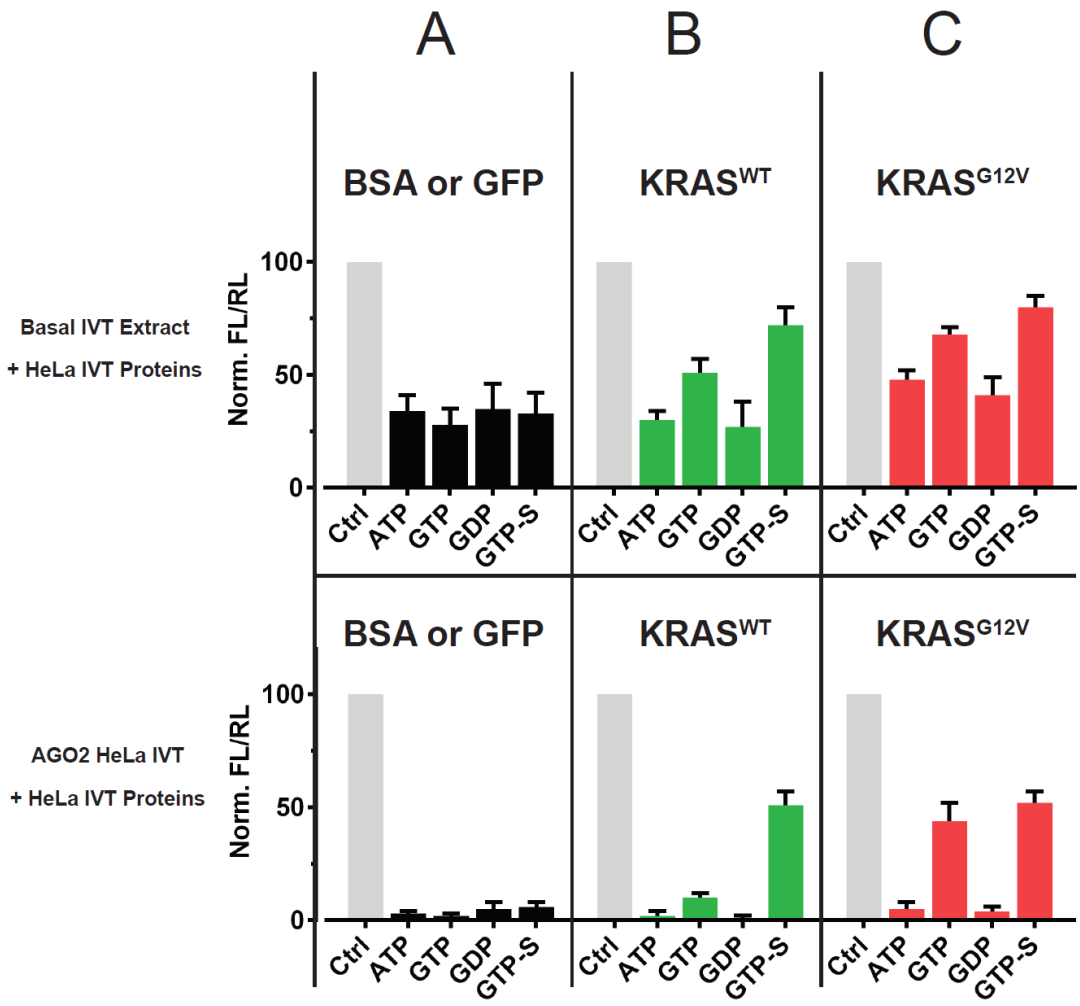

Supplemental Figure 4.3 AGO2 *in vitro* cleavage assay with KRAS WT vs G12V
AGO2 FL/RL *in vitro* cleavage assay with siRNA targeting FL. Proteins were generated via HeLa IVT system, and incubated as described in Chapter 4. Row (1) is basal IVT extract with mixed proteins as indicated below, and Row (2) is AGO2 IVT overexpression mixed the same. Each protein mixture was incubated with indicated nucleotide

(A) BSA or GFP Control
(B) WT KRAS
(C) G12V KRAS

Supplemental Figure 4.4

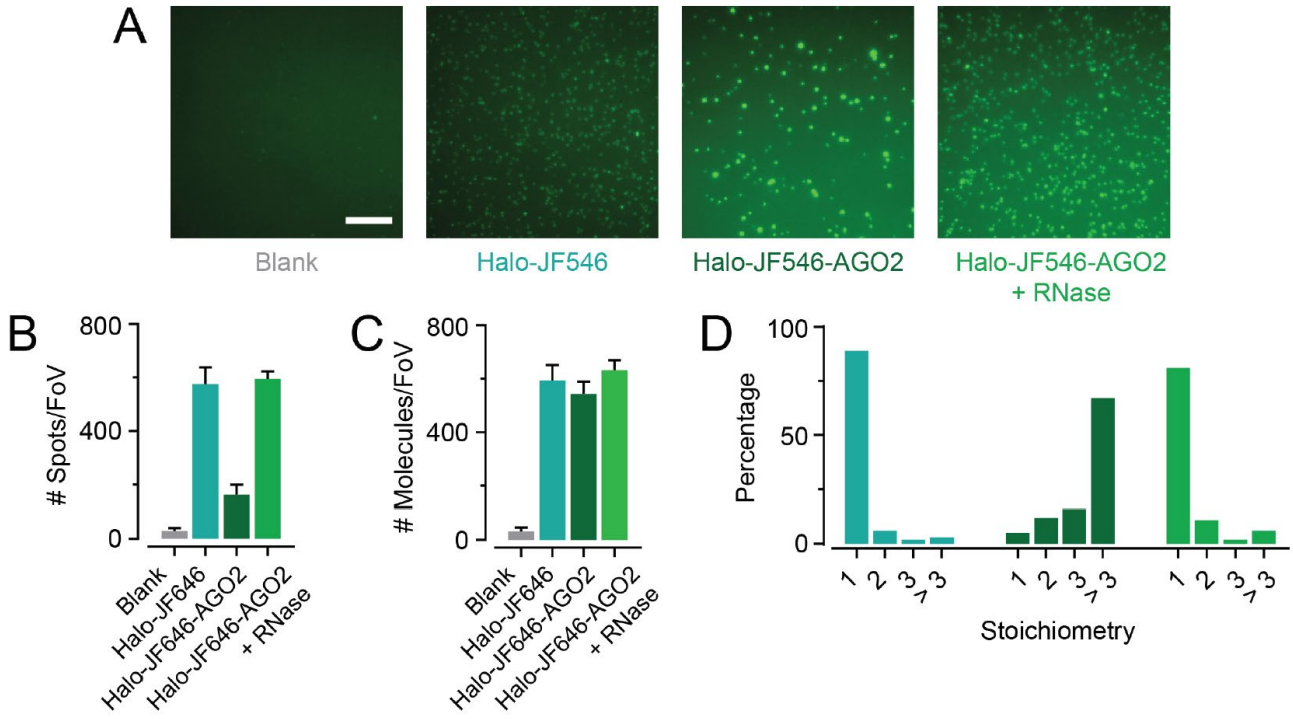

Supplemental Figure 4.4 RNase Treatment Disrupts AGO2's Formation of Higher Order Complexes *in vitro*

(A) Raw single molecule images from a black slide, HaloTag alone, Halo-AGO2, and Halo-AGO2 with RNase Treatment

(B) Number of spots per field of view in each of the four conditions above

(C) Number of molecules per field of view in each of the four conditions above

(D) Stoichiometry of Halo spots visualized in the four conditions

Author Contributions

Chapter 1
This chapter was written by Ronald Francis Siebenaler, and figures were generated via Biorender with protein structures from Jessica Waninger.

Chapter 2
This chapter was previously published in the article below:
Sunita Shankar*, Jean Ching-Yi Tien*, Ronald F. Siebenaler*, Seema Chugh*, Vijaya L. Dommeti, Sylvia Zelenka-Wang, Xiao-Ming Wang, Ingrid J. Apel, Jessica Waninger, Sanjana Eyunni, Alice Xu, Malay Mody, Andrew Goodrum, Yuping Zhang, John J. Tesmer, Rahul Mannan, Xuhong Cao, Pankaj Vats, Sethuramasundaram Pitchiaya, Jiaqi Shi, Chandan Kumar-Sinha, Howard C. Crawford, and Arul M. Chinnaiyan.
An Essential Role for *Argonaute 2* in EGFR-KRAS Signaling in Pancreatic Cancer Development. *Nat Comm*, 2020. *These authors contributed equally

Author Contributions
Mouse experimental data were generated by J.C.T., S.C., A.G., A.X., V.L.D., and S.S. Contributions to other experimental data were made by S.S., R.F.S, V.L.D., S.Z.-W., S.E., X.C., M.M., S.P., I.J.A., and C.K.-S. R.M. and J. S. coordinated the pathology assessment. J. S. provided the human TMA and performed IHC scoring. X.W. performed RNA ISH. J.W. and J.T. supported work on AGO2 phosphorylation. P.V. and Y.Z. provided bioinformatics support. X.C. helped with project management. H.C.C. supervised the pancreatitis experiments. S.S. and A.M.C. jointly conceived the study. S.S., R.F.S., C.K-S., and A.M.C. wrote the manuscript. Funding and overall supervision of the study was provided by A.M.C.

Chapter 3
This chapter is currently in preparation for submission:
Siebenaler R.F., Chugh S., Waninger J., Chu A., Dommeti L.V., Mody M., Gautam A., Kenum C., Steiert L., Patel N., Cao X, Kumar-Sinha C., Shankar S., and Chinnaiyan A.M.

Author Contributions
Contributions to experimental data were made by R.F.S, S.C., J.W., S.S., V.L.D., M.M., A.G., C.K, L.S., and N.P. Zebrafish experimental data were generated by A.C. and R.F.S. J.W. provided protein crystal structures. X.C. helped with project management. R.F.S. and A.M.C. jointly conceived the study. R.F.S. and A.M.C. wrote the manuscript. Funding and overall supervision of the study was provided by A.M.C.

Chapter 4

Author Contributions

Contributions to experimental data were made by Ronald F. Siebenaler, Sethuramasundaram Pitchiaya, Visha Krishnan, Sujay Ray, Xia Jiang, Malay Mody, Anudeeta Gautam, Carson Kenum, Logan Steiert, Nidhi Patel, and Meike Stoldt. Data analyses were conducted by S.P. and R.F.S. R.F.S. and S.P. wrote the manuscript. Funding and overall supervision of the study was provided by Nils Walter and Arul Chinnaiyan.

Chapter 5

This chapter was written by Ronald Francis Siebenaler.